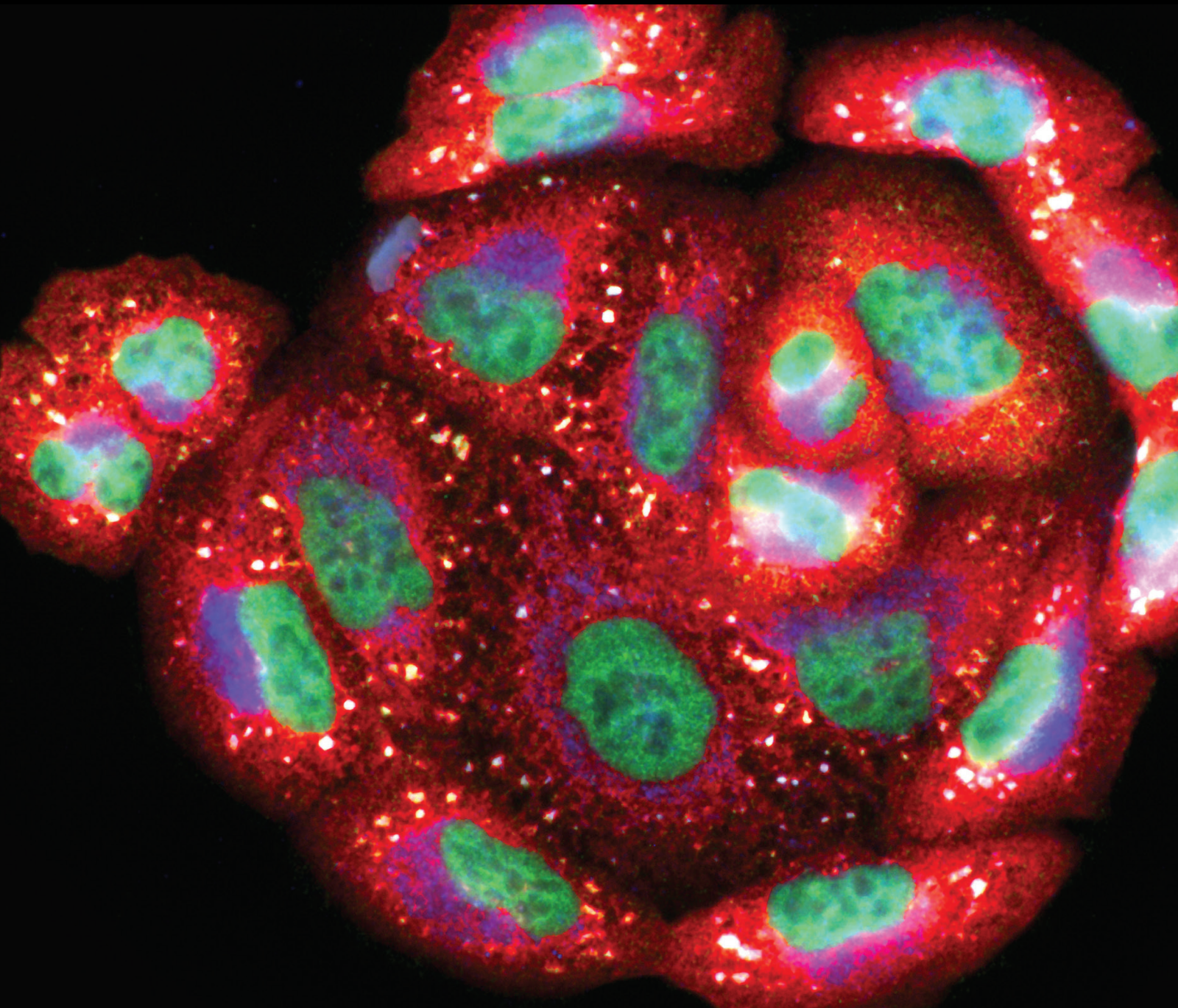


# Glial Cells and Oxidative Stress in Neurodegenerative Diseases

Lead Guest Editor: Xu Wu

Guest Editors: Alexei Verkhratsky and Robert Zorec





---

# **Glial Cells and Oxidative Stress in Neurodegenerative Diseases**

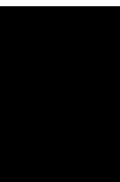
Oxidative Medicine and Cellular Longevity

---

## **Glial Cells and Oxidative Stress in Neurodegenerative Diseases**

Lead Guest Editor: Xu Wu

Guest Editors: Alexei Verkhratsky and Robert  
Zorec



---

Copyright © 2022 Hindawi Limited. All rights reserved.

This is a special issue published in "Oxidative Medicine and Cellular Longevity" All articles are open access articles distributed under the Creative Commons Attribution License, which permits unrestricted use, distribution, and reproduction in any medium, provided the original work is properly cited.

# Chief Editor

Jeannette Vasquez-Vivar, USA

## Associate Editors

Amjad Islam Aqib, Pakistan  
Angel Catalá , Argentina  
Cinzia Domenicotti , Italy  
Janusz Gebicki , Australia  
Aldrin V. Gomes , USA  
Vladimir Jakovljevic , Serbia  
Thomas Kietzmann , Finland  
Juan C. Mayo , Spain  
Ryuichi Morishita , Japan  
Claudia Penna , Italy  
Sachchida Nand Rai , India  
Paola Rizzo , Italy  
Mithun Sinha , USA  
Daniele Vergara , Italy  
Victor M. Victor , Spain

## Academic Editors

Ammar AL-Farga , Saudi Arabia  
Mohd Adnan , Saudi Arabia  
Ivanov Alexander , Russia  
Fabio Altieri , Italy  
Daniel Dias Rufino Arcanjo , Brazil  
Peter Backx, Canada  
Amira Badr , Egypt  
Damian Bailey, United Kingdom  
Rengasamy Balakrishnan , Republic of Korea  
Jiaolin Bao, China  
Ji C. Bihl , USA  
Hareram Birla, India  
Abdelhakim Bouyahya, Morocco  
Ralf Braun , Austria  
Laura Bravo , Spain  
Matt Brody , USA  
Amadou Camara , USA  
Marcio Carcho , Portugal  
Peter Celec , Slovakia  
Giselle Cerchiaro , Brazil  
Arpita Chatterjee , USA  
Shao-Yu Chen , USA  
Yujie Chen, China  
Deepak Chhangani , USA  
Ferdinando Chiaradonna , Italy

Zhao Zhong Chong, USA  
Fabio Ciccarone, Italy  
Alin Ciobica , Romania  
Ana Cipak Gasparovic , Croatia  
Giuseppe Cirillo , Italy  
Maria R. Ciriolo , Italy  
Massimo Collino , Italy  
Manuela Corte-Real , Portugal  
Manuela Curcio, Italy  
Domenico D'Arca , Italy  
Francesca Danesi , Italy  
Claudio De Lucia , USA  
Damião De Sousa , Brazil  
Enrico Desideri, Italy  
Francesca Diomede , Italy  
Raul Dominguez-Perles, Spain  
Joël R. Drevet , France  
Grégory Durand , France  
Alessandra Durazzo , Italy  
Javier Egea , Spain  
Pablo A. Evelson , Argentina  
Mohd Farhan, USA  
Ioannis G. Fatouros , Greece  
Gianna Ferretti , Italy  
Swaran J. S. Flora , India  
Maurizio Forte , Italy  
Teresa I. Fortoul, Mexico  
Anna Fracassi , USA  
Rodrigo Franco , USA  
Juan Gambini , Spain  
Gerardo García-Rivas , Mexico  
Husam Ghanim, USA  
Jayeeta Ghose , USA  
Rajeshwary Ghosh , USA  
Lucia Gimeno-Mallench, Spain  
Anna M. Giudetti , Italy  
Daniela Giustarini , Italy  
José Rodrigo Godoy, USA  
Saeid Golbidi , Canada  
Guohua Gong , China  
Tilman Grune, Germany  
Solomon Habtemariam , United Kingdom  
Eva-Maria Hanschmann , Germany  
Md Saquib Hasnain , India  
Md Hassan , India




Tim Hofer , Norway  
John D. Horowitz, Australia  
Silvana Hrelia , Italy  
Dragan Hrnčić, Serbia  
Zebo Huang , China  
Zhao Huang , China  
Tariq Hussain , Pakistan  
Stephan Immenschuh , Germany  
Norsharina Ismail, Malaysia  
Franco J. L. , Brazil  
Sedat Kacar , USA  
Andleeb Khan , Saudi Arabia  
Kum Kum Khanna, Australia  
Neelam Khaper , Canada  
Ramoji Kosuru , USA  
Demetrios Kouretas , Greece  
Andrey V. Kozlov , Austria  
Chan-Yen Kuo, Taiwan  
Gaocai Li , China  
Guoping Li , USA  
Jin-Long Li , China  
Qiangqiang Li , China  
Xin-Feng Li , China  
Jialiang Liang , China  
Adam Lightfoot, United Kingdom  
Christopher Horst Lillig , Germany  
Paloma B. Liton , USA  
Ana Lloret , Spain  
Lorenzo Loffredo , Italy  
Camilo López-Alarcón , Chile  
Daniel Lopez-Malo , Spain  
Massimo Lucarini , Italy  
Hai-Chun Ma, China  
Nageswara Madamanchi , USA  
Kenneth Maiese , USA  
Marco Malaguti , Italy  
Steven McAnulty, USA  
Antonio Desmond McCarthy , Argentina  
Sonia Medina-Escudero , Spain  
Pedro Mena , Italy  
V́ctor M. Mendoza-Núñez , Mexico  
Lidija Milkovic , Croatia  
Alexandra Miller, USA  
Sara Missaglia , Italy

Premysl Mladenka , Czech Republic  
Sandra Moreno , Italy  
Trevor A. Mori , Australia  
Fabiana Morroni , Italy  
Ange Mouithys-Mickalad, Belgium  
Iordanis Mourouzis , Greece  
Ryoji Nagai , Japan  
Amit Kumar Nayak , India  
Abderrahim Nemmar , United Arab Emirates  
Xing Niu , China  
Cristina Nocella, Italy  
Susana Novella , Spain  
Hassan Obied , Australia  
Pál Pacher, USA  
Pasquale Pagliaro , Italy  
Dilipkumar Pal , India  
Valentina Pallottini , Italy  
Swapnil Pandey , USA  
Mayur Parmar , USA  
Vassilis Paschalis , Greece  
Keshav Raj Paudel, Australia  
Ilaria Peluso , Italy  
Tiziana Persichini , Italy  
Shazib Pervaiz , Singapore  
Abdul Rehman Phull, Republic of Korea  
Vincent Pialoux , France  
Alessandro Poggi , Italy  
Zsolt Radak , Hungary  
Dario C. Ramirez , Argentina  
Erika Ramos-Tovar , Mexico  
Sid D. Ray , USA  
Muneeb Rehman , Saudi Arabia  
Hamid Reza Rezvani , France  
Alessandra Ricelli, Italy  
Francisco J. Romero , Spain  
Joan Roselló-Catafau, Spain  
Subhadeep Roy , India  
Josep V. Rubert , The Netherlands  
Sumbal Saba , Brazil  
Kunihiro Sakuma, Japan  
Gabriele Saretzki , United Kingdom  
Luciano Saso , Italy  
Nadja Schroder , Brazil

Anwen Shao , China  
Iman Sherif, Egypt  
Salah A Sheweita, Saudi Arabia  
Xiaolei Shi, China  
Manjari Singh, India  
Giulia Sita , Italy  
Ramachandran Srinivasan , India  
Adrian Sturza , Romania  
Kuo-hui Su , United Kingdom  
Eisa Tahmasbpour Marzouni , Iran  
Hailiang Tang, China  
Carla Tatone , Italy  
Shane Thomas , Australia  
Carlo Gabriele Tocchetti , Italy  
Angela Trovato Salinaro, Italy  
Rosa Tundis , Italy  
Kai Wang , China  
Min-qi Wang , China  
Natalie Ward , Australia  
Grzegorz Wegrzyn, Poland  
Philip Wenzel , Germany  
Guangzhen Wu , China  
Jianbo Xiao , Spain  
Qiongming Xu , China  
Liang-Jun Yan , USA  
Guillermo Zalba , Spain  
Jia Zhang , China  
Junmin Zhang , China  
Junli Zhao , USA  
Chen-he Zhou , China  
Yong Zhou , China  
Mario Zoratti , Italy




## Contents

### **Icariside II Attenuates Methamphetamine-Induced Neurotoxicity and Behavioral Impairments via Activating the Keap1-Nrf2 Pathway**

Jian Huang, Jiuyang Ding , Zhuo Wang, Yanning Li, Yitong He, Xiaohan Wang, Haoliang Fan , Qiqian Xie, and Pingming Qiu 





Research Article (23 pages), Article ID 8400876, Volume 2022 (2022)

### **Glial Purinergic Signaling-Mediated Oxidative Stress (GPOS) in Neuropsychiatric Disorders**

Lumei Huang , Yong Tang , and Beata Sperlagh 



Review Article (12 pages), Article ID 1075440, Volume 2022 (2022)

### **Cross-Talking Pathways of Forkhead Box O1 (FOXO1) Are Involved in the Pathogenesis of Alzheimer's Disease and Huntington's Disease**

Liyang Liu , Jun Bai, Fangxi Liu, Ying Xu, Mei Zhao , Chuansheng Zhao , and Zhike Zhou 

Research Article (14 pages), Article ID 7619255, Volume 2022 (2022)

### **Neuroprotective Effect of Ceftriaxone on MPTP-Induced Parkinson's Disease Mouse Model by Regulating Inflammation and Intestinal Microbiota**

Xiaoting Zhou, Jiachen Lu, Kehong Wei, Jing Wei, Puyuan Tian, Mengyun Yue, Yun Wang, Daojun Hong, Fangjun Li, Bo Wang, Tingtao Chen , and Xin Fang 




Research Article (15 pages), Article ID 9424582, Volume 2021 (2021)

### **mTORC1 Activation in *Chx10*-Specific *Tsc1* Knockout Mice Accelerates Retina Aging and Degeneration**

Yu-Qing Rao , Yu-Tong Zhou , Wenchuan Zhou , Jia-Kai Li , Baojie Li , and Jing Li 

Research Article (21 pages), Article ID 6715758, Volume 2021 (2021)

### **Trilobatin Alleviates Cognitive Deficits and Pathologies in an Alzheimer's Disease Mouse Model**

Jiuyang Ding , Jian Huang, Dan Yin, Ting Liu , Zheng Ren, Shanshan Hu, Yuanliang Ye, Cuiyun Le, Na Zhao, Hongmei Zhou, Zhu Li, Xiaolan Qi, and Jiang Huang 









Research Article (15 pages), Article ID 3298400, Volume 2021 (2021)

### **Food-Origin Mycotoxin-Induced Neurotoxicity: Intend to Break the Rules of Neuroglia Cells**

Xingyao Pei , Wenjuan Zhang, Haiyang Jiang , Dingkuo Liu, Xinyu Liu, Liuan Li, Cun Li, Xilong Xiao, Shusheng Tang , and Daowen Li 

Review Article (14 pages), Article ID 9967334, Volume 2021 (2021)

### **Mitochondrial Protection and Against Glutamate Neurotoxicity via Shh/Ptch1 Signaling Pathway to Ameliorate Cognitive Dysfunction by Kaixin San in Multi-Infarct Dementia Rats**

Xiaoqiong Li , Wen Wen , Ping Li , Ying Fu , Hao Chen , Fushun Wang , Yuan Dai , and Shijun Xu 

Research Article (15 pages), Article ID 5590745, Volume 2021 (2021)



**Downregulation of ATP6V1A Involved in Alzheimer's Disease via Synaptic Vesicle Cycle, Phagosome, and Oxidative Phosphorylation**

Zhike Zhou, Jun Bai, Shanshan Zhong, Rongwei Zhang, Kexin Kang, Xiaoqian Zhang, Ying Xu, Chuansheng Zhao , and Mei Zhao 

Research Article (15 pages), Article ID 5555634, Volume 2021 (2021)

## Research Article

# Icariside II Attenuates Methamphetamine-Induced Neurotoxicity and Behavioral Impairments via Activating the Keap1-Nrf2 Pathway

Jian Huang,<sup>1</sup> Jiuyang Ding<sup>1,2</sup>,, Zhuo Wang,<sup>3</sup> Yanning Li,<sup>1</sup> Yitong He,<sup>1</sup> Xiaohan Wang,<sup>1</sup> Haoliang Fan<sup>1</sup>,, Qiqian Xie,<sup>1</sup> and Pingming Qiu<sup>1</sup>

<sup>1</sup>School of Forensic Medicine, Southern Medical University, Guangzhou 510515, China

<sup>2</sup>School of Forensic Medicine, Guizhou Medical University, Guiyang 550004, China

<sup>3</sup>Department of Infertility and Sexual Medicine, The Third Affiliated Hospital of Sun Yat-sen University, Guangzhou 510630, China

Correspondence should be addressed to Pingming Qiu; [qiupmfy@126.com](mailto:qiupmfy@126.com)

Received 18 August 2021; Revised 26 November 2021; Accepted 11 March 2022; Published 28 March 2022

Academic Editor: Daniel Lopez Malo

Copyright © 2022 Jian Huang et al. This is an open access article distributed under the Creative Commons Attribution License, which permits unrestricted use, distribution, and reproduction in any medium, provided the original work is properly cited.

Chronic and long-term methamphetamine (METH) abuse is bound to cause damages to multiple organs and systems, especially the central nervous system (CNS). Icariside II (ICS), a type of flavonoid and one of the main active ingredients of the traditional Chinese medicine *Epimedium*, exhibits a variety of biological and pharmacological properties such as anti-inflammatory, antioxidant, and anticancer activities. However, whether ICS could protect against METH-induced neurotoxicity remains unknown. Based on a chronic METH abuse mouse model, we detected the neurotoxicity after METH exposure and determined the intervention effect of ICS and the potential mechanism of action. Here, we found that METH could trigger neurotoxicity, which was characterized by loss of dopaminergic neurons, depletion of dopamine (DA), activation of glial cells, upregulation of  $\alpha$ -synuclein ( $\alpha$ -syn), abnormal dendritic spine plasticity, and dysfunction of motor coordination and balance. ICS treatment, however, alleviated the above-mentioned neurotoxicity elicited by METH. Our data also indicated that when ICS combated METH-induced neurotoxicity, it was accompanied by partial correction of the abnormal Kelch 2 like ECH2 associated protein 1 (Keap1)-nuclear factor erythroid-2-related factor 2 (Nrf2) pathway and oxidative stress response. In the presence of ML385, an inhibitor of Nrf2, ICS failed to activate the Nrf2-related protein expression and reduce the oxidative stress response. More importantly, ICS could not attenuate METH-induced dopaminergic neurotoxicity and behavioral damage when the Nrf2 was inhibited, suggesting that the neuroprotective effect of ICS on METH-induced neurotoxicity was dependent on activating the Keap1-Nrf2 pathway. Although further research is needed to dig deeper into the actual molecular targets of ICS, it is undeniable that the current results imply the potential value of ICS to reduce the neurotoxicity of METH abusers.

## 1. Introduction

Methamphetamine (METH), an amphetamine-type stimulant that appears as white transparent irregular crystals, commonly known as “ice,” is rapidly and widely abused across the world due to easy access to raw materials, simple synthetic methods, and low production costs [1]. The *World Drug Report 2020* issued by the United Nations Office on Drugs and Crime pointed out that in the past year, about 27 million people worldwide have used amphetamine-type stimulants including METH. METH is known for its strong

excitability and high potency for addiction, which can lead to repeated withdrawal and relapse. Some researchers defined it as a chronic recurrent disease characterized by compulsive drug taking, inability to control intake, and strong drug cravings [2]. Chronic and long-term METH abuse is bound to cause serious toxic effects on abusers ending with multiple organ and system damages. Especially, the pathological changes of the central nervous system (CNS) result in mental disorders such as psychosis, anxiety, and depression [3, 4] and in cognitive dysfunctions such as impairment of executive function, attention disability, and

working memory loss [2, 5]. Nevertheless, there is still a lack of reliable and effective drugs to prevent and treat METH-induced neurotoxicity.

Dopaminergic neurons are one of the main attacked targets by METH, and its damage caused by METH is similar to the pathological changes of Parkinson's disease (PD). While the mechanism of METH-induced neurotoxicity is not well understood, our previous studies and those of other researchers' works have indicated that involves the regulation of neuronal excitotoxicity, oxidative stress, neuroinflammation, apoptosis, and autophagy [6–11]. Among these molecular and cellular processes, oxidative stress seems to be a bridge connecting neuroinflammation, apoptosis, and autophagy [4, 12, 13]. When oxidative stress occurs, the endogenous antioxidant system is also activated, thereby inhibiting the injury from the oxidative stress and keeping the body in a balanced state. The pathway involving Kelch 2 like ECH2 associated protein 1 (Keap1) and nuclear factor erythroid-2-related factor 2 (Nrf2) is crucial in the endogenous antioxidant system. Nrf2 is a redox-sensitive transcription factor containing the basic structure of the leucine zipper [14]. Under physiological conditions, Nrf2 mainly concentrates in the cytoplasm and forms a complex with Keap1, which could mediate the degradation of Nrf2 through the ubiquitin-proteasome system [14, 15]. When reactive oxygen species (ROS) or other substances stimulate, Nrf2 will dissociate from Keap1 and enter the nucleus, where it interacts with the antioxidant-response element and activates the expression of antioxidant enzymes such as heme oxygenase 1 (HO-1) and NAD(P)H:quinone oxidoreductase 1 (NQO-1) [14, 15]. However, when the damage is severe enough to exceed the regulatory range, the Keap1-Nrf2 pathway will also be affected and lead to a vicious circle of oxidative stress. Recent studies have confirmed that the Keap1-Nrf2 pathway dysfunction plays an important role in METH-induced neurotoxicity [16–19].

Icariside II (ICS), a type of flavonoid, is one of the main active ingredients of the traditional Chinese medicine *Epimedium* [20]. Extensive data have shown that ICS could exhibit a variety of biological and pharmacological properties, including anti-inflammatory [21, 22], antioxidant [23, 24], and anti-cancer [20, 25] activities. Recent studies have also found that ICS has a protective effect against CNS damage. For example, ICS could attenuate lipopolysaccharide-induced amyloid production and inflammation in astrocytes [21] and suppress oxygen-glucose deprivation/reperfusion- (OGD/R-) induced hippocampal neuronal death [26]. However, there are no research reports on whether ICS could protect against METH-induced neurotoxicity. And if it does so, the relevant molecular mechanisms are worthy of further study.

To verify this hypothesis, we observed the intervention effect of ICS and investigated the potential influence of the Keap1-Nrf2 pathway in a chronic METH-abuse mouse model that developed CNS injury.

## 2. Materials and Methods

**2.1. Reagents.** METH (purity  $\geq 99.1\%$ ) was obtained from the National Institute for the Control of Pharmaceutical

and Biological Products (Beijing, China). ICS (Figure 1(a)) was purchased from the ZZBIO Co., Ltd. (Shanghai, China), and ML385 was purchased from the Macklin Biochemical Co., Ltd. (Shanghai, China). The antibodies used in this study were TH (AB152, Millipore, Germany), DAT (bs-1714R, Bioss, China),  $\alpha$ -syn (A7215, Abclonal, China), GFAP (16825-1-AP, Proteintech, China), Iba1 (ab220815, Abcam, USA), Keap1 (60027-1-Ig, Proteintech, China), Nrf2 (66504-1-Ig, Proteintech, China), HO-1 (70081S, CST, USA), NQO1 (ab80588, Abcam, USA),  $\beta$ -actin (bs-0061R, Bioss, China), and corresponding secondary antibodies (BL003A and BL001A, Biosharp, China).

**2.2. Animal Treatments.** Male C57BL/6J mice (20–22 g, 8 weeks old) were purchased from the Laboratory Animal Center of Southern Medical University (Guangzhou, China) and housed in a standard animal room with temperature ( $22 \pm 2^\circ\text{C}$ ), humidity ( $55 \pm 5\%$ ), light cycles (12 h light and 12 h dark), and free access to food and water. All experiments were approved by the Animal Care and Use Committee of Southern Medical University (No. L2017208) and were performed according to ethical standards described in the NIH guidelines. The chronic METH-abuse mice model was established according to the 14-day administration schedule (Table 1), which was determined based on our previous studies [8, 27, 28]. And 10 mg/kg or 30 mg/kg of ICS was administered orally to investigate the intervention effect of ICS on METH-induced neurotoxicity by referring to an earlier study [29]. As shown in Figure 1(b), the animal experiments were divided into two phases.

In the first phase, the mice were randomly divided into five groups (16 mice per group):

- (1) Control: saline (orally, once a day for four weeks)+saline (saline in place of METH, intraperitoneal injection, according to the 14-day dosing schedule)
- (2) ICS<sub>H</sub>: 30 mg/kg of ICS (orally, once a day for four weeks)+saline (saline in place of METH, intraperitoneal injection, according to the 14-day dosing schedule)
- (3) METH: saline (orally, once a day for four weeks)+METH (intraperitoneal injection, according to the 14-day dosing schedule)
- (4) METH+ICS<sub>L</sub>: 10 mg/kg of ICS (orally, once a day for four weeks)+METH (intraperitoneal injection, according to the 14-day dosing schedule)
- (5) METH+ICS<sub>H</sub>: 30 mg/kg of ICS (orally, once a day for four weeks)+METH (intraperitoneal injection, according to the 14-day dosing schedule)

In the second phase, the mice were randomly divided into six groups (16 mice per group):

- (1) Control: saline (intraperitoneal injection, once a week for four weeks)+saline (orally, once a day for four weeks)+saline (intraperitoneal injection, according to the 14-day dosing schedule, but replace METH with saline)

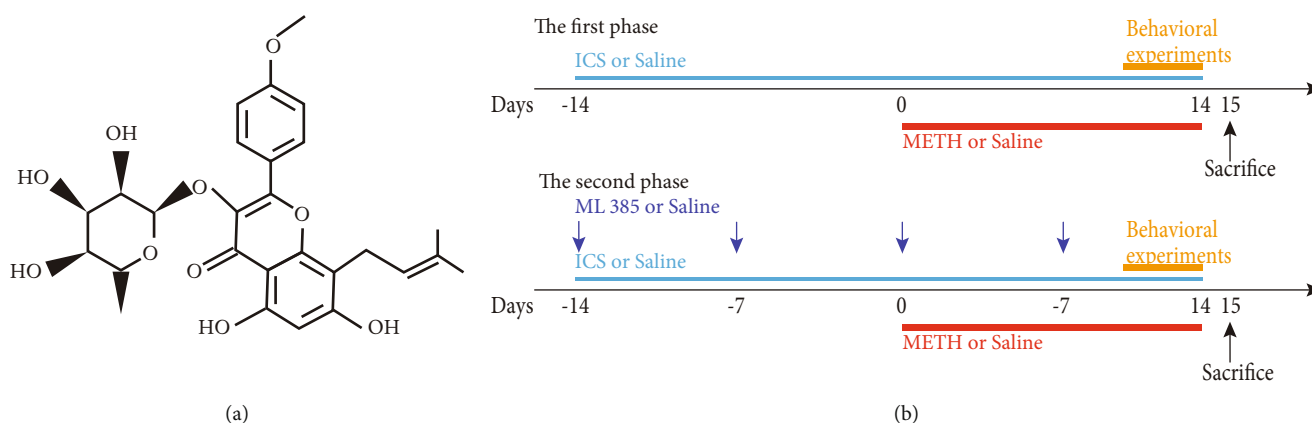


FIGURE 1: (a) Molecular structure of ICS. (b) Experimental protocol.

TABLE 1: The METH (mg/kg) administration schedule.

Day	1	2	3	4	5	6	7	8	9	10	11	12	13	14
8:00	1.0	1.0	1.0	1.0	1.5	1.5	2.0	2.0	2.5	3.0	3.5	4.0	4.5	5.0
10:00				1.0	1.5	1.5	2.0	2.0	2.5	3.0	3.5	4.0	4.5	5.0
12:00				1.0	1.5	1.5	2.0	2.0	2.5	3.0	3.5	4.0	4.5	5.0
14:00		1.0	1.0	1.0	1.5	1.5	2.0	2.0	2.5	3.0	3.5	4.0	4.5	5.0

- (2) METH: saline (intraperitoneal injection, once a week for four weeks)+saline (orally, once a day for four weeks)+METH (intraperitoneal injection, according to the 14-day dosing schedule)
- (3) METH+ICS<sub>H</sub>: saline (intraperitoneal injection, once a week for four weeks)+30 mg/kg of ICS (orally, once a day for four weeks)+METH (intraperitoneal injection, according to the 14-day dosing schedule)
- (4) ML385: 30 mg/kg of ML385 (intraperitoneal injection, once a week for four weeks)+saline (orally, once a day for four weeks)+saline (intraperitoneal injection, according to the 14-day dosing schedule, but replace METH with saline)
- (5) METH+ML385: 30 mg/kg of ML385 (intraperitoneal injection, once a week for four weeks)+saline (orally, once a day for four weeks)+METH (intraperitoneal injection, according to the 14-day dosing schedule)
- (6) METH+ICS<sub>H</sub>+ML385: 30 mg/kg of ML385 (intraperitoneal injection, once a week for four weeks)+30 mg/kg of ICS (orally, once a day for four weeks)+METH (intraperitoneal injection, according to the 14-day dosing schedule)

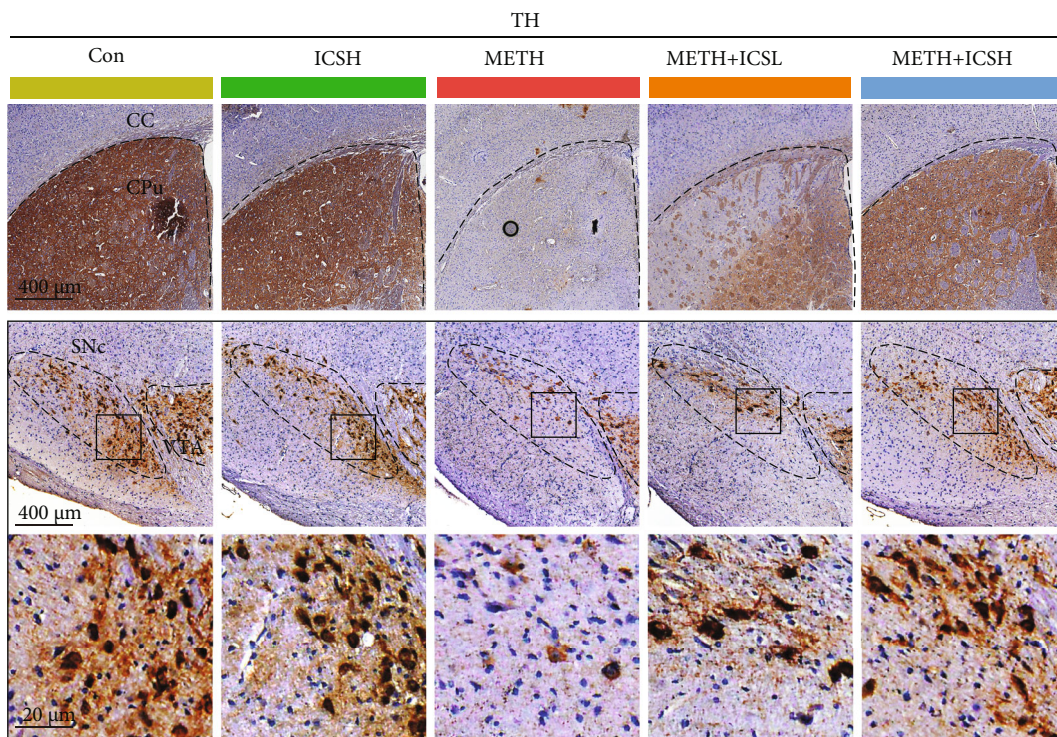
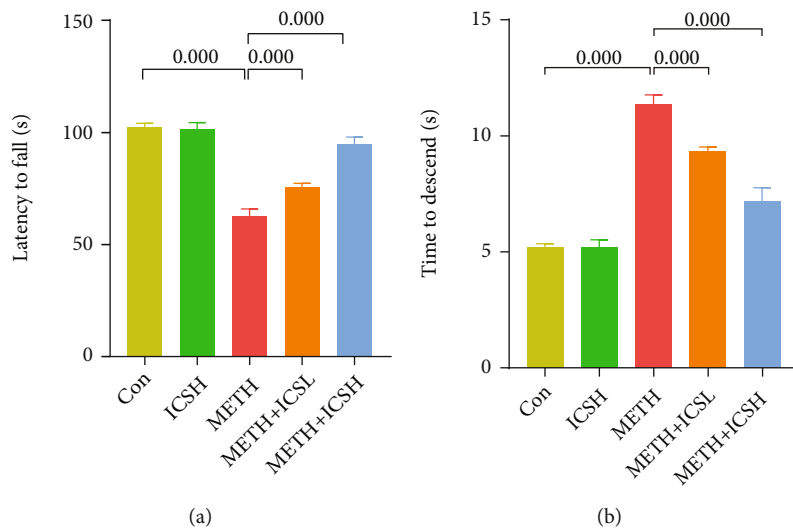
All mice were euthanized 24 h after behavioral tests and the brains were harvested for further analysis.

**2.3. Behavioral Tests.** For pole test, the pole (length: 75 cm and diameter: 1.5 cm) was placed on the ground vertically. The mice were placed near the top (5 cm from the top) of the pole facing upwards. The total time taken to reach the bottom of the pole was recorded. For rotarod test, the mice

were placed on a wheel and the time of latency to fall was recorded. The speed of the rotarod started from 4 to 40 rpm, and the acceleration rate was 20 rpm/min. Each test was conducted 3 times after 2 days of training. For gait test, the apparatus is a U-shaped runway (length: 60 cm, width: 10 cm, and height: 10 cm). The paper was placed on the bottom of the runway. The mice were allowed to run from one side to the other side. Before the test, the mice were trained for 2 days. In the test trials, the mice forepaws were painted red and hindpaws black using nontoxic dyes. The mice were placed on the runway, and the footprints were acquired. Stride length was measured between each of the forepaw and hindpaw footprints.

**2.4. Immunohistochemical (IHC) Staining.** The mice brains were fixed in 4% paraformaldehyde and then dehydrated in gradient alcohol. After being embedded in paraffin, the brain tissues were sectioned at the coronal plane using a microtome (RM 2235, Leica, Germany). Sections containing substantia nigra (SNc) and caudate and putamen (CPu) areas were subjected to IHC staining. Briefly, the sections were immersed into sodium citrate solution for antigen recovery. The sections were then incubated with the anti-TH antibody for 12 h at 4°C. Thereafter, the targeted proteins were visualized by 3'3-diaminobenzidine Kits (CW2069, CW Bio, China). The images were captured by a microscope (CX23, Olympus, Japan).

**2.5. Nissl Staining.** The Nissl staining was performed by using a Nissl staining kit (G 1434, Solarbio Life Sciences, China). The paraffin-embedded brains were sectioned using a microtome (RM 2235, Leica, Germany). The sections were dewaxed, rehydrated, and then immersed into methylene



(c)

FIGURE 2: Continued.

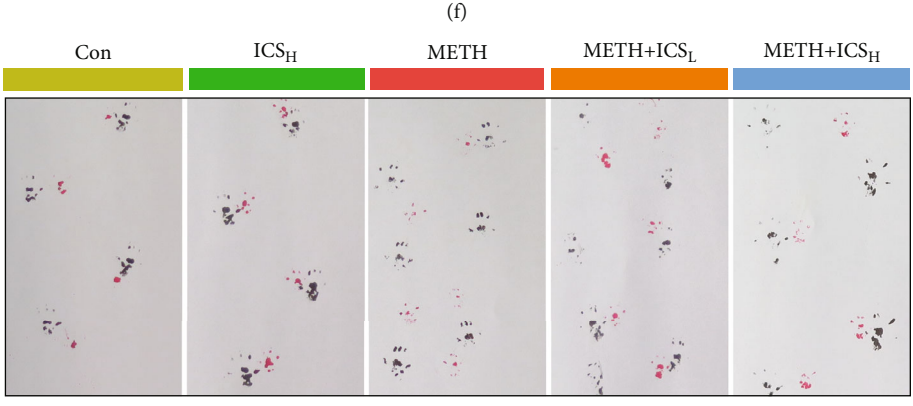
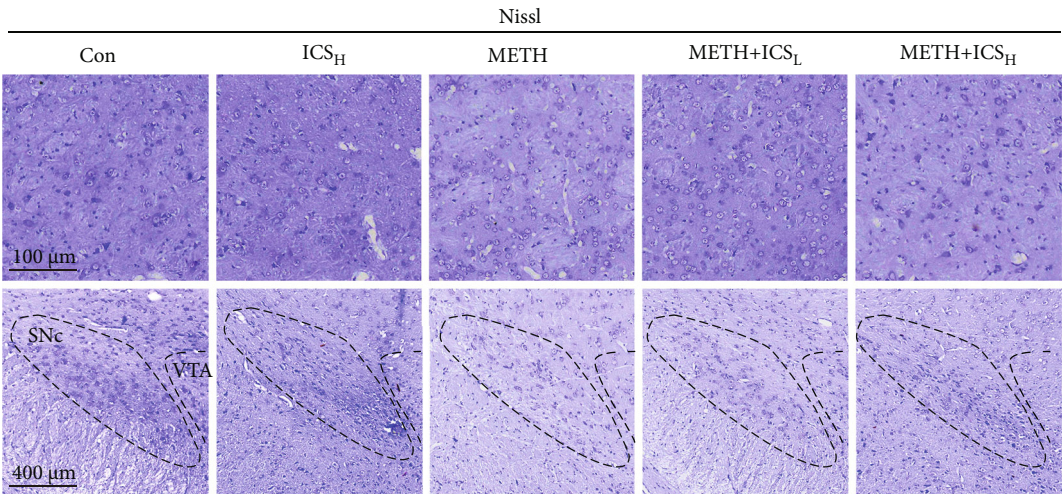
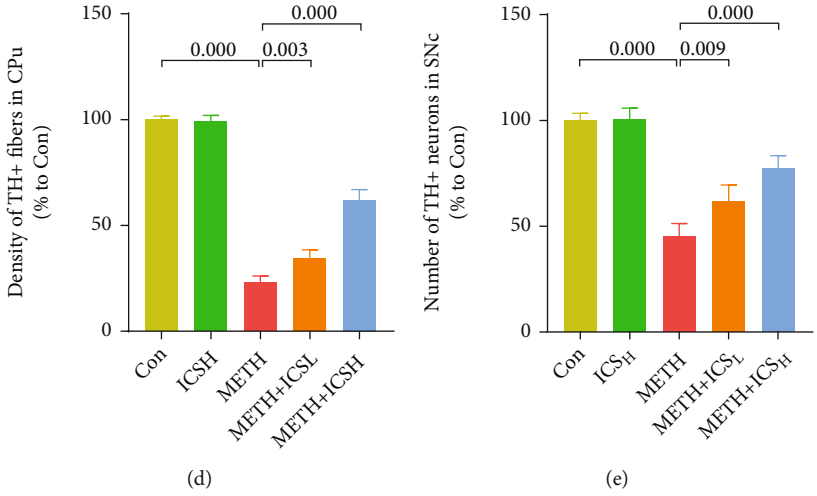


FIGURE 2: Continued.

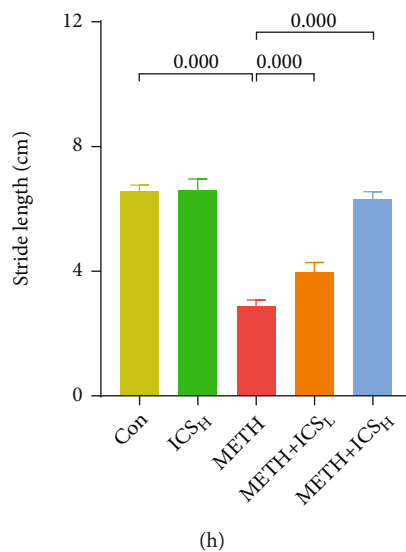


FIGURE 2: ICS attenuated neuronal loss and improved behavioral performance in chronic METH abuse mice model. (a) The fall latency was determined by rotarod test. (b) The descend time was determined by pole test. (c) Representative micrographs of TH staining in CPu and SNc (scale bar = 400  $\mu\text{m}$  for the low-magnification images and 20  $\mu\text{m}$  for the high-magnification images). (d) Quantification of TH-positive fibers in CPu. (e) Quantification of TH-positive neurons in SNc. (f) Representative micrographs of Nissl staining in CPu (scale bar = 100  $\mu\text{m}$ ) and SNc (scale bar = 400  $\mu\text{m}$ ). (g) Representative footprint patterns from gait test. (h) Analysis of stride length.  $n = 6$  per group for behavioral tests and  $n = 4$  per group for IHC staining and Nissl staining.

blue staining solution for 10 min. After being immersed in the Nissl differentiation solution for 3 s, the sections were rinsed in water and then dehydrated in pure alcohol. A microscope (CX23, Olympus, Japan) was used to obtain images.

**2.6. Western Blot.** The striatum tissues were homogenized in a protein extraction buffer (Beyotime, China) containing protease and phosphatase inhibitors. After centrifugation (12,000 g, 10 min, 4°C), the protein supernatant was collected and measured with a Protein Quantitative Analysis kit (Biocolors, China). The protein loading buffer was added to the supernatant and boiled at 99°C for 10 min. The samples were separated by SDS-PAGE and transferred to 0.45  $\mu\text{m}$  PVDF membranes (Millipore, USA). After blocking in 5% nonfat milk at room temperature for 1 h, the membranes were then incubated overnight at 4°C with the following primary antibodies: TH, DAT,  $\alpha$ -syn, GFAP, Iba1, Keap1, Nrf2, HO-1, NQO1, and  $\beta$ -actin. The dilution ratios for all antibodies were 1:1000. In the next day, the membranes were incubated with the secondary antibody at room temperature for 1 h, and electrochemiluminescence reagents (Bio-Rad, USA) were added to visualize the immunoblot signals. ImageJ software was used to measure band densities.

**2.7. Measurement of Dopamine (DA) Levels.** The striatum was homogenized in an ice-cold buffer containing 0.01 mM of  $\text{HClO}_4$  and 0.01% EDTA. After centrifugation (20,000 g, 20 min, 4°C), DA levels in the supernatant were assessed by using HPLC.

**2.8. Dendritic Spine Analysis.** Brain tissues were fixed in 4% paraformaldehyde for 6 h. The sections (thick in 200  $\mu\text{m}$ )

were acquired using a vibratome (VT1200S, Leica, Germany). Lucifer yellow dye (L453, MA, USA) was loaded in a pipette for injection into the neurons of CPu. The dye was injected into a neuron for 25 min with a 1-3 nA current. The pipettes were removed when the dendritic branches were visualized. Dendritic images were acquired under a confocal microscope (LSM 880, Zeiss Carl, Germany). The numbers of dendritic spines were analyzed using ImageJ software.

**2.9. Measurement of ROS, MDA, SOD, and GSH Levels.** The ROS levels in striatum were measured by using an ELISA assay kit (MEIMIAN, China). Briefly, the striatum was homogenized in ice-cold saline, and the supernatant was collected after centrifugation (3500 rpm, 15 min, 4°C). After a series of incubation and washing, a microplate reader (BioTek, USA) was used to detect the absorbance at 450 nm, which can be used to calculate the ROS levels. The MDA, SOD, and GSH levels in striatum were measured by using commercial kits (Nanjing Jiancheng Bioengineering Institute, China) according to the manufacturer's instructions. The samples from striatum were measured with a microplate reader (BioTek, USA) at 532, 450, and 405 nm for further calculating MDA, SOD, and GSH levels, respectively.

**2.10. Data Analysis.** All experiments were repeated at least four times and data were represented as the mean  $\pm$  SD. One-way ANOVA (followed by the Tukey HSD and LSD tests) was performed by using SPSS 21 (IBM SPSS, Chicago, United States), and  $p < 0.05$  was considered statistically significant.

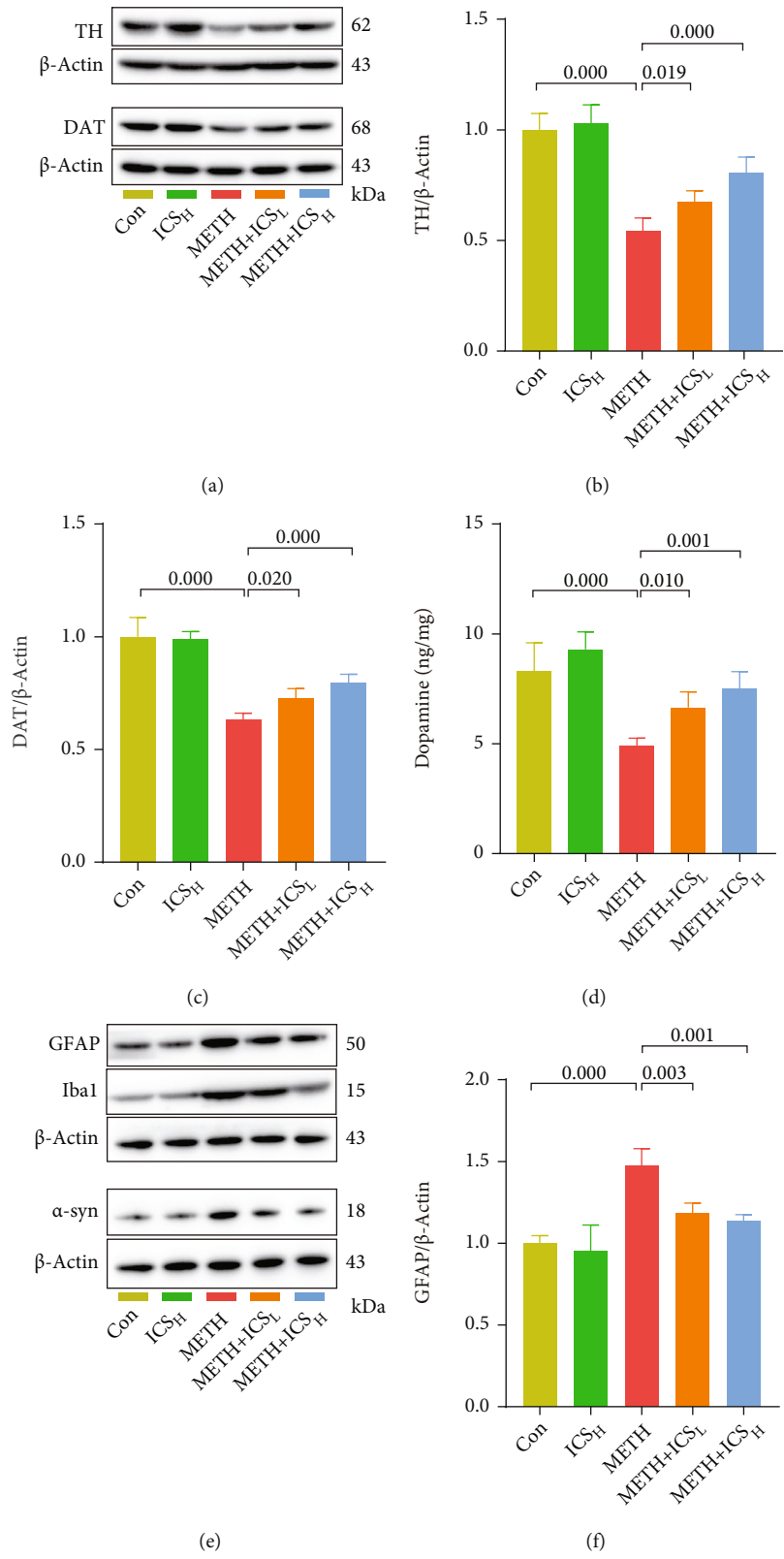


FIGURE 3: Continued.



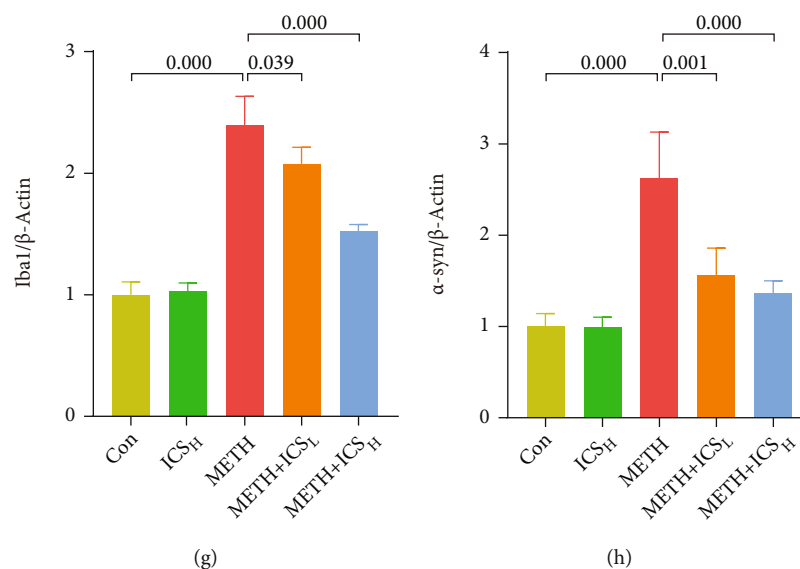


FIGURE 3: ICS increased TH, DAT, and DA levels and decreased GFAP, Iba1, and  $\alpha$ -syn levels in striatum of METH mice model. Figures 3(a)–3(c) Representative WB images and quantification of TH and DAT. (d) Measurement of DA levels by using HPLC. Figures 3(e)–3(h) Representative WB images and quantification of GFAP, Iba1, and  $\alpha$ -syn.  $n = 4$  per group.

### 3. Results

**3.1. ICS Attenuated Neuronal Loss and Improved Behavioral Performance in Chronic METH-Abuse Mice Model.** Rotarod test, pole test, and gait test revealed that chronic METH abuse induced the impairment of motor coordination and balance, while both low (10 mg/kg) and high (30 mg/kg) dosages of ICS could improve these impaired behavioral performances elicited by METH (Figures 2(a), 2(b), 2(g), and 2(h)). We next performed IHC staining of TH to detect the dopaminergic neuron number in SNc and CPu of each group of mice (Figure 2(c)). Quantitative analysis of TH staining showed that both 10 mg/kg and 30 mg/kg of ICS could attenuate the loss of dopaminergic neurons in METH-treated mice (Figures 2(d) and 2(e)). Similarly, the numbers of Nissl-positive cells were increased in SNc and CPU of ICS+METH mice compared to METH mice (Figure 2(f)).

**3.2. ICS Increased TH, DAT, and DA Levels and Decreased GFAP, Iba1, and  $\alpha$ -Syn Levels in Striatum of METH Mice Model.** To further verify the protective effects of ICS on dopaminergic neurons decreased by METH, WB and HPLC analyses were used to detect DAT, TH, and DA levels in striatum of each group of mice, respectively. We found that the levels of DAT, TH, and DA remarkably decreased in METH mice compared to control mice. However, treatment with ICS increased TH, DAT, and DA levels reduced by METH (Figures 3(a)–3(d)). Considering that glial activation and high expression of  $\alpha$ -syn are manifestations of METH neurotoxicity, we continued to detect the expression of GFAP, Iba1, and  $\alpha$ -syn in striatum of each group of mice. The WB results suggested that METH-induced high-level expressions of GFAP, Iba1, and  $\alpha$ -syn were suppressed in ICS-received mice (Figures 3(e)–3(h)).

**3.3. ICS Alleviated the Abnormalities of Dendritic Spines of Neurons in CPu of METH Mice Model.** We next conducted morphology analysis for dendritic spines of neurons in CPu area. Compared with the control mice, METH-treated mice exhibited decreased numbers of total dendritic spines, mushroom-type dendritic spines, and stubby-type dendritic spines in neurons. Both low and high dosage ICS intervention alleviated the abnormalities of dendritic spines of neurons in CPu of METH mice model (Figures 4(a)–4(d)). In addition, we found that there was no difference in the numbers of thin-type dendritic spines of neurons between each group of mice (Figure 4(e)).

**3.4. ICS Activated the Keap1-Nrf2 Pathway and Reduced Oxidative Stress in Striatum of METH Mice Model.** Given the crucial role of oxidative stress in METH neurotoxicity, we then investigated whether the Keap1-Nrf2 pathway and its mediated antioxidative stress were countable for the neuroprotective ability of ICS. Here, we found that METH inhibited the Keap1-Nrf2 pathway and elicited a severe oxidative stress response, which was featured by the upregulation of ROS (Figure 5(a)), MDA (Figure 5(b)), and Keap1 (Figures 5(h) and 5(i)) levels and by the downregulation of SOD (Figure 5(c)), GSH (Figure 5(d)), Nrf2 (Figures 5(e) and 5(f)), NQO1 (Figures 5(e) and 5(g)), and HO-1 (Figures 5(h) and 5(j)) levels in striatum of METH mice, whereas the decrease or increase of these indicators was all recovered to some extent in both ICS<sub>L</sub>+METH mice and ICS<sub>H</sub>+METH mice compared to METH mice (Figures 5(a)–5(j)). These data implied that ICS might protect against METH-induced neurotoxicity by activating the Keap1-Nrf2 pathway and reducing oxidative stress.

**3.5. In the Presence of ML385, an Inhibitor of Nrf2, ICS Failed to Activate the Nrf2-Related Protein Expression and Reduce Oxidative Stress in Striatum of METH Mice Model.**

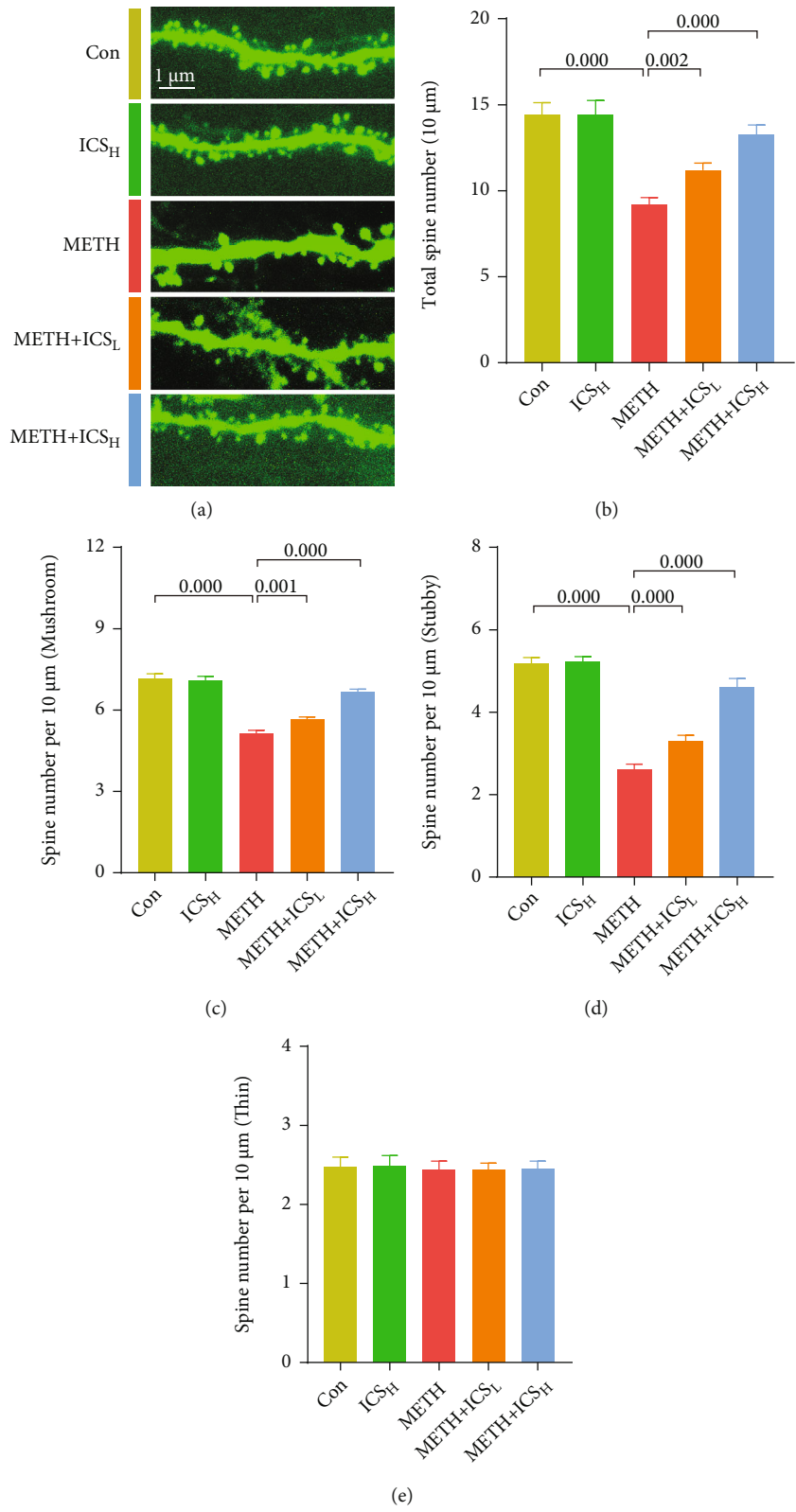


FIGURE 4: ICS alleviated the abnormalities of dendritic spines of neurons in CPu of METH mice model. Figure 4(a) Representative images of dendritic spines (scale bar = 1 μm). Figures 4(b)–4(e) Analysis of the numbers of total dendritic spines, mushroom-type dendritic spines, stubby-type dendritic spines, and thin-type dendritic spines. *n* = 4 per group.

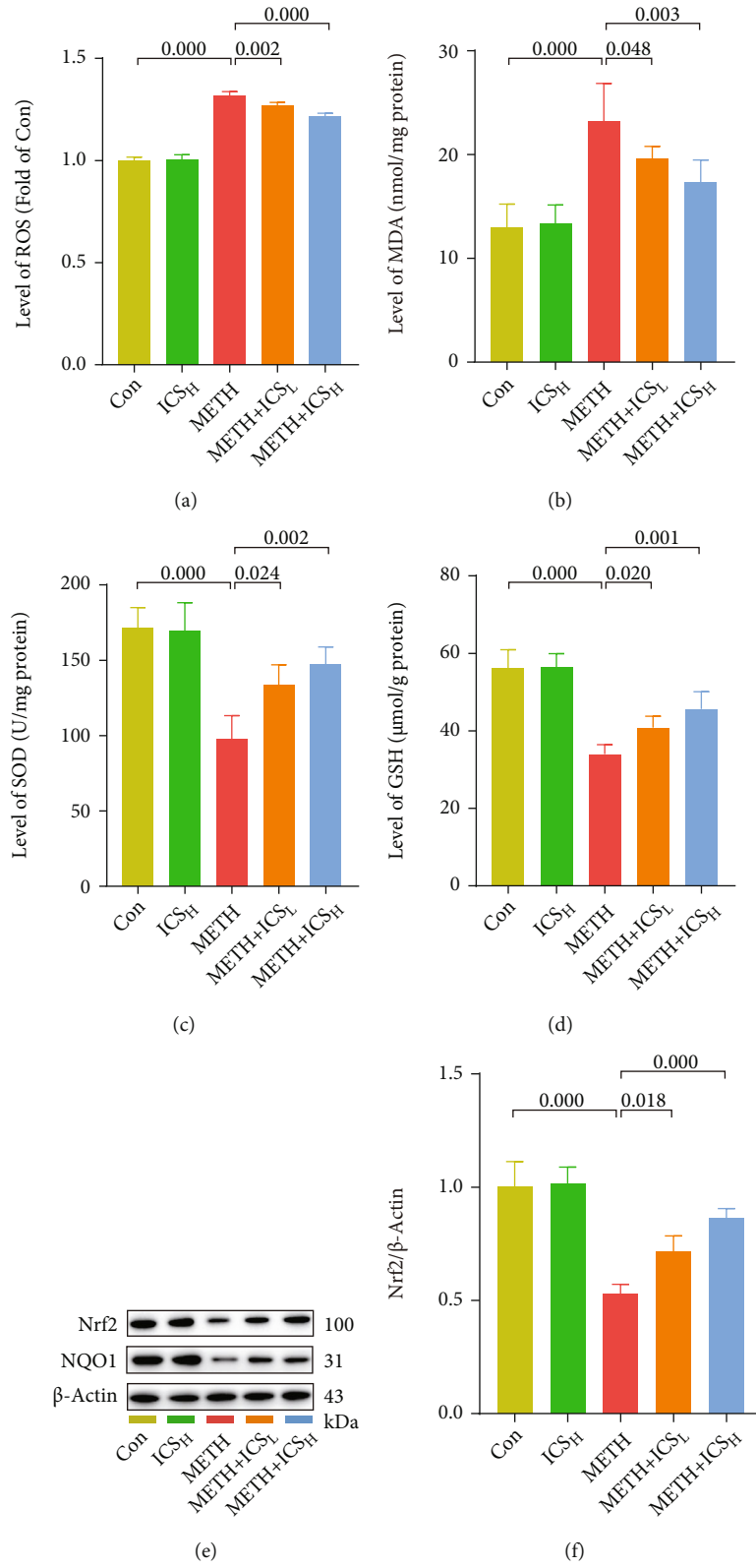


FIGURE 5: Continued.

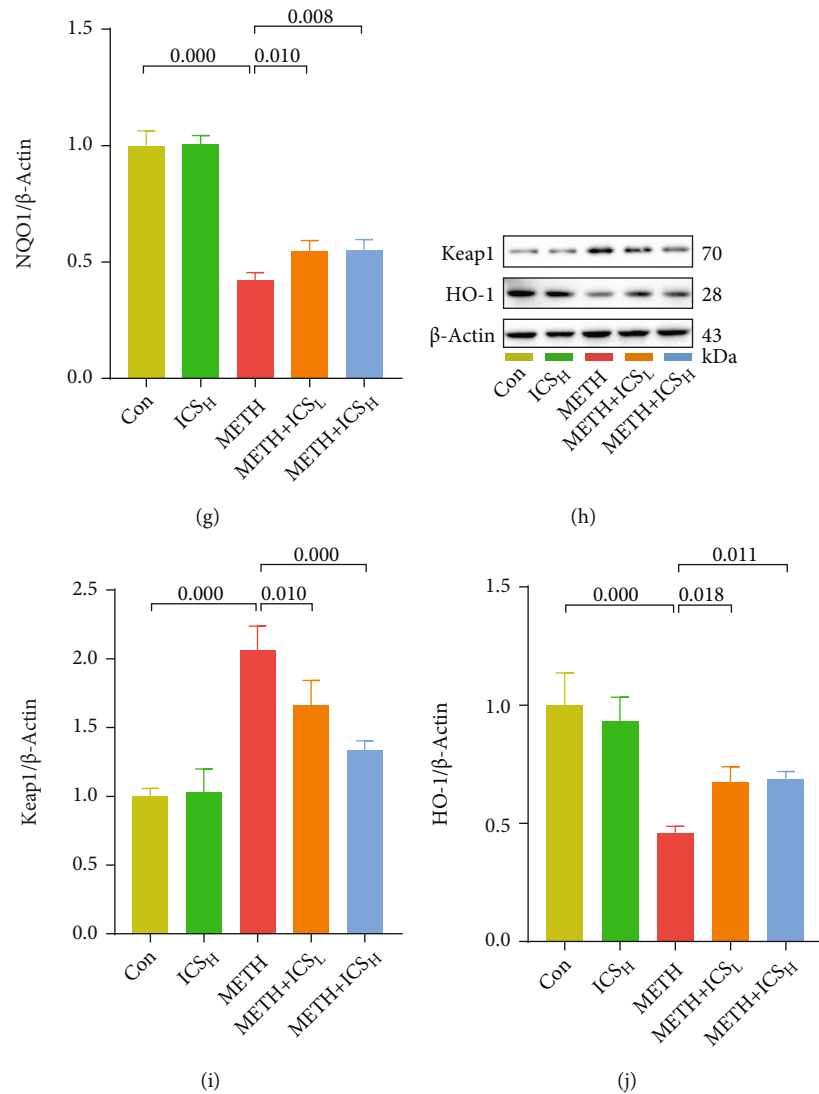


FIGURE 5: ICS activated the Keap1-Nrf2 pathway and reduced oxidative stress in striatum of METH mice model. Figure 5(a) The ROS levels were measured by using an Elisa kit. Figures 5(b)–5(d) The MDA, SOD, and GSH levels were measured by using commercial kits. Figures 5(e)–5(j) Representative WB images and quantification of Nrf2, NQO1, Keap1, and HO-1.  $n = 4$  per group.

ML385, an inhibitor of Nrf2 [30], was used to further confirm whether the Keap1-Nrf2 pathway and its mediated antioxidative stress were involved in the protective effect of ICS on METH neurotoxicity. First, we focused on the effect of ML385, ICS, and METH on the Keap1-Nrf2 pathway and oxidative stress response. Consistent with the first phase of the experiment, we found that ICS activated the Keap1-Nrf2 pathway and reduced oxidative stress in striatum of METH mice (Figures 6(a)–6(j)). Besides, the mice treated with ML385 alone exhibited lower levels of Nrf2, NQO1, HO-1, GSH, and SOD but higher levels of ROS and MDA than the control mice. The changes of these indicators were more obvious in ML385+METH mice compared to METH alone mice (Figures 6(a)–6(h) and 6(j)). In addition, we found that the regulation of Keap1 by ICS was not affected in the presence of ML385 (Figures 6(h) and 6(i)). Nevertheless, after inhibiting Nrf2 by ML385, ICS failed to activate

the Nrf2-related protein expression and to reduce oxidative stress in striatum of METH mice model (Figures 6(a)–6(h) and 6(j)).

3.6. When Nrf2 Was Suppressed, ICS Could Not Attenuate Dopaminergic Neurotoxicity, nor Improve Impaired Behavioral Performance in Chronic METH Abuse Mice Model. Next, we will determine if ICS, when Nrf2 was suppressed, could still attenuate dopaminergic neurotoxicity and improve impaired behavioral performance in chronic METH abuse mice model. Compared with the METH alone group, the indicators that reflected the damage to dopaminergic neurons and motor coordination and balance became more serious in METH+ML385 group. In behavioral performance, the fall latency in rotarod test was lower (Figure 7(a)), the descend time in pole test was longer (Figure 7(b)), and the stride length in gait test was shorter

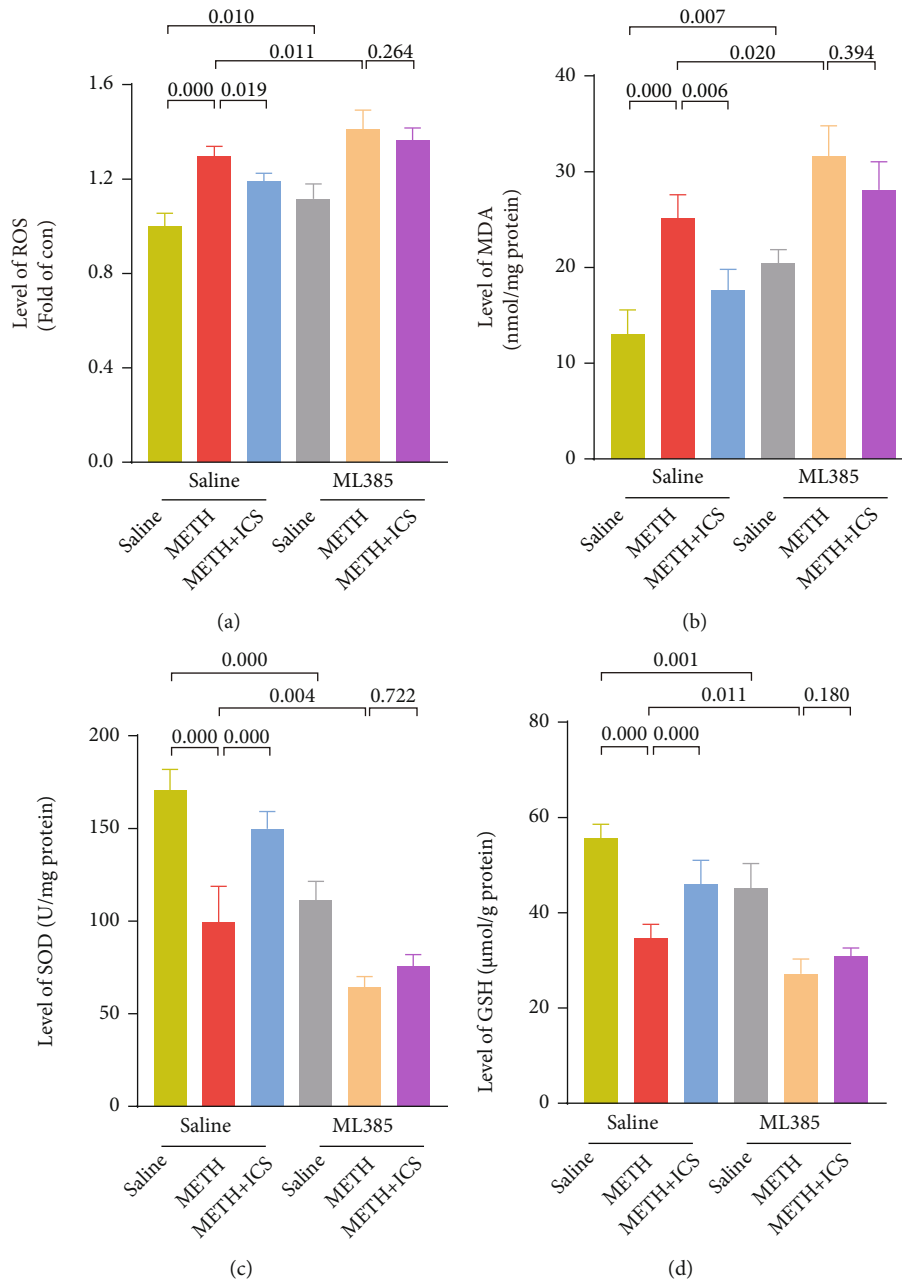
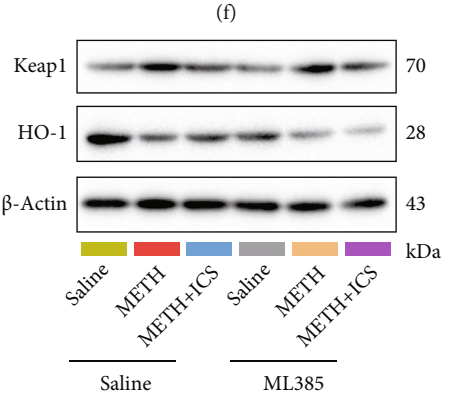
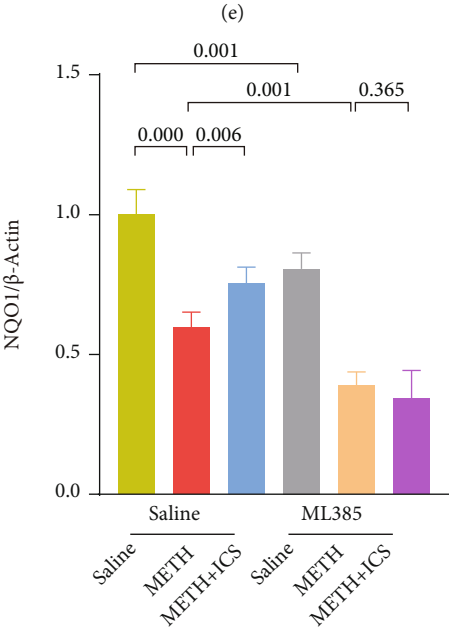
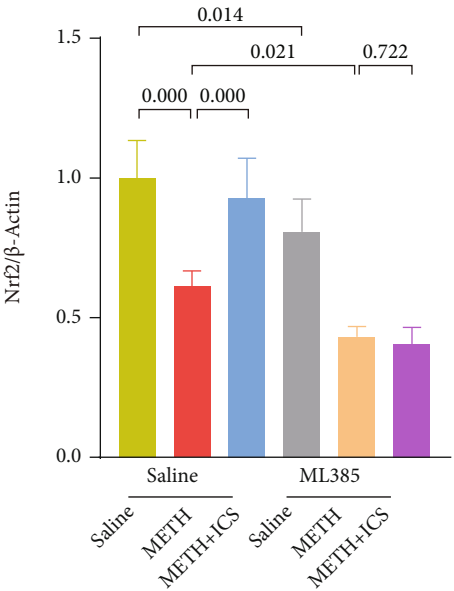
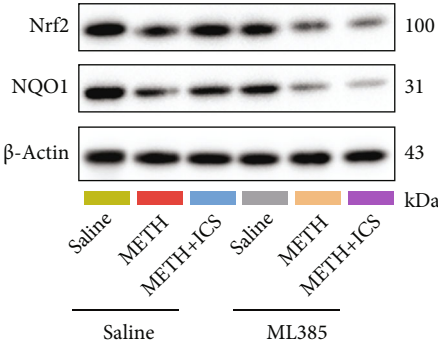


FIGURE 6: Continued.



(h)

(g)

FIGURE 6: Continued.

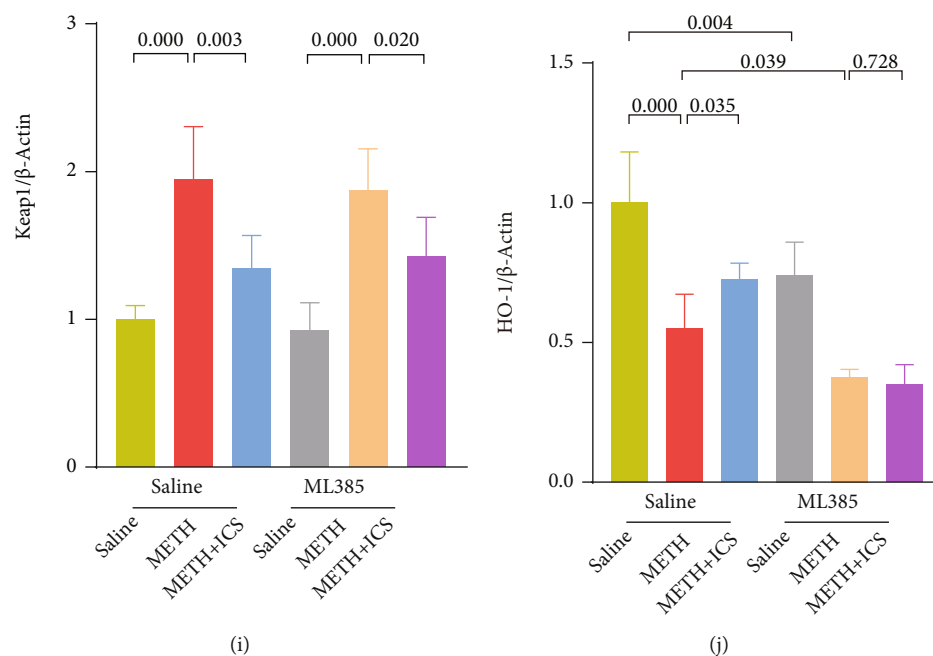


FIGURE 6: In the presence of ML385, an inhibitor of Nrf2, ICS failed to activate the Nrf2-related protein expression and to reduce oxidative stress in striatum of METH mice model. Figure 1(a) The ROS levels were measured by using an Elisa kit. Figures 6(b)–6(d) The MDA, SOD, and GSH levels were measured by using commercial kits. Figures 6(e)–6(j) Representative WB images and quantification of Nrf2, NQO1, Keap1, and HO-1.  $n = 4$  per group.

(Figures 7(h) and 7(g)). In morphological and molecular studies, the numbers of TH-positive neurons and Nissl-positive neurons were lower in SNc and CPU (Figures 7(c)–7(f)). The TH, DAT, and DA levels were lower (Figures 8(a)–8(d)), and the GFAP, Iba1, and  $\alpha$ -syn levels were higher (Figures 8(a) and 8(e)–8(g)). The decreased numbers of total dendritic spines, mushroom-type dendritic spines, and stubby-type dendritic spines in neurons were also more obvious (Figures 9(a)–9(d)). More importantly, while ICS treatment could alleviate the above-mentioned neurotoxicity and behavioral damage induced by METH, however, when Nrf2 was suppressed, ICS failed to show its neuroprotective effects in chronic METH abuse mice model (Figures 7–9). This suggests that the neuroprotective effect of ICS on METH-induced neurotoxicity was achieved by activating the Keap1-Nrf2 pathway.

#### 4. Discussion

This study showed that METH could trigger neurotoxicity, which was characterized by dopaminergic neurons loss, glial cell activation,  $\alpha$ -syn upregulation, DA depletion, and dendritic spines abnormalities. The neurotoxicity is also accompanied by behavioral impairments (specifically, dysfunction of motor coordination and balance). ICS treatment alleviated the above-mentioned neurotoxicity and behavioral impairments induced by METH. We also found that the neuroprotective effect of ICS on METH-induced neurotoxicity was achieved by activating the Keap1-Nrf2 pathway and decreasing the oxidative stress response.

The toxic effect of METH on dopaminergic neurons is one of its most representative neurotoxic manifestations,

which has been extensively studied. Due to the high lipid solubility, METH can cross the blood-brain barrier (recent studies suggested that METH can destroy it [31]) and enter the brain parenchyma. METH infiltrates the brain further into dopaminergic neurons through the DAT and exerts its toxic effects there. METH initially enhances DA release and inhibits DA reuptake, thereby activating dopaminergic signals in the reward pathway to trigger reward behavior and subsequently drug addiction. However, with the prolonged METH exposure, neurotoxic effects on dopaminergic neurons occur, specifically manifested as the downregulation of TH and DAT levels and DA depletion [10, 32]. Using positron emission tomography imaging, Volkow et al. [33] found that the DAT density in striatum of METH abusers was decreased compared to those of healthy individuals. Previous studies have also found that METH treatment could reduce the expression levels of TH, DAT, and DA in laboratory animals [6, 8, 34, 35]. Consistent with these studies, we duplicated the dopaminergic neurotoxic phenotype in mice after chronic METH exposure. Considering the various pharmacological properties of ICS, we selected it as a candidate to study whether it could reduce the neurotoxicity induced by METH. We have collected evidence showing that ICS could attenuate the loss of dopaminergic neurons and the decrease of DA concentrations in the METH mice model. The neuroprotective effects of ICS have been mentioned in other animal disease models. Xu et al. [26] demonstrated that ICS could mitigate OGD/R-induced primary hippocampal neuron injury. ICS also remarkably ameliorated beta-amyloid ( $A\beta$ ) generation and neuronal degradation in APP/PS1 double transgenic mice [29]. Interestingly, a recent study found that human amniotic mesenchymal

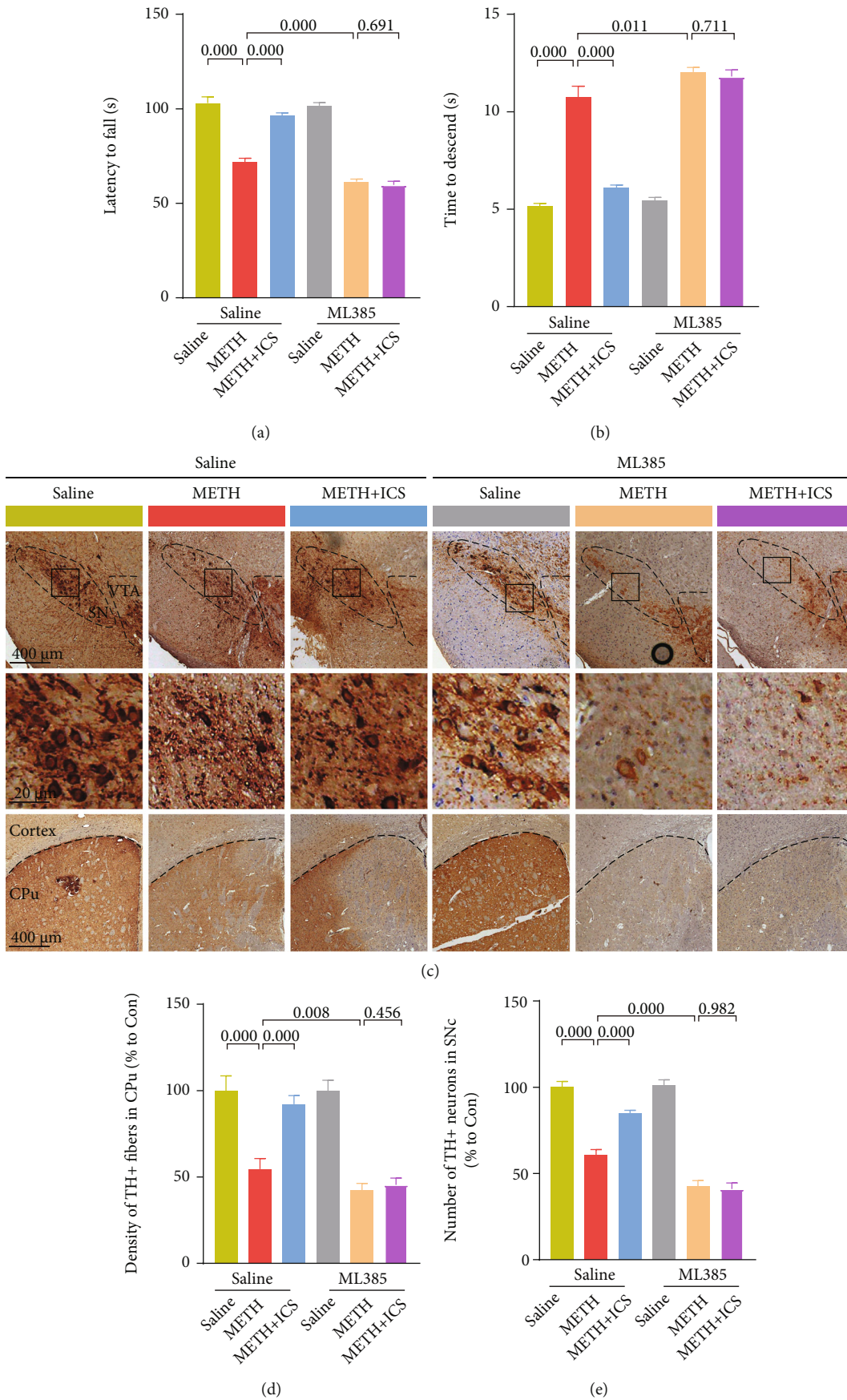
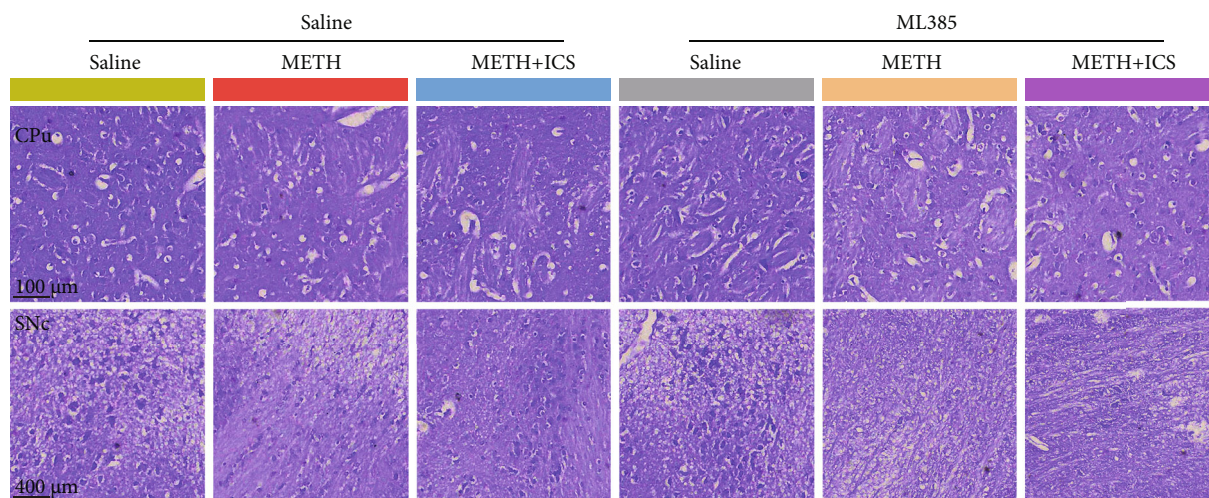
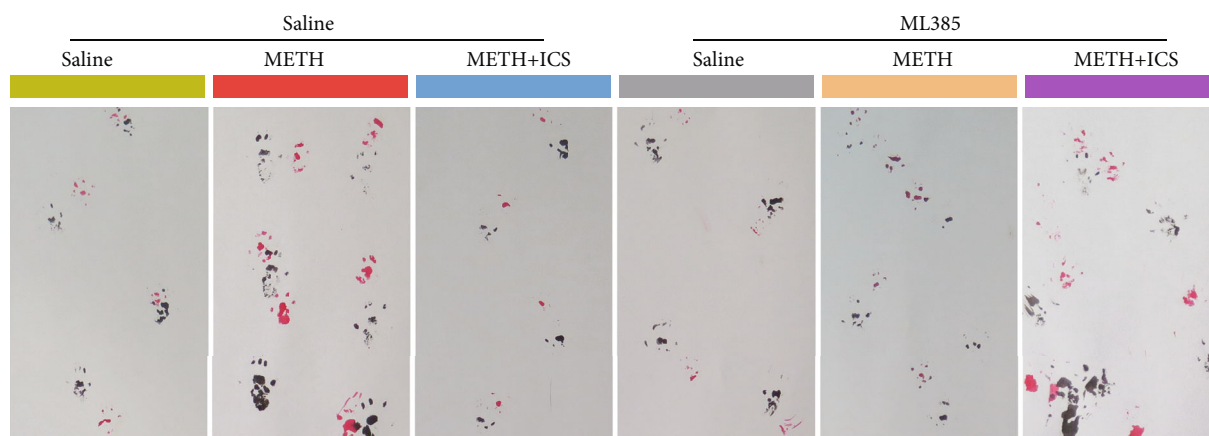


FIGURE 7: Continued.

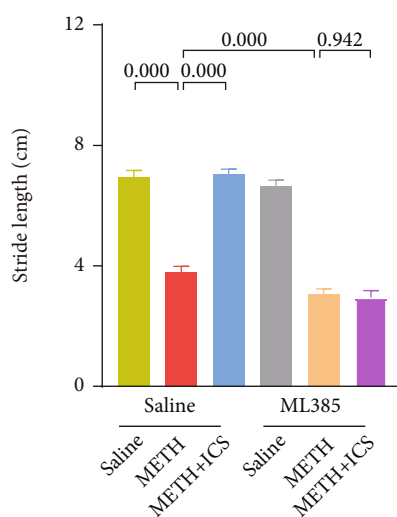




(f)



(g)



(h)

FIGURE 7: ML385 blocked the protective effects of ICS on neuronal loss and behavioral impairment in METH mice model. Figure 7(a) The fall latency was determined by rotarod test. Figure 7(b) The descend time was determined by pole test. Figure 7(c) Representative micrographs of TH staining in CPu and SNc (scale bar = 400  $\mu\text{m}$  for the low-magnification images and 20  $\mu\text{m}$  for the high-magnification images). Figure 7(d) Quantification of TH-positive fibers in CPu. Figure 7(e) Quantification of TH-positive neurons in SNc. Figure 7(f) Representative micrographs of Nissl staining in CPu (scale bar = 100  $\mu\text{m}$ ) and SNc (scale bar = 400  $\mu\text{m}$ ). Figure 7(g) Representative footprint patterns from gait test. Figure 7(h) Analysis of stride length.  $n = 6$  per group for behavioral tests and  $n = 4$  per group for IHC staining and Nissl staining.

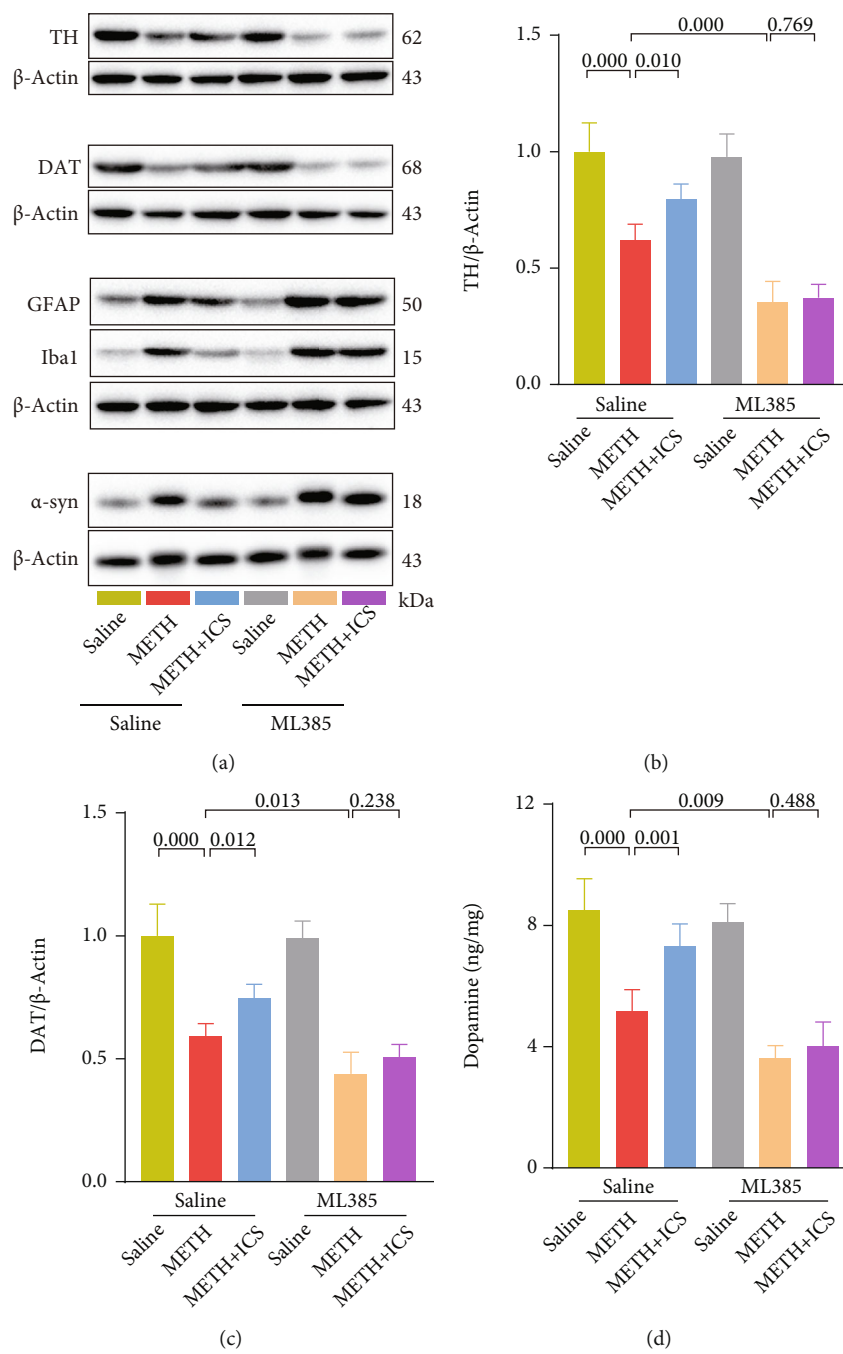


FIGURE 8: Continued.

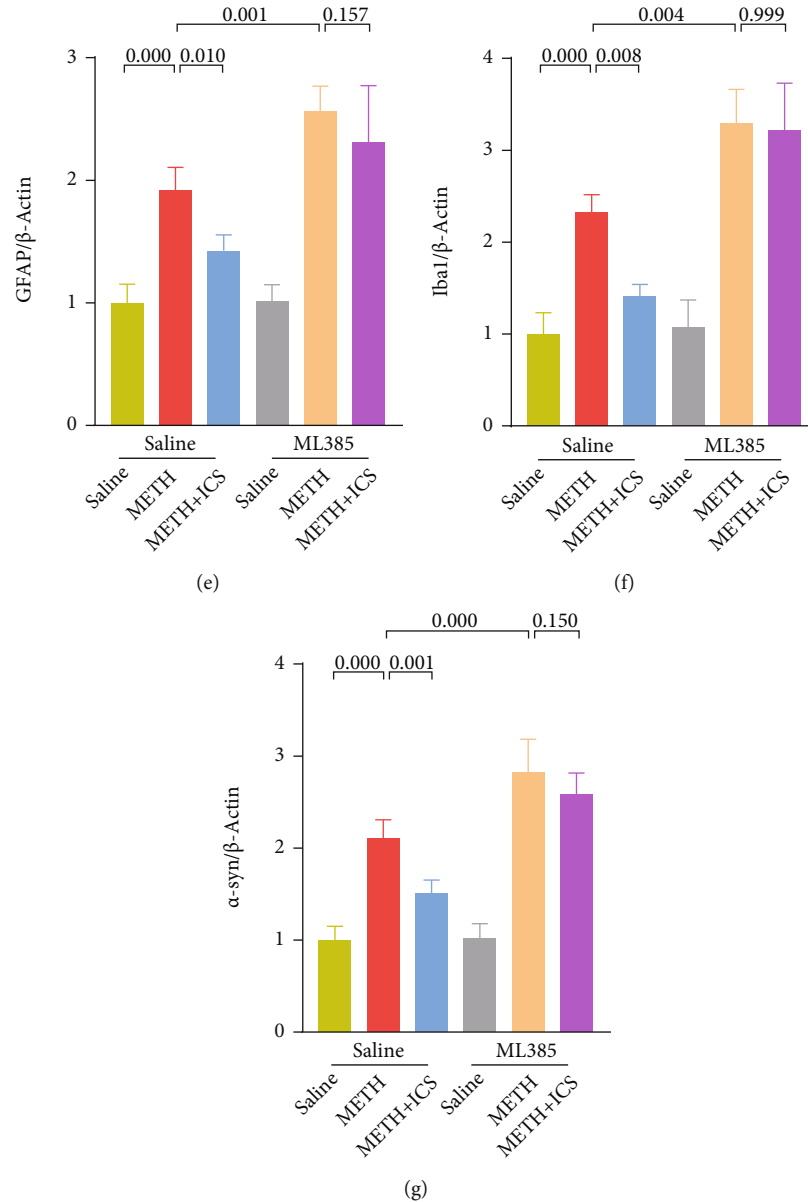


FIGURE 8: Inhibition of Nrf2 eliminated the regulatory effect of ICS on the abnormal expression of TH, DAT, DA, GFAP, Iba1, and  $\alpha$ -syn in striatum of METH mice model. (a–c and e–g) Representative WB images and quantification of TH, DAT, GFAP, Iba1, and  $\alpha$ -syn. (d) Measurement of DA levels by using HPLC.  $n = 4$  per group.

stem cells could differentiate into dopaminergic neuron-like cells under the influence of ICS [36]. Thus, both this study and previous studies suggest the neuroprotective potential of ICS.

METH-induced dopaminergic neuron damage is similar to the pathological changes of PD, which is an increased risk for METH abusers [37]. In this study, a high-level expression of  $\alpha$ -syn was observed in striatum of METH mice model, which was consistent with our previous studies [35, 38, 39]. The abnormalities in the dendritic spines of striatal neurons were observed in PD [40]; therefore, the pathological changes of dendritic spines of neurons in CPU were analyzed after METH exposure. We found that METH caused abnormal dendritic spine morphology and spine number.

We then detected the motor coordination and balance ability of METH-treated mice through pole test, rotarod test, and gait test. Compared with the control mice, mice treated with METH exhibited poorer behavioral performance. The above results further proved that METH could induce PD-like symptoms [35]. Surprisingly, unlike the protective effects of ICS on the Alzheimer’s disease (AD) model [41–44], we found in this study that ICS could alleviate METH-induced high-level expression of  $\alpha$ -syn, dendritic spines abnormalities, and dysfunction of motor coordination and balance.

Oxidative stress plays an essential role in METH-induced neurotoxicity [45], and it always has crosstalk with inflammatory response, apoptosis, autophagy, and other

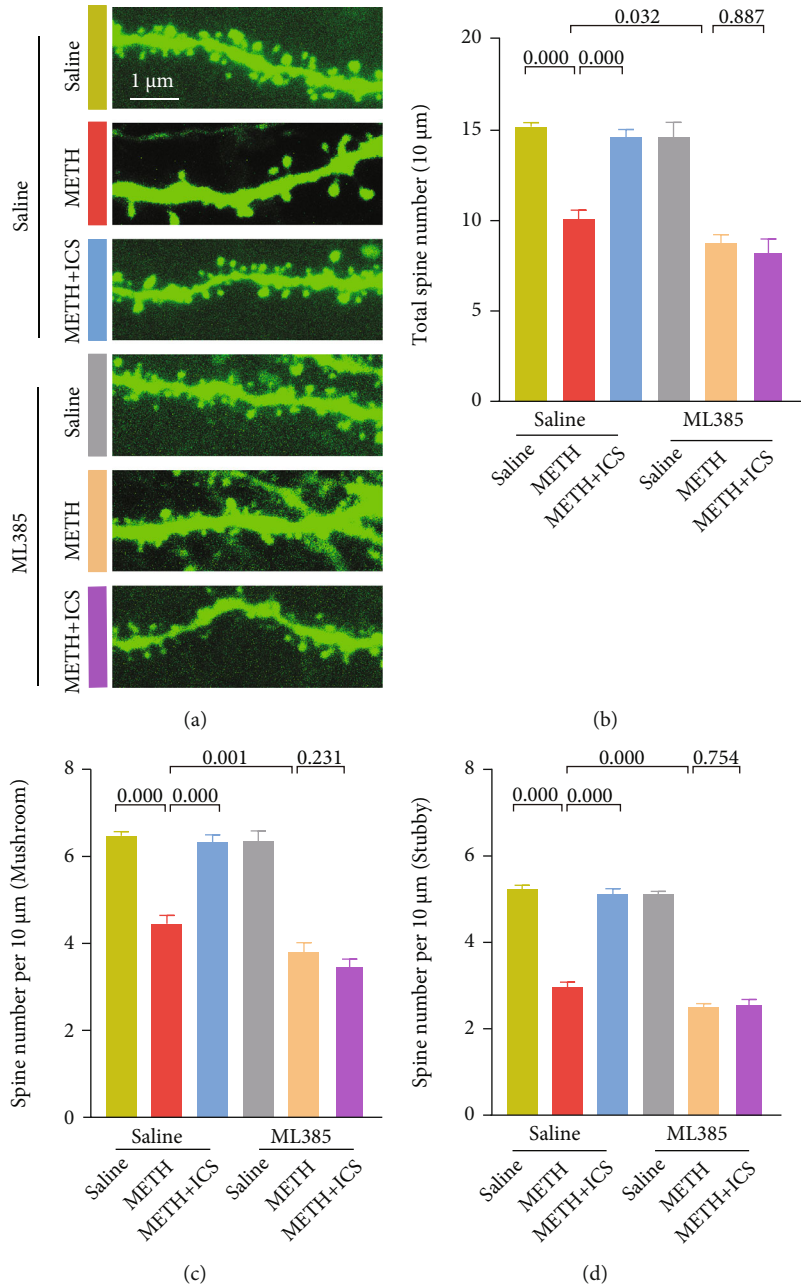
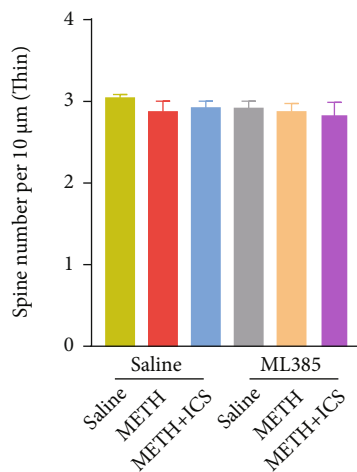


FIGURE 9: Continued.



(e)

FIGURE 9: When Nrf2 was suppressed, ICS could not alleviate the abnormalities of dendritic spines of neurons in CPU of METH mice model. Figure 9(a) Representative images of dendritic spines (scale bar = 1  $\mu\text{m}$ ). Figures 9(b)–9(e) Analysis of the numbers of total dendritic spines, mushroom-type dendritic spines, stubby-type dendritic spines, and thin-type dendritic spines.  $n = 4$  per group.

molecular pathological mechanisms [4, 12, 46]. ROS is a by-product of aerobic metabolism, including superoxide anion, hydroxyl radical, and hydrogen peroxide. Under the dynamic equilibrium between the oxidation system and antioxidant system, excess ROS will be cleared in time. However, when the body's antioxidant system is weakened or ROS is greatly increased, oxidative stress damage will occur. Due to the strong oxidative effect, METH abuse will result in oxidative stress damage. Zeng et al. [46] pointed out that METH augmented intracellular ROS levels and downregulated the level of glutathione peroxidase 1 (GPX1) and SOD1. This severe oxidative stress further induced autophagy and apoptosis in human SH-SY5Y neuroblastoma cells and rat striatum.

Nrf2 exerts an antioxidant effect by dissociating from Keap1 and transferring into nuclear, where it interacts with the antioxidant response element and activates the expression of antioxidant enzymes. When Nrf2 nuclear translocation and its downstream gene expression be inhibited, it will cause redox imbalance and oxidative stress injury [47]. Conversely, activating the Keap1-Nrf2 pathway by increasing the expression and effect of Nrf2 will play a protective role against disease states [48, 49]. Unfortunately, multiple exposures to METH increased Keap1 expression but decreased Nrf2 expression and thus downregulated downstream antioxidant enzyme expressions like HO-1 and glutamyl-cysteine synthetase- $\gamma$  [18]. Besides, METH not only enhanced ROS production but also inhibited the Keap1-Nrf2 pathway, thus resulting in damage to neurons in ventral tegmental area of rats [19]. In line with these previous results, in this study, we also found that chronic METH abuse inhibited the Keap1-Nrf2 pathway and elicited oxidative stress. Moreover, ICS exhibited positive effects on activating the Keap1-Nrf2 pathway and attenuating oxidative stress in striatum of METH mice model, implying the involvement of the Keap1-Nrf2 pathway and oxidative stress in ICS-regulated METH neurotoxicity.

We next used ML385, an inhibitor of Nrf2, to further confirm whether the Keap1-Nrf2 pathway and oxidative stress were involved in the protective effect of ICS on METH neurotoxicity. Just as expected, in the presence of ML385, ICS failed to activate the Keap1-Nrf2 pathway and to reduce oxidative stress in striatum of METH mice. More importantly, ML385 blocked the protective effects of ICS on neuronal loss, dendritic spines abnormalities, and behavioral impairments induced by METH. Also, inhibition of Nrf2 eliminated the regulatory ability of ICS on the abnormal expression of TH, DAT, DA, GFAP, Iba1, and  $\alpha$ -syn. These results proved that ICS could attenuate the METH-induced neurotoxicity via modulating the Keap1-Nrf2 pathway and the oxidative stress. Although previous studies have shown that ICS might achieve antioxidant effects by activating Nrf2-related protein expression and decreasing ROS levels in several diseases [50–52], we collected evidence for the first time that ICS could combat METH-induced neurotoxicity and PD-like symptoms through mediating the classic anti-oxidant Keap1-Nrf2 pathway and oxidative stress.

For decades, accumulative evidence from preclinical studies has shown that many natural plants and their active ingredients have preventive and therapeutic effects on neurodegenerative diseases. For example, in the 1-methyl-4-phenyl-1,2,3,6-tetrahydropyridine- (MPTP-) induced PD mice model, chlorogenic acid, ursolic acid, *Tinospora cordifolia*, and *Mucuna pruriens* could exhibit antiapoptotic, anti-inflammatory, antioxidant, or other pharmacological properties, which contribute to protection against neurotoxicity elicited by MPTP [53–57]. Similarly, our study found that ICS, a type of flavonoid and one of the main active ingredients of the traditional Chinese medicine *Epimedium*, could confer neuroprotection against METH-induced neurotoxicity via the Keap1-Nrf2 pathway activation and subsequent antioxidant and anti-inflammatory reinforcement.

While the mechanism of how Nrf2 dissociates from Keap1 is unclear, studies have shown that several kinases,

such as advanced protein kinase B (AKT) and extracellular signal-regulated kinase (ERK), may be involved in Nrf2 activation and nuclear translocation. Lv et al. [58] found that Licochalcone A could enhance Nrf2 nuclear translocation and HO-1 expression through AKT and ERK activation in *tert*-butyl hydroperoxide-treated RAW 264.7 cells. The protective effect of sesamin on ulcerative colitis was also involved in the activation of AKT/ERK and subsequent enhancement of Nrf2 signaling [59]. The limitation of this study was that we did not investigate the prime target molecules directly affected by ICS in the METH exposure model. Therefore, the exact mechanism by which ICS activates the Keap1-Nrf2 pathway remains to be answered in the future.

Besides, the anti-inflammatory role of the Keap1-Nrf2 pathway has been fully verified and widely recognized. The nuclear factor kappa B (NF- $\kappa$ B) is one of the most concerned transcription factors in inflammatory pathways. It has been suggested that there is complex crosstalk between the Nrf2 and NF- $\kappa$ B pathways. A review written by Bellezza et al. [60] pointed out that compounds that suppress NF- $\kappa$ B signaling could activate the Nrf2 pathway, and activated NF- $\kappa$ B could also stimulate the Nrf2 pathway, which could inhibit NF- $\kappa$ B activity conversely. Previous studies indicated that ICS could attenuate lipopolysaccharide-induced neuroinflammation by regulating the NF- $\kappa$ B pathway [21, 22]. Consistently, in this study, ICS activated the Keap1-Nrf2 pathway suppressed by METH to decrease glial cell activation. However, this positive influence was blocked when Nrf2 was inhibited.

In sum, the major findings of this work are that ICS can attenuate the METH-induced neurotoxicity and PD-like behavioral impairments via activating the Keap1-Nrf2 pathway. Although further research is needed to dig deeper into the actual molecular targets of ICS, it is undeniable that the current results imply the potential value of ICS to reduce the neurotoxicity of METH abusers.

## Data Availability

The original contributions presented in the study are included in the article.

## Conflicts of Interest

The authors declare no conflicts of interest.

## Authors' Contributions

Jian Huang, Jiuyang Ding, Zhuo Wang, Yanning Li, Yitong He, Xiaohan Wang, Haoliang Fan, and Qiqian Xie participated in literature search, experimental validation, writing the manuscript, and creating figures and tables. Pingming Qiu supervised the study design and critically read and edited the manuscript. All authors read and approved the manuscript. Jian Huang, Jiuyang Ding, and Zhuo Wang contributed equally to this work.

## Acknowledgments

This work was supported by the National Natural Science Foundation of China (Grant No. 81971786) to Pingming Qiu, Research Foundation for Advanced Talents of Guizhou Medical University (Grant No. University Contract of Doctors J [2021] 014), and Natural Science Foundation of Guizhou Medical University Incubation Program (Grant No. 20NSP084) to Jiuyang Ding.

## References

- [1] J. Huang, G. Yang, Z. Li et al., "Involvement of dopamine D3 receptor and dopamine transporter in methamphetamine-induced behavioral sensitization in tree shrews," *Brain and Behavior*, vol. 10, no. 2, article e01533, 2020.
- [2] H. Mizoguchi and K. Yamada, "Methamphetamine use causes cognitive impairment and altered decision-making," *Neurochemistry International*, vol. 124, pp. 106–113, 2019.
- [3] Z. Wang, C. Li, J. Ding et al., "Basolateral amygdala serotonin 2C receptor regulates emotional disorder-related symptoms induced by chronic methamphetamine administration," *Frontiers in Pharmacology*, vol. 12, article 627307, 2021.
- [4] S. Jayanthi, A. P. Daiwile, and J. L. Cadet, "Neurotoxicity of methamphetamine: main effects and mechanisms," *Experimental Neurology*, vol. 344, article 113795, 2021.
- [5] S. Sabrini, G. Y. Wang, J. C. Lin, J. K. Ian, and L. E. Curley, "Methamphetamine use and cognitive function: a systematic review of neuroimaging research," *Drug Alcohol Dependence*, vol. 194, pp. 75–87, 2019.
- [6] Y. Tai, L. Chen, E. Huang et al., "Protective effect of alpha-synuclein knockdown on methamphetamine-induced neurotoxicity in dopaminergic neurons," *Neural Regeneration Research*, vol. 9, no. 9, pp. 951–958, 2014.
- [7] J. Ding, Y. Wang, J. Huang et al., "Role of alpha-synuclein phosphorylation at serine 129 in methamphetamine-induced neurotoxicity in vitro and in vivo," *Neuroreport*, vol. 31, no. 11, pp. 787–797, 2020.
- [8] J. Ding, S. Hu, Y. Meng et al., "Alpha-synuclein deficiency ameliorates chronic methamphetamine induced neurodegeneration in mice," *Toxicology*, vol. 438, article 152461, 2020.
- [9] B. Kim, J. Yun, and B. Park, "Methamphetamine-induced neuronal damage: neurotoxicity and neuroinflammation," *Biomolecules & Therapeutics*, vol. 28, no. 5, pp. 381–388, 2020.
- [10] X. Yang, Y. Wang, Q. Li et al., "The main molecular mechanisms underlying methamphetamine-induced neurotoxicity and implications for pharmacological treatment," *Frontiers in Molecular Neuroscience*, vol. 11, p. 186, 2018.
- [11] F. Limanaqi, C. L. Busceti, R. Celli, F. Biagioni, and F. Fornai, "Autophagy as a gateway for the effects of methamphetamine: from neurotransmitter release and synaptic plasticity to psychiatric and neurodegenerative disorders," *Progress in Neurobiology*, vol. 204, article 102112, 2021.
- [12] H. R. Yun, Y. H. Jo, J. Kim, Y. Shin, S. S. Kim, and T. G. Choi, "Roles of autophagy in oxidative stress," *International Journal of Molecular Sciences*, vol. 21, no. 9, 2020.
- [13] J. Zhang, X. Wang, V. Vikash et al., "ROS and ROS-mediated cellular signaling," *Oxidative Medicine and Cellular Longevity*, vol. 2016, Article ID 4350965, 18 pages, 2016.

- [14] A. Osama, J. Zhang, J. Yao, X. Yao, and J. Fang, "Nrf2: a dark horse in Alzheimer's disease treatment," *Ageing Research Reviews*, vol. 64, article 101206, 2020.
- [15] C. Bento-Pereira and A. T. Dinkova-Kostova, "Activation of transcription factor Nrf2 to counteract mitochondrial dysfunction in Parkinson's disease," *Medicinal Research Reviews*, vol. 41, no. 2, pp. 785–802, 2021.
- [16] X.-L. Xie, J.-T. He, Z.-T. Wang et al., "Lactulose attenuates METH-induced neurotoxicity by alleviating the impaired autophagy, stabilizing the perturbed antioxidant system and suppressing apoptosis in rat striatum," *Toxicology Letters*, vol. 289, pp. 107–113, 2018.
- [17] A. Ramkissoon and P. G. Wells, "Methamphetamine oxidative stress, neurotoxicity, and functional deficits are modulated by nuclear factor-E2-related factor 2," *Free Radical Biology and Medicine*, vol. 89, pp. 358–368, 2015.
- [18] Q. Zeng, Q. Xiong, M. Zhou et al., "Resveratrol attenuates methamphetamine-induced memory impairment via inhibition of oxidative stress and apoptosis in mice," *Journal of Food Biochemistry*, vol. 45, no. 2, article e13622, 2021.
- [19] X. Meng, C. Zhang, Y. Guo et al., "TBHQ attenuates neurotoxicity induced by methamphetamine in the VTA through the Nrf2/HO-1 and PI3K/AKT signaling pathways," *Oxidative Medicine and Cellular Longevity*, vol. 2020, Article ID 8787156, 13 pages, 2020.
- [20] F. Xu, Q. Wu, L. Li, J. Gong, R. Huo, and W. Cui, "Icariside II: anticancer potential and molecular targets in solid cancers," *Frontiers in Pharmacology*, vol. 12, article 663776, 2021.
- [21] Y. Zheng, Y. Deng, J.-m. Gao et al., "Icariside II inhibits lipopolysaccharide-induced inflammation and amyloid production in rat astrocytes by regulating IKK/IkappaB/NF-kappaB/BACE1 signaling pathway," *Acta Pharmacologica Sinica*, vol. 41, no. 2, pp. 154–162, 2020.
- [22] J. Zhou, Y. Deng, F. Li, C. Yin, J. Shi, and Q. Gong, "Icariside II attenuates lipopolysaccharide-induced neuroinflammation through inhibiting TLR4/MyD88/NF-kappaB pathway in rats," *Biomedicine & Pharmacotherapy*, vol. 111, pp. 315–324, 2019.
- [23] J. Zhang, S. Li, S. Li et al., "Effect of icariside II and metformin on penile erectile function, glucose metabolism, reaction oxygen species, superoxide dismutase, and mitochondrial autophagy in type 2 diabetic rats with erectile dysfunction," *Translational Andrology and Urology*, vol. 9, no. 2, pp. 355–366, 2020.
- [24] L. Feng, J. Gao, Y. Liu, J. Shi, and Q. Gong, "Icariside II alleviates oxygen-glucose deprivation and reoxygenation-induced PC12 cell oxidative injury by activating Nrf2/SIRT3 signaling pathway," *Biomedicine & Pharmacotherapy*, vol. 103, pp. 9–17, 2018.
- [25] Y. S. Sun, K. Thakur, F. Hu, J. G. Zhang, and Z. J. Wei, "Icariside II inhibits tumorigenesis via inhibiting AKT/Cyclin E/CDK 2 pathway and activating mitochondria-dependent pathway," *Pharmacological Research*, vol. 152, article 104616, 2020.
- [26] F. Xu, C. Lv, Y. Deng, Y. Liu, and Q. Gong, "Icariside II, a PDE5 inhibitor, suppresses oxygen-glucose deprivation/reperfusion-induced primary hippocampal neuronal death through activating the PKG/CREB/BDNF/TrkB signaling pathway," *Frontiers in Pharmacology*, vol. 11, p. 523, 2020.
- [27] Y. Meng, J. Ding, C. Li, H. Fan, Y. He, and P. Qiu, "Transfer of pathological  $\alpha$ -synuclein from neurons to astrocytes via exosomes causes inflammatory responses after METH exposure," *Toxicology Letters*, vol. 331, pp. 188–199, 2020.
- [28] J. Ding, J. Huang, B. Xia et al., "Transfer of alpha-synuclein from neurons to oligodendrocytes triggers myelin sheath destruction in methamphetamine administration mice," *Toxicology Letters*, vol. 352, pp. 34–45, 2021.
- [29] L. Yan, Y. Deng, J. Gao et al., "Icariside II effectively reduces spatial learning and memory impairments in Alzheimer's disease model mice targeting beta-amyloid production," *Frontiers in Pharmacology*, vol. 8, p. 106, 2017.
- [30] W. Cui, J. Chen, F. Yu, W. Liu, and M. He, "GYY4137 protected the integrity of the blood-brain barrier via activation of the Nrf2/ARE pathway in mice with sepsis," *The FASEB Journal*, vol. 35, no. 7, article e21710, 2021.
- [31] J. Li, J. Huang, Y. He et al., "The protective effect of gastrodin against the synergistic effect of HIV-Tat protein and METH on the blood-brain barrier via glucose transporter 1 and glucose transporter 3," *Toxicology Research*, vol. 10, no. 1, pp. 91–101, 2021.
- [32] D. O. Sambo, J. J. Lebowitz, and H. Khoshbouei, "The sigma-1 receptor as a regulator of dopamine neurotransmission: a potential therapeutic target for methamphetamine addiction," *Pharmacology & Therapeutics*, vol. 186, pp. 152–167, 2018.
- [33] N. D. Volkow, G.-J. Wang, L. Smith et al., "Recovery of dopamine transporters with methamphetamine detoxification is not linked to changes in dopamine release," *Neuroimage*, vol. 121, pp. 20–28, 2015.
- [34] A. L. Blaker, E. A. Rodriguez, and B. K. Yamamoto, "Neurotoxicity to dopamine neurons after the serial exposure to alcohol and methamphetamine: protection by COX-2 antagonism," *Brain, Behavior, and Immunity*, vol. 81, pp. 317–328, 2019.
- [35] J. Ding, Y. Lian, Y. Meng et al., "The effect of  $\alpha$ -synuclein and Tau in methamphetamine induced neurotoxicity in vivo and in vitro," *Toxicology Letters*, vol. 319, pp. 213–224, 2020.
- [36] W. Kuang, T. Liu, F. He, L. Yu, Q. Wang, and C. Yu, "Icariside II promotes the differentiation of human amniotic mesenchymal stem cells into dopaminergic neuron-like cells," *In Vitro Cellular & Developmental Biology-Animal*, vol. 57, no. 4, pp. 457–467, 2021.
- [37] J. M. Lappin, S. Darke, and M. Farrell, "Methamphetamine use and future risk for Parkinson's disease: evidence and clinical implications," *Drug Alcohol Dependence*, vol. 187, pp. 134–140, 2018.
- [38] Y. Meng, H. Qiao, J. Ding et al., "Effect of Parkin on methamphetamine-induced alpha-synuclein degradation dysfunction in vitro and in vivo," *Brain and Behavior*, vol. 10, no. 4, article e01574, 2020.
- [39] L. N. Zhu, H. H. Qiao, L. Chen et al., "SUMOylation of alpha-synuclein influences on alpha-synuclein aggregation induced by methamphetamine," *Frontiers in Cellular Neuroscience*, vol. 12, p. 262, 2018.
- [40] T. H. McNeill, S. A. Brown, J. A. Rafols, and I. Shoulson, "Atrophy of medium spiny I striatal dendrites in advanced Parkinson's disease," *Brain Research*, vol. 455, no. 1, pp. 148–152, 1988.
- [41] S. Liu, X. Li, J. Gao, Y. Liu, J. Shi, and Q. Gong, "Icariside II, a phosphodiesterase-5 inhibitor, attenuates beta-amyloid-induced cognitive deficits via BDNF/TrkB/CREB signaling," *Cellular Physiology and Biochemistry*, vol. 49, no. 3, p. 985, 2018.
- [42] L. He, Y. Deng, J. Gao, L. Zeng, and Q. Gong, "Icariside II ameliorates ibotenic acid-induced cognitive impairment and

- apoptotic response via modulation of MAPK pathway in rats,” *Phytomedicine*, vol. 41, pp. 74–81, 2018.
- [43] Y. Deng, L. Long, K. Wang et al., “Icariside II, a broad-spectrum anti-cancer agent, reverses beta-amyloid-induced cognitive impairment through reducing inflammation and apoptosis in rats,” *Frontiers in Pharmacology*, vol. 8, p. 39, 2017.
- [44] C. Yin, Y. Deng, J. Gao, X. Li, Y. Liu, and Q. Gong, “Icariside II, a novel phosphodiesterase-5 inhibitor, attenuates streptozotocin-induced cognitive deficits in rats,” *Neuroscience*, vol. 328, pp. 69–79, 2017.
- [45] Y. L. Zhao, W. Zhao, M. Liu, L. Liu, and Y. Wang, “TBHQ-overview of multiple mechanisms against oxidative stress for attenuating methamphetamine-induced neurotoxicity,” *Oxidative Medicine and Cellular Longevity*, vol. 2020, Article ID 8874304, 10 pages, 2020.
- [46] X. F. Zeng, Q. Li, J. Li et al., “HIV-1 Tat and methamphetamine co-induced oxidative cellular injury is mitigated by N-acetylcysteine amide (NACA) through rectifying mTOR signaling,” *Toxicology Letters*, vol. 299, pp. 159–171, 2018.
- [47] D. Yang, Q. Yang, N. Fu et al., “Hexavalent chromium induced heart dysfunction via Sesn2-mediated impairment of mitochondrial function and energy supply,” *Chemosphere*, vol. 264, article 128547, 2021.
- [48] Y. Lv, H. Jiang, S. Li et al., “Sulforaphane prevents chromium-induced lung injury in rats via activation of the Akt/GSK-3beta/Fyn pathway,” *Environmental Pollution*, vol. 259, article 113812, 2020.
- [49] Q. Yang, B. Han, S. Li et al., “The link between deacetylation and hepatotoxicity induced by exposure to hexavalent chromium,” *Journal of Advanced Research*, vol. 35, 2022.
- [50] J. Gu, X. Sun, G. Wang, M. Li, and M. Chi, “Icariside II enhances Nrf2 nuclear translocation to upregulate phase II detoxifying enzyme expression coupled with the ERK, Akt and JNK signaling pathways,” *Molecules*, vol. 16, no. 11, pp. 9234–9244, 2011.
- [51] J. Gao, Y. Deng, C. Yin et al., “Icariside II, a novel phosphodiesterase 5 inhibitor, protects against H<sub>2</sub>O<sub>2</sub>-induced PC12 cells death by inhibiting mitochondria-mediated autophagy,” *Journal of Cellular and Molecular Medicine*, vol. 21, no. 2, pp. 375–386, 2017.
- [52] Y. Li and F. Meng, “Effects of icariside II on brain tissue oxidative stress and Nrf2/HO-1 expression in rats with cerebral ischemia-reperfusion injury1,” *Acta Cirurgica Brasileira*, vol. 34, no. 2, article e201900208, 2019.
- [53] S. S. Singh, S. N. Rai, H. Birla et al., “Neuroprotective Effect of Chlorogenic Acid on Mitochondrial Dysfunction-Mediated Apoptotic Death of DA Neurons in a Parkinsonian Mouse Model,” *Oxidative Medicine and Cellular Longevity*, vol. 2020, Article ID 6571484, 14 pages, 2020.
- [54] S. N. Rai, W. Zahra, S. S. Singh et al., “Anti-inflammatory activity of ursolic acid in MPTP-induced Parkinsonian mouse model,” *Neurotoxicity Research*, vol. 36, no. 3, pp. 452–462, 2019.
- [55] H. Birla, S. N. Rai, S. S. Singh et al., “*Tinospora cordifolia* suppresses neuroinflammation in Parkinsonian mouse model,” *Neuromolecular Medicine*, vol. 21, no. 1, pp. 42–53, 2019.
- [56] S. S. Singh, S. N. Rai, H. Birla et al., “Effect of chlorogenic acid supplementation in MPTP-intoxicated mouse,” *Frontiers in Pharmacology*, vol. 9, p. 757, 2018.
- [57] S. N. Rai, H. Birla, S. S. Singh et al., “*Mucuna pruriens* protects against MPTP intoxicated neuroinflammation in Parkinson’s disease through NF-kappaB/pAKT signaling pathways,” *Frontiers in Aging Neuroscience*, vol. 9, p. 421, 2017.
- [58] H. Lv, H. Ren, L. Wang, W. Chen, and X. Ci, “Lico A enhances Nrf2-mediated defense mechanisms against t-BHP-induced oxidative stress and cell death via Akt and ERK activation in RAW 264.7 cells,” *Oxidative Medicine and Cellular Longevity*, vol. 2015, Article ID 709845, 13 pages, 2015.
- [59] X. Bai, X. Gou, P. Cai et al., “Sesamin enhances Nrf2-mediated protective defense against oxidative stress and inflammation in colitis via AKT and ERK activation,” *Oxidative Medicine and Cellular Longevity*, vol. 2019, Article ID 2432416, 20 pages, 2019.
- [60] I. Bellezza, I. Giambanco, A. Minelli, and R. Donato, “Nrf2-Keap1 signaling in oxidative and reductive stress,” *Biochimica et Biophysica Acta (BBA)-Molecular Cell Research*, vol. 1865, no. 5, pp. 721–733, 2018.



## Review Article

# Glial Purinergic Signaling-Mediated Oxidative Stress (GPOS) in Neuropsychiatric Disorders

Lumei Huang <sup>1,2</sup>, Yong Tang <sup>3</sup>, and Beata Sperlagh <sup>1,2</sup>

<sup>1</sup>Laboratory of Molecular Pharmacology, Institute of Experimental Medicine, Budapest, Hungary

<sup>2</sup>János Szentágotthai Doctoral School, Semmelweis University, Budapest, Hungary

<sup>3</sup>International Collaborative Centre on Big Science Plan for Purinergic Signalling, Chengdu University of Traditional Chinese Medicine, Acupuncture and Chronobiology Key Laboratory of Sichuan Province, Chengdu, China

Correspondence should be addressed to Lumei Huang; [lumei.huang@koki.mta.hu](mailto:lumei.huang@koki.mta.hu)

Received 19 August 2021; Revised 21 January 2022; Accepted 9 February 2022; Published 4 March 2022

Academic Editor: Cinzia Signorini

Copyright © 2022 Lumei Huang et al. This is an open access article distributed under the Creative Commons Attribution License, which permits unrestricted use, distribution, and reproduction in any medium, provided the original work is properly cited.

Oxidative stress (OS) has been implicated in the progression of multiple neuropsychiatric disorders, including schizophrenia (SZ), major depressive disorder (MDD), bipolar disorder, and autism. However, whether glial purinergic signaling interaction with oxidative/antioxidative system displays an important role in neuropsychiatric disorders is still unclear. In this review, we firstly summarize the oxidative/antioxidative pathways shared in different glial cells and highlight the cell type-specific difference in response to OS. Then, we collect the evidence showing the regulation of purinergic signaling in OS with an emphasis on adenosine and its receptors, P2Y1 receptor in the P2Y family and P2X7 receptor in the P2X family. Available data shows that the activation of P1 receptors and P2X accelerates the OS; reversely, the activation of the P2Y family (P2Y1) causes protective effect against OS. Finally, we discuss current findings demonstrating the contribution of the purinergic signaling system to neuropsychiatric disorders and point out the potential role of OS in this process to propose a “glial purinergic-oxidative stress” (“GPOS”) hypothesis for future development of therapeutic strategies against a variety of neuropsychiatric disorders.

## 1. Introduction

After the discovery of cell energy carrier adenosine 5'-triphosphate (ATP) as a neurotransmitter, the term “purinergic” was introduced by Burnstock for the first time in 1972 [1–3]. Years later, the purinergic receptors were identified in succession. Until now, there are two families of receptors that have been identified, including P1 (adenosine activation) and P2 (ATP and its metabolite activation). P1 receptors have been classified into four groups: A1, A2A, A2B, and A3. Similarly, P2 receptors have further been categorized into P2X (1, 2, 3, 4, 5, 6, and 7) and P2Y (1, 2, 4, 6, 11, 12, 13, and 14) [4–6]. ATP is released through various mechanisms into the synaptic cleft and then hydrolyzed into ADP, AMP, and adenosine, to further bind to different receptors, triggering a series of intracellular signaling pathways that have been well investigated to establish a “purinergic signaling system” [7]. In the central nervous system (CNS), growing evidence shows that purinergic signaling plays a key role not only in

physiological conditions but also in various central nervous disorders, referring to neurodegenerative disorders associated with Alzheimer's disease (AD) [8, 9], Parkinson's disease (PD) [10], Huntington's disease (HD) [11], and Amyotrophic Lateral Sclerosis (ALS) [12] and neuropsychiatric disorders, including schizophrenia (SZ) [13], major depression disorder (MDD), [14], autism [15]. Notably, one of the important underlying mechanisms associated with the regulatory effect of the purinergic system in a variety of brain disorders is the interactive effect between the purinergic system and oxidative stress (OS).

OS is a pathological condition produced by the imbalance between oxidants and antioxidants in a living system and has been recognized as one of most important pathogenic factors for multiple brain disorders. On the one hand, repetitive exposure to oxidative stress accelerates a cascade of intracellular events, including mitochondrial dysfunction, DNA and mDNA impairment, and neuroinflammation, which, in turn, cause even more ROS production [16]. On

the other hand, the oxidative stress-induced byproducts from the cell could further diffuse in the extracellular space to affect other tissues, exacerbate neuronal damage, and contribute to development of neurodegenerative and neuropsychiatric disorders [17, 18]. Despite the “neuron doctrine” that has governed brain research for a long time, the importance of glial cells as architects in CNS has been gradually recognized and rapidly expanded in past decades [19]. The interplay between OS and glial cells is bidirectional. OS could trigger the activation of glial cells, leading to inflammation [20]. Reversely, chronic inflammation further induces cellular OS via inflammatory cytokines [21, 22].

However, whether glial purinergic signaling interaction with the oxidative/antioxidative system participates as a major pathway in the development and therapeutic of neuropsychiatric disorders is still unclear. Therefore, the aim of this review is to firstly summarize the regulatory effect of the glial cell in response to OS and shed light on the involvement of glial purinergic signaling in this process to establish a new pathological hypothesis of “GPOS” (glial purinergic signaling-mediated oxidative stress). Then, we will discuss the potential application of this hypothesis in neuropsychiatric disorders with an emphasis on schizophrenia (SZ) and major depressive disorder (MDD).

## 2. Glial Purinergic Signaling-Mediated Oxidative Stress (“GPOS”)

The hypothesis of GPOS is mainly based on evidence shows the association of glial cells with the balance of oxidant/antioxidant and regulation of the glial-specific purinergic signaling system in this process.

**2.1. Glial Cells and Oxidative Stress.** The brain, as a high oxygen consumption organ, is particularly subjective to OS, resulting in ROS production. Overaccumulation of ROS damages DNA, lipids, and proteins, ultimately contributing to necrosis and apoptosis. Besides neurons, the crucial role of glial cell-related OS also has been comparatively investigated in the past decade. However, different types of glial cells not only share the same mechanism to produce OS but also display their unique feature to deal with OS.

**2.1.1. Microglia, Astrocyte, and Oligodendrocyte Share the Same Intracellular Pathway to Generate and Resist OS.** Neuroinflammation and OS are common properties of neurodegenerative diseases in CNS. Neuroinflammatory stimuli can lead to elevation of reactive oxygen and nitrogen species (ROS and RNS), causing neuronal damage. Reversely, neuronal damage induced the release of proinflammatory factors which further act as a trigger to generate more OS to shape a feed-forward loop of neurodegeneration. Therefore, it is reasonable to assume an interactive pathway between inflammation and OS.

In fact, increasing evidence has confirmed that ERK/NF- $\kappa$ B, P38 AMPK/NF- $\kappa$ B, and JNK/BF- $\kappa$ B exert the basic pathway to generate RNS and ROS in response to inflammatory stimuli in microglia, astrocyte, and oligodendrocyte. In microglia, activation of murine microglial cell lines (N11

and BV-2) with LPS and interferon-gamma (IFN- $\gamma$ ) caused the induction of inducible nitric oxide synthase (iNOS), subsequently increasing nitric oxide (NO) release to the surrounding environment [23]. As the two most common inflammatory signaling pathways, MAPKs and NF- $\kappa$ B were associated with iNOS/NO induction [24, 25]. Additionally, the transfection rat microglial cell line with TAK1, the upstream kinase to activate MAPKs and BF- $\kappa$ B pathways and its activator protein, TAK1-binding protein 1 (TAB1), caused iNOS promoter-reporter construct activity in microglia through p38 MAPK-, JNK-, and NF- $\kappa$ B-dependent manner [26]. Meanwhile, protein kinase C (PKC) also regulated iNOS production via MAPK and NF- $\kappa$ B pathways in an isoform-dependent fashion in reactive microglia [27]. The generation of ROS also associated with activation of these intracellular pathways. Treating BV-2 cell lines with fluoride led to the increase in ROS partly via increasing the JNK phosphorylation level. The increasing levels of intracellular O<sub>2</sub> could be markedly reduced by using the JNK inhibitor P600125 [28]. Efforts have also been made to investigate further downstream pathways. It turned out that LPS-induced mitochondrial ROS generation not only activated MAPKs, including ERK, JNK, and p38, but also regulated I $\kappa$ B activation and NF- $\kappa$ B nuclear localization [29]. In primary human fetal astrocyte culture, direct interleukin- (IL-) 1 stimulation increased iNOS expression via activation of NF- $\kappa$ B [30]. The source of IL-1 could be from microglia, since the study suggested that gp41 only could trigger iNOS mRNA expression and NO production in astrocyte in the presence of microglial cell IL-1 expression [23, 31]. Zn<sup>2+</sup> application also augmented LPS-induced NO production by the phosphorylation of p38 MAPK and activation of NF- $\kappa$ B in rat astrocytes [32]. In response to LPS-induced inflammation, tyrosine kinase Fyn regulated iNOS expression via modulation of ERK phosphorylation [33]. Matrix metalloproteinase- (MMP-) 9, one of the zinc-dependent endopeptidases, has been shown to raise an impact on cell migration and inflammation modulation [34]. OS, especially the (NOX)/ROS-dependent pathway, is essential for MMP-9 expression under various stimuli. Japanese encephalitis virus-induced expression of the MMP-9 in rat brain astrocytes (RBA-1 cells) has been tested via the generation of ROS, followed by activation of p38, p42/p44 MAPK, and JNK1/2, subsequently leading to NF- $\kappa$ B activation [35]. Furthermore, stimulating RBA-1 cells with LPS elevated MMP-9 expression and boosted the cell migration via the (NOX)/ROS-dependent NF- $\kappa$ B pathway [36]. In agreement with microglia and astrocyte, the OS-induced MAPK pathway is also present in the oligodendrocyte. Early research found H<sub>2</sub>O<sub>2</sub>-induced oligodendrocyte death mainly through the activation of MAPK, ERK1/2, and p38 pathways [37].

Likely, these three types of glial cells also implicated the same pathway against OS, called antioxidative pathway. It is well known that activated nuclear factor erythroid 2-related factor 2 (Nrf2) could translocate and bind to the antioxidant response element (ARE), subsequently regulating the expression of a large battery of genes involved in the cellular antioxidant and anti-inflammatory defense. Meanwhile, Nrf2 is regulated by its negative regulator Kelch-like ECH-associated protein 1 (Keap1). Therefore, the Keap1/Nrf2/

ARE signaling pathway was recognized as the classical anti-oxidative and anti-inflammatory pathway [38]. Glial cells also comply with this pathway in response to OS. In BV2 microglia, kolaviron produced antioxidant effect by increasing HO-1 via the Nrf2/ARE pathway [39]. Antioxidation and anti-inflammatory effect of icariin also depended on the activation of Nrf2 signaling in microglia [40]. In line with microglia, activation of the Nrf2/ARE pathway in astrocyte reduced OS in Parkinson's disease model [41], spinal cord injury [42], and AD [43]. In oligodendrocyte, release of Nrf2/ARE protected the oligodendrocyte from axonal damage, demyelination, and neuroinflammation [44]. Interestingly, the Nrf2/ARE pathway could partially work together with peroxisome proliferator-activated receptor gamma (PPAR- $\gamma$ ) to preserve mitochondrial function, defend against OS, and promoted OPC differentiation [45]. PPAR- $\gamma$  self-activation induced a protective effect on oligodendrocyte mitochondria attributed to the elevation of the expression of PGC-1 $\alpha$  (a mitochondrial biogenesis master regulator), UCP2 (a mitochondrial protein known to reduce ROS production), and cytochrome oxidase subunit COX1 and influenced oscillatory Ca<sup>2+</sup> waves to defend against TNF- $\alpha$  damage [46, 47].

*2.1.2. Microglia, Astrocyte, and Oligodendrocyte Displayed Their Unique Features in Response to OS.* NADPH oxidases (NOXes) are one of the major sources of cellular ROS. Under physiological condition, suitable regulation of NADPH oxidase activity is crucial to maintain a healthy level of ROS in the body. However, overactivity of these enzymes could overproduce ROS, which further leads to OS and cell damage. To date, there are 7 human isoforms of the complex, including NOX1, NOX2, NOX3, NOX4, NOX5, DUOX1, and DUOX2. Interestingly, different types of glial cells showed different expression patterns which could implicate distinct therapeutic potential.

The experiments performed on neuron-glia mixed culture from NADPH oxidase-deficient (PHOX<sup>-/-</sup>) and wild-type mice demonstrated that LPS-induced dopaminergic neurotoxicity mainly was caused by microglial activation through NADPH oxidase, producing the ROS accumulation [48]. Among the NOX family (NOX1–5 and DUOX1–2) [49], NOX 2 was highly expressed in microglia. In contrast, expression of NOX1 and NOX4 in microglia is still controversial due to the lack of specific antibodies [50]. Although evidence showed the increase in both NOX2 and NOX4 levels in microglia-neuron mixed culture exposed to iron and LPS [51], the spotlight has been focused on NOX2. By employing p47<sup>phox</sup>-deficient mice, a study demonstrated that the functional subunit of NOX2 switched microglia to an activation state in response to an inflammatory challenge [52]. With an exception of p47<sup>phox</sup>, the increased expression of the p67<sup>phox</sup> subunit also has been observed when N9 microglia lines and primary microglia culture were treated with angiotensin II [53]. Unlike microglia, the expression of NOXs in astrocytes and oligodendrocytes is quite low. In astrocyte, NOX is activated by PKC and intracellular calcium. The activity of NOX could be modulated by intracellular pH environment, suppressed by intracellular alkalinization, and enhanced by acidi-

fication [54]. Regardless of less expression of NOXs, treatment of oligodendrocytes with injured astrocyte media with a reduction in zinc levels was sufficient to result in NADPH oxidase activation by gp91 phox [55]. A study by using the cell line MO3-13 displaying the molecular and cellular features of OL precursors was performed to determine the effect of NOXs on oligodendrocyte differentiation. The elevated expression of NOX3 and NOX 5 in human OLs was observed for the first time after H<sub>2</sub>O<sub>2</sub> treatment, and selective depletion of these proteins inhibited differentiation induced by the protein kinase C (PKC) activator, phorbol-12-myristate-13-acetate (PMA). Furthermore, NOX5 silencing down-regulated NOX3 mRNA levels, suggesting that ROS produced by NOX5 upregulated NOX3 expression [56].

Another distinct feature for different types of glial cells is their antioxidant gene expression, especially the expression of glutathione (GSH), a major cellular antioxidant and redox regulator in the brain against OS. Microglia and astrocyte showed higher expression compared to oligodendrocyte [57, 58]. This feature makes oligodendrocyte more susceptible to OS in comparison with microglia and astrocyte. Another enzyme, which could inhibit ROS production, is SHP-1, a non-receptor-type protein tyrosine phosphatase. The presence of SHP-1 had an inhibitory effect on the activation of transcription factors NF- $\kappa$ B, STAT3, and STAT6, further suppressing ROS production [59, 60]. The expression of SHP-1 mainly depended on the physiopathological conditions. Although the expression of SHP1 could dramatically increase in all types of glial cells under pathological stimulation, the physiological expression of SHP1 varied from microglia and astrocyte to oligodendrocyte. Under physiological condition, immunohistochemistry showed that SHP1 immunoreactivity colocalized with GFAP-positive astrocytes, but not with microglia [61]. In either mixed glial culture or pure culture, oligodendrocytes expressed high levels of SHP-1 in the cytoplasm of cell bodies and processes [62]. The unique expression pattern probably could implicate a dominant antioxidative effect of astrocyte and oligodendrocyte compared to microglia.

## 2.2. Glia Purinergic Signaling-Mediated OS

*2.2.1. P1 Family Member Adenosine and Its Receptors Exerted an Opposite Effect in Response to OS.* Under physiological condition, extracellular ATP could be rapidly converted into ADP, AMP, and adenosine in the presence of enzymes CD39 and CD73. To keep the homeostasis, the nucleoside transporters (ENTs) expressed on the membrane of glial cells take up the excessive adenosine from extracellular into intracellular part. Intracellular adenosine is either further hydrolyzed to inosine by adenosine deaminase or phosphorylated to AMP by adenosine kinase (ADK) to efficiently regulate adenosine levels. In an OS-loaded brain, the elevated extracellular adenosine could significantly protect neurons from damage. The study from cultured astrocytes found that OS induced extracellular adenosine accumulation partially via decreasing the function of ENT1 without expression alteration [63]. However, pretreating microglia with adenosine could significantly decrease H<sub>2</sub>O<sub>2</sub>-induced

ROS overproduction compared to the nontreated group. This benefit is accompanied by expression of antioxidative enzyme hemoxygenase-1 (HO-1) expression through Nrf2/ARE and PI3K/Akt pathways. Furthermore, the effects of adenosine are independent of its receptors, since pharmacological activation and inhibition of A1, A2A, and A3 had small impact on ROS generation and HO-1 expression [64].

Inconsistent with the beneficial effect of adenosine itself, it exerts a harmful effect on OS once it activates its receptors. For example, extracellular adenosine activated A3 receptors, which further caused OS and disturbed mitochondrial membrane potentials in oligodendrocytes [65]. After retinal detachment, blockade of A2A receptors could protect the photoreceptor by inhibiting microglia proliferation, decreasing IL-1, and suppressing ROS overproduction [66]. In LPS-treated mixed glia cultures with astrocyte and microglia, the A2A agonist CGS21680 potentiated LPS-induced NO release and NO synthase II expression, and the potentiation was inhibited by the A2A antagonist ZM-241385 [67].

**2.2.2. P2X Family Especially P2X7 Receptor Activation Exacerbated OS.** The P2 receptor family also participates in the regulation of OS. Among the P2X subgroup, most of interests have been focused on P2X7 receptors due to their unique low affinity to ATP, especially under pathological conditions. Using mixed neuron and microglia culture from wild-type and P2X7-deficient mice confirmed that microglial P2X7 receptor activation dramatically increased the release of superoxide and nitric oxide, contributing to cortical neuronal death [68]. Further experiments from  $\beta$ -amyloid-stimulated microglia indicated that microglial P2X7 activation could not only induce the release of superoxide but also increase the level of ROS. This experiment uncovered the important contribution of the influx of extracellular  $Ca^{2+}$  to the production of ROS. Interestingly, the source of  $Ca^{2+}$  influx was attributed to P2X7 activation induced by  $\beta$ -amyloid-stimulated ATP release directly from microglia in an autocrine fashion [69]. However, P2X7 activation-induced ROS production also could be  $Ca^{2+}$  independent. In the murine microglial EOC13 cell line, researchers found that cells had higher ATP-induced ROS formation in the absence of  $Ca^{2+}$  compared to the presence of  $Ca^{2+}$  without P2X7 function alteration. Results were confirmed by incubation of the  $Ca^{2+}$  chelator EGTA. Similarly, high extracellular  $K^+$  incubation also was unable to impair P2X7-induced ROS formation [70]. P2X7-induced ROS production could be influenced by extracellular acidification in different ways in the BV-2 microglial line. Short-time acidification efficiently suppressed maximal ionic current response of P2X7 at the upstream level. However, long-lasting acidification induced intracellular OS by coordinating enhancement with P2X7 activation for mitochondrial toxicity [71].

The intracellular pathways of P2X7 activation-induced OS also have been investigated. In primary rat microglia culture, both ATP and P2X7 agonist BzATP stimulations caused the production of superoxide by activation of NADPH oxidase and pharmacological inhibition of P38 MAPK attenuated the superoxide production. This experiment indicated that microglial P2X7 activation induced cor-

tical neuron death by the NADPH-P38 MAPK pathway [72]. Although the ATP/P2X7/ROS-/ASK1/p38 pathway has been identified in macrophage [73], other studies addressed this pathway in microglia, the resident immune cells of the CNS. Therefore, BV2 and MG6 microglia lines were used for this purpose. By using the immunoblot method, researchers found ATP-induced P38 phosphorylation which could be reversed by the p38 inhibitor SB, ROS scavengers, and P2X7 inhibitor CBB. Together with all the results, it turned out that P2X7 activation-induced ROS generation was a necessary process to activate the ASK1-p38 pathway. Furthermore, the CaMKII inhibitor KN-93 that suppressed ASK1 activation, p38 activation, and cell death further identified the upstream signaling of ASK1-p38 [74]. Compared to the MAPK signaling pathway which was largely related to cellular proliferation, differentiation, and survival, the AMPK signaling regulates cellular metabolism and cellular energy homeostasis by monitoring the AMP:ADP:ATP ratio [75]. Therefore, to uncover if P2X7 activation-induced OS via the AMPK pathway further contributes to mitochondrial dysfunction will be particularly important in future. The influx of  $Ca^{2+}$  and efflux of  $K^+$  are two major upstream events after P2X7 receptor activation. Intracellular overload of  $Ca^{2+}$  together with robust efflux of  $K^+$  interrupted the cytosol pH and mitochondrial electron transport, followed by ROS overproduction. To our knowledge, ROS overproduction parallel with  $Ca^{2+}$ /CaMKII resulted in phosphorylation of AMPK. The consequence of AMPK activation further increased mitochondrial fission and caused cell death in cultured BV-2 microglia cells [76]. In astrocyte, P2X7 receptor activation increased ROS production through NADPH oxidase, subsequently leading to IL-6 release [77].

**2.2.3. P2Y Family Especially P2Y1 Receptor Activation Alleviated OS.** Parallel with ion channel P2X receptors, the G protein-coupled P2Y family is also associated with regulation of OS in a different way. In cultured astrocytes, short-time ATP incubation displayed a protective effect against  $H_2O_2$ -induced cell death. However, preapplication of the P2Y1 receptor antagonist MRS2179 efficiently reversed the protective action, which confirmed the involvement of P2Y1. The results from DNA microarray analysis and quantitative RT-PCR analysis demonstrated that ATP incubation upregulated oxidoreductase genes such as TrxR, CBR, and superoxide dismutase-like gene. However, detailed connection between P2Y1-related protection and the upregulated genes was still unclear [78]. In coculture with astrocyte and neurons, they found that the protective effect induced by P2Y1 receptor activation against  $H_2O_2$  attributed to IL-6 release from astrocyte instead of neuron [79]. The mechanism of P2Y1 induced protective effect against  $H_2O_2$  in astrocyte has been tested. Researchers found that  $H_2O_2$  evoked the activation of src tyrosine kinase, which further enhanced ERK1/2 phosphorylation, resulting in cell death. Therefore, inhibition the activation of src tyrosine kinase was a crucial process to protect the cell from death. Remarkably, P2Y1 agonist 2MeSADP enhanced the gene expression and activity of protein tyrosine phosphatase (PTP), which

was responsible for the inhibition of src tyrosine kinase. Thus, P2Y1-PTP- src tyrosine kinase-ERK1/2 pathway could be essential for the protective effect [80]. In addition, there are still some other mechanisms showing the involvement of P2Y1 in OS. In mixed hippocampal culture with astrocyte and neurons, P2Y1 activation directly contributed to ROS decrease and mitochondrial depolarization [81]. With an exception of P2Y1 receptor, other P2Y receptors in astrocytes also have been showed to regulate the OS. The P2Y12/13 agonist 2MeADP application decreased ROS generation and mitochondrial depolarization. In contrast, the P2Y6 agonist UDP increased ROS production, whereas that of P2Y2/4 did not show any effect on ROS overproduction [82]. In astrocyte-microglia interaction experiment, UDP activated microglia P2Y6 and further coupled to the phospholipase C (PLC)/PKC pathway, which mediated an increase in inducible nitric oxide synthase (iNOS) expression and in nitric oxide (NO) release. Consequently, the diffusible NO mediated astroglial apoptosis [83].

### 3. GPOS in Neuropsychiatric Disorders

**3.1. GPOS in SZ.** Schizophrenia (SZ) is a common psychiatric disorder characterized by positive, negative, and cognitive symptoms. It has been identified that genetic susceptibility factors combined with environment insults together contribute to the development of SZ. To date, several pathogenesis models of SZ have been proposed from different aspects. (1) Cell-specific involvement, including hyperdopaminergic, hypoglutamatergic, hypo-GABAergic, and hypo-serotonergic; (2) gene-related involvement; (3) energy metabolism disturbance [84, 85]; and (4) oxidative and antioxidant imbalance [86].

Based on evidence suggesting that purine derivative allopurinol administration exerted a beneficial therapeutic effect on patients with SZ, Lara and colleagues first proposed a purinergic hypothesis of SZ [87, 88]. To date, the participant of the purinergic system in SZ is mainly related to adenosine receptors (P1 family), P2X7 receptors (P2X family), and P2Y1 receptors (P2Y family). Purinergic receptor activation or inhibition affected the behavior alteration in SZ. A clinical study supported that the reduction of A2AR levels accompanied by an altered motor phenotype in a subgroup of SZ patients, but A1 kept unchanged [89]. Few clinical data are available regarding P2Y and P2X receptors participation in SZ pathophysiology. By using bilateral microinfusions of the selective agonist MRS2365 into the medial prefrontal cortex (mPFC), the study addressed that activation of P2Y1 in mPFC reduced prepulse inhibition (PPI) while having no impact on startle amplitude [90]. Two antipsychotics drugs, prochlorperazine and trifluoperazine, acted as a negative allosteric modulator to inhibit human P2X7 receptor function [13]. Furthermore, in the phencyclidine-induced SZ model, genetic deletion and pharmacological inhibition of P2X7Rs alleviated schizophrenia-like behavioral alterations, increasing social interactions and alleviating hyperlocomotion and stereotype behavior [91, 92].

However, the underlying mechanism mainly focused on purinergic receptor polymorphisms and interaction with

dopamine receptors and NMDA receptors. The link between adenosine A2A receptor gene polymorphism located on chromosome 22q and susceptibility to SZ was reported [93, 94]. By measuring the polymorphisms in ADORA1, ADORA2A, and ADORA3, a study found a correlation between ADORA1 rs3766566 and positive psychopathological symptoms, ADORA2A rs2298383 and general psychopathological symptoms, and ADORA2A rs5751876 and akathisia [95]. In contrast, no association between SZ and polymorphisms of P2X7 receptor has been observed so far [96].

The dopamine hypothesis of SZ is largely based on the effects of D2R antagonists and agonists to alleviate and to accelerate the symptoms, respectively. The interaction between A2A and dopamine D2 [97] and A2A and NMDA [98] made A2A a potential target to SZ. By forming A2A/D2 heteromers, the reduction of adenosine level caused the elevation of dopamine level in SZ [99, 100]. Besides adenosine receptors, P2Y (P2Y1) and P2X (P2X7) also have been found to associate with SZ mainly through interacting with dopamine receptors and glutamate receptors. The emerging experimental evidence found that stimulation of P2Y1 receptors was related to elevation of dopamine release [101]. In contrast, activation of these receptors also caused the hypofunction of NMDA [102]. Importantly, the activation of dopamine receptor D2 could diminish the excessive production of ROS and RNS induced by bradykinin, a pro-inflammatory B2R-activating peptide. Together with the previous evidence implicating that A2A activation accumulated ROS, it suggested that A2A/D2 heteromers may play a complex role in the regulation of OS in SZ. In animal study, A1 receptors agonists could protect against neuropathological changes in rat retrosplenial cortex after administration of the NMDA receptor antagonist MK-801 [103]. It has been reported that MK-801 administration caused ROS and RNS production in rat [104, 105]. However, whether A1-induced protective effect involves the regulation of ROS and RNS is still masked due to the lack of direct evidence.

It is worth noting that glial expressed purinergic receptors probably devote to the pathogenesis of SZ. In the study of mice with A2A receptors deficiency from astrocytes, MK-801-induced inhibition of psychomotor functions and memory as well as suppression of glutamine transporter activity was observed [106]. This study revealed the expression of A2A receptors in astrocyte contributed to MK-801 induced psychotic symptoms. Under normal condition, the expression of A2A in astrocyte is lower than in certain population of neurons. The A2A expression could dramatically increase when responded to pathological stimulation. For example, study found that astrocytic A2A but not microglial A2A is increased in AD model [107]. Compared to the expression and function of microglia P2Y1, the role of astrocytic P2Y1 is less debated as it turned out to perform a variety of brain functions by regulating neuron-to-glia communications. With regard to P2X7, the research spotlight has been put on glial cells since the function or existence of neuronal P2X7 receptor remained a matter of debate [108, 109]. However, recently it was reported that there is no detectable microglia activation and neuroinflammation under sub-chronic PCP treatment [91]. Nevertheless, this study did

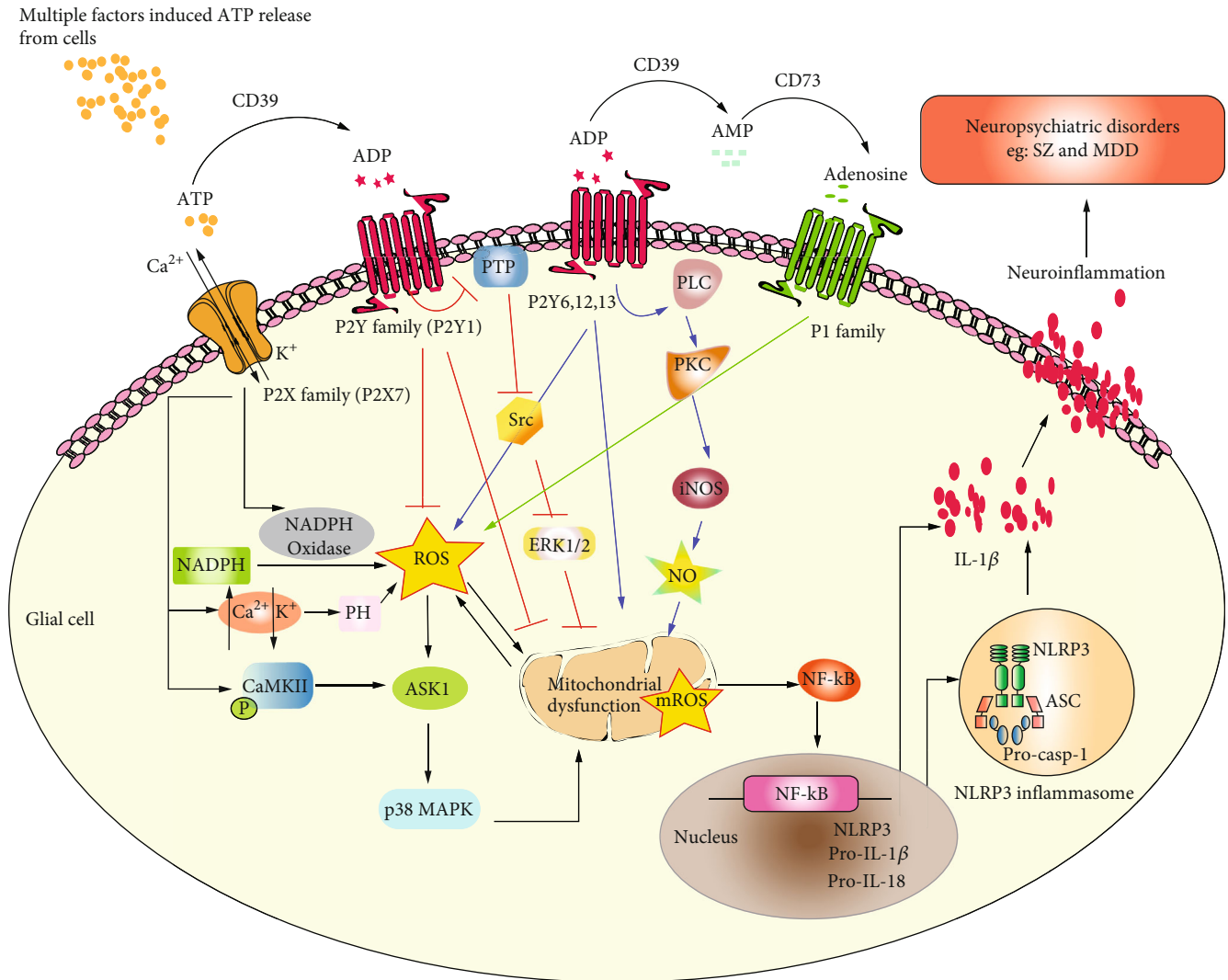


FIGURE 1: “Glial purinergic-oxidative stress” (“GPOS”) hypothesis in neuropsychiatric disorders (SZ and MDD). Multiple factor-induced ATP release from cells, on the one hand, is hydrolyzed into ADP, AMP, and adenosine in the presence of CD39 and CD73. On the other hand, ATP, ADP, and adenosine receptors triggering an intracellular pathway. The P2X family especially P2X7 activation by ATP increases the ROS through several pathways, including to activate NADPH oxidase, to adjust pH level, and to phosphorylate CaMKII. The increase in ROS further activates ASK1/p38 MAPK, subsequently resulting in mitochondrial dysfunction. In the P2Y family, P2Y1 exerts a protective role in suppressing ROS overproduction through inhibiting the PTP/Src ERK1/2 pathway. In contrast, P2Y6, 12, and 13 increase ROS by activating PLC/PKC/NO. P1 family activation also could elevate the ROS production. ROS overproduction interacts with mitochondrial dysfunction; could activate and translocate NF- $\kappa$ B to the nucleus and increase inflammatory cytokine gene expression, especially IL-1 $\beta$ , IL-8, and NLRP3. After NLRP3 inflammasome assembly, mature IL-1 $\beta$  and IL-8 could be released from the glia cell and cause neuroinflammation further contributing to neuropsychiatric disorders such as SZ and MDD.

not check the activation of glial cells in a chronic model and OS markers. In a rat SZ model, PCP administration could generate OS in hippocampus by measuring OS marker nitrotyrosine and chronic antipsychotics quetiapine application could significantly attenuate OS and object recognition memory impairment [110]. Therefore, more direct evidence should be provided in future to elucidate whether the regulation of P2X7 on PCP-induced SZ via glial involved OS.

**3.2. GPOS in MDD.** Major depressive disorder (MDD) is a common psychiatric disease prevalent worldwide and characterized by severe and persistent emotional symptoms (feelings of guilt and anhedonia), cognitive symptoms (low self-esteem)

and somatic symptoms (loss of sleeplessness and mental irritancy). Compared to SZ, purinergic signaling also received relatively considerable attention in MDD. The excellent review from Bartoli et al. elaborately summarized the promising role of the purinergic system in depression, highlighting potential antidepressant effect of A2A and P2X7 selective antagonists and detection of purinergic system peripheral metabolites as biomarkers of depression [111].

Recent reviews have also summarized the evidence from both human and animal studies concerning the involvement of the adenosinergic system in pathophysiology and treatment of MDD [112, 113]. In these two reviews, authors collected evidence in support of the involvement of the

adenosinergic system in MDD from adenosine synthesis, adenosine cleanup, and catabolism to adenosine receptor regulation. Herein, we only focused on the glial-related purinergic system in MDD. It is well known that sleeplessness, one of typical symptoms of MDD, was related to the level of adenosine [114, 115]. Sleep deprivation for 12 h led to the elevation of adenosine levels in the rodent frontal cortex. Importantly, astrocyte was capable of modulating changes in nonrapid eye movement slow wave activity in response to sleep deprivation [116, 117]. Another study found that selective expression of dnSNARE (dominant negative SNARE domain of the vesicle protein VAMP2) in astrocytes reduced extracellular adenosine accumulation mediated by the A1 receptor [118]. Wakefulness is related to high neuronal metabolism to maintain neuronal activity, which requires a great amount of oxygen, further resulting in oxidant production. Thus, sleep was a particularly important process for the brain to recover or increase antioxidant activity against free radicals such as ROS and RNS [119]. Together, we speculate that the regulation of the astrocytic A1 receptor in sleep might undergo OS pathways.

Along with adenosine, ATP signaling via the P2 receptor might also play a pivotal role in the neuropathological mechanisms of MDD. The blockade of P2 receptors has been shown antidepressant-like effects in the animal model [120]. Among P2 receptors, the P2X7 receptor has received lot of research interest. Polymorphism research pointed out the association of nonsynonymous coding of single-nucleotide polymorphism (SNP) rs2230912 in the P2X7 gene with MDD [121, 122]. Evidence showed an antidepressant-like profile and higher responsivity to the antidepressant treatment in P2X7 knockout mice [123, 124]. Most of studies emphasized that the antidepressant effect induced by P2X7 blockage was a result of monoamine and glutamate regulation [120, 121]. Indeed, P2X7 activation induced neuroinflammation might contribute to pathogenesis of MDD, although the role of direct neuronal mechanisms cannot be excluded either.

P2X7 receptor and its mediated signaling pathway play an important role in microglia activation. In microglia, there are two major inflammatory pathways involved into P2X7 activation, including P2X7/NLRP3/IL-1 $\beta$  [125] and P2X7/NF- $\kappa$ B/IL-1 $\beta$ . Chronic uncontrolled stress was a major cause of depression, which led to the activation of caspase-1 by the NLRP3 inflammasome, followed by production of inflammatory cytokine such as IL-18 and IL-1 $\beta$  [126]. In MDD model, the increased expression of NLRP3 inflammasome mRNA and IL-1 $\beta$  have been detected after LPS application, suggesting NLRP3 inflammasome and IL-1 $\beta$  acted as mediators of inflammation [127]. Similarly, the enhancement of IL-1 $\beta$  signaling in the hippocampus led to the development of depressive symptoms [128]. P2X7 activation could directly activate NLRP3, further resulting in IL-1 $\beta$  release. Besides this, the activation of inflammasome in microglia required potassium efflux, ROS production and cathepsin B function [129]. In particular, inflammasome-activating signal reactive oxygen species (mtROS) served as direct activator of the NLRP3: ASC: pro-Caspase-1 complex [130]. Another essential element for NLRP3-inflammasome activation is the transcription factor NF- $\kappa$ B, which acts

downstream of TLRs and other immune receptors. Surprisingly, P2X7 activation also served as the upstream signaling molecule of NF- $\kappa$ B [131]. NF- $\kappa$ B signaling could be activated and repressed by ROS in a phase and context dependent manner. The NF- $\kappa$ B pathway can have both anti- and prooxidant roles in the setting of OS [132]. Together with previous evidence showing that P2X7 activation caused ROS overproduction, we could assume that P2X7 activation induced inflammation pathway probably interacts with the OS pathway, contributing to the development of MDD.

#### 4. Conclusive Remarks and Perspective

Based on evidence showing that the purinergic system participates in the regulation of oxidative/antioxidative pathways in glial cells, we proposed a new neuropathological hypothesis termed as “GPOS” (glial purinergic system-mediated OS) for the first time. Then, we collectively elucidated the participation of the glial purinergic system in SZ and MDD and discussed the potential application of “GPOS” in neuropsychiatric disorders (Figure 1). However, there are still questions to be answered in support of this hypothesis. First of all, the direct evidence should be provided to confirm the role of “GPOS” in neuropsychiatric disorders and in other neurodegenerative disorders. Secondly, cell type-specific or subgroup dominant regulation of the purinergic system should be addressed by using multiple genetic manipulation approaches. Thirdly, given the correlation between redox status and the vitagenes network and its possible biological relevance in neuroprotection, it is important to further address whether it is a hormesis-dependent mechanism in neurodegenerative/neuroprotective disorders [133–136]. Whether the purinergic system alters oxidant/antioxidant balance or hormesis response in a neurodevelopment manner also should be further confirmed. And whether or not GPOS will be a potential promising target for the treatment of SZ and MDD, it is necessary to shorten the gap between the basic and translational research.

#### Conflicts of Interest

The authors declare no conflict of interest.

#### Acknowledgments

This work was supported by the Hungarian Research and Development Fund (grant number 131629); the Hungarian Brain Research Program (2017-1.2.1-NKP-2017-00002 to B.S.); the European Union’s Horizon 2020 Research, Innovation Programme under the Marie Skłodowska Curie grant agreement no. 766124, where LH is a recipient of the Marie-Curie PhD fellowship; the Project First-Class Disciplines Development of Chengdu University of Traditional Chinese Medicine (CZYHW1901); the Science and Technology Program of Sichuan Province, China (2019YFH0108); and the Innovation Team and Talents Cultivation Program of National Administration of Traditional Chinese Medicine (ZYYCXTD-D-202003).

## References

- [1] G. Burnstock, "Introduction to purinergic signaling," in *Purinergic Signaling*, pp. 1–15, Humana, New York, 2020.
- [2] M. P. Abbracchio, K. A. Jacobson, C. E. Müller, and H. Zimmermann, "Professor Dr. Geoffrey Burnstock (1929–2020)," vol. 16, no. 2, pp. 137–149, 2020.
- [3] A. Verkhratsky, H. Zimmermann, M. P. Abbracchio, P. Illes, and F. DiVirgilio, "In memoriam Geoffrey Burnstock: creator of purinergic signaling," *Function*, vol. 1, no. 1, 2020.
- [4] G. Burnstock, "Introductory overview of purinergic signaling," *Frontiers in Bioscience (Elite Edition)*, vol. 3, no. 1, pp. 896–900, 2011.
- [5] P. Illes, C. E. Müller, K. A. Jacobson et al., "Update of P2X receptor properties and their pharmacology: IUPHAR review 30," *British Journal of Pharmacology*, vol. 178, no. 3, pp. 489–514, 2021.
- [6] K. A. Jacobson, E. G. Delicado, C. Gachet et al., "Update of P2Y receptor pharmacology: IUPHAR review 27," *British Journal of Pharmacology*, vol. 177, no. 11, pp. 2413–2433, 2020.
- [7] L. Huang, L. Otrókocsi, and B. Sperlágh, "Role of P2 receptors in normal brain development and in neurodevelopmental psychiatric disorders," *Brain Research Bulletin*, vol. 151, pp. 55–64, 2019.
- [8] B. S. Thawkar and G. Kaur, "Inhibitors of NF- $\kappa$ B and P2X7/NLRP3/caspase 1 pathway in microglia: novel therapeutic opportunities in neuroinflammation induced early-stage Alzheimer's disease," *Journal of Neuroimmunology*, vol. 326, pp. 62–74, 2019.
- [9] M. Cieślak and A. Wojtczak, "Role of purinergic receptors in the Alzheimer's disease," *Purinergic Signalling*, vol. 14, no. 4, pp. 331–344, 2018.
- [10] A. Tóth, Z. Antal, D. Bereczki, and B. Sperlágh, "Purinergic signalling in Parkinson's disease: a multi-target system to combat neurodegeneration," *Neurochemical Research*, vol. 44, no. 10, pp. 2413–2422, 2019.
- [11] T. Glaser, R. Andrejew, A. Oliveira-Giacomelli et al., "Purinergic receptors in basal ganglia diseases: shared molecular mechanisms between Huntington's and Parkinson's disease," *Neuroscience bulletin*, vol. 36, no. 11, pp. 1299–1314, 2020.
- [12] P. Fabbri, S. Apolloni, A. Bianchi et al., "P2X7 activation enhances skeletal muscle metabolism and regeneration in SOD1G93A mouse model of amyotrophic lateral sclerosis," *Brain Pathology*, vol. 30, no. 2, pp. 272–282, 2020.
- [13] B. Koványi, C. Csölle, S. Calovi et al., "The role of P2X7 receptors in a rodent PCP-induced schizophrenia model," *Scientific Reports*, vol. 6, no. 1, pp. 1–16, 2016.
- [14] P. Illes, A. Verkhratsky, and Y. Tang, "Pathological ATPergic signaling in major depression and bipolar disorder," *Frontiers in Molecular Neuroscience*, vol. 12, p. 331, 2020.
- [15] G. Horváth, L. Otrókocsi, K. Beko et al., "P2X7 receptors drive poly (I: C) induced autism-like behavior in mice," *Journal of Neuroscience*, vol. 39, no. 13, pp. 2542–2561, 2019.
- [16] H. I. Chen, W. S. Hu, M. Y. Hung et al., "Protective effects of luteolin against oxidative stress and mitochondrial dysfunction in endothelial cells," *Nutrition Metabolism and Cardiovascular Diseases*, vol. 30, no. 6, pp. 1032–1043, 2020.
- [17] A. Singh, R. Kukreti, L. Saso, and S. Kukreti, "Oxidative stress: a key modulator in neurodegenerative diseases," *Molecules*, vol. 24, no. 8, p. 1583, 2019.
- [18] R. Wadhwa, R. Gupta, and P. K. Maurya, "Oxidative stress and accelerated aging in neurodegenerative and neuropsychiatric disorder," *Current Pharmaceutical Design*, vol. 24, no. 40, pp. 4711–4725, 2018.
- [19] N. J. Allen and D. A. Lyons, "Glia as architects of central nervous system formation and function," *Science*, vol. 362, no. 6411, pp. 181–185, 2018.
- [20] I. D. Akinrinade, A. E. Memudu, O. M. Ogundele, and O. I. Ajetunmobi, "Interplay of glia activation and oxidative stress formation in fluoride and aluminium exposure," *Pathophysiology*, vol. 22, no. 1, pp. 39–48, 2015.
- [21] N. Khansari, Y. Shakiba, and M. Mahmoudi, "Chronic inflammation and oxidative stress as a major cause of age-related diseases and cancer," *Recent Patents on Inflammation & Allergy Drug Discovery*, vol. 3, no. 1, pp. 73–80, 2009.
- [22] D. M. Hardbower, T. de Sablet, R. Chaturvedi, and K. T. Wilson, "Chronic inflammation and oxidative stress: the smoking gun for Helicobacter pylori-induced gastric cancer?," *Gut Microbes*, vol. 4, no. 6, pp. 475–481, 2013.
- [23] D. W. Moss and T. E. Bates, "Activation of murine microglial cell lines by lipopolysaccharide and interferon- $\gamma$  causes NO-mediated decreases in mitochondrial and cellular function," *European Journal of Neuroscience*, vol. 13, no. 3, pp. 529–538, 2001.
- [24] Y.-J. Kim, S.-Y. Hwang, O. Eok-Soo, O. Seikwan, and I.-O. Han, "IL-1 $\beta$ , an immediate early protein secreted by activated microglia, induces iNOS/NO in C6 astrocytoma cells through p38 MAPK and NF- $\kappa$ B pathways," *Journal of Neuroscience Research*, vol. 84, no. 5, pp. 1037–1046, 2006.
- [25] L. Connelly, M. Palacios-Callender, C. Ameixa, S. Moncada, and A. J. Hobbs, "Biphasic regulation of NF- $\kappa$ B activity underlies the pro- and anti-inflammatory actions of nitric oxide," *The Journal of Immunology*, vol. 166, no. 6, pp. 3873–3881, 2001.
- [26] N. R. Bhat, Q. Shen, and F. Fan, "TAK1-mediated induction of nitric oxide synthase gene expression in glial cells," *Journal of Neurochemistry*, vol. 87, no. 1, pp. 238–247, 2003.
- [27] J. Wen, R. Ribeiro, and Y. Zhang, "Specific PKC isoforms regulate LPS-stimulated iNOS induction in murine microglial cells," *Journal of Neuroinflammation*, vol. 8, no. 1, pp. 1–13, 2011.
- [28] L. Yan, S. Liu, C. Wang et al., "JNK and NADPH oxidase involved in fluoride-induced oxidative stress in BV-2 microglia cells," *Mediators of Inflammation*, vol. 2013, 10 pages, 2013.
- [29] J. Park, J.-S. Min, B. Kim et al., "Mitochondrial ROS govern the LPS-induced pro-inflammatory response in microglia cells by regulating MAPK and NF- $\kappa$ B pathways," *Neuroscience Letters*, vol. 584, pp. 191–196, 2015.
- [30] C. C. Chao, J. R. Lokensgard, W. S. Sheng, S. Hu, and P. K. Peterson, "IL-1-induced iNOS expression in human astrocytes via NF- $\kappa$ B," *Neuroreport*, vol. 8, no. 14, pp. 3163–3166, 1997.
- [31] W.-Y. Wang, M.-S. Tan, J.-T. Yu, and L. Tan, "Role of pro-inflammatory cytokines released from microglia in Alzheimer's disease," *Annals of Translational Medicine*, vol. 3, no. 10, 2015.
- [32] M. Moriyama, S. Fujitsuka, K. Kawabe, K. Takano, and Y. Nakamura, "Zinc potentiates lipopolysaccharide-induced nitric oxide production in cultured primary rat astrocytes," *Neurochemical Research*, vol. 43, no. 2, pp. 363–374, 2018.



- [33] H. M. Ko, S. H. Lee, M. Bang et al., "Tyrosine kinase Fyn regulates iNOS expression in LPS-stimulated astrocytes via modulation of ERK phosphorylation," *Biochemical and Biophysical Research Communications*, vol. 495, no. 1, pp. 1214–1220, 2018.
- [34] G. A. Cabral-Pacheco, I. Garza-Veloz, J. M. Ramirez-Acuña et al., "The roles of matrix metalloproteinases and their inhibitors in human diseases," *International Journal of Molecular Sciences*, vol. 21, no. 24, p. 9739, 2020.
- [35] W.-H. Tung, H.-W. Tsai, I.-T. Lee et al., "Japanese encephalitis virus induces matrix metalloproteinase-9 in rat brain astrocytes via NF- $\kappa$ B signalling dependent on MAPKs and reactive oxygen species," *British Journal of Pharmacology*, vol. 161, no. 7, pp. 1566–1583, 2010.
- [36] C.-C. Yang, L.-D. Hsiao, H.-C. Tseng, C.-M. Kuo, and C.-M. Yang, "Pristimerin inhibits MMP-9 expression and cell migration through attenuating NOX/ROS-dependent NF- $\kappa$ B activation in rat brain astrocytes challenged with LPS," *Journal of Inflammation Research*, vol. Volume 13, pp. 325–341, 2020.
- [37] N. R. Bhat and P. Zhang, "Hydrogen peroxide activation of multiple mitogen-activated protein kinases in an oligodendrocyte cell line," *Journal of Neurochemistry*, vol. 72, no. 1, pp. 112–119, 1999.
- [38] W. Tu, H. Wang, S. Li, Q. Liu, and H. Sha, "The anti-inflammatory and anti-oxidant mechanisms of the Keap1/Nrf2/ARE signaling pathway in chronic diseases," *Aging and Disease*, vol. 10, no. 3, pp. 637–651, 2019.
- [39] S. A. Onasanwo, R. Velagapudi, A. El-Bakoush, and O. A. Olajide, "Inhibition of neuroinflammation in BV2 microglia by the biflavonoid kolaviron is dependent on the Nrf2/ARE antioxidant protective mechanism," *Molecular and Cellular Biochemistry*, vol. 414, no. 1-2, pp. 23–36, 2016.
- [40] Y. Zheng, G. Zhu, J. He, G. Wang, D. Li, and F. Zhang, "Icariin targets Nrf2 signaling to inhibit microglia-mediated neuroinflammation," *International Immunopharmacology*, vol. 73, pp. 304–311, 2019.
- [41] T. P. Williamson, D. A. Johnson, and J. A. Johnson, "Activation of the Nrf2-ARE pathway by siRNA knockdown of Keap1 reduces oxidative stress and provides partial protection from MPTP-mediated neurotoxicity," *Neurotoxicology*, vol. 33, no. 3, pp. 272–279, 2012.
- [42] Z. Zhou, C. Liu, S. Chen et al., "Activation of the Nrf2/ARE signaling pathway by probucol contributes to inhibiting inflammation and neuronal apoptosis after spinal cord injury," *Oncotarget*, vol. 8, no. 32, pp. 52078–52093, 2017.
- [43] P. Ren, J. Chen, B. Li et al., "Nrf2 ablation promotes Alzheimer's disease-like pathology in APP/PS1 transgenic mice: the role of neuroinflammation and oxidative stress," *Oxidative medicine and cellular longevity*, vol. 2020, 13 pages, 2020.
- [44] A. Nellesen, S. Nyamoya, A. Zendedel et al., "Nrf2 deficiency increases oligodendrocyte loss, demyelination, neuroinflammation and axonal damage in an MS animal model," *Metabolic Brain Disease*, vol. 35, no. 2, pp. 353–362, 2020.
- [45] D. Nuccio, A. B. Chiara, C. Troiano et al., "NRF2 and PPAR- $\gamma$  pathways in oligodendrocyte progenitors: focus on ROS protection, mitochondrial biogenesis and promotion of cell differentiation," *International Journal of Molecular Sciences*, vol. 21, no. 19, p. 7216, 2020.
- [46] C. De Nuccio, A. Bernardo, C. Cruciani, R. De Simone, S. Visentin, and L. Minghetti, "Peroxisome proliferator activated receptor- $\gamma$  agonists protect oligodendrocyte progenitors against tumor necrosis factor-alpha-induced damage: effects on mitochondrial functions and differentiation," *Experimental Neurology*, vol. 271, pp. 506–514, 2015.
- [47] D. Nuccio, A. B. Chiara, R. De Simone et al., "Peroxisome proliferator-activated receptor  $\gamma$  agonists accelerate oligodendrocyte maturation and influence mitochondrial functions and oscillatory Ca<sup>2+</sup> waves," *Journal of Neuropathology & Experimental Neurology*, vol. 70, no. 10, pp. 900–912, 2011.
- [48] L. Qin, Y. Liu, T. Wang et al., "NADPH oxidase mediates lipopolysaccharide-induced neurotoxicity and proinflammatory gene expression in activated microglia," *Journal of Biological Chemistry*, vol. 279, no. 2, pp. 1415–1421, 2004.
- [49] K. Bedard and K.-H. Krause, "The NOX family of ROS-generating NADPH oxidases: physiology and pathophysiology," *Physiological Reviews*, vol. 87, no. 1, pp. 245–313, 2007.
- [50] J. Haslund-Vinding, G. McBean, V. Jaquet, and F. Vilhardt, "NADPH oxidases in oxidant production by microglia: activating receptors, pharmacology and association with disease," *British Journal of Pharmacology*, vol. 174, no. 12, pp. 1733–1749, 2017.
- [51] Y. J. Yauger, S. Bermudez, K. E. Moritz, E. Glaser, B. Stoica, and K. R. Byrnes, "Iron accentuated reactive oxygen species release by NADPH oxidase in activated microglia contributes to oxidative stress in vitro," *Journal of Neuroinflammation*, vol. 16, no. 1, pp. 1–15, 2019.
- [52] S.-H. Choi, S. Aid, H.-W. Kim, S. H. Jackson, and F. Bosetti, "Inhibition of NADPH oxidase promotes alternative and anti-inflammatory microglial activation during neuroinflammation," *Journal of Neurochemistry*, vol. 120, no. 2, pp. 292–301, 2012.
- [53] A. I. Rodriguez-Perez, A. Borrajo, J. Rodriguez-Pallares, M. J. Guerra, and J. L. Labandeira-Garcia, "Interaction between NADPH-oxidase and Rho-kinase in angiotensin II-induced microglial activation," *Glia*, vol. 63, no. 3, pp. 466–482, 2015.
- [54] A. Y. Abramov, J. Jacobson, F. Wientjes, J. Hothersall, L. Canevari, and M. R. Duchen, "Expression and modulation of an NADPH oxidase in mammalian astrocytes," *Journal of Neuroscience*, vol. 25, no. 40, pp. 9176–9184, 2005.
- [55] J. T. Johnstone, P. D. Morton, A. R. Jayakumar et al., "Inhibition of NADPH oxidase activation in oligodendrocytes reduces cytotoxicity following trauma," *PLoS One*, vol. 8, no. 11, article e80975, 2013.
- [56] R. Accetta, S. Damiano, A. Morano et al., "Reactive oxygen species derived from NOX3 and NOX5 drive differentiation of human oligodendrocytes," *Frontiers in Cellular Neuroscience*, vol. 10, p. 146, 2016.
- [57] F. Vilhardt, J. Haslund-Vinding, V. Jaquet, and G. McBean, "Microglia antioxidant systems and redox signalling," *British Journal of Pharmacology*, vol. 174, no. 12, pp. 1719–1732, 2017.
- [58] R. Dringen, M. Brandmann, M. C. Hohnholt, and E.-M. Blumrich, "Glutathione-dependent detoxification processes in astrocytes," *Neurochemical Research*, vol. 40, no. 12, pp. 2570–2582, 2015.
- [59] T. A. Sarafian, C. Montes, T. Imura et al., "Disruption of astrocyte STAT3 signaling decreases mitochondrial function and increases oxidative stress in vitro," *PLoS One*, vol. 5, no. 3, article e9532, 2010.
- [60] N. Shulga and J. G. Pastorino, "GRIM-19 mediated translocation of STAT3 to mitochondria is necessary for TNF induced

- necroptosis," *Journal of Cell Science*, vol. 125, no. 12, pp. 2995–3003, 2012.
- [61] A. Horvat, F.-W. Schwaiger, G. Hager et al., "A novel role for protein tyrosine phosphatase shp1 in controlling glial activation in the normal and injured nervous system," *Journal of Neuroscience*, vol. 21, no. 3, pp. 865–874, 2001.
- [62] P. T. Massa, S. Saha, C. Wu, and K. W. Jarosinski, "Expression and function of the protein tyrosine phosphatase SHP-1 in oligodendrocytes," *Glia*, vol. 29, no. 4, pp. 376–385, 2000.
- [63] A. Tanaka, K. Nishida, H. Okuda et al., "Peroxynitrite treatment reduces adenosine uptake via the equilibrative nucleoside transporter in rat astrocytes," *Neuroscience Letters*, vol. 498, no. 1, pp. 52–56, 2011.
- [64] K. M. Choi, S. J. Gibbons, T. V. Nguyen et al., "Heme oxygenase-1 protects interstitial cells of Cajal from oxidative stress and reverses diabetic gastroparesis," *Gastroenterology*, vol. 135, no. 6, pp. 2055–2064.e2, 2008.
- [65] E. González-Fernández, M. V. Sánchez-Gómez, A. Pérez-Samartín, R. O. Arellano, and C. Matute, "A3 adenosine receptors mediate oligodendrocyte death and ischemic damage to optic nerve," *Glia*, vol. 62, no. 2, pp. 199–216, 2014.
- [66] S. Gao, N. Li, Y. Wang, Y. Zhong, and X. Shen, "Blockade of adenosine A2A receptor protects photoreceptors after retinal detachment by inhibiting inflammation and oxidative stress," *Oxidative Medicine and Cellular Longevity*, vol. 2020, 12 pages, 2020.
- [67] J. Saura, E. Angulo, A. Ejarque et al., "Adenosine A2A receptor stimulation potentiates nitric oxide release by activated microglia," *Journal of Neurochemistry*, vol. 95, no. 4, pp. 919–929, 2005.
- [68] A. Melani, S. Amadio, M. Gianfriddo et al., "P2X7 receptor modulation on microglial cells and reduction of brain infarct caused by middle cerebral artery occlusion in rat," *Journal of Cerebral Blood Flow & Metabolism*, vol. 26, no. 7, pp. 974–982, 2006.
- [69] S. Y. Kim, J. H. Moon, H. G. Lee, S. U. Kim, and Y. B. Lee, "ATP released from  $\beta$ -amyloid-stimulated microglia induces reactive oxygen species production in an autocrine fashion," *Experimental & Molecular Medicine*, vol. 39, no. 6, pp. 820–827, 2007.
- [70] B. Wang and R. Sluyter, "P2X7 receptor activation induces reactive oxygen species formation in erythroid cells," *Purinergic Signalling*, vol. 9, no. 1, pp. 101–112, 2013.
- [71] P. Sekar, D.-Y. Huang, S.-F. Chang, and W.-W. Lin, "Coordinate effects of P2X7 and extracellular acidification in microglial cells," *Oncotarget*, vol. 9, no. 16, pp. 12718–12731, 2018.
- [72] L. K. Parvathenani, S. Tertysnikova, C. R. Greco, S. B. Roberts, B. Robertson, and R. Posmantur, "P2X<sub>7</sub> mediates superoxide production in primary microglia and is up-regulated in a transgenic mouse model of Alzheimer's disease," *Journal of Biological Chemistry*, vol. 278, no. 15, pp. 13309–13317, 2003.
- [73] G. Martel-Gallegos, G. Casas-Pruneda, F. Ortega-Ortega et al., "Oxidative stress induced by P2X7 receptor stimulation in murine macrophages is mediated by c-Src/Pyk2 and ERK1/2," *Biochimica et Biophysica Acta (BBA)-General Subjects*, vol. 1830, no. 10, pp. 4650–4659, 2013.
- [74] Y. Hirata, Y. Nada, Y. Yamada et al., "Elaidic acid potentiates extracellular ATP-induced apoptosis via the P2X<sub>7</sub>-ROS-ASK1-p38 axis in microglial cell lines," *Biological and Pharmaceutical Bulletin*, vol. 43, no. 10, pp. 1562–1569, 2020.
- [75] Y. Lin, H. Lin, M. Lin et al., "Hydrogen peroxide reduced ATPase activity and the levels of ATP, ADP, and energy charge and its association with pulp breakdown occurrence of longan fruit during storage," *Food Chemistry*, vol. 311, p. 126008, 2020.
- [76] P. Sekar, D.-Y. Huang, S.-L. Hsieh, S.-F. Chang, and W.-W. Lin, "AMPK-dependent and independent actions of P2X7 in regulation of mitochondrial and lysosomal functions in microglia," *Cell Communication and Signaling*, vol. 16, no. 1, pp. 1–15, 2018.
- [77] F. M. Munoz, P. A. Patel, X. Gao et al., "Reactive oxygen species play a role in P2X7 receptor-mediated IL-6 production in spinal astrocytes," *Purinergic Signalling*, vol. 16, no. 1, pp. 97–107, 2020.
- [78] Y. Shinozaki, S. Koizumi, S. Ishida, J.-I. Sawada, Y. Ohno, and K. Inoue, "Cytoprotection against oxidative stress-induced damage of astrocytes by extracellular ATP via P2Y1 receptors," *Glia*, vol. 49, no. 2, pp. 288–300, 2005.
- [79] T. Fujita, H. Tozaki-Saitoh, and K. Inoue, "P2Y1 receptor signaling enhances neuroprotection by astrocytes against oxidative stress via IL-6 release in hippocampal cultures," *Glia*, vol. 57, no. 3, pp. 244–257, 2009.
- [80] Y. Shinozaki, S. Koizumi, Y. Ohno, T. Nagao, and K. Inoue, "Extracellular ATP counteracts the ERK1/2-mediated death-promoting signaling cascades in astrocytes," *Glia*, vol. 54, no. 6, pp. 606–618, 2006.
- [81] S. Kahlert, T. Blaser, M. Tulapurkar, and G. Reiser, "P2Y receptor-activating nucleotides modulate cellular reactive oxygen species production in dissociated hippocampal astrocytes and neurons in culture independent of parallel cytosolic Ca<sup>2+</sup> rise and change in mitochondrial potential," *Journal of Neuroscience Research*, vol. 85, no. 15, pp. 3443–3456, 2007.
- [82] C. Quintas, D. Pinho, C. Pereira, L. Saraiva, J. Gonçalves, and G. Queiroz, "Microglia P2Y<sub>6</sub> receptors mediate nitric oxide release and astrocyte apoptosis," *Journal of Neuroinflammation*, vol. 11, no. 1, pp. 1–12, 2014.
- [83] S. Salim, "Oxidative stress and psychological disorders," *Current Neuropharmacology*, vol. 12, no. 2, pp. 140–147, 2014.
- [84] B. S. Pruetz and J. H. Meador-Woodruff, "Evidence for altered energy metabolism, increased lactate, and decreased pH in schizophrenia brain: a focused review and meta-analysis of human postmortem and magnetic resonance spectroscopy studies," *Schizophrenia Research*, vol. 223, pp. 29–42, 2020.
- [85] A. Bryll, J. Skrzypek, W. Krzyściak et al., "Oxidative-antioxidant imbalance and impaired glucose metabolism in schizophrenia," *Biomolecules*, vol. 10, no. 3, p. 384, 2020.
- [86] D. R. Lara, P. Belmonte-de-Abreu, and D. O. Souza, "Allopurinol for refractory aggression and self-inflicted behaviour," *Journal of Psychopharmacology*, vol. 14, no. 1, pp. 81–83, 2000.
- [87] D. R. Lara, M. R. S. Cruz, F. Xavier, D. O. Souza, and E. H. Moriguchi, "Allopurinol for the treatment of aggressive behaviour in patients with dementia," *International clinical psychopharmacology*, vol. 18, no. 1, pp. 53–55, 2003.
- [88] D. Boison, P. Singer, H.-Y. Shen, J. Feldon, and B. K. Yee, "Adenosine hypothesis of schizophrenia - opportunities for pharmacotherapy," *Neuropharmacology*, vol. 62, no. 3, pp. 1527–1543, 2012.
- [89] H. Koch, A. Bepalov, K. Drescher, H. Franke, and U. Krügel, "Impaired cognition after stimulation of P2Y<sub>1</sub> receptors in

- the rat medial prefrontal cortex,” *Neuropsychopharmacology*, vol. 40, no. 2, pp. 305–314, 2015.
- [90] C. Hempel, W. Nörenberg, H. Sobottka et al., “The phenothiazine-class antipsychotic drugs prochlorperazine and trifluoperazine are potent allosteric modulators of the human P2X7 receptor,” *Neuropharmacology*, vol. 75, pp. 365–379, 2013.
- [91] S. Calovi, P. Mut-Arbona, P. Tod et al., “P2X7 receptor-dependent layer-specific changes in neuron-microglia reactivity in the prefrontal cortex of a phencyclidine induced mouse model of schizophrenia,” *Frontiers in molecular neuroscience*, vol. 13, 2020.
- [92] J. Deckert, M. M. Nöthen, S. P. Bryant et al., “Mapping of the human adenosine A<sub>2A</sub> receptor gene: relationship to potential schizophrenia loci on chromosome 22q and exclusion from the CATCH 22 region,” *Human Genetics*, vol. 99, no. 3, pp. 326–328, 1997.
- [93] J. Miao, L. Lu, C. Yan et al., “Association between ADORA2A gene polymorphisms and schizophrenia in the North Chinese Han population,” *Neuropsychiatric Disease and Treatment*, vol. 15, pp. 2451–2458, 2019.
- [94] A. Turčin, V. Dolžan, S. Porcelli, A. Serretti, and B. K. Plesničar, “Adenosine hypothesis of antipsychotic drugs revisited: pharmacogenomics variation in nonacute schizophrenia,” *OmicS: A Journal of Integrative Biology*, vol. 20, no. 5, pp. 283–289, 2016.
- [95] R. Andrejew, Á. Oliveira-Giacomelli, D. E. Ribeiro et al., “The P2X7 receptor: central hub of brain diseases,” *Neuroscience*, vol. 13, p. 124, 2020.
- [96] J. I. Real, A. P. Simões, R. A. Cunha, S. G. Ferreira, and D. Rial, “Adenosine A<sub>2A</sub> receptors modulate the dopamine D<sub>2</sub> receptor-mediated inhibition of synaptic transmission in the mouse prefrontal cortex,” *European Journal of Neuroscience*, vol. 47, no. 9, pp. 1127–1134, 2018.
- [97] R. Franco, R. Rivas-Santisteban, M. Casanovas, A. Lillo, C. A. Saura, and G. Navarro, “Adenosine A<sub>2A</sub> receptor antagonists affects NMDA glutamate receptor function. Potential to address neurodegeneration in Alzheimer’s disease,” *Cells*, vol. 9, no. 5, p. 1075, 2020.
- [98] S. Ferré, J. Bonaventura, W. Zhu et al., “Essential control of the function of the striatopallidal neuron by pre-coupled complexes of adenosine A<sub>2A</sub>-dopamine D<sub>2</sub> receptor heterotetramers and adenylyl cyclase,” *Frontiers in pharmacology*, vol. 9, p. 243, 2018.
- [99] D. O. Borroto-Escuela, L. Ferraro, M. Narvaez et al., “Multiple adenosine-dopamine (A<sub>2A</sub>-D<sub>2</sub> like) heteroreceptor complexes in the brain and their role in schizophrenia,” *Cell*, vol. 9, no. 5, p. 1077, 2020.
- [100] S. J. Guzman, H. Schmidt, H. Franke et al., “P<sub>2</sub>Y<sub>1</sub> receptors inhibit long-term depression in the prefrontal cortex,” *Neuropharmacology*, vol. 59, no. 6, pp. 406–415, 2010.
- [101] G. Gonzalez-Burgos and D. A. Lewis, “GABA neurons and the mechanisms of network oscillations: implications for understanding cortical dysfunction in schizophrenia,” *Schizophrenia Bulletin*, vol. 34, no. 5, pp. 944–961, 2008.
- [102] N. Okamura, K. Hashimoto, E. Shimizu, C. Kumakiri, N. Komatsu, and M. Iyo, “Adenosine A<sub>1</sub> receptor agonists block the neuropathological changes in rat retrosplenial cortex after administration of the NMDA receptor antagonist dizocilpine,” *Neuropsychopharmacology*, vol. 29, no. 3, pp. 544–550, 2004.
- [103] B. Ozyurt, H. Ozyurt, N. Akpolat, H. Erdogan, and M. Sarsilmaz, “Oxidative stress in prefrontal cortex of rat exposed to MK-801 and protective effects of CAPE,” *Progress in Neuro-Psychopharmacology and Biological Psychiatry*, vol. 31, no. 4, pp. 832–838, 2007.
- [104] K. Kuroda, K. Suzumura, T. Shirakawa et al., “Investigation of mechanisms for MK-801-induced neurotoxicity utilizing metabolomic approach,” *Toxicological Sciences*, vol. 146, no. 2, pp. 344–353, 2015.
- [105] M. Matos, H. Y. Shen, E. Augusto et al., “Deletion of adenosine A<sub>2A</sub> receptors from astrocytes disrupts glutamate homeostasis leading to psychomotor and cognitive impairment: relevance to schizophrenia,” *Biological Psychiatry*, vol. 78, no. 11, pp. 763–774, 2015.
- [106] A. G. Orr, E. C. Hsiao, M. M. Wang et al., “Astrocytic adenosine receptor A<sub>2A</sub> and G<sub>s</sub>-coupled signaling regulate memory,” *Nature neuroscience*, vol. 18, no. 3, pp. 423–434, 2015.
- [107] A. Verkhratsky and E. C. Toescu, “Neuronal-glia networks as substrate for CNS integration,” *Journal of Cellular and Molecular Medicine*, vol. 10, no. 4, pp. 869–879, 2006.
- [108] M. Miras-Portugal, Á. Sebastián-Serrano, L. de Diego García, and M. Díaz-Hernández, “Neuronal P2X7 receptor: involvement in neuronal physiology and pathology,” *Journal of Neuroscience*, vol. 37, no. 30, pp. 7063–7072, 2017.
- [109] B. Sperlágh, A. Köfalvi, J. Deuchars et al., “Involvement of P2X7 receptors in the regulation of neurotransmitter release in the rat hippocampus,” *Journal of Neurochemistry*, vol. 81, no. 6, pp. 1196–1211, 2002.
- [110] J. He, F. Liu, Z. Qian et al., “Chronic administration of quetiapine attenuates the phencyclidine-induced recognition memory impairment and hippocampal oxidative stress in rats,” *Neuroreport*, vol. 29, no. 13, pp. 1099–1103, 2018.
- [111] F. Bartoli, G. Burnstock, C. Crocamo, and G. Carrà, “Purinergic signaling and related biomarkers in depression,” *Brain Sciences*, vol. 10, no. 3, p. 160, 2020.
- [112] J. I. Gomes, M. Farinha-Ferreira, N. Rei et al., “Of adenosine and the blues: the adenosinergic system in the pathophysiology and treatment of major depressive disorder,” *Pharmacological Research*, vol. 163, article 105363, 2021.
- [113] N. Gass, H. M. Ollila, S. Utge et al., “Contribution of adenosine related genes to the risk of depression with disturbed sleep,” *Journal of Affective Disorders*, vol. 126, no. 1–2, pp. 134–139, 2010.
- [114] D. J. Hines and P. G. Haydon, “Astrocytic adenosine: from synapses to psychiatric disorders,” *Philosophical Transactions of the Royal Society B: Biological Sciences*, vol. 369, no. 1654, p. 20130594, 2014.
- [115] M. M. Halassa, C. Florian, T. Fellin et al., “Astrocytic modulation of sleep homeostasis and cognitive consequences of sleep loss,” *Neuron*, vol. 61, no. 2, pp. 213–219, 2009.
- [116] T. Blutstein and P. G. Haydon, “The importance of astrocyte-derived purines in the modulation of sleep,” *Glia*, vol. 61, no. 2, pp. 129–139, 2013.
- [117] C. Florian, C. G. Vecsey, M. M. Halassa, P. G. Haydon, and T. Abel, “Astrocyte-derived adenosine and A<sub>1</sub> receptor activity contribute to sleep loss-induced deficits in hippocampal synaptic plasticity and memory in mice,” *Journal of Neuroscience*, vol. 31, no. 19, pp. 6956–6962, 2011.
- [118] E. Reimund, “The free radical flux theory of sleep,” *Medical Hypotheses*, vol. 43, no. 4, pp. 231–233, 1994.

- [119] C. R. A. F. Diniz, M. Rodrigues, P. C. Casarotto et al., "Monoamine involvement in the antidepressant-like effect induced by P2 blockade," *Brain Research*, vol. 1676, pp. 19–27, 2017.
- [120] A. M. Basso, N. A. Bratcher, R. R. Harris, M. F. Jarvis, M. W. Decker, and L. E. Rueter, "Behavioral profile of P2X<sub>7</sub> receptor knockout mice in animal models of depression and anxiety: relevance for neuropsychiatric disorders," *Behavioural Brain Research*, vol. 198, no. 1, pp. 83–90, 2009.
- [121] S. Lucae, D. Salyakina, N. Barden et al., "P2RX7, a gene coding for a purinergic ligand-gated ion channel, is associated with major depressive disorder," *Human Molecular Genetics*, vol. 15, no. 16, pp. 2438–2445, 2006.
- [122] A. Vereczkei, O. Abdul-Rahman, Z. Halmi et al., "Association of purinergic receptor P2RX7 gene polymorphisms with depression symptoms," *Progress in Neuro-Psychopharmacology and Biological Psychiatry*, vol. 92, pp. 207–216, 2019.
- [123] A. A. Boucher, J. C. Arnold, G. E. Hunt et al., "Resilience and reduced c-Fos expression in P2X7 receptor knockout mice exposed to repeated forced swim test," *Neuroscience*, vol. 189, pp. 170–177, 2011.
- [124] L. Papp, E. S. Vizi, and B. Sperl agh, "Lack of ATP-evoked GABA and glutamate release in the hippocampus of P2X7 receptor−/− mice," *Neuroreport*, vol. 15, no. 15, pp. 2387–2391, 2004.
- [125] D. Wang, H. Wang, H. Gao et al., "P2X7 receptor mediates NLRP3 inflammasome activation in depression and diabetes," *Cell & Bioscience*, vol. 10, no. 1, pp. 1–9, 2020.
- [126] M. Iwata, K. T. Ota, X.-Y. Li et al., "Psychological stress activates the inflammasome via release of adenosine triphosphate and stimulation of the purinergic type 2X7 receptor," *Biological Psychiatry*, vol. 80, no. 1, pp. 12–22, 2016.
- [127] Y. Zhang, L. Liu, Y.-L. Peng et al., "Involvement of inflammasome activation in lipopolysaccharide-induced mice depressive-like behaviors," *CNS neuroscience & therapeutics*, vol. 20, no. 2, pp. 119–124, 2014.
- [128] D. Kovacs, N. Eszlari, P. Petschner et al., "Effects of IL1B single nucleotide polymorphisms on depressive and anxiety symptoms are determined by severity and type of life stress," *Brain, Behavior, and Immunity*, vol. 56, pp. 96–104, 2016.
- [129] A. Gustin, M. Kirchmeyer, E. Koncina et al., "NLRP3 inflammasome is expressed and functional in mouse brain microglia but not in astrocytes," *PLoS One*, vol. 10, no. 6, article e0130624, 2015.
- [130] Z. Zhong, Y. Zhai, S. Liang et al., "TRPM2 links oxidative stress to NLRP3 inflammasome activation," *Nature Communications*, vol. 4, no. 1, pp. 1–11, 2013.
- [131] Y. Liu, Y. Xiao, and Z. Li, "P2X7 receptor positively regulates MyD88-dependent NF-κB activation," *Cytokine*, vol. 55, no. 2, pp. 229–236, 2011.
- [132] T. Lawrence, "The nuclear factor NF-kappaB pathway in inflammation," *Cold Spring Harbor Perspectives in Biology*, vol. 1, no. 6, p. a001651, 2009.
- [133] V. Calabrese, C. Cornelius, A. T. Dinkova-Kostova, E. J. Calabrese, and M. P. Mattson, "Cellular stress responses, the hormesis paradigm, and vitagenes: novel targets for therapeutic intervention in neurodegenerative disorders," *Antioxidants & Redox Signaling*, vol. 13, no. 11, pp. 1763–1811, 2010.
- [134] V. Calabrese, C. Mancuso, M. Calvani, E. Rizzarelli, D. A. Butterfield, and A. M. Giuffrida Stella, "Nitric oxide in the central nervous system: neuroprotection versus neurotoxicity," *Nature Reviews Neuroscience*, vol. 8, no. 10, pp. 766–775, 2007.
- [135] V. Calabrese, A. Copani, D. Testa et al., "Nitric oxide synthase induction in astroglial cell cultures: effect on heat shock protein 70 synthesis and oxidant/antioxidant balance," *Journal of Neuroscience Research*, vol. 60, no. 5, pp. 613–622, 2000.
- [136] S. Dattilo, C. Mancuso, G. Koverech et al., "Heat shock proteins and hormesis in the diagnosis and treatment of neurodegenerative diseases," *Immunity & Ageing*, vol. 12, no. 1, pp. 1–19, 2015.

## Research Article

# Cross-Talking Pathways of Forkhead Box O1 (FOXO1) Are Involved in the Pathogenesis of Alzheimer's Disease and Huntington's Disease

Liyang Liu <sup>1</sup>, Jun Bai,<sup>2</sup> Fangxi Liu,<sup>1</sup> Ying Xu,<sup>2,3</sup> Mei Zhao <sup>4</sup>, Chuansheng Zhao <sup>1</sup>, and Zhike Zhou <sup>5</sup>

<sup>1</sup>Department of Neurology, The First Affiliated Hospital, China Medical University, Shenyang, 110001 Liaoning, China

<sup>2</sup>Cancer Systems Biology Center, The China-Japan Union Hospital, Jilin University, Changchun, 130033 Jilin, China

<sup>3</sup>Computational Systems Biology Lab, Department of Biochemistry and Molecular Biology and Institute of Bioinformatics, The University of Georgia, USA

<sup>4</sup>Department of Cardiology, The Shengjing Affiliated Hospital, China Medical University, Shenyang, 110004 Liaoning, China

<sup>5</sup>Department of Geriatrics, The First Affiliated Hospital, China Medical University, Shenyang, 110001 Liaoning, China

Correspondence should be addressed to Chuansheng Zhao; [cszhao@cmu.edu.cn](mailto:cszhao@cmu.edu.cn) and Zhike Zhou; [zkzhou@cmu.edu.cn](mailto:zkzhou@cmu.edu.cn)

Received 25 April 2021; Revised 18 December 2021; Accepted 11 January 2022; Published 3 February 2022

Academic Editor: Ana Lloret

Copyright © 2022 Liyang Liu et al. This is an open access article distributed under the Creative Commons Attribution License, which permits unrestricted use, distribution, and reproduction in any medium, provided the original work is properly cited.

Alzheimer's disease (AD) and Huntington's disease (HD) are destructive worldwide diseases. Efforts have been made to elucidate the process of these two diseases, yet the pathogenesis remains elusive as it involves a combination of multiple factors, including genetic and environmental ones. To explore the potential role of forkhead box O1 (FOXO1) in the development of AD and HD, we identified 1,853 differentially expressed genes (DEGs) from 19,414 background genes in both the AD&HD/control and FOXO1-low/high groups. Four coexpression modules were predicted by the weighted gene coexpression network analysis (WGCNA), among which blue and turquoise modules had the strongest correlation with AD&HD and high expression of FOXO1. Functional enrichment analysis showed that DEGs in these modules were enriched in phagosome, cytokine-cytokine receptor interaction, cellular senescence, FOXO signaling pathway, pathways of neurodegeneration, GABAergic synapse, and AGE-RAGE signaling pathway in diabetic complications. Furthermore, the cross-talking pathways of FOXO1 in AD and HD were jointly determined in a global regulatory network, such as the FOXO signaling pathway, cellular senescence, and AGE-RAGE signaling pathway in diabetic complications. Based on the performance evaluation of the area under the curve of 85.6%, FOXO1 could accurately predict the onset of AD and HD. We then identified the cross-talking pathways of FOXO1 in AD and HD, respectively. More specifically, FOXO1 was involved in the FOXO signaling pathway and cellular senescence in AD; correspondingly, FOXO1 participated in insulin resistance, insulin, and the FOXO signaling pathways in HD. Next, we use GSEA to validate the biological processes in AD&HD and FOXO1 expression. In GSEA analysis, regulation of protein maturation and regulation of protein processing were both enriched in the AD&HD and FOXO1-high groups, suggesting that FOXO1 may have implications in onset and progression of these two diseases through protein synthesis. Consequently, a high expression of FOXO1 is a potential pathogenic factor in both AD and HD involving mechanisms of the FOXO signaling pathway, AGE-RAGE signaling pathway in diabetic complications, and cellular senescence. Our findings provide a comprehensive perspective on the molecular function of FOXO1 in the pathogenesis of AD and HD.

## 1. Introduction

Neurodegenerative disease (ND), a heterogeneous group of devastating and irreversible disorders, is characterized by a

progressive loss of neurons due to the deposition of isomerism proteins, such as amyloid-beta ( $A\beta$ ), prion, huntingtin protein (HTT), tau, and alpha-synuclein [1, 2]. With the extension of life expectancy in general population, the

incidence of ND is on the rise. Herein, our study focused on two types of NDs, namely, Alzheimer's disease (AD) and Huntington's disease (HD). As the most common cause of dementia worldwide, AD is pathologically characterized by deposition of  $A\beta$  plaques composed of amyloid-beta protein and neurofibrillary tangles (NFTs) consisting of hyperphosphorylated tau protein, which are attributed to the overproduction and impaired clearance [3, 4]. The main manifestation of HD is motor impairment and cognitive deficit derived from neuronal dysfunction and death, which is due to the toxicity of the expansion of the polyglutamine region in the HTT protein as a consequence of the mutated gene [5, 6]. Of note, these two diseases are associated with aberrant proteins. Since there is no cure for either condition, efforts are under way to halt or even prevent them by studying genetic factors along with their underlying mechanisms in aberrant protein metabolism. So far, multiple mechanisms have been found to be involved in the occurrence and development of AD and HD [7].

FOXO belongs to the family of transcription factor forkhead box O genes with four isoforms (i.e., FOXO1, FOXO3a, FOXO4, and FOXO6), all of which share highly conserved domains [8]. The functions of FOXO proteins are thought to regulate the expression of genes during biological events including apoptosis, cell cycle control, glucose metabolism, antioxidative stress, and life longevity. Hence, dysfunction of FOXOs leads to diseases and conditions involving shortened life span, cancer, metabolic diseases, immune system disorders, and ND [9–11]. The processes of phosphorylation through the PI3K/Akt, JNK/c-Jun, or AMPK pathway in response to growth factors, insulin/IGF-1, oxidative, and nutrient stress are the main regulatory mechanisms of FOXO proteins. Although all the four isoforms have highly conserved domains and overlapping functions to certain extent [12], additional evidence shows that different isoforms of FOXO regulate a nonredundant set of genes [13]. For instance, FOXO1 plays critical roles in the processes of energy metabolism, longevity, cell cycle arrest, and cellular senescence. Suppression of FOXO1 protein by insulin/IGF-1 or growth factors through the PI3K/Akt pathway decreases its transcriptional function to mediate nutrient metabolism against food deprivation and energy deficiency. Dysfunction of such pathway could lead to metabolic diseases including diabetes, insulin resistance, and increase of food intake [14]. Moreover, FOXO1 mediates cell cycle arrest and apoptosis via the JNK/c-Jun pathway, which has been observed in cells under the condition of growth factor deprivation or oxidative stress [15–17]. With the presence of reactive oxygen species (ROS) or energy deficiency, FOXO1 is activated via the AMPK pathway to induce autophagy, an important mechanism for the clearance of abnormal proteins and organelles; conversely, this process is inhibited by activation of the PI3K/Akt pathway in non-neuronal systems [18, 19]. One plausible interpretation is that activation of FOXO1 protein induces neuronal loss, resulting in persistent neurodegeneration [20]. Although the regulatory role of FOXO1 proteins has been investigated, few studies have focused on the coordinated mechanism of FOXO1-related pathways in the development of AD and

HD. Accordingly, we performed a comprehensive genomic analysis of FOXO1 based on gene expression data and functional annotations with the aim of illuminating the common underlying role of FOXO1 in the pathogenesis of AD and HD.

## 2. Materials and Methods

**2.1. Data Processing.** We downloaded the RNA gene expression profiles of GSE33000 from the Gene Expression Omnibus (GEO) database, which included 467 patients with neurodegenerative diseases (310 AD and 157 HD) and 157 nondementia controls [21]. We then selected a total of 465 patients and controls over 60 years of age, including 367 patients (305 AD and 62 HD) and 98 controls for analysis. The *normalizeBetweenArrays* function in the *limma* package of R software (version 3.6.2) was used to normalize the gene expression profile [22]. Based on clinical data recorded in previous studies, the age and gender between cases and controls were matched [23, 24]. The mean age of AD and HD was  $79.24 \pm 9.11$  years (range: 60–100 years), and the mean age of nondementia was  $69.06 \pm 7.70$  years (range: 60–106 years). The enrolled samples were divided into the FOXO1-high and low groups by defining the mean expression value of FOXO1 as the cut-off point.

**2.2. Identification of Differentially Expressed Genes (DEGs).** DEGs were generated in the AD&HD/control and FOXO1-high/low groups using the *lmFit* and *eBayes* functions of *limma* package in R software. The fold changes (FC) in the expression of individual genes were calculated, with  $|\log_{2}FC| > 0.15$  and false discovery rate- (FDR-) adjusted  $P < 0.05$  considered thresholds [25].

**2.3. Coexpression Network Construction and Functional Enrichment Analysis of Coexpressed Modules.** Using the WGCNA package in R software, the gene coexpression network analysis was constructed by clustering overlapping DEGs between the AD&HD/control and FOXO1-high/low groups into multiple functional modules. Weight gene correlation network analysis (WGCNA), an advanced data exploration technique, not only allows the construction of interconnected node modules that represent network-based data volumes and alleviate the problem of multiple testing but also screens for modules that are relevant to clinical traits [26]. The *hclust* function was used to eliminate outliers from the samples. A *pickSoftThreshold* function was used to determine the appropriate power value of 16 when the degree of independence was set to 0.8. To ensure high reliability of the results, each module contained at least 30 genes. From thousands of genes, interesting modules of DEGs were identified by WGCNA, and then, the Kyoto Encyclopedia of Genes Genomes (KEGG) pathway analysis was performed on the genes in each module using the *ClusterProfiler* package in R software. FDR adjusted  $P < 0.05$  was used as the threshold to define the significant differences in biological functions and enrichment pathways enriched in each module.

**2.4. Construction of Module-Pathway Network of FOXO1.** Correlations between intramodular connectivity and clinical phenotype were used to estimate module-pathway associations, so that highly phenotypically related expression modules could be readily identified. Gene significance (GS) was calculated as the absolute value of the correlation between the gene expression profile and each trait; module membership (MM) was defined as the correlation between the gene expression profiles in each module. Scatterplot of GS vs. MM in each module was plotted using the *verboseScatterplot* function to represent the correlation between intramodular connectivity and clinical trait. In modules related to the trait of interest, genes with higher module membership tend to have higher genetic significance and biological importance [27]. The global regulatory network of module genes with the highest interest was constructed using the Search Tool for the Retrieval of Interacting Genes (STRING; <http://STRING-db.org>) online database [28], in which cross-talking pathways of FOXO1 were annotated by the functional enrichment analysis of the KEGG pathway. The visualization of global regulatory network and cross-talking pathways of FOXO1 were accomplished by employing Cytoscape software [29].

**2.5. Analysis of the Area under the Curve (AUC).** Adopting the *pROC* package, AUC analysis was performed to predict the diagnostic performance of FOXO1 in differentiation between AD&HD and controls. Bilateral *P* value of less than 0.05 was considered statistically significant.

**2.6. Gene Set Enrichment Analysis (GSEA).** According to the median expression of FOXO1, samples were divided into the FOXO1-high and low expression groups. After normalization of the gene expression profile, GSEA was performed to screen for the biological process of Gene Ontology (GO) terms in the AD&HD and FOXO1-high groups [30]. The threshold of significant enrichment was obtained based on the permutation test (the number of permutations was set to 1000, with a *P* value less than 0.05) applying default weighting statistic for each parameter. Enriched data in GSEA analysis was visualized using packages of *ClusterProfiler*, *ggplot2*, *enrichplot*, and *GSEABase*.

**2.7. Workflow.** To investigate the functions of FOXO1 in the pathogenesis of AD and HD, we conducted systematic analysis following the steps in Figure 1. Differential expression analysis of genes was conducted on basis of 19,414 background genes. GSEA was set to analyze biological processes related to AD&HD and FOXO1. The overlapping DEGs between the AD&HD/control and FOXO1-high/low groups were further analyzed by WGCNA. Coexpression gene modules were predicted for further functional enrichment analysis. A global regulation network was constructed to identify cross-talking pathways of FOXO1, thus exploring the potential mechanism of FOXO1 in these two diseases. Thenceforth, we applied the same method to screen out the cross-talking pathways of FOXO1 in AD and HD, respectively. AUC analysis was carried out to assess the

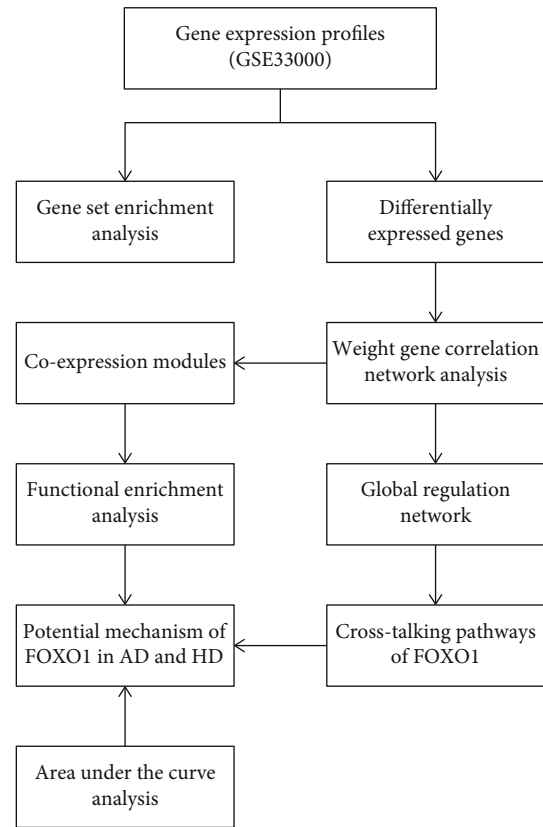


FIGURE 1: The workflow diagram of the present study. AD: Alzheimer's disease; HD: Huntington's disease.

diagnostic performance of FOXO1 in differentiating AD and HD from nondementia controls.

### 3. Results

**3.1. Identification of DEGs.** In the present study, 367 patients and 98 nondementia controls over the age of 60 were included for this computational analysis (Supplementary Table 1). Figure 2(a) shows the comparison of mean expressions of FOXO1 between patients and controls. The expression of FOXO1 in the AD&HD group ( $0.10 \pm 0.11$ ) was significantly higher than those in controls ( $-0.11 \pm 0.15$ ) ( $P < 0.0001$ ). After removal of unannotated or duplicated genes, 19,414 background genes were summarized for further differential expression analysis. A total of 2,103 genes were differentially expressed in AD&HD compared with nondementia controls. Among them, 1,001 DEGs were found to be significantly upregulated, while 1,102 were downregulated (Figure 2(b)). In subjects with high versus low expression of FOXO1, in total, 2,124 DEGs consisted of 1,089 up- and 1,035 downregulated genes were identified (Figure 2(c)). Of these, 1,657 DEGs were overlapped between the AD&HD/control and FOXO1-low/high groups. The cluster heatmap of the top 25 up- and downregulated overlapping DEGs is shown in Figure 2(d).

**3.2. Coexpression Network Construction by WGCNA.** The set of DEGs was used for hierarchical clustering analysis and

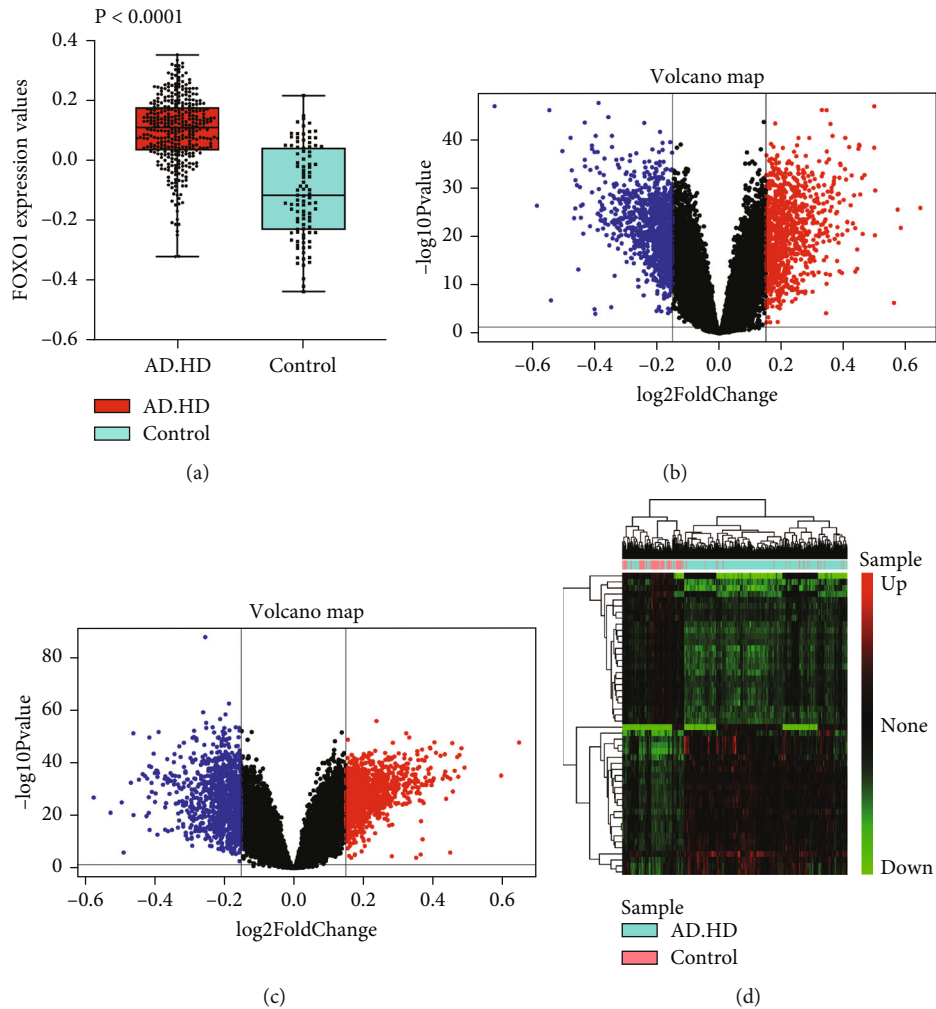


FIGURE 2: Differential expression gene analysis. FOXO1 expression between AD&HD and nondementia controls (a). Volcano plot of the AD&HD/control (b) and FOXO1-high/low group (c): blue, black, and red, respectively, indicate downregulated, nonsignificant, and upregulated DEGs. The heatmap of the top 25 down- and upregulated DEGs (d). AD: Alzheimer's disease; HD: Huntington's disease; DEGs: differential expression genes.

module-trait heatmap plotting. All samples passed the pre-defined cut-off line (height = 16) for the next step of bioinformatic analysis (Figure 3(a)). Using WGCNA, we predicted four coexpression modules with different colours based on the overlapping DEGs between the AD&HD/control and FOXO1-high/low groups (Figure 3(b)). As shown in the module-trait relationships (Figure 3(c)), the blue module of 344 DEGs had the strongest positive correlation with AD&HD (correlation coefficient = 0.61,  $P = 5e - 49$ ) and FOXO1 (correlation coefficient = 0.71,  $P = 4e - 73$ ); the turquoise module of 1,151 DEGs had the strongest negative correlation with AD&HD (correlation coefficient = -0.6,  $P = 1e - 46$ ) and FOXO1 (correlation coefficient = -0.85,  $P = 9e - 133$ ), while the brown module of 127 DEGs was positively correlated with AD&HD (correlation coefficient = 0.48,  $P = 5e - 28$ ) and FOXO1 (correlation coefficient = 0.56,  $P = 1e - 39$ ); and for the grey module, 35 noncoexpressed DEGs were clustered. These data suggest that DEGs in blue and turquoise modules had the strongest correlation with AD and HD.

**3.3. Functional Enrichment Analysis of Coexpressed Modules.** The mainly enriched KEGG pathways in the blue module were pathways of phagosome and cytokine-cytokine receptor interaction; brown module was enriched in transforming growth factor- (TGF-)  $\beta$  signaling pathway, extracellular matrix (ECM)-receptor interaction, and advanced glycation end product- (AGE-) receptors for AGEs (RAGE) signaling pathway in diabetic complications; for turquoise module, DEGs were involved in pathway of neurodegeneration, GABAergic synapse, FOXO signaling pathway, cellular senescence, and AGE -RAGE signaling pathway in diabetic complications (Figure 3(d)).

**3.4. Construction of Module-Pathway Network of FOXO1.** According to the scatter plot of relationship between GS and MM, DEGs in blue and turquoise modules showed the strongest correlation of intramodular connectivity with genetic phenotype (blue: correlation coefficient = 0.59,  $P = 1.2e - 33$ ; turquoise: correlation coefficient = 0.73,  $P = 3.8e - 192$ ) (Figure 4(a)). We extracted DEGs from the blue



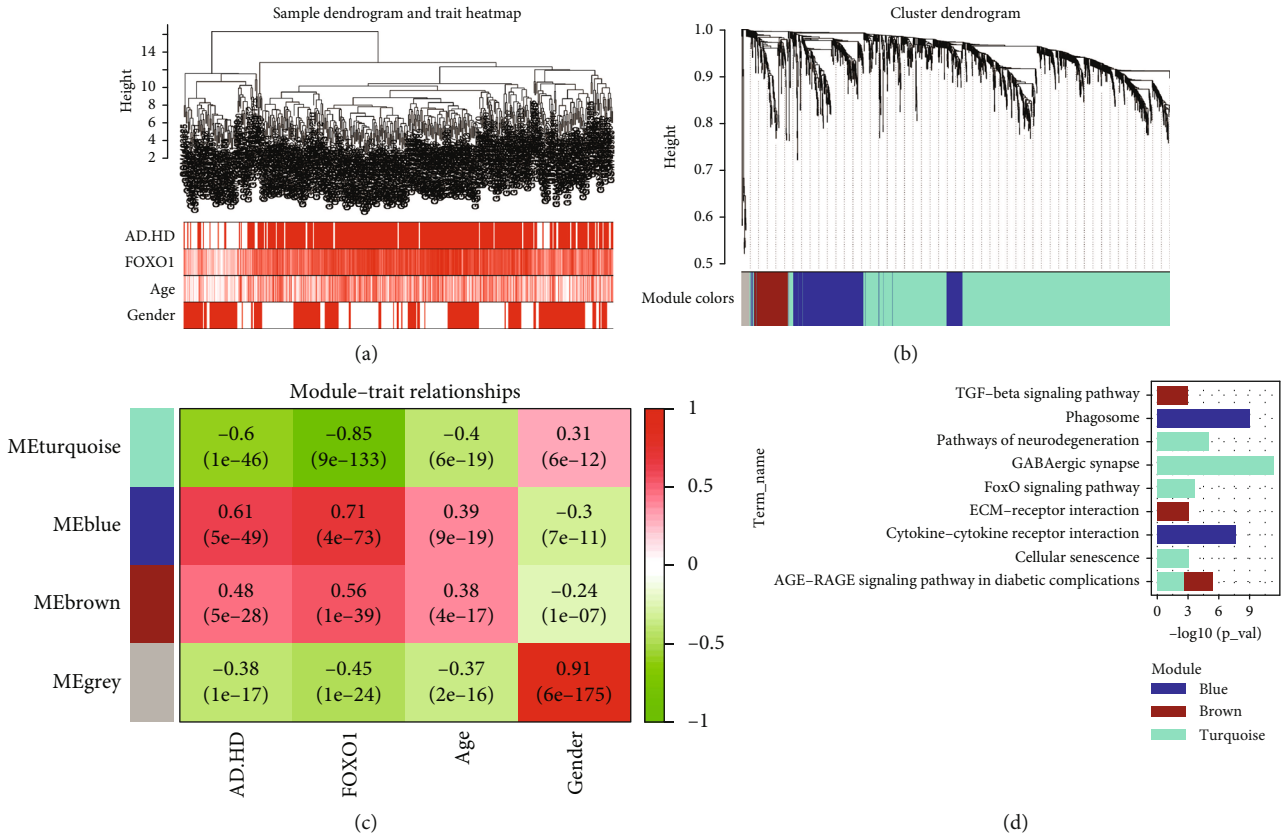


FIGURE 3: Weighted correlation network analysis. Sample dendrogram and trait heatmap (a). Four different coloured modules are used to form clustering dendrogram (b): grey stands for nonclustering genes. Heatmap of module-trait relationships (c): red indicates a positive correlation, green a negative correlation. Enrichment analysis of KEGG pathways for genes in coexpression modules (d). AD: Alzheimer’s disease; HD: Huntington’s disease; KEGG: Kyoto Encyclopedia of Genes and Genomes.

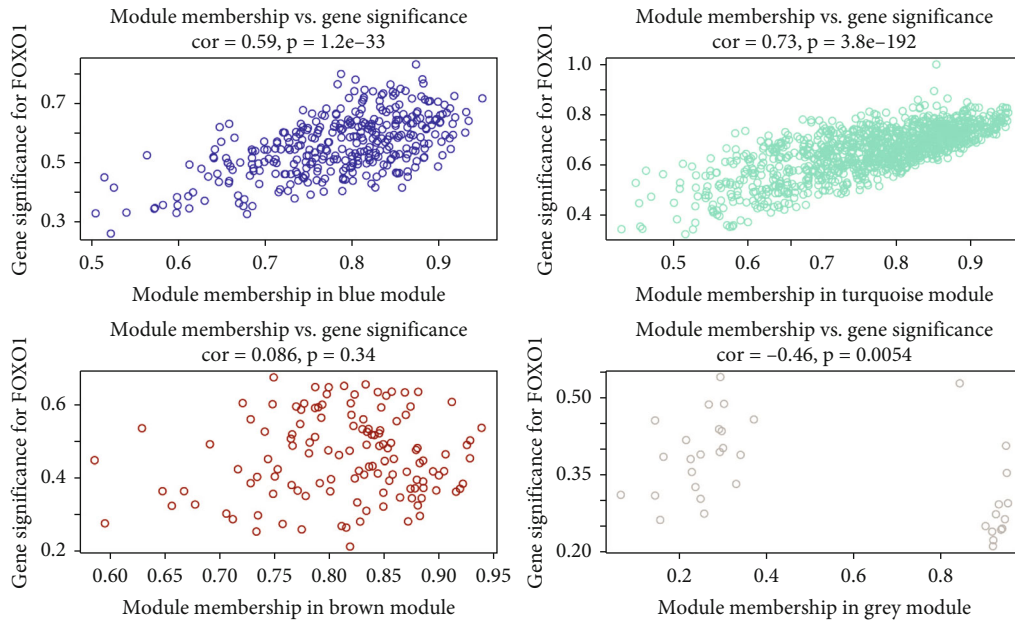
and turquoise modules and displayed them in the global regulatory network (Figure 4(b)). As shown in Figure 4(c), the cross-talking pathways of FOXO1 were identified, including cellular senescence, FOXO signaling pathway, and AGE-RAGE signaling pathway in diabetic complications. According to the AUC value of 85.6%, FOXO1 has potential predict value and may be a biomarker for AD and HD (Figure 4(d)). Separately, we found that the cross-pathways of FOXO1 in AD were related to FOXO signaling pathway and cellular senescence (Figure 5(a)); and the cross-pathways of FOXO1 in HD were linked to insulin resistance, insulin signaling pathway, and FOXO signaling pathway (Figure 5(b)).

**3.5. GSEA Validation in Biological Processes.** GSEA was adopted to validate the biological processes in the AD&HD and FOXO1-high groups. There were five biological processes significantly enriched in AD&HD, including B cell-mediated immunity, regulation of protein maturation, regulation of protein processing, immunoglobulin-mediated immune response, and T cell activation involved in immune response (Figure 5(c)). Five biological processes including regulation of postsynaptic membrane potential, regulation of protein maturation, regulation of protein processing, regulation of synaptic vesicle cycle, and respiratory electron transport chain were significantly enriched in the FOXO1-high group (Figure 5(d)). Of these, regulation of protein

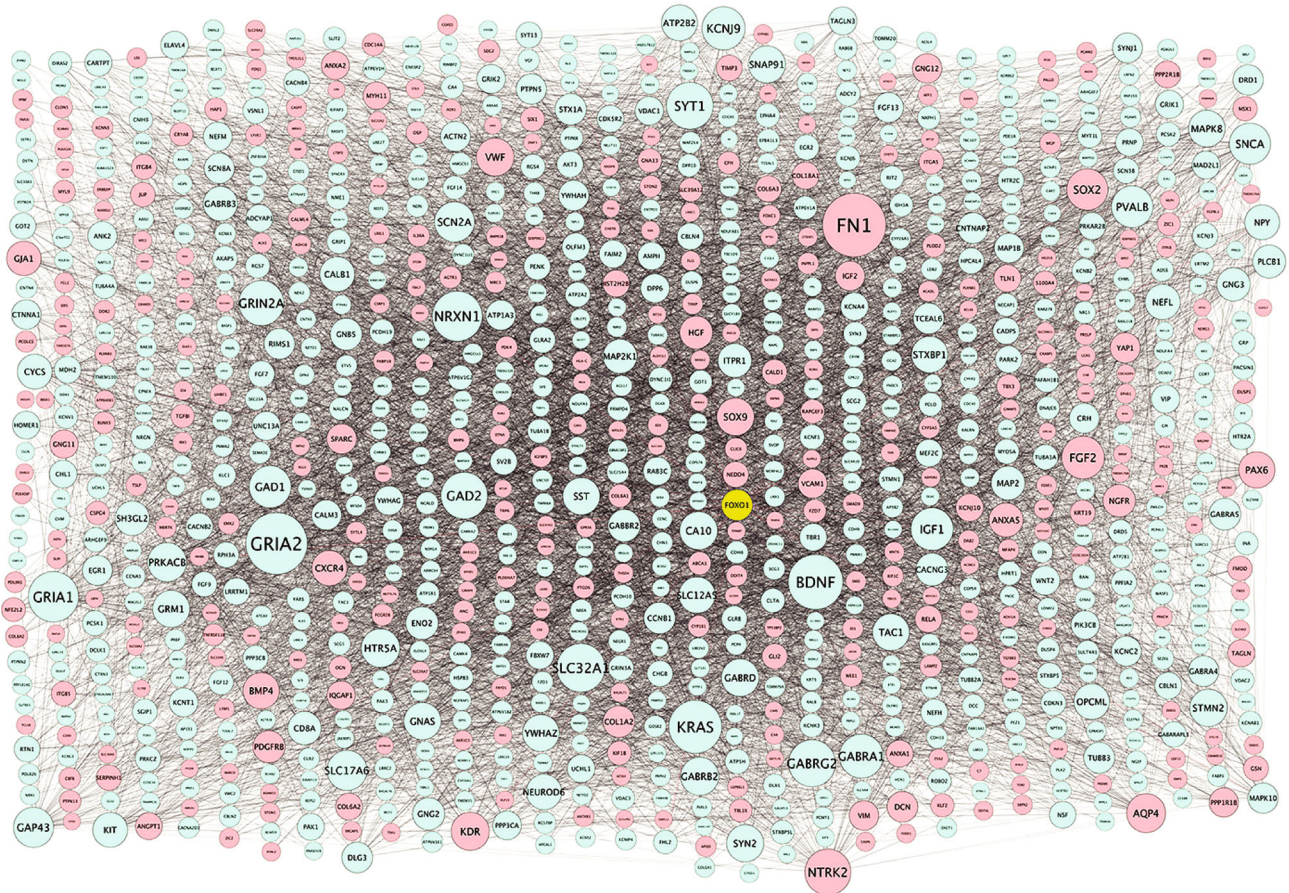
maturation and processing were both enriched in the AD&HD and FOXO1-high groups, suggesting that FOXO1 have implications in the onset and progression of these two diseases through protein synthesis.

**4. Discussion**

The GSEA results showed that the background genes in both AD&HD/control and FOXO1-high/low expression cohorts were enriched in biological processes of protein maturation and processing regulation. The newly synthesized proteins are processed in the endoplasmic reticulum (ER) to form mature proteins with physiological functions. In the presence of cellular crowding, gene mutations, oxidative stress, etc., protein processing in the ER is compromised, resulting in the formation of misfolded proteins. Subsequently, the accumulation of misfolded proteins leads to a state of ER stress to degrade these misfolded proteins. FOXO1 protein participates in such processes by modulating autophagy of misfolded proteins or apoptosis of impaired cells [31–33], consistent with our results of functional enrichment analysis. However, prolonged ER stress can also cause cell damage. It has been reported that ER stress in glial cells elicits the secretion of TNF- $\alpha$ , IL-1 $\beta$ , IL-6, and IL-8 [34]. These proinflammatory factors, in turn, facilitate the production of nitric oxide (NO) involving oxidative damage in glial cells



(a)



(b)

FIGURE 4: Continued.

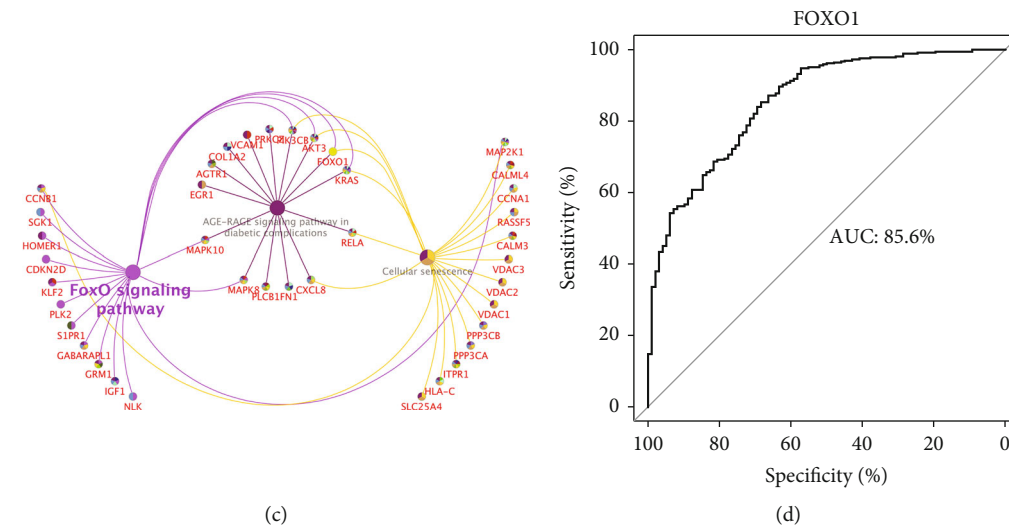


FIGURE 4: Module-pathway regulatory network of FOXO1 and AUC analysis. Scatterplot of module membership versus gene significance (a). Global regulatory network of turquoise and blue module (b): node size represents the degree of gene connectivity; blue represents low expression of the gene; yellow and red represent high expression. The cross-talking pathways of FOXO1 (c). Performance evaluation of AUC analysis (d). AUC: area under the curve.

[35]. Indeed, increased NO synthetase has been found in glia cells surrounding NFTs and amyloid deposition in AD brains [36], along with upregulated immunoreactivity in neurons adjacent to NO in these regions [37]. The mutant Huntingtin in cultured cells and neurons of postmortem HD brains exacerbates ER stress to impair ER-associated protein degradation (ERAD) early in the onset of HD [38–40]. Moreover, translocation of mutant Huntingtin into the nucleus is also inhibited, leading to persistent ER stress and long-term autophagic damage [41]. In addition, reduced organelle synthesis in ER that degrades misfolded proteins is also closely associated with the development of neurodegenerative diseases [42, 43]. It is reported that ER stress can be induced by mutations in the PSEN1 gene contributing consequently to dysfunctional lysosome synthesis, a cause potentially responsible for familial AD [44]. Therefore, these findings lend strong support to our notion that FOXO1 plays an essential role in protein processing and maturation and is closely associated with the pathology of proteotoxicity-related diseases such as AD and HD.

FOXO factors lie in the center of a complex regulatory network of multiple upstream pathways and downstream target genes, receiving upstream signals simultaneously or sequentially to regulate transcriptional activity of downstream target genes in normal or pathological cells. The PI3K/Akt/FOXO pathway is one of the major FOXO pathways that regulates the activation and localization of FOXO1. Knockdown of the upstream insulin receptor substrate (IRS) of this pathway leads to hyperactivation of FOXO1 [45]. Subsequently, activated FOXO1 disrupts mitochondrial oxidative and phosphorylation activities (OXPHOS), resulting in deficient ATP synthesis and metabolic disorders [46]. Notably, the resultant bioenergetic deficits in astrocytes and neurons are one of the most prevalent early features of AD [47]. This is in line with evidence in HD mouse models that mutant HTT (mHTT) aggregation recruits IRS-2 to

activate FOXO1 via the PI3K/Akt/FOXO1 pathway, which contributes to mitochondrial dysfunction [48]. Furthermore, mHTT affects mitochondrial oxygenation to enhance anaerobic metabolism in the basal ganglia and hippocampus of HD patients, leading to increased levels of ROS; in turn, this process accelerates mitochondrial dysfunction and thus to form a vicious circle [49]. Several experiments have found a strong link of impaired insulin secretion and insulin resistance to HD. The incidence of diabetes in HD patients is seven times higher than that of normal diabetes, whose pathological features are reduced insulin secretion and increased insulin resistance. Moreover, even in HD patients with normal glycaemia, there is substantial insulin resistance [50]. Yamamoto et al. have demonstrated that activation of IRS-2 not only affects mitochondrial function but also leads to autophagy of accumulated mHTT proteins via the PI3K/Akt pathway, a branch of insulin signaling pathway highlighting the importance of insulin regulatory mechanisms for HD pathogenesis [47]. This is consistent with our results on the cross-talking pathways of FOXO1 in HD patients.

ROS are mainly produced by and act on mitochondria to regulate cell growth and differentiation at low concentrations [51]. JNKs belong to the mitogen-activated protein kinase (MAPK) family. The JNK pathway is predominantly activated by oxidative stress, and activation of phosphorylated substrates by JNK extensively induces apoptosis [52]. It is well known that aberrant accumulation of ROS leading to neuronal exposure to oxidative stress is a common feature of both AD and HD [53]. And a major consequence of this feature is an increase of cellular apoptosis. Specifically, MAPK kinase (MAP3K) is activated to form the JNK/FOXO1 signaling pathway, which induces neuronal apoptosis by nuclear translocation and phosphorylation of FOXO1 [54, 55]. In experiments of APP transgenic mouse brains, it has been shown that ROS-induced oxidative stress enhanced neuronal apoptosis [56]. Aggregation of A $\beta$  induces excessive

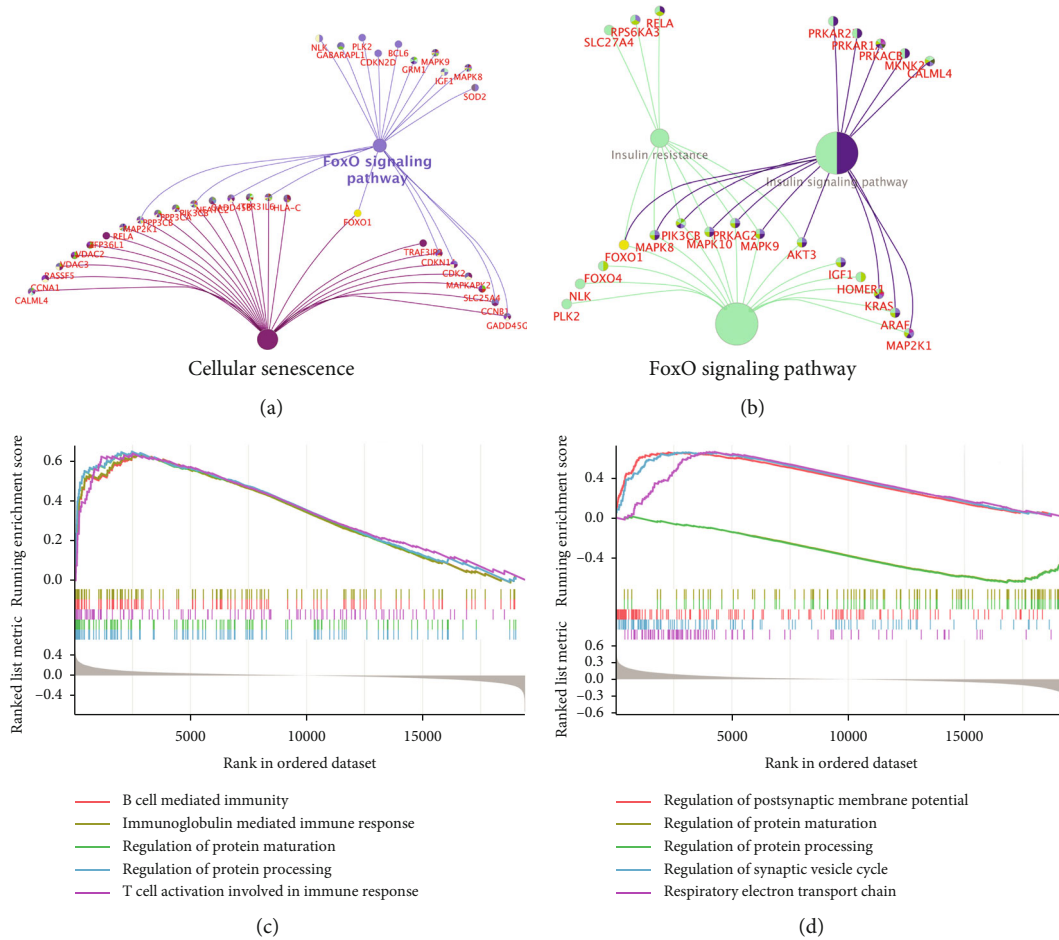


FIGURE 5: Module-pathway regulatory network of FOXO1 in single disease and gene set enrichment analysis. The pathways of FOXO1 enriched in AD (a) and HD (b). Biological processes enriched in AD&HD (c) and high expression of FOXO1 (d). AD: Alzheimer's disease; HD: Huntington's disease.

mitochondrial production of ROS; conversely, sustained activation of the JNK pathway induces increased expression of  $\beta$ -secretase and  $\gamma$ -secretase under conditions of oxidative stress, which in turn promotes  $A\beta$  production [57]. In HD pathology, mutant HTT increases the length of CAG repeats in neurons to overproduce mitochondrial ROS, which then activates the JNK pathway [58, 59], upregulating the expression of proapoptotic genes and thus to apoptosis [60, 61].

Following the process of apoptosis, the removal of apoptotic and senescent cells by phagocytosis contributes to the emergence of phagosomes, which are vesicles formed by the fusion of the cell membrane of the phagocyte around the granule. Fusion with lysosomes results in maturation of phagosome, which not only contains hydrolases and ROS to digest debris but also forms proinflammatory factors via activation of MAPK signaling and PI3K/Akt pathways [62]. Microglia, as special phagocytes of the central nervous system (CNS), recognize aggregated  $A\beta$  and mHTT, leading to a sustained release of neuroinflammatory factors for inflammatory damage and cell death [63]. Neuroinflammatory cell infiltration and microglia activation are inhibited through the PI3K/Akt/FOXO1 pathway, thus alleviating apoptosis and neurologic impairment after intracerebral

hemorrhage [64]. Similarly, Chen et al. found that neurocognitive disorders could be ameliorated through the PI3K/Akt/FOXO1 pathway [65], consistent with our enrichment analysis of the blue module.

Autophagy is another essential mechanism for eliminating organelles in response to stress or starvation. It is involved in the phosphorylation of the downstream target FOXO1 in dynamic equilibrium through synergistic, inhibitory, or cross-talking action of the AMPK, PI3K/Akt, and JNK pathways [66]. Recent experiments have confirmed that JNK activation responds to oxidative stress by inhibiting FOXO-induced autophagy related gene expression, leading to reduced clearance of cell debris and aggregative proteins [67]. Thus, the JNK pathway plays a deleterious role in neurological impairment in neurodegenerative models by promoting apoptosis and inhibiting autophagy [68]. Under oxidative stress caused by aberrant protein synthesis, aggregation, or mitochondrial dysfunction, neurons or glial cells regulate nuclear translocation and activity of FOXO1 through PI3K/Akt and JNK pathways, hence mediating the pathological process of neurodegeneration. Likewise, these findings are in line with functional enrichment analyses of AD and HD obtained in combination or separately.

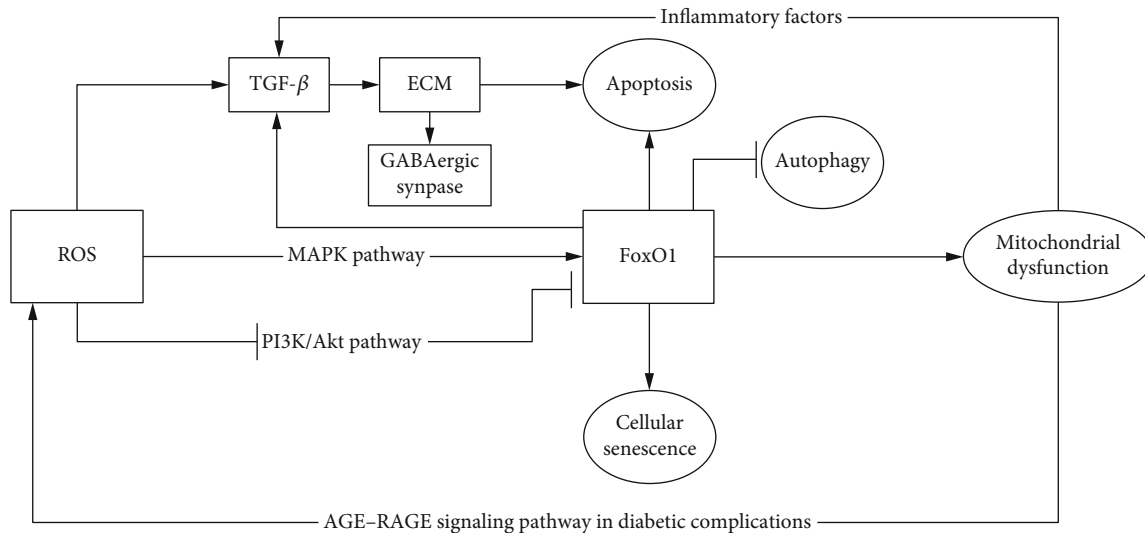


FIGURE 6: Cross-talking pathways of FOXO1 in AD and HD. AD: Alzheimer's disease; HD: Huntington's disease.

Oxidative stimulation acts on cellular components through different signaling pathways or exerts varying effects via the same pathways, determining diverse or even completely opposite cell fates. The precise mechanism is not fully understood, and the results of related experiments are variable and controversial. Salih and Brunet reported that apoptosis was the preferred cellular mechanism of FOXO1-activated neurons exposed to oxidative stress [69]. Nevertheless, Li et al. presented evidence that autophagy was initially triggered and only after prolonged stress could cells undergo apoptosis, which degraded aggregated proteins and damaged cells [70]. Hence, additional experiments are needed to prove the most realistic conclusion.

Cellular senescence participates in physiological processes including wound healing, tissue repair, and embryonic development, which is also a protective mechanism against tumor propagation triggered by oxidative stress-induced DNA damage or oncogenic signals. Moreover, it has also been observed that increased cellular senescence may contribute to senescence-associated diseases including ND [71]. Senescent cells alter proteostasis, promote the secretion of inflammatory cytokines, or allow the synthesis and aggregation of misfolded proteins, either of which ultimately leads to AD [72]. Cell senescence can also trigger iron accumulation, giving rise to oxidative death of neurons and glia cells associated with AD pathology [73]. Sirtuin 1 (SIRT1), a cellular senescence regulatory gene, has been shown to suppress FOXO1 expression in animal models of AD and HD, thereby attenuating neuronal degeneration and death [74, 75]. Additional evidence of *in vivo* HD model has also confirmed that SIRT1 activation provides a positive complement to mitochondrial failure, improving motor coordination and learning in HD [76].

The glycosylate modification of proteins by sugars and aldehydes in an oxygenated environment can produce AGEs [77]. AGEs binding to their receptors namely, RAGEs, promote the synthesis of inflammatory factors and the production of ROS, [78], leading to the accumulation of glyco-

sylated proteins in different organs and tissues [79–81]. The coupling of AGE with RAGE and their interaction in the development of diabetes and its complications have been well established [82]. In the CNS, neurons exposed to oxidative stress also tend to form glycosylated proteins. Glycosylation of mitochondrial enzymes leads to disruption of energy transduction, affecting adenosine triphosphate (ATP) synthesis and subsequent biological processes [83]. The resultant deposition of glycosylated proteins utilizes ROS as second messengers to synthesize and bind inflammatory factors involved in HD and AD through the AGE-RAGE signaling pathway [84–86]. In fibroblasts, ROS generated via the AGE-RAGE signaling pathway acts on JNK to activate FOXO1, thus inducing apoptosis and preventing diabetic wound healing [87]. The vast majority of experiments on the role of FOXO1 in the AGE-RAGE signaling pathway have focused on diabetes and its complications. However, our findings suggest that this pathway may also be involved in AD and HD through the action of ROS and inflammatory factors. And the findings on endothelial cell integrity [87] may provide novel insights into investigating the integrity of cerebrovascular endothelium in relation to FOXO1-mediated AGE-RAGE signaling pathway in AD or HD.

Cumulating evidence suggested that GABAergic synaptic dysfunction aggravated cognitive impairment in patients with dementia [88–90]. Although few studies have linked GABAergic synapses to FOXO1, Zullo et al. found that GABAergic neurotransmitters and FOXO1 are regulated by the same transcription factors involved in life longevity [91]. Recently, GABA has been reported to be essential for the localization of DAF-16, a homologous transcription factor of the FOXO family in *C. elegans*, which triggers nuclear translocation by inhibiting insulin phosphorylation of FOXO via the DAF-2/IGF1R pathway [92].

The multifunctional TGF- $\beta$  signaling pathway plays an important role in maintaining cellular homeostasis through apoptosis, autophagy, and cellular senescence in a variety

of cells [93–95]. As a signal transducer, FOXO1 binds to Smad complex to activate the TGF- $\beta$ /Smad signaling pathway, thus hampering neuronal growth and participating in the pathogenesis of AD [96, 97]. Alternatively, cellular senescence is regulated by the interaction of the TGF- $\beta$ /Smad pathway with the PI3K/Akt/FOXO1 pathway [98]. Likewise, the TGF- $\beta$  signaling pathway has implications in the pathology of neurodegeneration by interacting with the FOXO signaling pathway, which is consistent with the results of our functional enrichment analysis in the brown module.

ECM is a highly dynamic, continuously remodeling tissue with a specific structure [99]. Expression of collagen, a major component of ECM, is substantially upregulated in the subclinical and clinical phases of AD, which is associated with increased A $\beta$  deposition [100]. In addition, our enrichment analysis has clarified that FOXO1 is associated with the regulation of ECM-receptor interaction pathway, in line with evidence of osteoarthritis for the involvement of aberrant FOXO1 expression in ECM-receptor interaction pathway [101].

The onset and progression of AD or HD are the outcomes of the interaction of multiple mechanistic pathways. The cells are always in homeostasis by means of coordination, cross-regulation, and even mutual restraint among various pathways (Figure 6). For instance, AGE-RAGE interaction induces the release of TGF- $\beta$  involving the synthesis of ECM proteins [102]. Furthermore, deposited glycosylated proteins modify the composition of ECM under oxidative stress, which triggers apoptosis of endothelial progenitor cells [103]. Additionally, previous studies in schizophrenia have demonstrated that abnormal EMC disturbs the connectivity of GABAergic synapses due to low expression of TGF- $\beta$ 1 [104, 105].

In the scatter plot between MM and GS, the strongest correlation between DEGs and FOXO1 expression was found in blue and turquoise modules. According to the cross-talking pathways of FOXO1 identified in the global regulatory network of DEGs, FOXO1 plays pleiotropic roles in the physiopathology of AD and HD via cellular senescence, FOXO signaling pathway, and AGE-RAGE signaling pathway in diabetic complications. The result of AUC analysis showed a good diagnostic performance in differentiating AD and HD patients from nondementia controls, which indicated that FOXO1 was possibly a predictive factor for the incidence of AD and HD. Collectively, the findings emerging from this study provide novel possible directions for experiments focusing on the timing and conditions whereby cells enter the senescence or apoptosis program and whether cerebrovascular endothelial integrity influences the progression of AD and HD through the interaction of FOXO1 and AGE-RAGE signaling pathways.

## 5. Conclusions

In summary, our findings support that the high expression of FOXO1 is responsible for the pathogenesis of AD and HD, possibly mediated by FOXO signaling pathway, cellular senescence, and the AGE-RAGE signaling pathway in diabetic complications.

## Data Availability

The data supporting this study is from previously reported studies and datasets, which are available in the GSE33000 repository of the GEO database.

## Conflicts of Interest

The authors declare that there is no conflict of interest regarding the publication of this paper.

## Acknowledgments

The research is supported by the National Natural Science Foundation of China (No. 81372104), the Natural Science Foundation of Liaoning Province (No. 20180540150), the Shenyang Population and Health Technical Critical Special Project (No. F16-206-9-01), the Program of the Distinguished Professor of Liaoning Province (Chuansheng Zhao), and Guidance Plan for Key Research and Development Plans of Liaoning Province (No. 2019JH8/10300002).

## Supplementary Materials

Supplementary Table 1: clinical phenotypic data of enrolled samples. (*Supplementary Materials*)

## References

- [1] J. Vaquer-Alicea and M. I. Diamond, "Propagation of protein aggregation in neurodegenerative diseases," *Annual Review of Biochemistry*, vol. 88, no. 1, pp. 785–810, 2019.
- [2] B. N. Dugger and D. W. Dickson, "Pathology of neurodegenerative diseases," *Cold Spring Harbor Perspectives in Biology*, vol. 9, no. 7, article a028035, 2017.
- [3] D. R. Thal and M. Fandrich, "Protein aggregation in Alzheimer's disease: A $\beta$  and tau and their potential roles in the pathogenesis of AD," *Acta Neuropathologica*, vol. 129, no. 2, pp. 163–165, 2015.
- [4] L. Forny-Germano, N. M. e Silva, A. F. Batista et al., "Alzheimer's disease-like pathology induced by amyloid- $\beta$  oligomers in nonhuman primates," *Journal of Neuroscience*, vol. 34, no. 41, pp. 13629–13643, 2014, *Erratum in: J Neurosci* 2020, 40, 42, 8204.
- [5] F. O. Walker, "Huntington's disease," *The Lancet*, vol. 369, no. 9557, pp. 218–228, 2007.
- [6] P. McColgan and S. J. Tabrizi, "Huntington's disease: a clinical review," *European Journal of Neurology*, vol. 25, no. 1, pp. 24–34, 2018.
- [7] P. L. De Jager, H. S. Yang, and D. A. Bennett, "Deconstructing and targeting the genomic architecture of human neurodegeneration," *Nature Neuroscience*, vol. 21, pp. 1310–1317, 2018.
- [8] W. Link, "Introduction to FOXO biology," *Methods in Molecular Biology*, vol. 1890, pp. 1–9, 2019, PMID: 30414140.
- [9] R. Martins, G. J. Lithgow, and W. Link, "Long live FOXO: unraveling the role of FOXO proteins in aging and longevity," *Aging Cell*, vol. 15, no. 2, pp. 196–207, 2016.
- [10] A. Eijkelenboom and B. M. Burgering, "FOXOs: signalling integrators for homeostasis maintenance," *Nature Reviews. Molecular Cell Biology*, vol. 14, no. 2, pp. 83–97, 2013.

- [11] M. Schmitt-Ney, "The FOXO's advantages of being a family: considerations on function and evolution," *Cell*, vol. 9, no. 3, p. 787, 2020.
- [12] M. F. Hoekman, F. M. Jacobs, M. P. Smidt, and J. P. Burbach, "Spatial and temporal expression of FoxO transcription factors in the developing and adult murine brain," *Gene Expression Patterns*, vol. 6, no. 2, pp. 134–140, 2006.
- [13] M. Potente, C. Urbich, K. Sasaki et al., "Involvement of Foxo transcription factors in angiogenesis and postnatal neovascularization," *The Journal of clinical investigation*, vol. 115, no. 9, pp. 2382–2392, 2005.
- [14] S. Peng, W. Li, N. Hou, and N. Huang, "A review of FoxO1-regulated metabolic diseases and related drug discoveries," *Cell*, vol. 9, no. 1, p. 184, 2020.
- [15] D. G. Sedding, "FoxO transcription factors in oxidative stress response and ageing—a new fork on the way to longevity?," *Biological Chemistry*, vol. 389, no. 3, pp. 279–283, 2008.
- [16] B. C. Ren, Y. F. Zhang, S. S. Liu et al., "Curcumin alleviates oxidative stress and inhibits apoptosis in diabetic cardiomyopathy via Sirt1-Foxo1 and PI3K-Akt signalling pathways," *Journal of Cellular and Molecular Medicine*, vol. 24, no. 21, pp. 12355–12367, 2020.
- [17] M. Yeste-Velasco, J. Folch, G. Casadesús, M. A. Smith, M. Pallàs, and A. Camins, "Neuroprotection by c-Jun NH2-terminal kinase inhibitor SP600125 against potassium deprivation-induced apoptosis involves the Akt pathway and inhibition of cell cycle reentry," *Neuroscience*, vol. 159, no. 3, pp. 1135–1147, 2009.
- [18] N. Nakamura, S. Ramaswamy, F. Vazquez, S. Signoretti, M. Loda, and W. R. Sellers, "Forkhead transcription factors are critical effectors of cell death and cell cycle arrest downstream of PTEN," *Molecular and Cellular Biology*, vol. 20, no. 23, pp. 8969–8982, 2000.
- [19] M. Saline, L. Badertscher, M. Wolter et al., "AMPK and AKT protein kinases hierarchically phosphorylate the N-terminus of the FOXO1 transcription factor, modulating interactions with 14-3-3 proteins," *Journal of Biological Chemistry*, vol. 294, no. 35, pp. 13106–13116, 2019.
- [20] K. N. Manolopoulos, L. O. Klotz, P. Korsten, S. R. Bornstein, and A. Barthel, "Linking Alzheimer's disease to insulin resistance: the FoxO response to oxidative stress," *Molecular Psychiatry*, vol. 15, pp. 1046–1052, 2010.
- [21] M. Narayanan, J. L. Huynh, K. Wang et al., "Common dysregulation network in the human prefrontal cortex underlies two neurodegenerative diseases," *Molecular Systems Biology*, vol. 10, no. 7, p. 743, 2014.
- [22] M. E. Ritchie, B. Phipson, D. Wu et al., "Limma powers differential expression analyses for RNA-sequencing and microarray studies," *Nucleic Acids Research*, vol. 43, no. 7, p. e47, 2015.
- [23] B. C. Riedel, P. M. Thompson, and R. D. Brinton, "Age, APOE and sex: triad of risk of Alzheimer's disease," *The Journal of steroid biochemistry and molecular biology*, vol. 160, pp. 134–147, 2016.
- [24] R. Lardenoije, A. Iatrou, G. Kenis et al., "The epigenetics of aging and neurodegeneration," *Progress in neurobiology*, vol. 131, pp. 21–64, 2015.
- [25] C. W. Law, Y. Chen, W. Shi, and G. K. Smyth, "voom: precision weights unlock linear model analysis tools for RNA-seq read counts," *Genome Biology*, vol. 15, no. 2, p. R29, 2014.
- [26] P. Langfelder and S. Horvath, "WGCNA: an R package for weighted correlation network analysis," *BMC Bioinformatics*, vol. 29, no. 9, p. 559, 2008.
- [27] G. Pei, L. Chen, and W. Zhang, "WGCNA application to proteomic and metabolomic data analysis," *Methods in Enzymology*, vol. 585, pp. 135–158, 2017.
- [28] D. Szklarczyk, J. H. Morris, H. Cook et al., "The STRING database in 2017: quality-controlled protein-protein association networks, made broadly accessible," *Nucleic acids research*, vol. 45, no. D1, pp. D362–D368, 2017.
- [29] D. Otasek, J. H. Morris, J. Bouças, A. R. Pico, and B. Demchak, "Cytoscape automation: empowering workflow-based network analysis," *Genome Biology*, vol. 20, no. 1, p. 185, 2019.
- [30] A. Subramanian, P. Tamayo, V. K. Mootha et al., "Gene set enrichment analysis: a knowledge-based approach for interpreting genome-wide expression profiles," *Proceedings of the National Academy of Sciences*, vol. 102, no. 43, pp. 15545–15550, 2005.
- [31] S. H. Tan, G. Shui, J. Zhou et al., "Critical role of SCD1 in autophagy regulation via lipogenesis and lipid rafts-coupled AKT-FOXO1 signaling pathway," *Autophagy*, vol. 10, no. 2, pp. 226–242, 2014.
- [32] A. Fernández, R. Ordóñez, R. J. Reiter, J. González-Gallego, and J. L. Mauriz, "Melatonin and endoplasmic reticulum stress: relation to autophagy and apoptosis," *Journal of Pineal Research*, vol. 59, no. 3, pp. 292–307, 2015.
- [33] R. L. Vidal, A. Figueroa, F. A. Court et al., "Targeting the UPR transcription factor XBP1 protects against Huntington's disease through the regulation of FoxO1 and autophagy," *Hum Mol Genet*, vol. 21, no. 10, pp. 2245–2262, 2012.
- [34] L. E. Santos and S. T. Ferreira, "Crosstalk between endoplasmic reticulum stress and brain inflammation in Alzheimer's disease," *Neuropharmacology*, vol. 136, Part B, pp. 350–360, 2018.
- [35] P. Pacher, J. S. Beckman, and L. Liaudet, "Nitric oxide and peroxynitrite in health and disease," *Physiological Reviews*, vol. 87, no. 1, pp. 315–424, 2007.
- [36] K. T. Akama and L. J. Van Eldik, "Beta-amyloid stimulation of inducible nitric-oxide synthase in astrocytes is interleukin-1beta- and tumor necrosis factor-alpha (TNFalpha)-dependent, and involves a TNFalpha receptor-associated factor- and NFkappaB-inducing kinase-dependent signaling mechanism," *The Journal of Biological Chemistry*, vol. 275, no. 11, pp. 7918–7924, 2000.
- [37] D. A. Butterfield, J. Drake, C. Pocernich, and A. Castegna, "Evidence of oxidative damage in Alzheimer's disease brain: central role for amyloid beta-peptide," *Trends in Molecular Medicine*, vol. 7, no. 12, pp. 548–554, 2001.
- [38] A. Carnemolla, E. Fossale, E. Agostoni et al., "Rrs1 is involved in endoplasmic reticulum stress response in Huntington disease," *Journal of Biological Chemistry*, vol. 284, no. 27, pp. 18167–18173, 2009.
- [39] F. Trettel, D. Rigamonti, P. Hilditch-Maguire et al., "Dominant phenotypes produced by the HD mutation in STHdh(Q111) striatal cells," *Human Molecular Genetics*, vol. 9, no. 19, pp. 2799–2809, 2000.
- [40] M. L. Duennwald and S. Lindquist, "Impaired ERAD and ER stress are early and specific events in polyglutamine toxicity," *Genes & development*, vol. 22, no. 23, pp. 3308–3319, 2008.

- [41] R. S. Atwal and R. Truant, "A stress sensitive ER membrane-association domain in huntingtin protein defines a potential role for huntingtin in the regulation of autophagy," *Autophagy*, vol. 4, no. 1, pp. 91–93, 2008.
- [42] D. Y. Lee, D. Arnott, and E. J. Brown, "Ubiquilin4 is an adaptor protein that recruits Ubiquilin1 to the autophagy machinery," *EMBO Reports*, vol. 14, no. 4, pp. 373–381, 2013.
- [43] A. Scrivo, M. Bourdenx, O. Pampliega, and A. M. Cuervo, "Selective autophagy as a potential therapeutic target for neurodegenerative disorders," *Lancet Neurology*, vol. 17, no. 9, pp. 802–815, 2018.
- [44] C. A. Deaton and G. V. W. Johnson, "Presenilin 1 regulates membrane homeostatic pathways that are dysregulated in Alzheimer's disease," *Journal of Alzheimer's Disease*, vol. 77, no. 3, pp. 961–977, 2020.
- [45] S. Guo, K. D. Copps, X. Dong et al., "The Irs1 branch of the insulin signaling cascade plays a dominant role in hepatic nutrient homeostasis," *Molecular and cellular biology*, vol. 29, no. 18, pp. 5070–5083, 2009.
- [46] Z. Cheng, Y. Tseng, and M. F. White, "Insulin signaling meets mitochondria in metabolism," *Trends in Endocrinology & Metabolism*, vol. 21, no. 10, pp. 589–598, 2010.
- [47] S. Patro, S. Ratna, H. A. Yamamoto et al., "ATP synthase and mitochondrial bioenergetics dysfunction in Alzheimer's disease," *International Journal of Molecular Sciences*, vol. 22, no. 20, p. 11185, 2021.
- [48] L. Li, Y. Sun, Y. Zhang, W. Wang, and C. Ye, "Mutant huntingtin impairs pancreatic  $\beta$ -cells by recruiting IRS-2 and disturbing the PI3K/AKT/FoxO1 signaling pathway in Huntington's disease," *Journal of Molecular Neuroscience*, vol. 71, no. 12, pp. 2646–2658, 2021.
- [49] M. Jodeiri Farshbaf and K. Ghaedi, "Huntington's disease and mitochondria," *Neurotoxicity Research*, vol. 32, no. 3, pp. 518–529, 2017.
- [50] N. M. Lalić, J. Marić, M. Svetel et al., "Glucose homeostasis in Huntington disease: abnormalities in insulin sensitivity and early-phase insulin secretion," *Archives of Neurology*, vol. 65, no. 4, pp. 476–480, 2008.
- [51] M. L. Circu and T. Y. Aw, "Reactive oxygen species, cellular redox systems, and apoptosis," *Free Radical Biology and Medicine*, vol. 48, no. 6, pp. 749–762, 2010.
- [52] K. Sabapathy, "Role of the JNK pathway in human diseases," *Progress in Molecular Biology and Translational Science*, vol. 106, pp. 145–169, 2012, PMID: 22340717.
- [53] M. W. Ma, J. Wang, Q. Zhang et al., "NADPH oxidase in brain injury and neurodegenerative disorders," *Molecular Neurodegeneration*, vol. 12, no. 1, p. 7, 2017.
- [54] Q. Weng, Z. Liu, B. Li, K. Liu, W. Wu, and H. Liu, "Oxidative stress induces mouse follicular granulosa cells apoptosis via JNK/FoxO1 pathway," *PLoS One*, vol. 11, no. 12, article e0167869, 2016.
- [55] M. Manczak, T. S. Anekonda, E. Henson, B. S. Park, J. Quinn, and P. H. Reddy, "Mitochondria are a direct site of A beta accumulation in Alzheimer's disease neurons: implications for free radical generation and oxidative damage in disease progression," *Human Molecular Genetics*, vol. 15, no. 9, pp. 1437–1449, 2006.
- [56] V. Galvan, S. Banwait, P. Spilman et al., "Interaction of ASK1 and the beta-amyloid precursor protein in a stress-signaling complex," *Neurobiol Dis*, vol. 28, no. 1, pp. 65–75, 2007.
- [57] E. K. Kim and E. J. Choi, "Pathological roles of MAPK signaling pathways in human diseases," *Biochimica et Biophysica Acta*, vol. 1802, no. 4, pp. 396–405, 2010.
- [58] S. Hands, M. U. Sajjad, M. J. Newton, and A. Wytenbach, "In vitro and in vivo aggregation of a fragment of huntingtin protein directly causes free radical production," *Journal of Biological Chemistry*, vol. 286, no. 52, pp. 44512–44520, 2011.
- [59] Y. Furukawa-Hibi, Y. Kobayashi, C. Chen, and N. Motoyama, "FOXO transcription factors in cell-cycle regulation and the response to oxidative stress," *Antioxidants & Redox Signaling*, vol. 7, no. 5-6, pp. 752–760, 2005, PMID: 15890021.
- [60] H. D. Chae and H. E. Broxmeyer, "SIRT1 deficiency downregulates PTEN/JNK/FOXO1 pathway to block reactive oxygen species-induced apoptosis in mouse embryonic stem cells," *Stem cells and development*, vol. 20, no. 7, pp. 1277–1285, 2011.
- [61] S. Ayala-Peña, "Role of oxidative DNA damage in mitochondrial dysfunction and Huntington's disease pathogenesis," *Free Radical Biology and Medicine*, vol. 62, pp. 102–110, 2013.
- [62] M. Gray and R. J. Botelho, "Phagocytosis: hungry, hungry cells," *Methods in Molecular Biology*, vol. 1519, pp. 1–16, 2017, PMID: 27815869.
- [63] S. A. Wolf, H. W. Boddeke, and H. Kettenmann, "Microglia in physiology and disease," *Annual Review of Physiology*, vol. 10, no. 79, pp. 619–643, 2017.
- [64] S. Deng, P. Jin, P. Sherchan et al., "Recombinant CCL17-dependent CCR4 activation alleviates neuroinflammation and neuronal apoptosis through the PI3K/AKT/Foxo1 signaling pathway after ICH in mice," *Journal of Neuroinflammation*, vol. 18, no. 1, p. 62, 2021.
- [65] Y. N. Chen, H. H. Sha, Y. W. Wang et al., "Histamine 2/3 receptor agonists alleviate perioperative neurocognitive disorders by inhibiting microglia activation through the PI3K/AKT/FoxO1 pathway in aged rats," *Journal of Neuroinflammation*, vol. 17, no. 1, p. 217, 2020.
- [66] M. Mofarrahi, Y. Guo, J. A. Haspel et al., "Autophagic flux and oxidative capacity of skeletal muscles during acute starvation," *Autophagy*, vol. 9, pp. 1604–1620, 2013.
- [67] Y. Wei, S. Pattinre, S. Sinha, M. Bassik, and B. Levine, "JNK1-mediated phosphorylation of Bcl-2 regulates starvation-induced autophagy," *Molecular Cell*, vol. 30, no. 6, pp. 678–688, 2008.
- [68] P. Xu, M. Das, J. Reilly, and R. J. Davis, "JNK regulates FoxO-dependent autophagy in neurons," *Genes & Development*, vol. 25, no. 4, pp. 310–322, 2011.
- [69] D. A. Salih and A. Brunet, "FoxO transcription factors in the maintenance of cellular homeostasis during aging," *Current opinion in cell biology*, vol. 20, no. 2, pp. 126–136, 2008.
- [70] C. Li, B. Xia, S. Wang, and J. Xu, "Folded or degraded in endoplasmic reticulum," *Advances in Experimental Medicine and Biology*, vol. 1248, pp. 265–294, 2020, PMID: 32185715.
- [71] P. Santos-Otte, H. Leysen, J. van Gestel, J. O. Hendrickx, B. Martin, and S. Maudsley, "G protein-coupled receptor systems and their role in cellular senescence," *Computational and Structural Biotechnology Journal*, vol. 23, no. 17, pp. 1265–1277, 2019.



- [72] M. Kritsilis, S. V. Rizou, P. N. Koutsoudaki, K. Evangelou, V. G. Gorgoulis, and D. Papadopoulos, "Ageing, cellular senescence and neurodegenerative disease," *International journal of molecular sciences*, vol. 19, no. 10, p. 2937, 2018.
- [73] S. Masaldan, A. A. Belaidi, S. Ayton, and A. I. Bush, "Cellular senescence and iron dyshomeostasis in Alzheimer's disease," *Pharmaceuticals*, vol. 12, no. 2, p. 93, 2019.
- [74] Y. Yang, H. Hou, E. M. Haller, S. V. Nicosia, and W. Bai, "Suppression of FOXO1 activity by FHL2 through SIRT1-mediated deacetylation," *The EMBO journal*, vol. 24, no. 5, pp. 1021–1032, 2005.
- [75] M. Tajés, J. Gutierrez-Cuesta, D. Ortuño-Sahagun, A. Camins, and M. Pallàs, "Anti-aging properties of melatonin in an in vitro murine senescence model: involvement of the sirtuin 1 pathway," *Journal of Pineal Research*, vol. 47, no. 3, pp. 228–237, 2009.
- [76] L. Naia, T. R. Rosenstock, A. M. Oliveira et al., "Comparative mitochondrial-based protective effects of resveratrol and nicotinamide in Huntington's disease models," *Molecular Neurobiology*, vol. 54, no. 7, pp. 5385–5399, 2017.
- [77] N. Chondrogianni, I. Petropoulos, S. Grimm et al., "Protein damage, repair and proteolysis," *Molecular Aspects of Medicine*, vol. 35, pp. 1–71, 2014.
- [78] A. Bierhaus, D. M. Stern, and P. P. Nawroth, "RAGE in inflammation: a new therapeutic target?," *Current Opinion in Investigational Drugs*, vol. 7, no. 11, pp. 985–991, 2006.
- [79] A. L. Tan, J. M. Forbes, and M. E. Cooper, "AGE, RAGE, and ROS in diabetic nephropathy," *Seminars in Nephrology*, vol. 27, no. 2, pp. 130–143, 2007.
- [80] J. C. Santos, I. B. Valentim, O. R. de Araújo, R. Ataíde Tda, and M. O. Goulart, "Development of nonalcoholic hepatopathy: contributions of oxidative stress and advanced glycation end products," *International Journal of Molecular Sciences*, vol. 14, no. 10, pp. 19846–19866, 2013.
- [81] K. Fukami, S. Yamagishi, and S. Okuda, "Role of AGEs-RAGE system in cardiovascular disease," *Current Pharmaceutical Design*, vol. 20, no. 14, pp. 2395–2402, 2014, PMID: 23844818.
- [82] S. Y. Goh and M. E. Cooper, "Clinical review: the role of advanced glycation end products in progression and complications of diabetes," *The Journal of Clinical Endocrinology and Metabolism*, vol. 93, no. 4, pp. 1143–1152, 2008.
- [83] I. S. Kil, J. H. Lee, A. H. Shin, and J. W. Park, "Glycation-induced inactivation of NADP(+)-dependent isocitrate dehydrogenase: implications for diabetes and aging," *Free Radical Biology & Medicine*, vol. 37, no. 11, pp. 1765–1778, 2004.
- [84] A. Maczurek, K. Shanmugam, and G. Münch, "Inflammation and the redox-sensitive AGE-RAGE pathway as a therapeutic target in Alzheimer's disease," *Annals of the New York Academy of Sciences*, vol. 1126, pp. 147–151, 2008.
- [85] Y. Sawikr, N. S. Yarla, I. Peluso, M. A. Kamal, G. Aliev, and A. Bishayee, "Neuroinflammation in Alzheimer's disease: the preventive and therapeutic potential of polyphenolic nutraceuticals," *Advances in Protein Chemistry and Structural Biology*, vol. 108, pp. 33–57, 2017.
- [86] S. Anzilotti, C. Giampà, D. Laurenti et al., "Immunohistochemical localization of receptor for advanced glycation end (RAGE) products in the R6/2 mouse model of Huntington's disease," *Brain Research Bulletin*, vol. 87, no. 2-3, pp. 350–358, 2012.
- [87] M. Alikhani, C. M. Maclellan, M. Raptis, S. Vora, P. C. Trackman, and D. T. Graves, "Advanced glycation end products induce apoptosis in fibroblasts through activation of ROS, MAP kinases, and the FOXO1 transcription factor," *American Journal of Physiology. Cell Physiology*, vol. 292, no. 2, pp. C850–C856, 2007.
- [88] J. J. Palop and L. Mucke, "Network abnormalities and interneuron dysfunction in Alzheimer disease," *Nature Reviews Neuroscience*, vol. 17, no. 12, pp. 777–792, 2016.
- [89] A. I. Smith-Dijak, M. D. Sepers, and L. A. Raymond, "Alterations in synaptic function and plasticity in Huntington disease," *Journal of Neurochemistry*, vol. 150, no. 4, pp. 346–365, 2019.
- [90] T. L. Spires-Jones and B. T. Hyman, "The intersection of amyloid beta and tau at synapses in Alzheimer's disease," *Neuron*, vol. 82, no. 4, pp. 756–771, 2014.
- [91] J. M. Zullo, D. Drake, L. Aron et al., "Regulation of lifespan by neural excitation and REST," *Nature*, vol. 574, no. 7778, pp. 359–364, 2019.
- [92] A. Urrutia, V. A. García-Angulo, A. Fuentes et al., "Bacterially produced metabolites protect *C. elegans* neurons from degeneration," *PLoS Biol*, vol. 18, no. 3, article e3000638, 2020.
- [93] A. Hata and Y. G. Chen, "TGF- $\beta$  signaling from receptors to Smads," *Cold Spring Harbor Perspectives in Biology*, vol. 8, no. 9, article a022061, 2016.
- [94] P. M. Siegel and J. Massagué, "Cytostatic and apoptotic actions of TGF-beta in homeostasis and cancer," *Nature Reviews Cancer*, vol. 3, pp. 807–821, 2003.
- [95] Y. Zhang, P. B. Alexander, and X. F. Wang, "TGF- $\beta$  family signaling in the control of cell proliferation and survival," *Cold Spring Harbor Perspectives in Biology*, vol. 9, no. 4, article a022145, 2017.
- [96] T. Town, Y. Laouar, C. Pittenger et al., "Blocking TGF-beta-Smad2/3 innate immune signaling mitigates Alzheimer-like pathology," *Nature medicine*, vol. 14, no. 6, pp. 681–687, 2008.
- [97] J. Seoane, H. V. Le, L. Shen, S. A. Anderson, and J. Massagué, "Integration of Smad and forkhead pathways in the control of neuroepithelial and glioblastoma cell proliferation," *Cell*, vol. 117, no. 2, pp. 211–223, 2004.
- [98] D. Muñoz-Espín, M. Cañamero, A. Maraver et al., "Programmed cell senescence during mammalian embryonic development," *Cell*, vol. 155, no. 5, pp. 1104–1118, 2013.
- [99] C. Frantz, K. M. Stewart, and V. M. Weaver, "The extracellular matrix at a glance," *Journal of Cell Science*, vol. 123, Part 24, pp. 4195–4200, 2010.
- [100] F. X. Lepelletier, D. M. Mann, A. C. Robinson, E. Pinteaux, and H. Boutin, "Early changes in extracellular matrix in Alzheimer's disease," *Neuropathology and Applied Neurobiology*, vol. 43, no. 2, pp. 167–182, 2017.
- [101] T. Duffy, H. Bekki, and M. K. Lotz, "Genome-wide occupancy profiling reveals critical roles of FoxO1 in regulating extracellular matrix and circadian rhythm genes in human chondrocytes," *Arthritis & rheumatology*, vol. 72, no. 9, pp. 1514–1523, 2020.
- [102] A. K. Pastino, T. M. Greco, R. A. Mathias, I. M. Cristea, and J. E. Schwarzbauer, "Stimulatory effects of advanced glycation endproducts (AGEs) on fibronectin matrix assembly," *Matrix Biology*, vol. 59, pp. 39–53, 2017.

- [103] J. Chen, J. Jing, S. Yu et al., “Advanced glycation endproducts induce apoptosis of endothelial progenitor cells by activating receptor RAGE and NADPH oxidase/JNK signaling axis,” *American journal of translational research*, vol. 8, no. 5, pp. 2169–2178, 2016.
- [104] I. Zaharieva, L. Georgieva, I. Nikolov et al., “Association study in the 5q31-32 linkage region for schizophrenia using pooled DNA genotyping,” *BMC Psychiatry*, vol. 25, no. 8, p. 11, 2008.
- [105] S. Berretta, “Extracellular matrix abnormalities in schizophrenia,” *Neuropharmacology*, vol. 62, no. 3, pp. 1584–1597, 2012.

## Research Article

# Neuroprotective Effect of Ceftriaxone on MPTP-Induced Parkinson's Disease Mouse Model by Regulating Inflammation and Intestinal Microbiota

Xiaoting Zhou,<sup>1,2</sup> Jiachen Lu,<sup>3</sup> Kehong Wei,<sup>3</sup> Jing Wei,<sup>3</sup> Puyuan Tian,<sup>3</sup> Mengyun Yue,<sup>1</sup> Yun Wang,<sup>1</sup> Daojun Hong,<sup>1</sup> Fangjun Li,<sup>1</sup> Bo Wang,<sup>1</sup> Tingtao Chen <sup>3</sup> and Xin Fang <sup>1</sup>

<sup>1</sup>Department of Neurology, The First Affiliated Hospital of Nanchang University, Nanchang, Jiangxi 330006, China

<sup>2</sup>Department of Neurology, Qingyuan People's Hospital, The Sixth Affiliated Hospital of Guangzhou Medical University, Qingyuan, Guangdong 511500, China

<sup>3</sup>National Engineering Research Center for Bioengineering Drugs and the Technologies, Institute of Translational Medicine, Nanchang University, Nanchang, Jiangxi 330031, China

Correspondence should be addressed to Tingtao Chen; [chentingtao1984@163.com](mailto:chentingtao1984@163.com) and Xin Fang; [fangx2011@163.com](mailto:fangx2011@163.com)

Received 8 August 2021; Revised 20 September 2021; Accepted 16 November 2021; Published 13 December 2021

Academic Editor: Xu Wu

Copyright © 2021 Xiaoting Zhou et al. This is an open access article distributed under the Creative Commons Attribution License, which permits unrestricted use, distribution, and reproduction in any medium, provided the original work is properly cited.

Parkinson's disease (PD) is a common degenerative disease of the central nervous system. Although some drugs can alleviate the progress of PD, their long-term use will lead to complications, so it is still necessary to find new drugs to delay or cure PD effectively. In view of the difficulty in developing new drugs, it is imperative to discover new functions of existing compounds that could be used to treat PD. In this study, 1-methyl-4-phenyl-1,2,3,6-tetrahydropyridine (MPTP) was used to induce PD symptoms in a mouse model. Subsequently, these mice were treated with the antibiotic ceftriaxone. Ceftriaxone alleviated the behavioural and neuropathological changes induced by MPTP, downregulated the expression of glial fibrillary acidic protein (GFAP) and ionised calcium-binding adapter molecule 1 (Iba1) as markers of astroglia and microglia, respectively, and reduced the expression of neuroinflammation-related Toll-like receptor 4 (TLR4), myeloid differentiation primary response 88 (MyD88), and phosphorylated nuclear factor kappa-B (p-NF- $\kappa$ B)/NF- $\kappa$ B in the brain of PD mice. In addition, ceftriaxone reduced the abundance of pathogenic bacteria of the genus *Proteus* and increased the abundance of probiotic *Akkermansia*. Finally, ceftriaxone treatment increased the expression of the tight junction proteins zona occludens-1 (ZO-1) and occludin in the colon, decreased the expression of the inflammation-related proteins TLR4, MyD88, and NF- $\kappa$ B in the colon, and decreased the serum concentration of the proinflammatory cytokines interleukin-1 $\beta$  (IL-1 $\beta$ ), IL-6, and tumour necrosis factor- $\alpha$  (TNF- $\alpha$ ). These results indicate that ceftriaxone had a neuroprotective effect on MPTP-induced PD mice, and its neuroprotective effect could be through regulating inflammation and intestinal microbiota. While we showed that ceftriaxone exerts a neuroprotective effect in an MPTP-induced PD mouse model, our findings are limited to the short-term effects of ceftriaxone. Additional work using transgenic mice is required to determine the long-term effects of ceftriaxone. In addition, the dose and frequency of ceftriaxone use should be evaluated.

## 1. Introduction

Parkinson's disease (PD) is a complex and progressively degenerative disease of the central nervous system; it affects more than 6 million people throughout the world [1]. The clinical features of PD include motor and nonmotor symptoms [2]. These symptoms severely affect the quality of life

of patients and bring great burden to society [3]. The main pathologies of PD are the loss of dopaminergic neurons in the substantia nigra pars compacta (SNc) of the midbrain and the accumulation of  $\alpha$ -synuclein in the cytoplasm of neurons form Lewy bodies. The aetiology of PD is not clear but may be related to various risk factors such as excitotoxicity, oxidative stress, and neuroinflammation. The current

treatment of PD includes levodopa, dopamine agonists, monoamine oxidase (MAO) inhibitors, anticholinergics, and amantadine, all of which can improve symptoms and slow disease progression. However, none of these treatments can completely cure the disease, and there are some side effects [4]. Although new treatments such as glutamate receptor antagonists, antiapoptotic agents, and antioxidants have been proposed—with the potential to protect nerve cells and slow the progression of PD—there is a lack of scientific evidence to support these claims in clinical practice [5].

Increasing evidence suggests there is bidirectional communication between the gut and the brain [6–8]. Patients with PD have an intestinal microbiota disorder, which is specifically manifested in the increased abundance of *Lactobacillus* and *Enterobacteriaceae* and the decreased abundance of *Prevotella*, *Clostridium coccooides*, and *Bacteroides fragilis* [9, 10]. Recently, GV-971 was approved for the treatment of Alzheimer's disease (AD) by the National Medical Products Administration for its ability to remodel the intestinal microbiota. Targeting the intestinal microbiota for the treatment of AD opens up a new way to treat other neurological diseases [11].

The use of antibiotics has a long-term impact on the composition and diversity of the intestinal microbiota, and it has been reported that the use of antibiotics—especially macrolides and lincosamides—is related to the increased risk of PD [12]. Nevertheless, some antibiotics, such as ceftriaxone, have been reported to have neuroprotective properties that are unrelated to their antibacterial activity [13]. Rothstein et al. [13] first reported that the  $\beta$ -lactam antibiotics (such as ceftriaxone) have a neuroprotective effect on ischaemic brain injury. Subsequent studies have proved that ceftriaxone exerts a neuroprotective effect in various neurodegenerative diseases, such as AD [14], PD [15], amyotrophic lateral sclerosis (ALS) [16], and Huntington's disease (HD) [17].

Although ceftriaxone has been used commonly in the clinic, little work has been done to explore its potential mechanisms of adjusting intestinal microorganisms in PD. In this study, ceftriaxone was injected intraperitoneally into a mouse model of PD, induced by 1-methyl-4-phenyl-1,2,3,6-tetrahydropyridine (MPTP), and the neuroprotective effect of ceftriaxone in these mice was explored using behavioural tests, immunofluorescence, Western blotting, and high-throughput 16S ribosomal DNA (rDNA) sequencing.

## 2. Materials and Methods

**2.1. Animals.** The mice used in this experiment were purchased from SJA Laboratory Animal Co. (Changsha, Hunan, China). All mice were male C57BL/6 and weighed 25–30 g. The purchased mice were allowed to adapt to the laboratory environment for 1 week before the experiment. The mice were kept on a 12-h photoperiod, with a temperature of  $22 \pm 2^\circ\text{C}$  and humidity of  $50\% \pm 15\%$ . Laboratory food and water were available *ad libitum*.

The study had been approved by the Laboratory Animal Ethics Committee of Nanchang Royo Biotech Co., Ltd.

(license No. RYE2019041502) on 15 April 2019, and all experiments were conducted according to the established guidelines.

**2.2. Experimental Design and Treatment.** After 1 week of adaptation, the mice were divided into six groups, each with 15 mic. (i) A control group received saline (C group). (ii) A group was given a daily intraperitoneal injection of MPTP (Sigma, Cat# M-0896) of 20 mg/kg for 7 days to establish a PD mouse model (M group). (iii) A group was treated with ceftriaxone (200 mg/kg, once a day, intraperitoneal injection) for 7 days while using MPTP to establish a PD mouse model (MCEF group). (iv) A group was treated with ceftriaxone (200 mg/kg, once a day, intraperitoneal injection) for 7 days while using MPTP to establish a PD mouse model. Behaviour was evaluated in these mice. Then, the mice were transplanted with 200  $\mu\text{l}$  of faecal microbiota (from PD mice), containing  $1 \times 10^7$  colony-forming units (CFU)/ml every day for 7 days (MCEFF group). (v) A group received faecal microbiota transplantation from PD mice, namely, 200  $\mu\text{l}$  (microbial content of  $1 \times 10^7$  CFU/ml) intragastric gavage per day for 7 days (FMT group). (vi) A group received faecal microbiota transplantation from PD mice, namely, 200  $\mu\text{l}$  (microbial content of  $10^7$  CFU/ml) gavage per day for 7 days. Behaviour was evaluated in these mice, followed by ceftriaxone administration (200 mg/kg, once a day, intraperitoneal injection) for 7 consecutive days (FCEF group). As shown in Figure 1, we performed behavioural tests on all mice on days 7–10, and euthanised mice in groups C, M, MCEF, and FMT. Then, the MCEFF group was transplanted with faecal bacteria, and the FCEF group was treated with ceftriaxone, and behavioural tests were performed on these mice on days 16–19. After the test, all mice were euthanised. Five mice were intracardially perfused with 30 ml of saline and then injected with 100 ml of 4% (*v/v*) paraformaldehyde (Sigma-Aldrich, Cat# P6148) prepared in phosphate-buffered saline (PBS). The entire perfusion process was completed within 5 min, and the perfusate was injected with a 50 ml syringe. The brain was collected immediately and then fixed in 4% (*v/v*) paraformaldehyde for immunofluorescence. The brains and colon tissues of the remaining mice were collected, quickly frozen in liquid nitrogen, and stored at  $-80^\circ\text{C}$  for future molecular biology experiments (Figure 1(a)).

**2.3. Preparation of Faecal Microbiota from PD Mice.** In this experiment, the donors of faecal microbiota transplantation were PD mice in the M group, and faeces of mice were collected after daily intraperitoneal injection of MPTP for 5–6 days. One or two grams of faeces were taken from the collected faeces and mixed with 1 ml of sterile saline, and then, the supernatant was filtered and counted on the plate after multiple dilutions. One gram of faeces contained  $1 \times 10^9$  to  $1 \times 10^{10}$  CFU of microbes; faeces were collected according to the calculated number of faecal microbiota. The faeces of mice were weighed and added to about 5-times the volume of sterile saline. After mixing, the faeces were added to saline (final volume of 50 ml) and oscillated in an oscillator for 2 min for full mixing. Faeces were placed at room

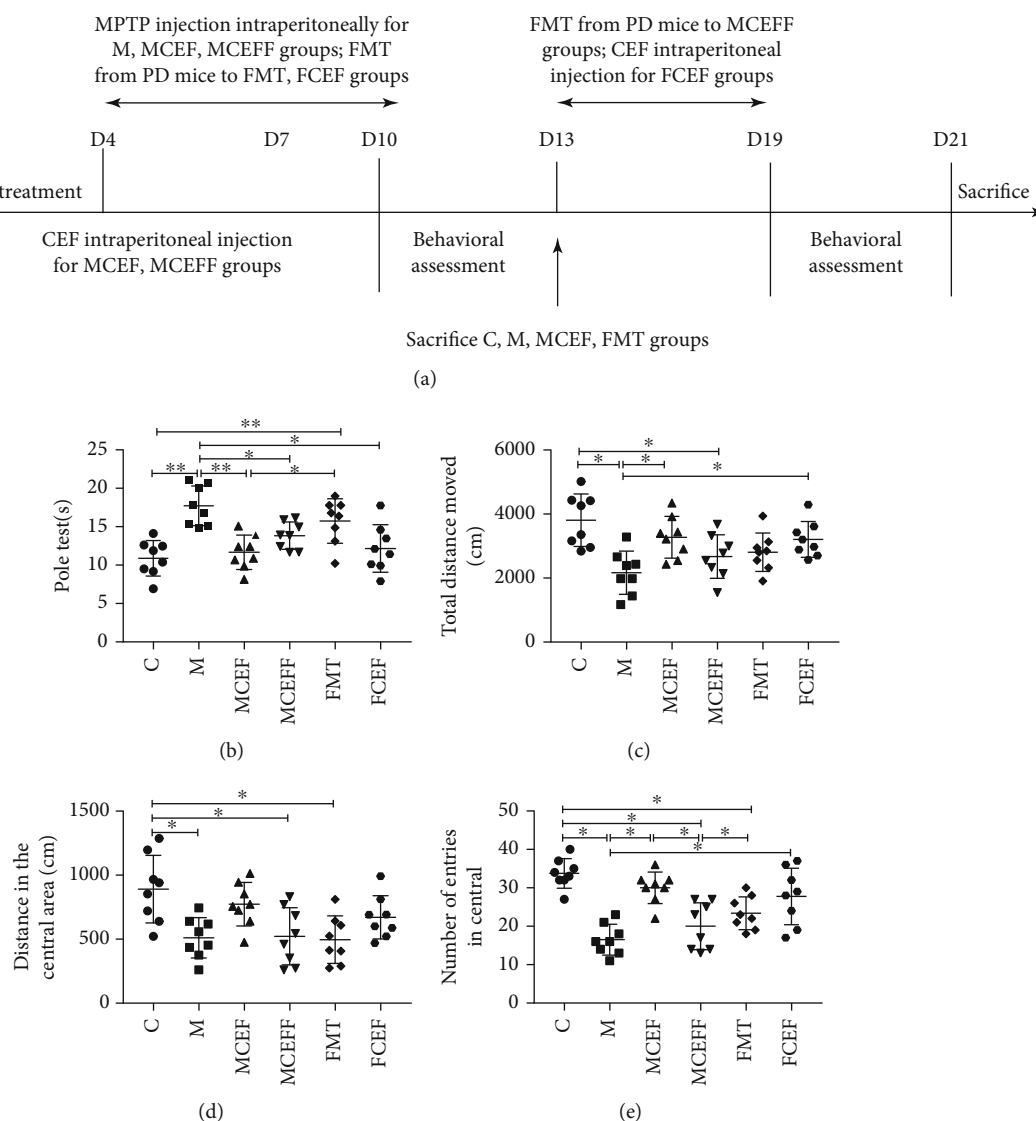


FIGURE 1: Ceftriaxone improved MPTP-induced motor dysfunction in PD mice. (a) Treatment schedule to explain the design of the whole experimental. (b) Ceftriaxone improved the bradykinesia mice induced by MPTP (pole test). (c) Ceftriaxone increased the total distance moved for PD mice (open-field test). (d) Ceftriaxone increased the distance in the central area moved for PD mice (open-field test). (e) Ceftriaxone increased the number of entries in central (open-field test). C group ( $N = 8$ ), control group; M group ( $N = 8$ ), MPTP group; MCEF group ( $N = 8$ ), MPTP + ceftriaxone group; MCEFF group ( $N = 8$ ), MPTP + ceftriaxone + fecal microbiota transplantation group; FMT group ( $N = 8$ ), fecal microbiota transplantation group, FCEF group ( $N = 8$ ), fecal microbiota transplantation group + ceftriaxone group. Data are presented as means  $\pm$  SD. One-way repeated-measures ANOVA with Tukey's test for multiple comparisons (b–e, respectively); \* $p < 0.05$ , \*\* $p < 0.01$ . CEF: ceftriaxone; MPTP: 1-methyl-4-phenyl-1, 2, 3, 6-tetra-hydropyridine.

temperature for 30 min, the supernatant was collected and centrifuged, and then, the precipitate was collected. The precipitate was washed twice with sterile normal saline, and the final precipitate was added to the appropriate volume of normal saline and mixed well. Finally, the preparation was given to the mice intragastrically.

**2.4. Behavioural Testing.** The pole test is often used to assess the motor coordination in PD mice. A metal rod with a diameter of 1 cm and a length of 50 cm was wrapped with bandage gauze to prevent the mice from slipping, and the bottom of the metal rod was placed in a cage. The mouse was placed head down on the top of the rod. The time it took

the mouse to return to the cage freely was recorded, ending when the hind limbs of the mouse reached the bottom of the cage. Before the formal test, the mice were trained for 2 days. Each mouse was tested three times, with 15 min between trials. Finally, we take the average of the three trials for analysis.

The open-field test was used to detect behavioural changes of the mice—such as exploration—in the new environment. The open-field test was performed in a square, with a length, width, and height of 50 cm  $\times$  50 cm  $\times$  40 cm, and black perimeter walls. It was divided into 25 squares with equal area, which were then divided into the edge area and the central area (the four small squares in the centre).

During the experiment, mice were put into a corner of the arena, and their free movement over 10 min was recorded with a camera. At the end of the experiment, the arena was swabbed with 75% alcohol to avoid the next mouse from disturbing by the left scent.

**2.5. Immunofluorescence.** The fixed brains were embedded in paraffin. The tissue was then sectioned, and the sections were dewaxed to water, subjected to antigen retrieval, and incubated with bovine serum albumin (BSA) to block non-specific protein binding. The tissues were incubated overnight at 4°C with the following primary antibodies: rabbit antityrosine hydroxylase (TH; 1:200; Proteintech, Cat# 25859-1-AP), rabbit antiglial fibrillary acidic protein (GFAP; 1:200; Proteintech; Cat# 16825-1-AP), and rabbit anti-ionised calcium-binding adapter molecule 1 (Iba1; 1:100; Abcam; Cat# ab178847). Subsequently, the tissues were washed on a decolourisation shaker with PBS and then incubated with the corresponding secondary antibody at room temperature for 50 min. After mounting the sections, they were observed under a fluorescence microscope and images captured.

**2.6. Western Blotting.** The brain and colon tissues were homogenised to extract proteins. The protein concentration was determined by using the BCA protein quantitative kit, and the protein was separated by polyacrylamide gel electrophoresis using 10%-12% gels. The electrophoresis time was adjusted according to the molecular weight of the protein of interest. After electrophoresis, the separated protein was transferred to polyvinylidene fluoride membrane. The membrane was incubated with 5% nonfat milk in Tris-buffered saline with Tween 20 (TBST) at room temperature for 1-2 h to block nonspecific protein binding. The membrane was then incubated overnight at 4°C with one of the following antibodies: rabbit anti-TH (1:2000; Proteintech, Cat# 25859-1-AP), rabbit antiexcitatory amino acid transporter 2 (EAAT2, GLT-1; 1:2000; Proteintech; Cat# 22515-1-AP), rabbit anti- $\alpha$ -synuclein ( $\alpha$ -syn; 1:1000; Cell Signaling Technology; Cat# 4179S), rabbit anti-brain-derived neurotrophic factor (BDNF; 1:5000; Abcam; Cat# ab108319), rabbit antiglial cell line-derived neurotrophic factor (GDNF; 1:5000; Abcam; Cat# ab176564), rabbit anti-GFAP (1:10000; Proteintech; Cat# 16825-1-AP), rabbit anti-Iba1 (1:1000; Abcam; Cat# ab178847), mouse anti-Toll-like receptor 4 (TLR4; 1:1000; Santa Cruz Biotechnology, Cat# sc-293072), rabbit antimyeloid differentiation primary response gene 88 (MyD88; 1:1000; Proteintech; Cat# 23230-1-AP), rabbit antiphosphorylated-p65 (p-p65; 1:1000; Abcam; Cat# ab86299), rabbit anti-p65 (1:1000; Cell Signaling Technology; Cat# 8242S), rabbit anti-zona occludens 1 (ZO-1; 1:5000; Proteintech; Cat# 21773-1-AP), rabbit antioccludin (1:1000; Proteintech; Cat# 13409-1-AP), and rabbit anti- $\beta$ -actin (1:1000; Cell Signaling Technology; Cat# 4970S). The membrane was washed with TBST and then incubated with the appropriate secondary antibody at room temperature for 1-2 h. The enhanced chemiluminescence detection system (Pierce) was used to observe the

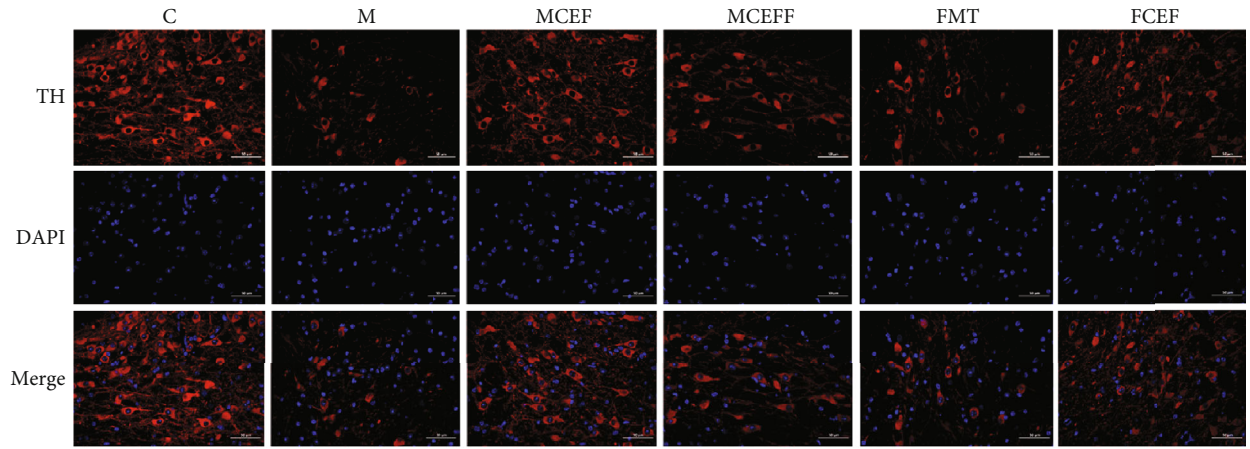
membranes. The ImageJ software (National Institutes of Health) was used to calculate the density determination.

**2.7. Serum Cytokine Measurement.** Blood (100-150  $\mu$ l) was collected after anaesthesia. The blood was incubated at 4°C for 30 min and then centrifuged at 1500 g for 15 min; the upper serum was collected and stored at -80°C. The levels of several cytokines were determined by using commercially available enzyme-linked immunosorbent assay (ELISA) kits according to manufacturer's protocols: IL-6 (Proteintech, Cat# KE10007), TNF- $\alpha$  (Proteintech, Cat# KE10002), and IL-1 $\beta$  (Proteintech, Cat# KE10003).

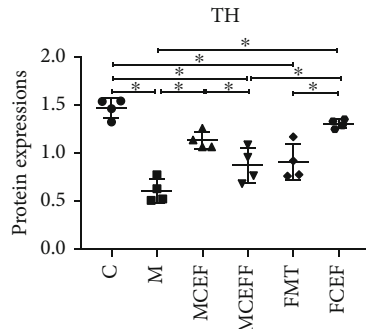
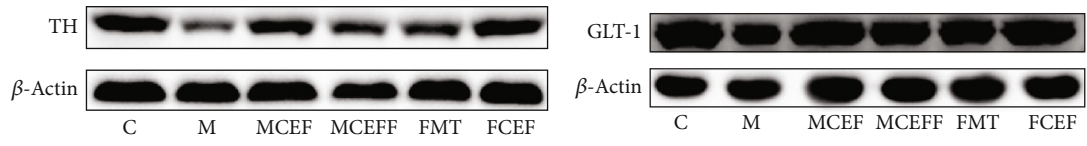
**2.8. DNA Extraction.** Faecal samples from groups C ( $N = 8$ ), M ( $N = 8$ ), MCEF ( $N = 8$ ), MCEFF ( $N = 8$ ), FMT ( $N = 8$ ), and FCEF ( $N = 8$ ) were collected after the behavioural testing, and the TIANamp Bacteria DNA Kit (TianGen) was used to extract microbiota genomic DNA. The extracted DNA was quantified by using a nanodrop spectrophotometer, and the quality of DNA extraction was visualised by using 1.2% agarose gel electrophoresis. The 16S rDNA V4 region was amplified using primers 515F (5'-GTGCCAGC MGCCGCGGTAA-3') and 806R (5'-GGACTACVSGGGT ATCTAAT-3'). Then, the polymerase chain reaction (PCR) products were sequenced on the IlluminaHiSeq 2000 platform (Illumina, Inc.) (GenBank accession number PRJNA659569).

**2.9. High-Throughput 16S rDNA Amplicon Sequencing Analysis.** The Illumina MiSeq/NovaSeq platform was used to conduct paired-end sequencing of community DNA fragments. The analysis software QIIME2 (version 2019.4, <https://docs.qiime2.org/2019.4/tutorials/>) and the QIIME2 dada2 analysis process were used. Sequences were quality filtered, denoised, and merged, and chimera were removed to obtain amplicon sequence variants (ASVs). In addition, the Vsearch software analysis process was used for quality filtering, merging, chimera removal, and clustering to obtain operational taxonomic units (OTUs) [18]. According to the distribution of ASV/OTU in different samples, the  $\alpha$ -diversity level of each sample was evaluated.

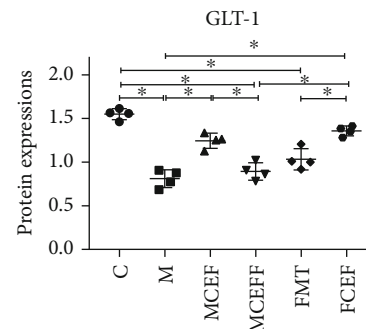
The Chao1 index estimates the number of species that actually exist in the community by calculating the ASV/OTU that are only detected once and twice in the community. The Faith\_pd index evaluates the degree of genetic diversity of the community by calculating the full length of the clade occupied by the ASV/OTU representative sequence in the sample in the phylogenetic tree constructed by it. The  $\beta$ -diversity index represents the difference between samples. Principal coordinate analysis (PCoA), nonmetric multidimensional scaling (NMDS), and other nonconstrained sorting methods were used to reduce the dimensionality of multidimensional microbial data and to display the distribution of samples on the continuous sort axis to show the main trend of the data changes. PCoA expands the sample distance matrix in a low-dimensional space after projecting it and preserves the distance relationship of the original sample to the utmost extent.



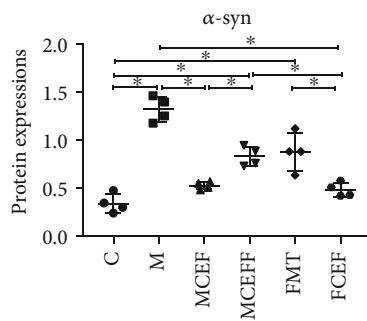
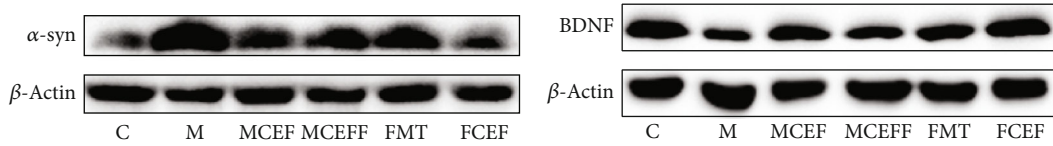
(a)



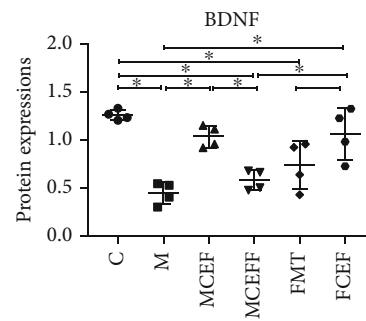
(b)



(c)



(d)



(e)

FIGURE 2: Continued.

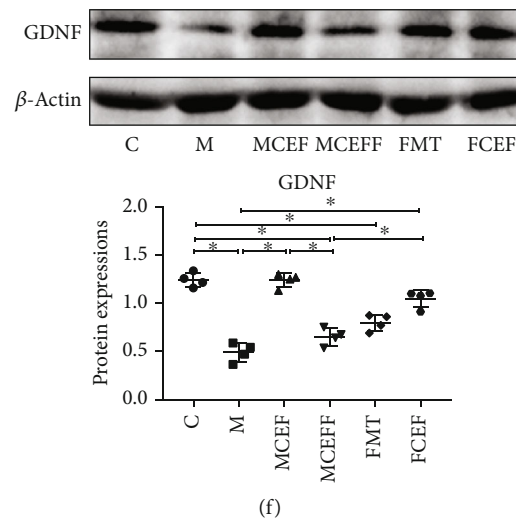


FIGURE 2: Ceftriaxone alleviated MPTP-induced neuropathologic changes in PD mice. (a) Ceftriaxone alleviated the reduction of dopamine neurons on mouse brain induced by MPTP (IF staining of substantia nigra). Western blotting of TH (b), GLT-1 (c),  $\alpha$ -syn (d), BDNF (e), and GDNF (f) expression in substantia nigra,  $\beta$ -actin was used as an internal control. C group ( $N = 4$ ), control group; M group ( $N = 4$ ), MPTP group; MCEF group ( $N = 4$ ), MPTP + ceftriaxone group; MCEFF group ( $N = 4$ ), MPTP + ceftriaxone + fecal microbiota transplantation group; FMT group ( $N = 4$ ), fecal microbiota transplantation group, FCEF group ( $N = 4$ ), fecal microbiota transplantation group + ceftriaxone group. Data are presented as means  $\pm$  SD. One-way repeated-measures ANOVA with Tukey's test for multiple comparisons (b–f, respectively); \* $p < 0.05$ , \*\* $p < 0.01$ . CEF: ceftriaxone; MPTP: 1-methyl-4-phenyl-1, 2, 3, 6-tetra-hydropyridine.

**2.10. Data Analysis.** Prism version 7.0 (GraphPad Software, San Diego, CA, USA) was used for data analysis. Statistical analysis was conducted by one-way analysis of variance (ANOVA) followed by Tukey's test for multiple comparisons, as indicated in the figure legends. The data are presented as mean  $\pm$  standard deviation (SD), and  $p < 0.05$  was regarded to be statistically significant.

### 3. Results

**3.1. Ceftriaxone Improved the Motor Dysfunction and Decreased Exploratory Ability Caused by MPTP.** To investigate the effects of ceftriaxone on PD mice, we established a subacute PD mouse model using MPTP and then conducted the faecal microbiota transplantation experiment (Figure 1(a)). In the pole test, MPTP-treated mice showed significant motor dysfunction compared with the control group (M vs. C = 17.72 s vs. 10.89 s;  $p < 0.001$ ), and ceftriaxone significantly alleviated MPTP-induced motor dysfunction (MCEF vs. M = 11.67 s vs. 17.72 s;  $p < 0.001$ ), and motor dysfunction recurred in the MCEFF group, which underwent transplantation of faecal microbiota from PD mice (MCEFF vs. MCEF = 13.83 s vs. 11.67 s) (Figure 1(b)). In addition, when we transplanted the faecal microbiota of PD mice to normal mice, the mice in the FMT group showed motor impairment compared with the control group (FMT vs. C = 15.74 s vs. 10.89 s;  $p < 0.01$ ). Notably, the use of ceftriaxone could reverse the movement impairment caused by faecal microbiota transplantation from PD mice (FCEF vs. FMT = 12.16 s vs. 15.74 s; Figure 1(b)).

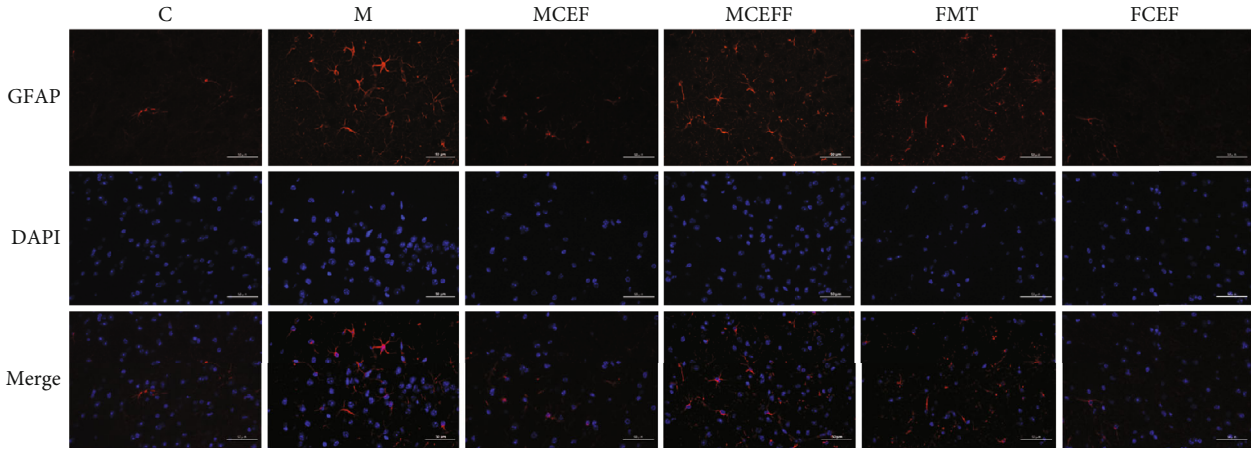
In the open field test, mice in the M group showed decreased exploratory ability after injection of MPTP compared with the C group, as indicated by the total movement distance (M vs. C = 2169 cm vs. 3806 cm; Figure 1(c)),

distance moved in the central area (M vs. C = 510.6 cm vs. 890.7 cm; Figure 1(d)), and the number of entries in the central area (M vs. C = 16.5 vs. 33.75; Figure 1(e)) ( $p < 0.001$ ). Additionally, the use of ceftriaxone increased the exploratory ability of MPTP-induced PD mice. In the MCEFF and FMT groups, the transplantation of PD microbiota decreased the exploratory ability of mice, and the use of ceftriaxone reversed the behavioural and mental changes of the mice caused by PD microbiota in the FCEF group (Figures 1(c)–1(e)).

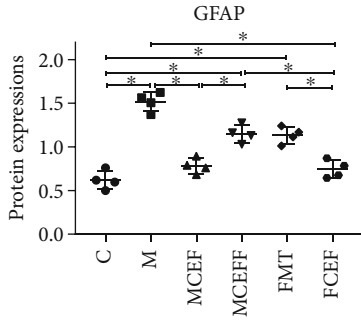
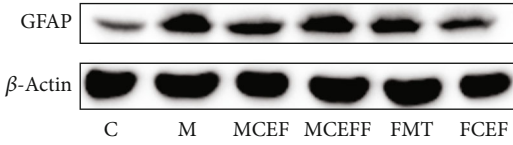
**3.2. Effect of Ceftriaxone on MPTP-Induced Neuropathological Changes.** To evaluate the effect of ceftriaxone on PD mice neuropathologically, immunofluorescence was used to detect TH expression in the substantia nigra of mice. MPTP significantly reduced the TH expression in the substantia nigra of mice in the M group (Figure 2(a)). Based on Western blotting, MPTP treatment significantly decreased the expression of TH, GLT-1, and neurotrophic factors, and significantly increased the expression of  $\alpha$ -syn compared with the C group (Figures 2(b)–2(f)). The transplantation of microbiota from PD mice worsened the neuropathological characteristics in the MCEFF and FMT groups, while the use of ceftriaxone greatly enhanced the expression of TH, GLT-1, and neurotrophic factors and reduced the expression of  $\alpha$ -syn (Figure 2).

We further studied the effect of ceftriaxone on astrocytes and microglia; ceftriaxone significantly reduced the activation of glia via downregulating the expression of GFAP (a marker of astrocytes) and Iba1 (a marker of microglia) in the substantia nigra of mice (Figures 3(a)–3(d)). In addition, this drug reduced inflammation by lowering the expression of TLR4, MyD88, and p-p65 in the TLR4/NF- $\kappa$ B inflammatory pathway in the substantia nigra of mice (Figure 3(e)).

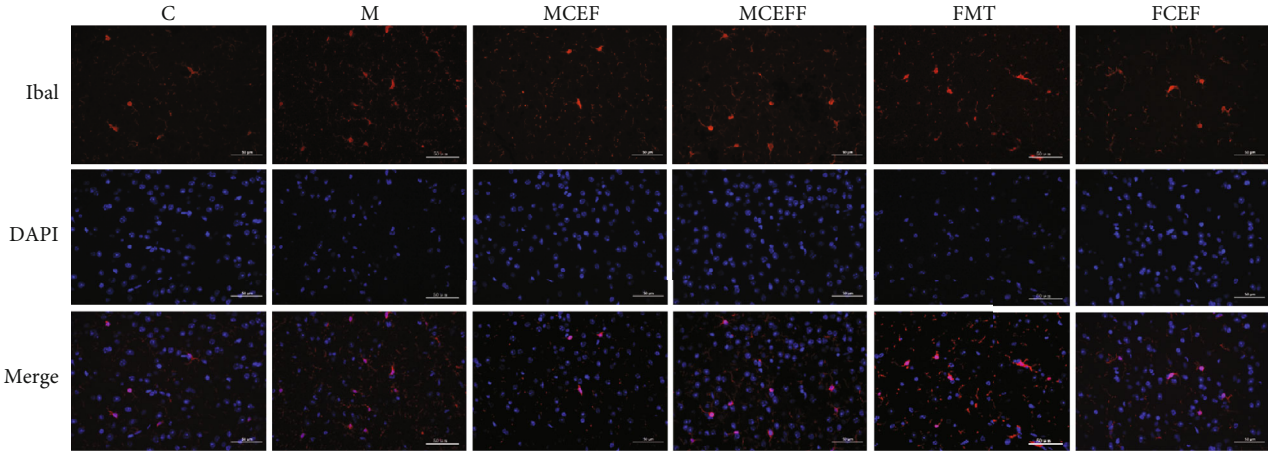




(a)



(b)



(c)

FIGURE 3: Continued.

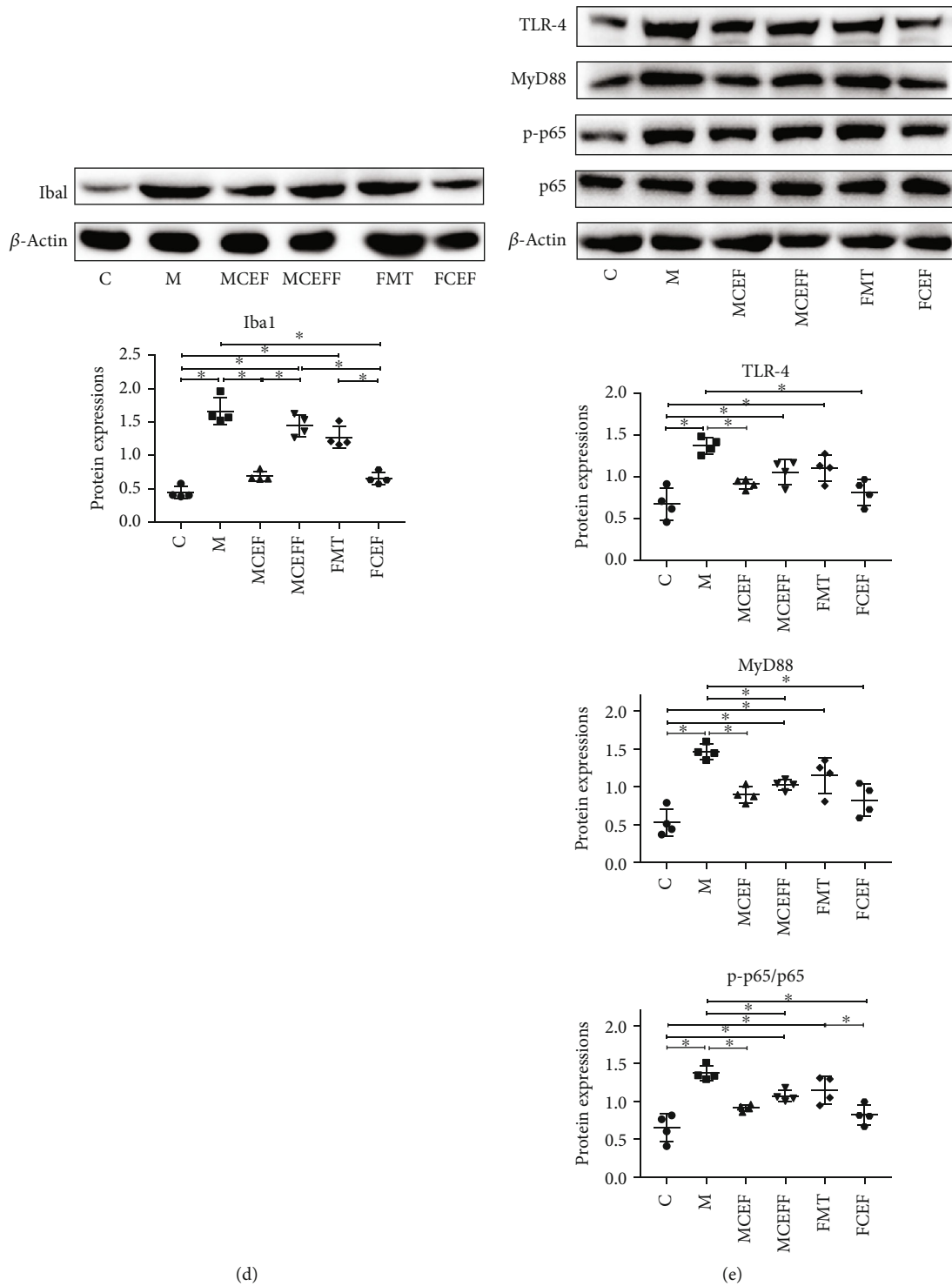


FIGURE 3: Ceftriaxone alleviates MPTP-induced neuroinflammation. (a) Ceftriaxone decreased the expression of GFAP on mouse brain induced by MPTP (IF staining of substantia nigra). (b) Western blotting of GFAP expression in substantia nigra,  $\beta$ -actin was used as an internal control. (c) Ceftriaxone decreased the expression of Iba1 on mouse brain induced by MPTP (IF staining of substantia nigra). (d) Western blotting of Iba1 expression in substantia nigra,  $\beta$ -actin was used as an internal control. (e) Western blotting of TLR-4, MyD88, p-NF $\kappa$ B, and NF $\kappa$ B expression in substantia nigra,  $\beta$ -actin was used as an internal control. C group ( $N = 4$ ), control group; M group ( $N = 4$ ), MPTP group; MCEF group ( $N = 4$ ), MPTP + ceftriaxone group; MCEFF group ( $N = 4$ ), MPTP + ceftriaxone + fecal microbiota transplantation group; FMT group ( $N = 4$ ), fecal microbiota transplantation group, FCEF group ( $N = 4$ ), fecal microbiota transplantation group + ceftriaxone group. Data are presented as means  $\pm$  SD. One-way repeated-measures ANOVA with Tukey's test for multiple comparisons (b, d, e, respectively); \* $p < 0.05$ , \*\* $p < 0.01$ . CEF: ceftriaxone; MPTP: 1-methyl-4-phenyl-1, 2, 3, 6-tetra-hydropyridine.

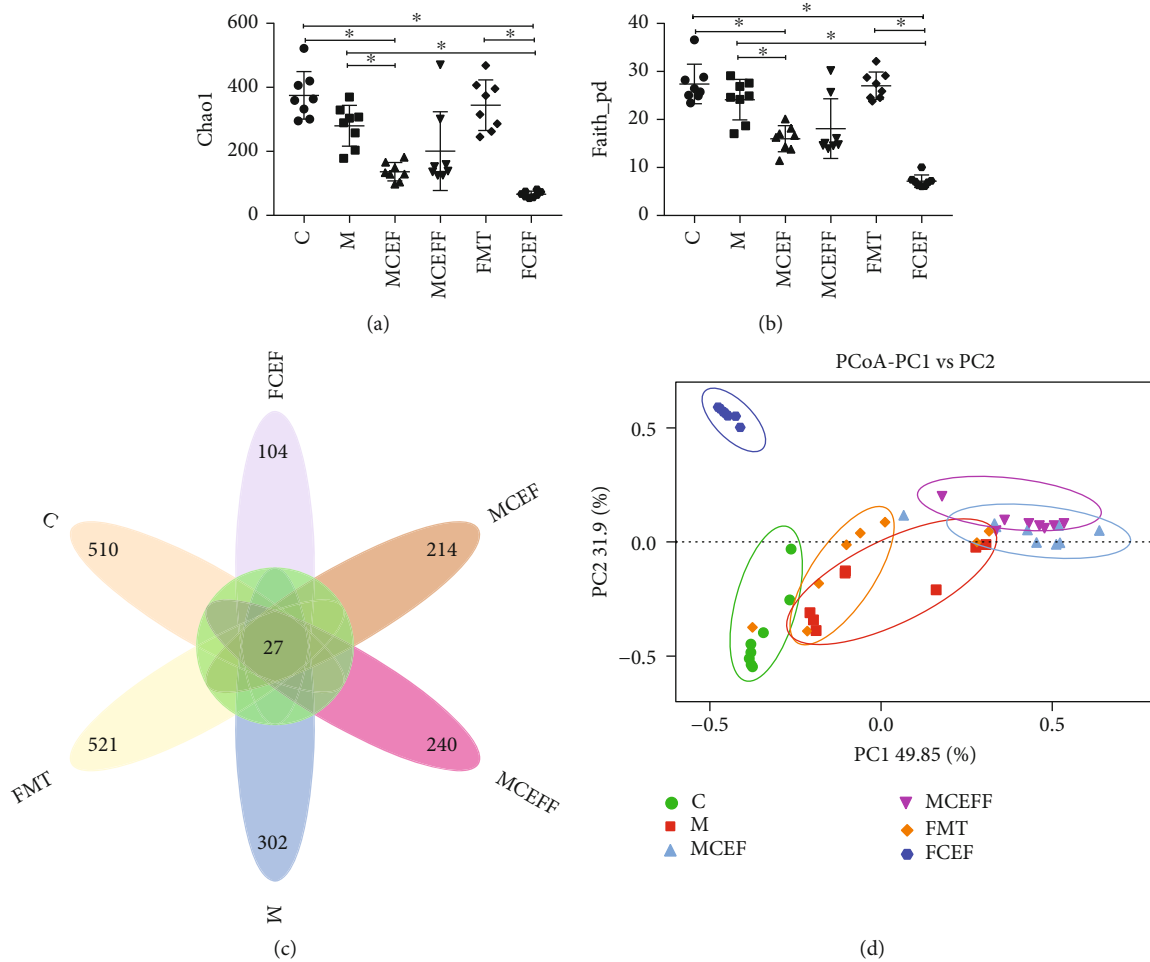


FIGURE 4: Gut microbial dysbiosis in PD mice is reduced by ceftriaxone. (a) The Chao1 index. (b) The Faith\_pd index. (c) Petal map representation of OTUs. (d) PCoA of  $\beta$  diversity index. C group ( $N = 8$ ), control group; M group ( $N = 8$ ), MPTP group; MCEF group ( $N = 8$ ), MPTP + ceftriaxone group; MCEFF group ( $N = 8$ ), MPTP + ceftriaxone + fecal microbiota transplantation group; FMT group ( $N = 8$ ), fecal microbiota transplantation group; FCEF group ( $N = 8$ ), fecal microbiota transplantation group + ceftriaxone group. Data are presented as means  $\pm$  SD. One-way repeated-measures ANOVA with Tukey's test for multiple comparisons (a, b, respectively); \* $p < 0.05$ , \*\* $p < 0.01$ . CEF: ceftriaxone; MPTP: 1-methyl-4-phenyl-1, 2, 3, 6-tetra-hydropyridine.

Transplantation of microbiota from PD mice enhanced the activation of glia and increased the levels of TLR4/NF- $\kappa$ B inflammatory proteins, and the use of ceftriaxone reversed these changes (Figure 3).

**3.3. Effect of Ceftriaxone on the Intestinal Microbiota of MPTP-Induced PD Mice.** The intestinal microbiota plays a key role in the development and treatment of PD through the brain-gut axis [9]. Therefore, 16S rDNA amplicon sequencing was used to evaluate the effect of ceftriaxone on the intestinal microbiota of PD mice. The Chao1 index and Faith\_pd index showed that there was no obvious difference between the C and M groups, while the use of ceftriaxone significantly reduced the  $\alpha$ -diversity in the MCEF, MCEFF, and FCEF groups (Figures 4(a) and 4(b)). The Venn results revealed 27 common OTUs in all groups, and the number of unique OTUs in the C, M, MCEF, MCEFF, FMT, and FCEF groups is 510, 302, 214, 240, 521, and 104, respectively (Figure 4(c)). PCoA analysis indicated that the samples in the M group were far from

samples in the C group, and the transplantation of faecal microbiota from PD mice (MCEFF and FMT groups) significantly changed the microbial diversity compared with the C group. Moreover, the use of ceftriaxone (MCEF, MCEFF, and FCEF groups) greatly changed the microbial diversity compared with the C group (Figure 4(d)), even though these mice had obvious changes in behaviour and neuroinflammation caused by MPTP and PD faecal microbiota transplantation.

Finally, we compared the relative abundance of probiotics and pathogens closely related to PD (Figure 5). MPTP reduced the abundance of the phylum Firmicutes and the genera *Akkermansia*, *Prevotella*, and *Ruminococcus* and markedly enhanced the abundance of the genera *Proteus*, *Adlercreutzia*, *Bifidobacterium*, *Clostridium*, and *Dorea* in the M group compared with the C group. Ceftriaxone treatment reduced the abundance of the genera *Bifidobacterium* and *Proteus* ( $p < 0.01$ ) and increased the abundance of the probiotic genera *Akkermansia* and *Prevotella* (Figure 5).

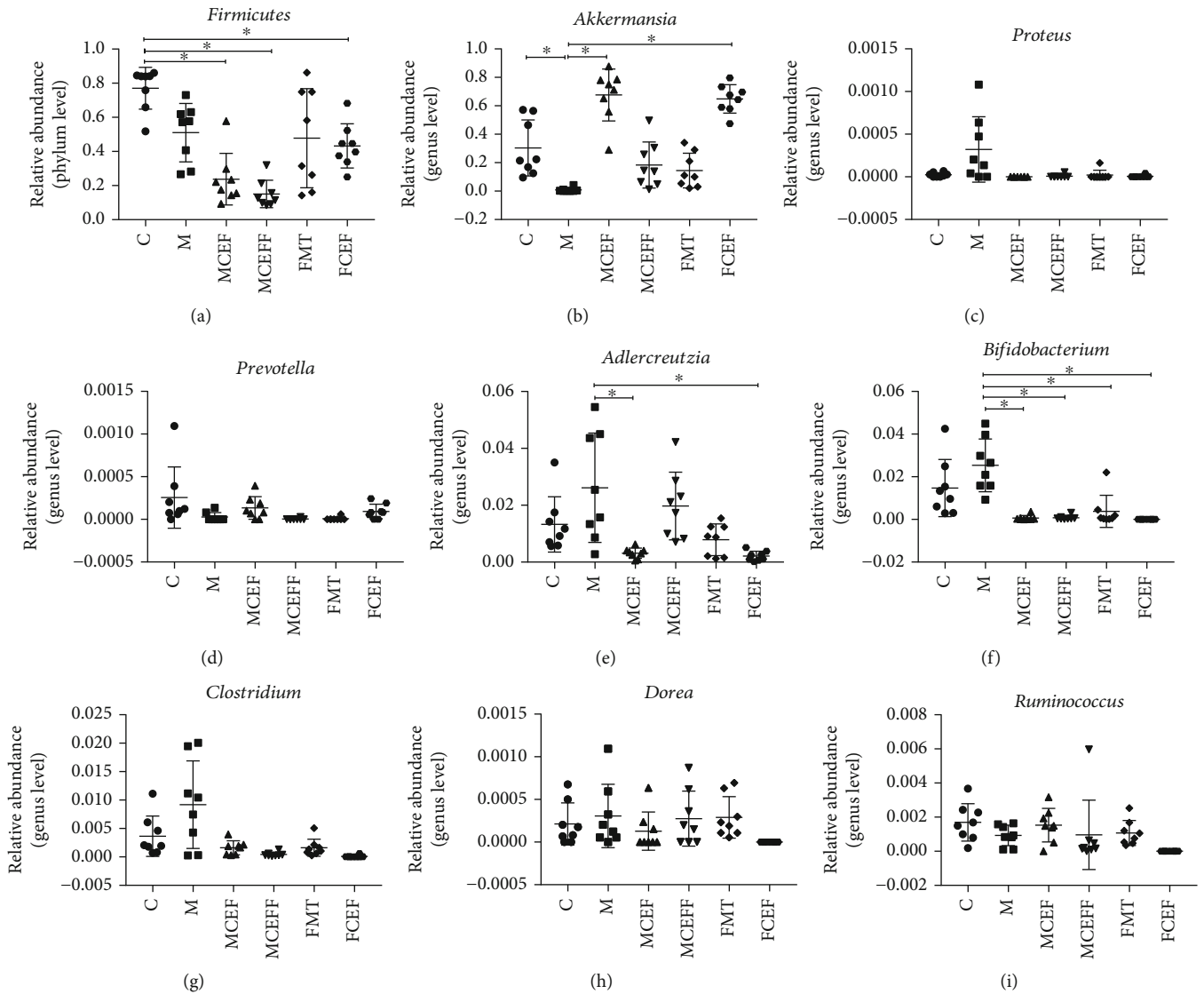


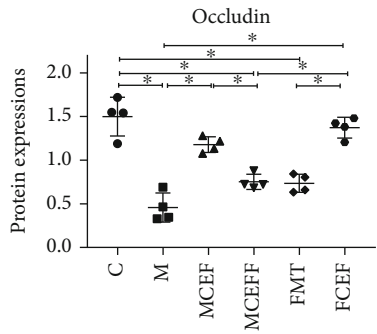
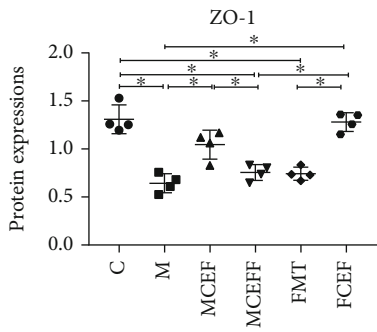
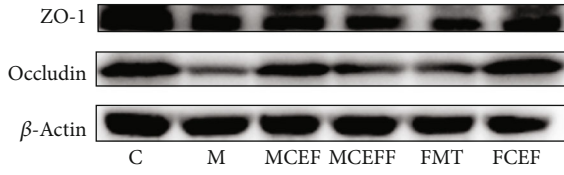
FIGURE 5: Effect of ceftriaxone on the relative abundance of gut microbial at phylum and genus level in feces of mice. The relative abundance of *Firmicutes* (a), *Akkermansia* (b), *Proteus* (c), *Prevotella* (d), *Adlercreutzia* (e), *Bifidobacterium* (f), *Clostridium* (g), *Dorea* (h), and *Ruminococcus* (i), in feces of PD mice. C group ( $N = 8$ ), control group; M group ( $N = 8$ ), MPTP group; MCEF group ( $N = 8$ ), MPTP + ceftriaxone group; MCEFF group ( $N = 8$ ), MPTP + ceftriaxone + fecal microbiota transplantation group; FMT group ( $N = 8$ ), fecal microbiota transplantation group, FCEF group ( $N = 8$ ), fecal microbiota transplantation group + ceftriaxone group. Data are presented as means  $\pm$  SD. One-way repeated-measures ANOVA with Tukey's test for multiple comparisons (a–i, respectively); \* $p < 0.05$ , \*\* $p < 0.001$ . CEF: ceftriaxone; MPTP: 1-methyl-4-phenyl-1, 2, 3, 6-tetra-hydropyridine.

**3.4. Ceftriaxone Regulated Intestinal Tight Junction Proteins and Inhibited Intestinal Inflammation and Systemic Inflammation Caused by MPTP.** To further investigate the role of intestinal microbiota in the brain-gut axis, we assessed the expression of intestinal tight-junction-associated proteins and proteins in the TLR4/NF- $\kappa$ B inflammatory pathway in the colon (Figure 6). MPTP significantly reduced the expression of ZO-1 and occludin (Figure 6(a)); increased the expression of TLR4, MyD88, and p-p65 in the M group compared with the C group (Figure 6(b)); and also promoted the expression of inflammatory cytokines IL-6 (M vs. C = 154.7 pg/ml vs. 17.94 pg/ml;  $p < 0.01$ ), IL-1 $\beta$  (M vs. C = 65.93 pg/ml vs. 12.74 pg/ml;  $p < 0.01$ ), and TNF- $\alpha$  (M vs. C = 147.2 pg/ml vs. 14.47 pg/ml;  $p < 0.01$ ) in the serum

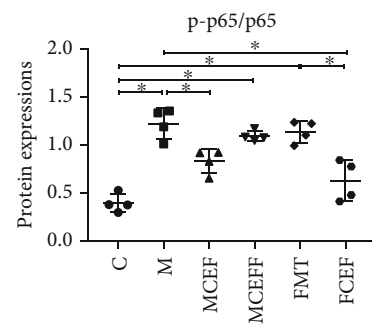
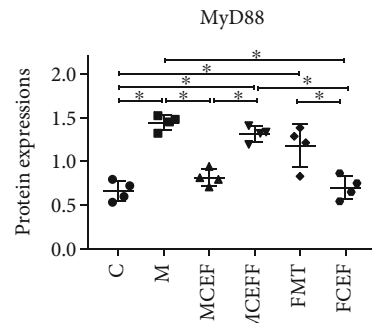
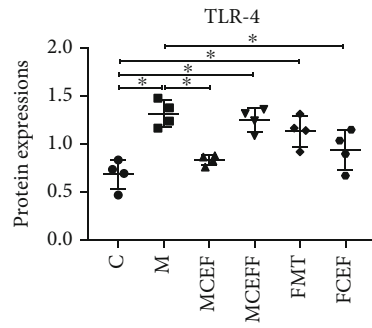
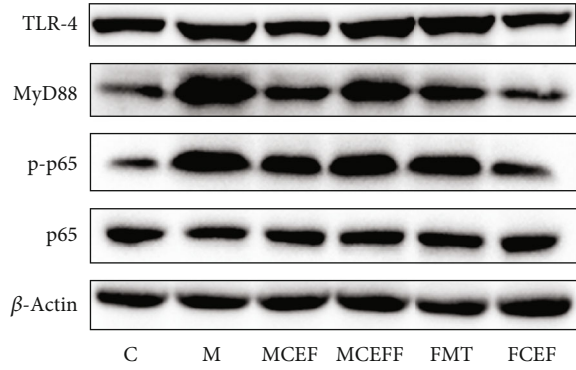
of mice (Figure 6(c)). The use of ceftriaxone significantly reduced the colonic inflammatory proteins and systemic inflammatory cytokines caused by MPTP and faecal microbiota transplantation from PD mice and greatly enhanced the expression of intestinal tight-junction-associated proteins.

#### 4. Discussion

PD is a common degenerative disease of the central nervous system; the number of patients with PD is predicted to exceed 17.5 million by 2040 [1]. At present, there is no specific medicine to cure PD [19]. Therefore, considering the difficulties of new drug development, exploiting new features



(a)



(b)

FIGURE 6: Continued.

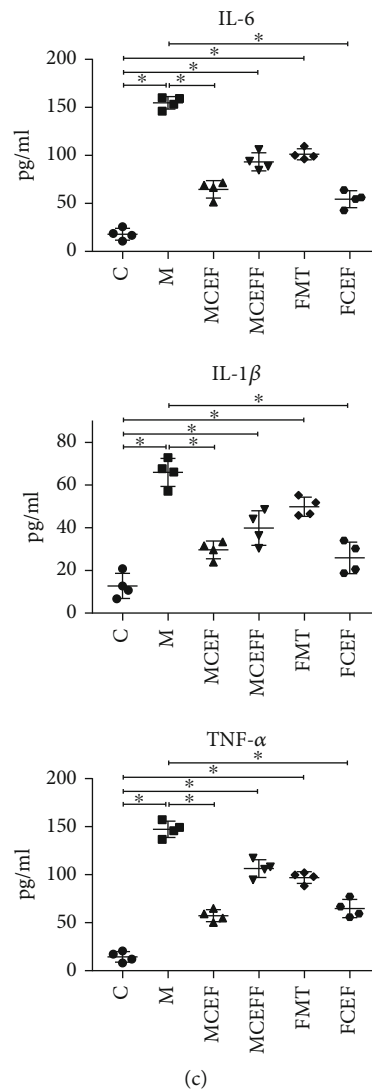


FIGURE 6: Ceftriaxone regulated intestinal tight junction proteins and inhibited intestinal inflammation and systemic inflammation caused by MPTP. (a) Western blot analysis of permeation-related proteins ZO-1, Occludin expression in the colon of mice,  $\beta$ -actin was used as an internal control. (b) Western blotting of TLR-4, MyD88, p-NF $\kappa$ B, and NF $\kappa$ B expression in the colon of mice,  $\beta$ -actin was used as an internal control. (c) The expression of inflammatory cytokines TNF- $\alpha$ , IL-6 and IL-1 $\beta$  in protein levels was detected by ELISA. C group ( $N = 4$ ), control group; M group ( $N = 4$ ), MPTP group; MCEF group ( $N = 4$ ), MPTP + ceftriaxone group; MCEFF group ( $N = 4$ ), MPTP + ceftriaxone + fecal microbiota transplantation group; FMT group ( $N = 4$ ), fecal microbiota transplantation group, FCEF group ( $N = 4$ ), fecal microbiota transplantation group + ceftriaxone group. Data are presented as means  $\pm$  SD. One-way repeated-measures ANOVA with Tukey's test for multiple comparisons (a-c, respectively); \* $p < 0.05$ , \*\* $p < 0.01$ . CEF: ceftriaxone; MPTP: 1-methyl-4-phenyl-1, 2, 3, 6-tetra-hydropyridine.

of old drugs is a good choice [13]. Ceftriaxone is a broad-spectrum antibiotic that is used commonly in the clinic to treat infections of the respiratory tract and urinary system [16]; it exhibits a neuroprotective effect in addition to its antibacterial effect in PD [15, 20] and AD [21]. However, little work has been done to explore the effect of ceftriaxone on the intestinal microbiota in PD.

In this study, a mouse model of subacute PD was used to evaluate the effect of ceftriaxone on PD, and faecal microbiota transplantation was performed (faecal microbiota from PD mice were transplanted into normal mice) to evaluate whether ceftriaxone plays an important role in regulating the intestinal microbiota of PD mice. MPTP caused signifi-

cant motor dysfunction and decreased the exploratory ability of mice, and the mice receiving faecal microbiota from PD mice also showed similar behaviours. Intraperitoneal injection of ceftriaxone reversed the behavioural changes caused by MPTP and PD faecal microbiota. These results are consistent with previous reports that ceftriaxone could improve the motor dysfunction of PD [20, 22].

The dopaminergic and glutamatergic systems in the brain work together to regulate motor and cognitive functions [23]. TH is the rate-limiting enzyme that participates in dopamine synthesis, and when it is reduced to a certain threshold, it will cause the motor symptoms of PD [24]. Meanwhile, the excitotoxicity of glutamate plays an

important role in the pathogenesis of PD [25]. Glutamate in the brain is mainly cleared by GLT-1, but GLT-1 shows dysfunction or decreased expression in patients with neurodegenerative diseases such as PD [26], AD [27], or ALS [17]. Ceftriaxone reportedly reduced the loss of dopaminergic neurons in PD patients by increasing GLT-1 expression [23], and our results also confirmed that ceftriaxone could increase TH and GLT-1 expression in mouse substantia nigra. In addition, BDNF and GDNF are dopamine-active neurotrophic proteins that can promote the survival of dopaminergic neurons and play an important role in neurite growth [28]. Our results showed that ceftriaxone restored the expression of BDNF and GDNF in MPTP-induced PD mice, a finding that is consistent with the results of Kaur and Prakash [15]. In summary, these results indicate that ceftriaxone could increase the expression of TH, GLT-1, and neurotrophic factors, thereby improving the motor symptoms of PD mice.

In recent years, increasing evidence has confirmed that the neuroinflammatory response is involved in the pathogenesis of PD. Neuroinflammation is characterised by the activation of microglia and astrocytes [29]. Microglia is the inherent immune effector cells in the central nervous system [30, 31]. Under normal circumstances, microglia are in a resting state. When brain tissue is damaged or stimulated by  $\alpha$ -syn or bacteria and their metabolites in the brain, TLR4 is activated on microglia, and then, the NF- $\kappa$ B pathway is activated to promote the secretion of proinflammatory factors such as IL-6, IL-1 $\beta$ , and TNF- $\alpha$ ; the ultimate outcome is the death of neurons [30, 32]. The signalling pathway mediated by TLR4 plays an important role in PD [33], and knockout of the *Tlr4* gene reduces rotenone-induced motor dysfunction, neuroinflammation, and corresponding neuropathological changes in PD mice [33]. In this study, we found that ceftriaxone reduced the expression of GFAP and Iba1 and downregulated the expression levels of TLR4, MyD88, and p-p65, all part of the inflammatory pathway.

To further explore the effect of ceftriaxone on the intestinal microbes of PD mice, 16S rDNA amplicon sequencing was used to detect changes in gut microbes in the mice. Through the Chao1 index and Faith\_pd index, we found that MPTP treatment reduced the  $\alpha$ -diversity of the intestinal microbiota. Although ceftriaxone treatment also significantly reduced the  $\alpha$ -diversity of the intestinal microbiota, when we analysed microbiota changes at the phylum and genus levels, we found that the abundance of the genera *Akkermansia* and *Prevotella* was increased in the ceftriaxone-treated groups. Many studies have shown that *Akkermansia* can effectively improve symptoms in mouse models of diseases such as ALS [34], progeria [35], and chronic colitis [36] by promoting healing and recovery of intestinal mucosal layer and reducing the expression of proinflammatory cytokines such as TNF- $\alpha$  and interferon gamma (IFN- $\gamma$ ) in the colon. *Prevotella* has been reported to be correlated negatively with PD [37] and autism spectrum disorder (ASD) [38]. In addition, MPTP administration increased the abundance of the genera *Proteus*, *Adlercreutzia*, *Bifidobacterium*, and *Clostridium*, as well as

the bacterium *Proteus mirabilis* that may trigger neuroinflammation and lead to pathological changes related to PD by its metabolites (such as lipopolysaccharide) [39]. Although studies have shown that *Lactobacillus acidophilus* and *Bifidobacterium infantis* can improve abdominal pain and bloating in PD patients [40], the results reported by Petrov et al. [37] and our research consistently showed that the abundance of *Bifidobacterium* in PD is increased.

The functions of the intestinal mucosal barrier are related to the intestinal microbiota, whose dysbiosis can lead to decreased expression of intestinal tight-junction-associated proteins. This reduction allows the entry of pathogenic bacteria and their metabolites into the blood and increases inflammatory factors such as IL-6, IL-1 $\beta$ , and TNF- $\alpha$  [36]. There is an increase in proinflammatory microorganisms in the intestinal microbiota of PD patients [41], and proinflammatory cytokines could play a role in the nonmotor symptoms of PD [42]. In our study, ceftriaxone therapy restored the MPTP-induced decrease in intestinal tight-junction-associated proteins, reducing TLR4-mediated intestinal inflammation as well as serum IL-6, IL-1 $\beta$ , and TNF- $\alpha$  expression.

## 5. Conclusion

We conclude that ceftriaxone regulates the intestinal microbiota of PD mice and alleviates the motor dysfunction and decreased exploratory ability. It also plays an important role in increasing the integrity of the intestinal barrier, reducing the inflammation of the colon and the brain, and has a neuroprotective effect (Supplemental Figure 1). Ceftriaxone could be a potential treatment for PD, but we only examined the short-term effects of ceftriaxone on PD through the establishment of an MPTP-induced PD mouse model. Further work is needed to determine the long-term effects of ceftriaxone by using transgenic mice. In addition, because ceftriaxone drug resistance could appear after long-term use, the dose and frequency of ceftriaxone should be explored.

## Data Availability

The datasets used and/or analyzed during the present study are available from the corresponding author on reasonable request.

## Conflicts of Interest

The authors declare that there is no conflict of interest regarding the publication of this paper.

## Authors' Contributions

XF and TTC contributed to conception and design of the study. XTZ, JCL, KHW, JW, PYT, and MYY performed the experiments. YW, DJH, FJL, and BW carried out data analysis. All authors participated in drafting of the

manuscript and critical revision of the draft and contributed to the article and approved the submitted version.

## Acknowledgments

This work was supported by grants from the National Natural Science Foundation of China (nos. 82060222 to XF and 82060638 to TC), Science and Technology Plan of Jiangxi Health Planning Committee (no. 20195092 to XF), the Major Disciplines of Academic and Technical Leaders Project of Jiangxi Province to XF, the Science and Technology Project of Jiangxi (nos. 20194BCJ22032 to TC and 20192BBG70031 to XF), and Double 10-Thousand Plan of Jiangxi Province to TC (innovation and technology professionals as the high-end talent).

## Supplementary Materials

Supplemental Figure 1: the graphical abstract of our study. Ceftriaxone can alleviate the motor dysfunction and decreased exploration ability. In addition, it also plays an important role in increasing the integrity of the intestinal barrier, reducing the inflammation of the colon and brain, and has the neuroprotective effect, and its neuroprotective effect may be through regulating inflammation and intestinal microbiota. (*Supplementary Materials*)

## References

- [1] O. B. Tysnes and A. Storstein, "Epidemiology of Parkinson's disease," *Journal of Neural Transmission*, vol. 2017, no. 124, pp. 901–905, 2017.
- [2] S. Sveinbjornsdottir, "The clinical symptoms of Parkinson's disease," *Journal of Neurochemistry*, vol. 139, Suppl 1, pp. 318–324, 2016.
- [3] P. Martinez-Martin, D. Macaulay, Y. J. Jalundhwala et al., "The long-term direct and indirect economic burden among Parkinson's disease caregivers in the United States," *Movement Disorders*, vol. 34, no. 2, pp. 236–245, 2019.
- [4] D. Grimes, M. Fitzpatrick, J. Gordon et al., "Canadian guideline for Parkinson disease," *Canadian Medical Association Journal*, vol. 191, no. 36, pp. E989–E1004, 2019.
- [5] F. I. Tarazi, Z. T. Sahli, M. Wolny, and S. A. Mousa, "Emerging therapies for Parkinson's disease: from bench to bedside," *Pharmacology & Therapeutics*, vol. 144, no. 2, pp. 123–133, 2014.
- [6] M. F. Sun, Y. L. Zhu, Z. L. Zhou et al., "Neuroprotective effects of fecal microbiota transplantation on MPTP-induced Parkinson's disease mice: gut microbiota, glial reaction and TLR4/TNF- $\alpha$  signaling pathway," *Brain, Behavior, and Immunity*, vol. 70, pp. 48–60, 2018.
- [7] E. M. M. Quigley, "Microbiota-brain-gut axis and neurodegenerative diseases," *Current Neurology and Neuroscience Reports*, vol. 17, no. 12, p. 94, 2017.
- [8] M. Obrenovich, H. Jaworski, T. Tadimalla et al., "The role of the microbiota-gut-brain axis and antibiotics in ALS and neurodegenerative diseases," *Microorganisms*, vol. 8, no. 5, p. 784, 2020.
- [9] M. F. Sun and Y. Q. Shen, "Dysbiosis of gut microbiota and microbial metabolites in Parkinson's disease," *Ageing Research Reviews*, vol. 45, pp. 53–61, 2018.
- [10] D. Yang, D. Zhao, S. Z. Ali Shah et al., "The role of the gut microbiota in the pathogenesis of Parkinson's disease," *Frontiers in Neurology*, vol. 10, p. 1155, 2019.
- [11] X. Wang, G. Sun, T. Feng et al., "Sodium oligomannate therapeutically remodels gut microbiota and suppresses gut bacterial amino acids-shaped neuroinflammation to inhibit Alzheimer's disease progression," *Cell Research*, vol. 29, no. 10, pp. 787–803, 2019.
- [12] T. H. Mertsalmi, E. Pekkonen, and F. Scheperjans, "Antibiotic exposure and risk of Parkinson's disease in Finland: a nationwide case-control study," *Movement Disorders*, vol. 35, no. 3, pp. 431–442, 2020.
- [13] J. D. Rothstein, S. Patel, M. R. Regan et al., " $\beta$ -Lactam antibiotics offer neuroprotection by increasing glutamate transporter expression," *Nature*, vol. 433, no. 7021, pp. 73–77, 2005.
- [14] M. A. Tikhonova, T. G. Amstislavskaya, V. M. Belichenko et al., "Modulation of the expression of genes related to the system of amyloid-beta metabolism in the brain as a novel mechanism of ceftriaxone neuroprotective properties," *BMC Neuroscience*, vol. 19, no. S1, p. 13, 2018.
- [15] B. Kaur and A. Prakash, "Ceftriaxone attenuates glutamate-mediated neuro-inflammation and restores BDNF in MPTP model of Parkinson's disease in rats," *Pathophysiology*, vol. 24, no. 2, pp. 71–79, 2017.
- [16] M. Nizzardo, M. Nardini, D. Ronchi et al., "Beta-lactam antibiotic offers neuroprotection in a spinal muscular atrophy model by multiple mechanisms," *Experimental Neurology*, vol. 229, no. 2, pp. 214–225, 2011.
- [17] B. R. Miller, J. L. Dorner, M. Shou et al., "Up-regulation of GLT1 expression increases glutamate uptake and attenuates the Huntington's disease phenotype in the R6/2 mouse," *Neuroscience*, vol. 153, no. 1, pp. 329–337, 2008.
- [18] B. J. Callahan, P. J. McMurdie, M. J. Rosen, A. W. Han, A. J. Johnson, and S. P. Holmes, "DADA2: high-resolution sample inference from Illumina amplicon data," *Nature Methods*, vol. 13, no. 7, pp. 581–583, 2016.
- [19] R. M. A. de Bie, C. E. Clarke, A. J. Espay, S. H. Fox, and A. E. Lang, "Initiation of pharmacological therapy in Parkinson's disease: when, why, and how," *The Lancet Neurology*, vol. 19, no. 5, pp. 452–461, 2020.
- [20] R. Bisht, B. Kaur, H. Gupta, and A. Prakash, "Ceftriaxone mediated rescue of nigral oxidative damage and motor deficits in MPTP model of Parkinson's disease in rats," *Neurotoxicology*, vol. 44, pp. 71–79, 2014.
- [21] E. M. Yimer, H. Z. Hishe, and K. B. Tuem, "Repurposing of the  $\beta$ -lactam antibiotic, ceftriaxone for neurological disorders: a review," *Frontiers in Neuroscience*, vol. 13, p. 236, 2019.
- [22] R. Collyer, A. Clancy, and T. Borody, "Faecal microbiota transplantation alleviates symptoms of depression in individuals with irritable bowel syndrome: a case series," *Medicine in Microecology*, vol. 6, article 100029, 2020.
- [23] T. Chotibut, R. W. Davis, J. C. Arnold et al., "Ceftriaxone increases glutamate uptake and reduces striatal tyrosine hydroxylase loss in 6-OHDA Parkinson's model," *Molecular Neurobiology*, vol. 49, no. 3, pp. 1282–1292, 2014.
- [24] S. C. Daubner, T. Le, and S. Wang, "Tyrosine hydroxylase and regulation of dopamine synthesis," *Archives of Biochemistry and Biophysics*, vol. 508, no. 1, pp. 1–12, 2011.
- [25] G. Ambrosi, S. Cerri, and F. Blandini, "A further update on the role of excitotoxicity in the pathogenesis of Parkinson's



- disease,” *Journal of Neural Transmission*, vol. 2014, no. 121, pp. 849–859, 2014.
- [26] C. Ferrarese, L. Tremolizzo, M. Rigoldi et al., “Decreased platelet glutamate uptake and genetic risk factors in patients with Parkinson's disease,” *Neurological Sciences*, vol. 22, no. 1, pp. 65–66, 2001.
- [27] S. Li, M. Mallory, M. Alford, S. Tanaka, and E. Masliah, “Glutamate transporter alterations in Alzheimer disease are possibly associated with abnormal APP expression,” *Journal of Neuropathology and Experimental Neurology*, vol. 56, no. 8, pp. 901–911, 1997.
- [28] M. G. Murer, Q. Yan, and R. Raisman-Vozari, “Brain-derived neurotrophic factor in the control human brain, and in Alzheimer's disease and Parkinson's disease,” *Progress in Neurobiology*, vol. 63, no. 1, pp. 71–124, 2001.
- [29] G. Dutta, P. Zhang, and B. Liu, “The lipopolysaccharide Parkinson's disease animal model: mechanistic studies and drug discovery,” *Fundamental & Clinical Pharmacology*, vol. 22, no. 5, pp. 453–464, 2008.
- [30] M. Colonna and O. Butovsky, “Microglia function in the central nervous system during health and neurodegeneration,” *Annual Review of Immunology*, vol. 35, no. 1, pp. 441–468, 2017.
- [31] J. R. White, P. Dauros-Singorenko, J. Hong, F. Vanholsbeeck, A. Phillips, and S. Swift, “The role of host molecules in communication with the resident and pathogenic microbiota: a review,” *Medicine in Microecology*, vol. 4, article 100005, 2020.
- [32] S. Voet, S. Srinivasan, M. Lamkanfi, and G. van Loo, “Inflammasomes in neuroinflammatory and neurodegenerative diseases,” *EMBO Molecular Medicine*, vol. 11, no. 6, 2019.
- [33] P. Perez-Pardo, H. B. Dodiya, P. A. Engen et al., “Role of TLR4 in the gut-brain axis in Parkinson's disease: a translational study from men to mice,” *Gut*, vol. 68, no. 5, pp. 829–843, 2019.
- [34] E. Blacher, S. Bashiardes, H. Shapiro et al., “Potential roles of gut microbiome and metabolites in modulating ALS in mice,” *Nature*, vol. 572, no. 7770, pp. 474–480, 2019.
- [35] C. Bárcena, R. Valdés-Mas, P. Mayoral et al., “Healthspan and lifespan extension by fecal microbiota transplantation into progeroid mice,” *Nature Medicine*, vol. 25, no. 8, pp. 1234–1242, 2019.
- [36] M. C. Collado, M. Derrien, E. Isolauri, W. M. de Vos, and S. Salminen, “Intestinal integrity and Akkermansia muciniphila, a mucin-degrading member of the intestinal microbiota present in infants, adults, and the elderly,” *Applied and Environmental Microbiology*, vol. 73, no. 23, pp. 7767–7770, 2007.
- [37] V. A. Petrov, I. V. Saltykova, I. A. Zhukova et al., “Analysis of gut microbiota in patients with Parkinson's disease,” *Bulletin of Experimental Biology and Medicine*, vol. 162, no. 6, pp. 734–737, 2017.
- [38] Z. Dan, X. Mao, Q. Liu et al., “Altered gut microbial profile is associated with abnormal metabolism activity of autism SPECTRUM disorder,” *Gut Microbes*, vol. 11, no. 5, pp. 1246–1267, 2020.
- [39] J. G. Choi, N. Kim, I. G. Ju et al., “Oral administration of *Proteus mirabilis* damages dopaminergic neurons and motor functions in mice,” *Scientific Reports*, vol. 8, no. 1, p. 1275, 2018.
- [40] D. Georgescu, O. E. Ancusa, L. A. Georgescu, I. Ionita, and D. Reisz, “Nonmotor gastrointestinal disorders in older patients with Parkinson's disease: is there hope?,” *Clinical Interventions in Aging*, vol. Volume 11, pp. 1601–1608, 2016.
- [41] T. R. Sampson, J. W. Debelius, T. Thron et al., “Gut microbiota regulate motor deficits and neuroinflammation in a model of Parkinson's disease,” *Cell*, vol. 167, no. 6, pp. 1469–80.e12, 2016.
- [42] D. Lindqvist, E. Kaufman, L. Brundin, S. Hall, Y. Surova, and O. Hansson, “Non-motor symptoms in patients with Parkinson's disease - correlations with inflammatory cytokines in serum,” *PLoS One*, vol. 7, no. 10, article e47387, 2012.

## Research Article

# mTORC1 Activation in *Chx10*-Specific *Tsc1* Knockout Mice Accelerates Retina Aging and Degeneration

Yu-Qing Rao <sup>1</sup>, Yu-Tong Zhou <sup>1</sup>, Wenchuan Zhou <sup>1</sup>, Jia-Kai Li <sup>1</sup>, Baojie Li <sup>2</sup>,  
and Jing Li <sup>1</sup>

<sup>1</sup>Department of Ophthalmology, Xinhua Hospital Affiliated to Shanghai Jiao Tong University School of Medicine, Shanghai, China

<sup>2</sup>Bio-X Institutes, Key Laboratory for the Genetics of Developmental and Neuropsychiatric Disorders, Ministry of Education, Shanghai Jiao Tong University, Shanghai, China

Correspondence should be addressed to Jing Li; [lijing@xinhumed.com.cn](mailto:lijing@xinhumed.com.cn)

Received 7 August 2021; Revised 14 October 2021; Accepted 25 October 2021; Published 5 November 2021

Academic Editor: Xu Wu

Copyright © 2021 Yu-Qing Rao et al. This is an open access article distributed under the Creative Commons Attribution License, which permits unrestricted use, distribution, and reproduction in any medium, provided the original work is properly cited.

Age-associated decline in retina function is largely responsible for the irreversible vision deterioration in the elderly population. It is also an important risk factor for the development of degenerative and angiogenic diseases. However, the molecular mechanisms involved in the process of aging in the retina remain largely elusive. This study investigated the role of mTORC1 signaling in aging of the retina. We showed that mTORC1 was activated in old-aged retina, particularly in the ganglion cells. The role of mTORC1 activation was further investigated in *Chx10-Cre;Tsc1<sup>fl/fl</sup>* mouse (*Tsc1*-cKO). Activation of mTORC1 was found in bipolar and some of the ganglion and amacrine cells in the adult *Tsc1*-cKO retina. Bipolar cell hypertrophy and Müller gliosis were observed in *Tsc1*-cKO since 6 weeks of age. The abnormal endings of bipolar cell dendritic tips at the outer nuclear layer resembled that of the old-aged mice. Microglial cell activation became evident in 6-week-old *Tsc1*-cKO. At 5 months, the *Tsc1*-cKO mice exhibited advanced features of old-aged retina, including the expression of p16<sup>Ink4a</sup> and p21, expression of SA- $\beta$ -gal in ganglion cells, decreased photoreceptor cell numbers, decreased electroretinogram responses, increased oxidative stress, microglial cell activation, and increased expression of immune and inflammatory genes. Inhibition of microglial cells by minocycline partially prevented photoreceptor cell loss and restored the electroretinogram responses. Collectively, our study showed that the activation of mTORC1 signaling accelerated aging of the retina by both cell autonomous and nonautonomous mechanisms. Our study also highlighted the role of microglia cells in driving the decline in retina function.

## 1. Introduction

Visual functions, including visual acuity, visual field sensitivity, contrast sensitivity, and dark adaptation threshold, deteriorate with age [1]. The age-related changes of the retina included the loss of retinal neurons, declined electroretinography (ERG) responses, increased oxidative stress, activation of microglial cells, and increased inflammatory responses. Aging is also an important risk factor for the development of degenerative and angiogenic retinal diseases, such as age-related macular degeneration, glaucomatous retinopathy, and diabetic retinopathy [2]. In humans, age-related thinning of inner retina, including the ganglion cell layer

(GCL), inner plexiform layer (IPL), and inner nuclear layer (INL), the loss of retinal ganglion cells (RGCs), bipolar cells, and rod photoreceptors, and increased expression of senescence-related proteins have been reported [1, 3, 4]. However, the mechanisms which regulate the aging process of retina (retina aging) are yet to be elucidated.

Mammalian target of rapamycin complex 1 (mTORC1) is a protein complex that senses and integrates environmental and intracellular nutrient, growth factors, energy, and redox status and regulates protein synthesis [5]. mTORC1 signaling pathway is involved in the regulation of cell growth, proliferation, apoptosis, and inflammatory responses. In cells, the tuberous sclerosis complex, a protein complex consisting of

TSC1 and TSC2, is a major upstream inhibitor of mTORC1 [6]. Deletion of *Tsc1* gene leads to the activation of mTORC1 in affected cells. On the other hand, rapamycin effectively inhibits mTORC1 therefore attenuates mTORC1-mediated signaling activity. The two best-characterized downstream effector molecules of mTORC1 are ribosomal protein S6 kinase (S6K) and eukaryotic translation initiation factor 4E- (eIF4E-) binding protein 1 (4E-BP1) [7]. mTORC1 phosphorylates and activates ribosomal protein S6 kinase (S6K), which subsequently phosphorylates ribosomal protein S6 (S6). Phosphorylation of 4E-BP1 by mTORC1 releases its binding from eIF4E, enabling it to form an active protein translation initiation complex and initiate cap-dependent protein translation.

*Chx10* is a transcriptional factor involved in retinal development and bipolar cell differentiation [8]. The expression of *Chx10* is restricted in the anterior part of the optic vesicle during retina genesis and is gradually restricted to bipolar cells in adult mice [9]. Using *Chx10-cre* driven *Tsc1* conditional knockout mice (*Tsc1-cKO*), Choi et al. found that the activation of mTORC1 in *Chx10*-expressing cells shortened retinal progenitor cell cycle and subsequently accelerated progenitor cell differentiation and retina development [10]. Depending on the timing of *Tsc1* knockout during retinal development, the activation of mTORC1 could also lead to the manifestation of ocular tuberous sclerosis complex [11]. Reduced mTORC1 signaling led to proliferation defect and excessive production of retinal ganglion cells [11]. mTORC1 is also expressed abundantly in adult retina, at a level higher than metabolically active brain and liver, especially in cells of the inner retina [12]. In ganglion cells, mTORC1 activity was needed for axonal survival after optic nerve injury [13–17]. However, Müller glial predominantly express mTORC2 rather than mTORC1 [12]. In photoreceptor cells, augmentation of mTORC1 activity extended the survival of cone cells in mouse with retinitis pigmentosa, possibly because it ameliorated the nutrition deprivation condition caused by rod cell death [18–20].

mTORC1 is also involved in the regulation of longevity and aging. Inhibition of mTORC1 signaling by rapamycin extended the longevity of all livings tested so far, from single cell yeast to nonhuman primates [21]. In human retinal pigment epithelial cells, the mTOR pathway showed age-associated changes [22]. In the OXYS rat, a rat model of accelerated aging due to overproduction of free radicals, rapamycin treatment ameliorated the incidence and severity of retinal degeneration [23]. However, it is not known whether mTORC1 signaling played a direct role in retina aging and neural retinal cell senescence. In this study, we showed that mTORC1 signaling was activated in old-aged retina. We found that ganglion cells of the old-aged retina had increased mTORC1 activity and the expression of senescence associated- $\beta$ -galactosidase (SA- $\beta$ -gal). To further study the effect of mTORC1 activation on retina aging, we used the adult *Tsc1-cKO* mice and found that the ablation of *Tsc1* in *Chx10*-expressing cells accelerated retinal aging as evidenced by progressively declined ERG responses, the elevation of oxidative stress level, the activation of microglial cells, the expression of senescence-related proteins, and a gene expres-

sion profile with features of aging retina. Furthermore, we found that the inhibition of microglial cells by minocycline prevented photoreceptor cells loss and partially restored the ERG responses. Collectively, our study demonstrated mTORC1 activation accelerated retina aging and retinal degeneration. Our results also suggested that microglial cell activation is an important factor which lead to overall functional deterioration in the retina.

## 2. Materials and Methods

**2.1. Animal Husbandry and Genotyping.** *Chx10-Cre* (*Tg(Chx10-EGFP/cre,-ALPP)2Clc/J*, cat. 005105), *Tsc1-flox* (*Tsc1<sup>tm1Dj</sup>/J*), cat. 005680), and the tdTomato reporter mice (*B6.Cg-Gt(ROSA)26-Sortm9(CAG-tdTomato)Hze/J*, cat. 007909) were obtained from the Jackson Laboratory and housed in a specific-pathogen-free (SPF) mouse facility under 12-hour light/dark cycle with unrestricted access to food and water in Xinhua Hospital Affiliated to Shanghai Jiao Tong University School of Medicine. They were mated to produce the *Chx10-Cre;Tsc1<sup>f/f</sup>* mice (*Tsc1-cKO*). Unless otherwise specified, the control mice used in this study were *Chx10-Cre;Tsc1<sup>+/+</sup>*. All procedures involving animals were in compliance with the ARVO statement for the Use of Animals in Ophthalmic and Vision Research and approved by the Institutional Animal Care and Use Committee of Xinhua Hospital.

Animals were genotyped by PCR analysis using genomic DNA extracted from tail biopsies. Cre recombinase DNA was detected using Cre-F (5'-TTTCCCAGAACCTG AAGA-3') and Cre-R (5'-GGTGCTAACCAGCGTTTTC GT-3'). A 430 basepair (bp) amplicon was expected. The floxed *Tsc1* was detected using IMR4008 (5'-GTCACG ACCGTAGGAGAAGC-3') and IMR4009 (5'-GAATCA ACCCCACAGAGCAT-3'). The floxP containing DNA yielded a 230 bp product, and the wildtype DNA yielded a 193 bp product.

**2.2. Histological and Immunofluorescent Microscopy.** Animals were given a lethal dose of sodium pentobarbital (120 mg/kg body weight) and were either enucleated or perfused immediately with fresh-made 4% paraformaldehyde (PFA). The retina cup free of vitreous and retinal pigment epithelium was fixed in PFA overnight at 4°C, followed by sequential dehydration in 10%, 20%, and 30% sucrose, embedded in optimal cutting temperature compound (OCT), and sectioned at 10  $\mu$ m thickness using a Leica microtome (CM1950, Leica Biosystems, Wetzlar, Germany).

Hematoxylin and eosin (H&E) staining was performed according to the standard protocol and visualized under light microscope. For immunofluorescent staining, the tissue sections were permeabilized with 0.5% Triton X-100 for 60 mins, blocked with 10% goat serum and 0.1% Triton X-100 in PBS at room temperature, and incubated with desired primary antibody at 4°C overnight. The antibodies used in the present study (including those for Western blot analysis below) are listed in Supplementary Table S1. The slides were visualized under fluorescent microscope (Leica DMi3000B) or confocal microscope (Leica TCS SP8).

**2.3. Senescence-Associated  $\beta$ -Galactosidase Staining.** A senescence-associated  $\beta$ -galactosidase (SA- $\beta$ -Gal) staining kit (Catalog no. 9860; Cell Signaling Technology, Danvers, MA, USA) was used according to the manufacturer's instruction. Briefly, frozen sections of mouse retina were restored to room temperature, fixed in the provided fixative for 15 mins, washed with PBS 3 times, and then incubated in freshly prepared staining solution for 12 hrs at 37°C. Pictures were taken under light microscope. The original blue stained images were converted to grayscales to increase the contrast.

**2.4. Western Blot Analysis.** Freshly isolated retina cup was lysed in RIPA buffer (Cat. 9806S, Cell Signaling Technology) containing 1 mM PMSF and 1x protease inhibitor cocktail (cOmplete Protease Inhibitor Cocktail Tablets, Cat. 5892970001, Roche Diagnostics, Basel, Switzerland) with sonication. Protein concentration was measured using Micro BCA protein assay kit (Cat. 23235, Thermo Fisher Scientific, Shanghai, China), and 30  $\mu$ g of total tissue lysates was loaded onto SDS-PAGE, transferred to nitrocellulose membrane (1620115, Bio-Rad Laboratories, Hercules, CA, USA), and probed with indicated antibodies (Supplementary Table S1). Proteins were visualized using chemiluminescent HRP substrate (Immobilon Western, WBKLS0500, MilliporeSigma, Shanghai, China), and the signals were captured by Bio-Rad Gel Doc XR+ system. For quantitative analysis, the densitometrical value of the protein bands was analyzed with ImageJ and normalized to  $\beta$ -actin.

**2.5. RNA Extraction and Real-Time PCR.** Total RNA was extracted using Trizol reagent (Thermo Fisher Scientific, Shanghai, China) and the RNA Clean & Concentrator-5 kit (R1013, Zymo Research, Irvine, CA, USA). Complementary DNA was synthesized using PrimeScript RT Reagent Kit (RR037A, Takara, Japan). Real-time PCR analysis was performed using TB Green Premix Ex Taq II reagent (RR820A, Takara, Japan). Gene expression was compared by  $\delta$ Ct method using *Actb* as internal control. Primer sequences were listed in Supplementary Table S2.

**2.6. Electroretinograms.** The Espion E3 console in conjunction with the Color Dome (Diagnosys LLC, Lowell, MA, USA) was used for Ganzfeld ERG recording. The procedure was adopted from a detailed description for mouse ERG examination [24]. Briefly, mice were weighted, tagged, and dark-adapted overnight before the experiment. Sodium pentobarbital was used as anesthesia at the dose of 80  $\mu$ g/g body weight and injected intraperitoneally in the dark. Once the mouse was anesthetized, it was gently moved to a warm metal plate to maintain the body temperature at 37°C. The pupil was dilated with 0.5% tropicamide-0.5% phenylephrine (Mydrin-P, Santen Pharmaceutical Co., Ltd., Japan) about 10 mins before the recording. A thin layer of ofloxacin eye ointment (Sinqi Pharmaceutical, Shenyang, China) was applied to the cornea surface which served as a preventative medication for infection and as a lubricant. Platinum wire ring electrodes were positioned on the surface of both cornea for binocular ERG recordings. A reference electrode was placed subcutaneously at the middle of the forehead region. A ground electrode was placed at the back near the tail.

For the dark-adapted single-flash ERG recording, the mouse was placed in the dome with no background illumination. Single white-flash stimuli at -4.3, -4, -3, -2, -1.5, -1, -0.5, 0, 0.4, 1, and 1.3 log cd•s/m<sup>2</sup> were given at the interstimulus intervals of 40 s. Band-pass filtering was applied from 0.3 to 300 Hz. For each stimulus, five responses were recorded and averaged. For the light-adapted ERG recording, the mouse was light adapted for 10 mins at a static background light of 1.3 log cd/m<sup>2</sup>. White-flash stimuli at -2, -1.5, -1, -0.5, 0, 0.5, 1, and 1.5 log cd•s/m<sup>2</sup> were given at the interstimulus intervals of 10 secs. For each stimulus, ten responses were taken and averaged.

The total recording time was 420 ms, including a 20 ms preflash recording time. The amplitude of a-wave was measured from the prestimulus baseline to the most negative trough of the ERG. The amplitude of the b-wave was measured from the trough of the a-wave to the most positive peak of the ERG which followed the a-wave. Peak times were measured from flash onset to the peak of a- and b-waves.

**2.7. Microarray Analysis of Gene Expression.** Three 5-month-old *Tsc1*-cKO mice, three age-matched control, two 24-month-old C57BL/6, and two 5-month-old *Tsc1*-cKO mice after rapamycin treatment were subjected to gene expression analysis. The Agilent SurePrint G3 Mouse Gene Expression v2 8x60K microarray (Design ID: 074809) was used. The array contained 56605 probes which covered 27307 genes. Total RNA was quantified by NanoDrop ND-2000, and the integrity of RNA was assessed using Agilent Bioanalyzer 2100. Sample labeling, microarray hybridization, and washing were performed according to the manufacturer's suggestions. Agilent Scanner G2505C was used to scan the arrays at the end.

The Feature Extraction software (version 10.7.1.1, Agilent Technologies) was used to analyze array images to get raw data. It was then normalized with the quantile algorithm. The probes that were flagged as "detected" in at least 1 out of 2 conditions were chosen for further analysis. For each expressed gene, the fold change between groups and *p* value was calculated. Differentially expressed genes (DEGs) were identified if the fold change was 2 or more and the *p* value equaled or less than 0.05. Afterwards, Gene Set Enrichment Analysis (GSEA) and Gene Ontology (GO) analysis were performed to explore the collective functions of the DEGs. GSEA was conducted based on the normalized gene expression values from microarray data according to the methods described previously [25]. The gene sets analyzed were acquired from the GO database. A gene set-based permutation test of 1000 permutations was applied, and genes were ranked according to the signal2noise method. All other parameters were set to GSEA defaults. GO enrichment analysis of differentially expressed genes was performed using R based on the hypergeometric distribution.

**2.8. Dihydroethidium (DHE) Fluorescent Staining.** DHE fluorescent staining was performed to determine the reactive oxygen species (ROS) level in the retina *in vivo* [26, 27]. Briefly, freshly made DHE (10 mg/mL in anhydrous dimethylsulfoxide mixed with equal volume of 2x sterile

PBS) was injected intraperitoneally at the dose of 50 mg/kg body weight. The mice were sacrificed 2 hrs after the injection, and the eyes were enucleated, embedded in OCT, and cryo-sectioned at a thickness of 10  $\mu$ m. The slides were then washed twice in PBS and mounted with ProlongGold antifade reagent (P10144, Thermo Fisher Scientific) and scanned using a 532 nm excitation laser and a 580 nm long-pass detection filter. The intensity of the fluorescence of the entire section was quantified using ImageJ and used for comparison between groups.

**2.9. Lipid Peroxidation Analysis.** The level of lipid peroxidation was indicated by measuring the concentration of malondialdehyde (MDA) in the retina (ab118970, Abcam, Shanghai, China) according to the manufacturer's instruction. Briefly, retina tissue was homogenized in 300  $\mu$ L MDA lysis buffer supplemented with lipid peroxidation inhibitor. After centrifugation, 10  $\mu$ L of the supernatant was used for protein quantification, and 200  $\mu$ L of the supernatant was used to determine the amount of MDA based on the reaction with thiobarbituric acid (TBA) in a 96-well microplate. The final product of MDA-TBA adduct was quantified colorimetrically on a microplate reader at 532 nm.

**2.10. Rapamycin Treatment.** Rapamycin (HY-10219, MedChemExpress) was dissolved in 100% alcohol at the concentration of 25 mg/mL and further diluted to 1 mg/mL using a water-based solvent containing 5% Tween-80 and 5% PEG-400. The experimental mice were given intraperitoneal injections of 5  $\mu$ g/g body weight every day for 30 days and sacrificed 3 days after the last injection [28]. The control group received solvent at the same time as the experimental group.

**2.11. Minocycline Treatment.** Minocycline hydrochloride (HY-17412, MedChemExpress, Shanghai, China) at the dose of 50 mg/kg was injected intraperitoneally to mice daily for 1 month as described [29, 30].

**2.12. Statistical Analysis.** The Statistical Package for the Social Sciences (SPSS) version 21 was used for data analysis. Unless otherwise specified, the average and standard error (SE) of data from repeated experiments were presented. Unpaired Students' *t*-test or two-way analysis of variance (ANOVA) was used to determine the statistical significance between two groups. A *p* value that equals or less than 0.05 was considered as statistically significant.

### 3. Results

**3.1. mTORC1 Activity Is Increased in Retina of Old-Aged C57BL/6 Mice.** The effect of mTORC1 activation on aging has been demonstrated in many cells and tissues [21]. To test whether retina aging is also associated with changes of mTORC1 activity, we compared the expression of total and phosphorylated ribosomal protein S6 (S6 and p-S6, respectively) and S6 kinase (S6K and p-S6K, respectively) in 3- and 24-month-old C57BL/6 mouse retinal tissue. Western blot analysis showed that the 24-month-old mouse retina expressed higher levels of p-S6 and p-S6K than the

3-month-old ones, while the total S6 and S6K proteins remained the same between the two groups (Figures 1(a) and 1(b)). Immunofluorescent staining of p-S6 protein revealed strong positive signals in GCL and sporadic positive signals at the INL of the 24-month-old retina, while weak and sporadic staining was found in the GCL of the 3-month-old retina (Figure 1(c)). Costaining of p-S6 with markers for cells of the inner retina showed that ganglion cells and bipolar and amacrine cells expressed p-S6 in the old-aged retina (arrowheads in Figure 1(d)). These results indicated the activation of mTORC1 in the inner retina of old-aged mice, which was consistent with previous report [12]. We also found that the bipolar cells of the 24-month-old retina had aberrant dendritic tips ending at outer nuclear layer (ONL) (arrows in Figure 1(d)), which was also consistent with previous report [31]. In addition, GFAP and Iba-1 staining showed the activation of Müller glial and microglial cells in old-aged retina, respectively (Figure 1(e)).

Next, we performed SA- $\beta$ -Gal staining on 3- and 24-month-old retina. We found positive staining only in ganglion cells of the old-aged retina (Figure 1(f)). Taken together, the results showed that old-aged retina was featured with increased mTORC1 signaling in the inner retina, activation of microglia and Müller glial cells, abnormal bipolar cell morphology, and ganglion cell senescence.

**3.2. Generation and Characterization of *Tsc1*-cKO Mice.** In order to understand the impact of mTORC1 activation on retina aging, we generated the *Tsc1*-cKO mice. Real-time PCR analysis of retina RNA showed that *Tsc1* gene expression in *Tsc1*-cKO retina was about 26% of controls (data not shown). Western blot analysis revealed 90% reduction of *Tsc1* protein in the *Tsc1*-cKO mouse retina compared to littermate controls (Figures 2(a) and 2(b)). At the meantime, increased expression of phosphorylated mTOR, 4E-BP1, and S6 kinase was found in *Tsc1*-cKO retina, indicating the activation of mTORC1 pathway (Figures 2(a) and 2(b)).

*Chx10* is expressed in retinal progenitor cells during retina genesis and is gradually restricted to bipolar cells in adult mice [8]. *Chx10*-cre was known to be expressed in bipolar and a significant number of Müller glial cells [9, 32]. To determine cells with *Chx10*-cre expression in this study, we used *Rosa26*-tdTomato reporter mice. Red fluorescent signal was found in mosaic pattern in embryonic and neonatal retina of *Chx10*-cre; *Rosa26*-tdTomato mice (Supplementary Figure S1). In postnatal day 10 (P10) mouse retina, tdTomato expression was found in bipolar cells, Müller glial cells, some of the amacrine, horizontal, and RGC cells (Supplementary Figure S1A-G). In 4-week-old *Chx10*-Cre mouse, red fluorescent signal was concentrated in the inner retina, and the expression of Cre was restricted to cells at the outer part of the INL, presumably bipolar cells (Supplementary Figure S2H-I). These results were consistent with previous reports [9, 33, 34], suggesting that *Chx10*-cre likely led to *Tsc1* ablation in bipolar cells, a significant number of Müller glial cells, some of the RGC, amacrine, and horizontal cells in *Tsc1*-cKO retina.

To determine if *Tsc1* ablation was associated with neural retinal cell mTORC1 activation, we performed p-S6

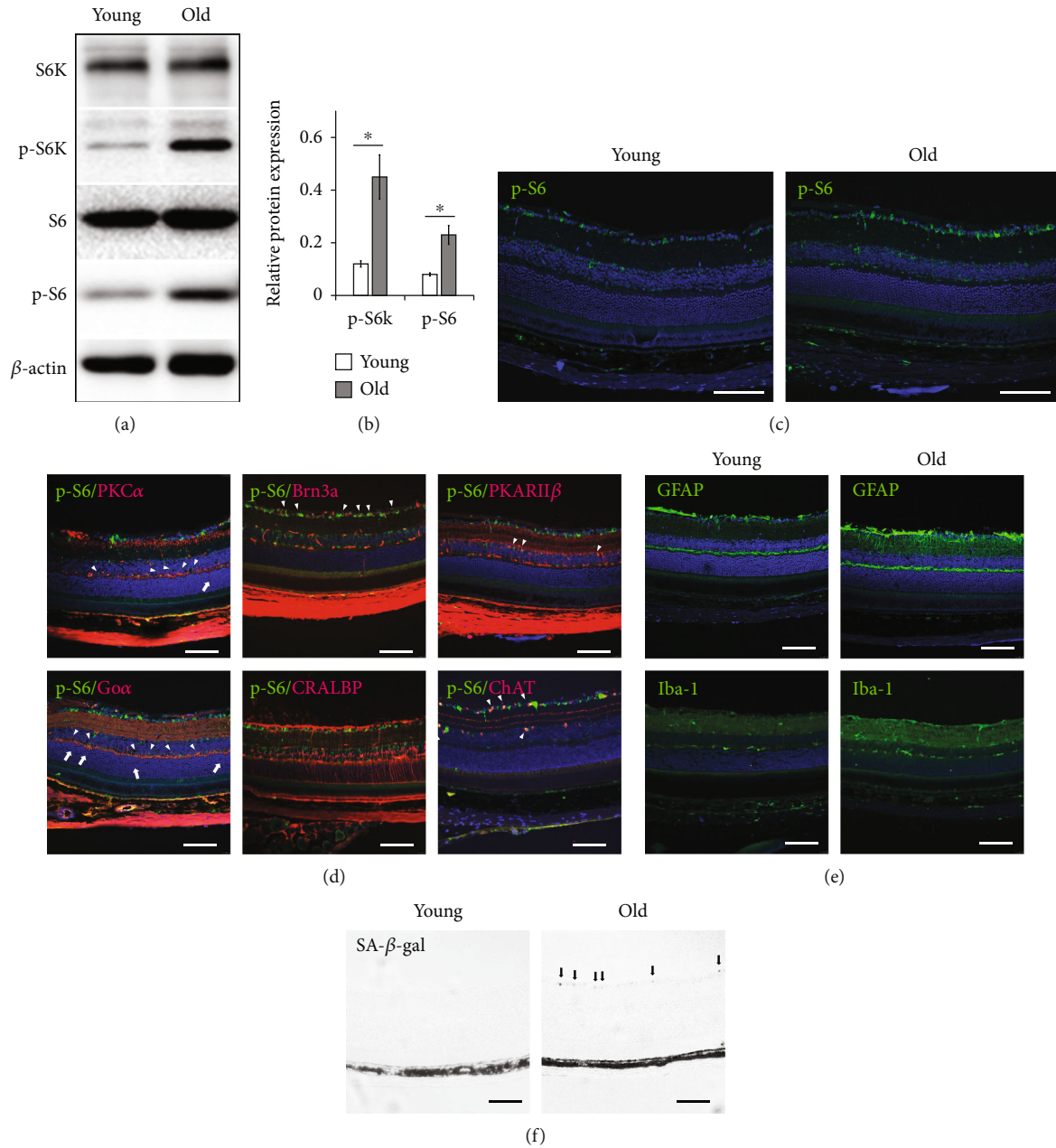


**FIGURE 1: Increased mTORC1 activity in 24-month-old C57BL/6 retina corresponded with cell senescence.** (a) Representative Western blot analysis of total ribosomal protein S6 (S6), phospho-S6 (p-S6), total S6 kinase (S6K), and phospho-S6 kinase (p-S6K) in retinal extracts of 24- (old) and 3-month-old (young) mice. The experiments were repeated three times with one pair of samples at each time. (b) Relative expression of phosphorylated S6 and S6K proteins in control and 24-month-old C57BL/6 retina. Phosphorylation status of each protein was calculated by dividing the intensity of the band of the phosphorylated protein by the intensity of the band of the corresponding total protein. The number from each experiment was averaged, and the error bars represented SE. \* $p < 0.05$  by unpaired Student's  $t$ -test between 24- and 3-month-old groups. (c) Representative immunofluorescent staining of p-S6 on 24- (old) and 3-month-old (young) mouse retina. (d) Costaining of p-S6 with markers for various retinal cells indicated the activation of mTORC1 in bipolar cells (PKC $\alpha$ , Go $\alpha$ , PKARII $\beta$ ), ganglion cells (Brn3a), and amacrine cells (ChAT) but not in Müller glial cells (CRALBP) (arrowheads) of 24-month-old C57BL/6 mouse retina. Arrows indicated aberrant dendritic tip endings of bipolar cells at ONL. (e) Representative immunofluorescent staining showed the activation of Müller glial (GFAP) and microglial (Iba-1) cells in old-aged retina. (f) Senescence-associated- $\beta$ -galactosidase (SA- $\beta$ -gal) staining of retinal ganglion cell layer (GCL) (arrows) of the 24-month-old mouse retina. The staining was absent in the retina of young mice. Scale bar: 100  $\mu$ m.

immunofluorescent staining in 2-month-old *Tsc1*-cKO retina and found that strong positive signals were predominantly localized at GCL and the inner part of the INL

(Figure 2(c)). Costaining revealed p-S6 expression in ganglion cells, bipolar cells, and a few of the amacrine cells (Figure 2(d)). We noticed very weak p-S6 staining in Müller

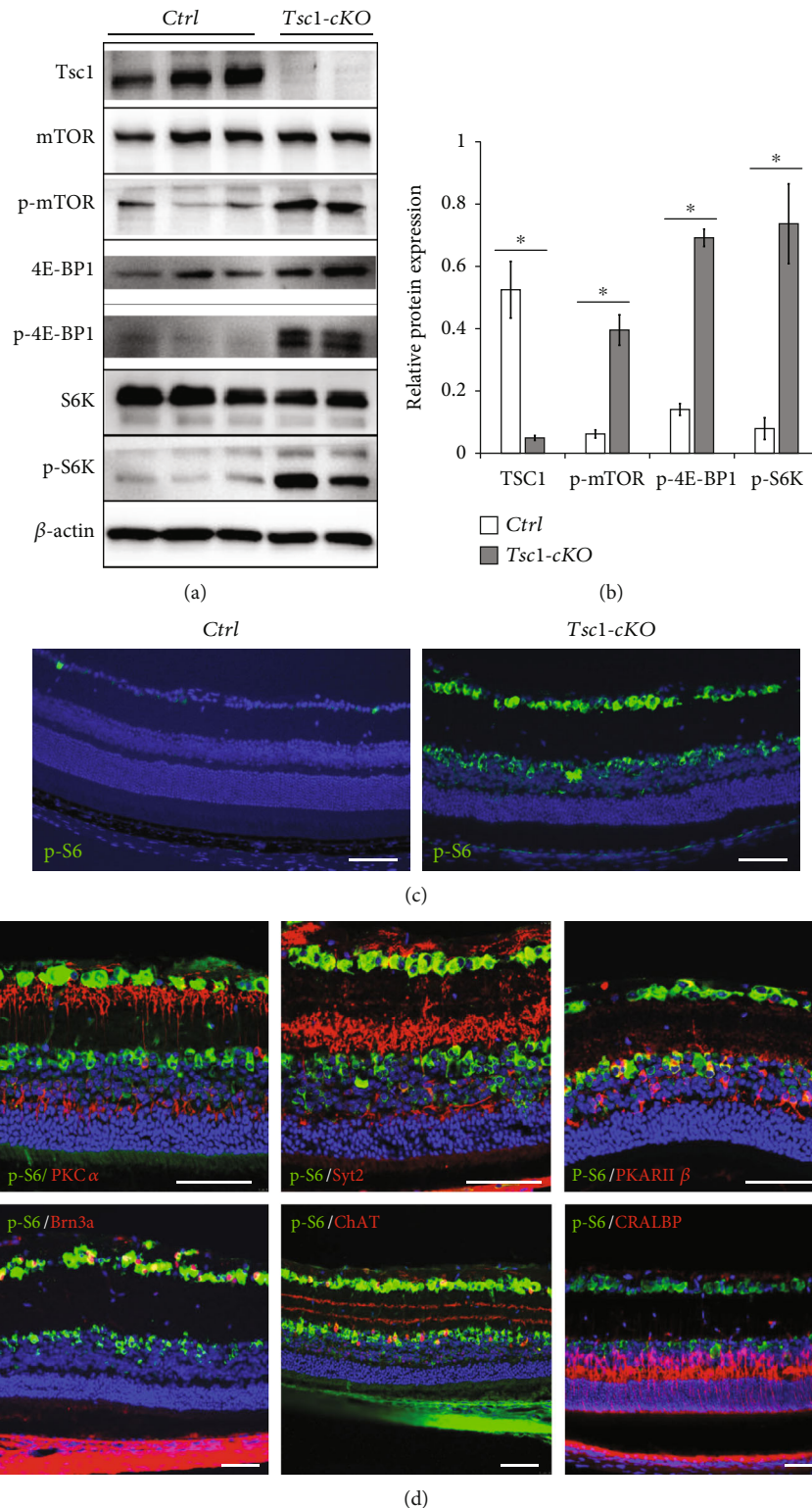


FIGURE 2: Characterization of Tsc1-cKO retina. (a) Western blot analysis of Tsc1, mTOR, phospho-mTOR (p-mTOR), 4E-BP1, phospho-4E-BP1 (p-4E-BP1), S6K, and p-S6K in total protein lysates of the Tsc1-cKO and control retina. The experiment was repeated twice. In total, 3 controls and 3 Tsc1-cKO retina samples were analyzed. (b) Relative quantification of protein expression. The density of the bands was normalized against actin for loading control and corresponding total protein for phosphorylated proteins. \* $p < 0.05$  by unpaired Student's  $t$ -test between control and Tsc1-cKO. (c) Staining of p-S6 indicated the activation of mTORC1 in Tsc1-cKO retina was predominantly at GCL and inner part of the INL layers. Only sporadic staining was found at GCL of control retina. (d) Immunofluorescent staining revealed the localization of p-S6 in bipolar cells (PKC $\alpha$ , Syt2, PKARII $\beta$ ), ganglion cells (Brn3a), and some of the amacrine cells (ChAT) of the 3-4-month-old Tsc1-cKO retina. Weak staining was found in Müller glial cells (CRALBP). Scale bar: 100  $\mu$ m.

glial cells. This was consistent with the results from a recent study showing that Müller glial cells predominantly express mTORC2 [12]. No significant p-S6 staining was found in photoreceptor cells. In rod- and cone-specific *Tsc1*-cKO mice, strong p-S6 staining was found in photoreceptor cells [18, 35]; therefore, the lack of p-S6 staining suggested negligible mTORC1 activation in photoreceptor cells of the *Tsc1*-cKO retina, which was consistent with the absence of *Chx10* expression in these cells. Collectively, the results showed that despite the broad expression of *Chx10*-cre during retinal development, the activation of mTORC1 was largely limited to cells of the inner retina, in particular, to bipolar cells, ganglion cells, and some of the amacrine cells.

**3.3. Histological Changes of *Tsc1*-cKO Retina.** Next we examined histological changes of the *Tsc1*-cKO retina. At the age of 1 month, no significant difference was found between *Tsc1*-cKO and control. At the age of 3 months, the eyes of the *Tsc1*-cKO were significantly bigger than the age-matched controls as indicated by the diameters of the eye balls and the surface areas of the retina (Figures 3(a) and 3(b), Supplementary Figure S2A). The surface areas of the 3- and 5-month-old *Tsc1*-cKO retina were about 4.4% and 11% bigger than controls at the same age, respectively. H&E staining of the retina at different ages showed progressive thickening of the IPL and INL layers of the *Tsc1*-cKO retina (Figures 3(c) and 3(d)). By the age of 7 months, the INL and IPL of the *Tsc1*-cKO retina were 57% and 81% thicker than the controls, respectively (Figure 3(d)). However, no retina hamartoma was found in any of the eyes examined. In contrast, the ONL layer of the *Tsc1*-cKO retina progressively thinned with age. At 5 months old, the ONL of the *Tsc1*-cKO mouse retina was 88% of the control ( $p = 0.034$ ). The increases in the thickness of INL and ONL in the *Tsc1*-cKO mice were also confirmed by optical coherence tomography of animals at the ages of 3 and 5 months old (data not shown).

We further compared the numbers of nuclear at the INL between *Tsc1*-cKO and control mice at different ages. No significant differences in the density of cell nuclear was found (data not shown). However, since the diameter of the *Tsc1*-cKO eye balls was slightly larger than that of controls, we could not exclude the possibility that the mature *Tsc1*-cKO retina had slightly more cells than controls. On the other hand, significant hypertrophy of the *Chx10*-cre expressing cells was observed in the *Tsc1*-cKO retina (Figure 4). This was most evident in bipolar cells. The average cell soma of the PKC-positive rod bipolar cells from 3-month-old *Tsc1*-cKO mice was about 22% larger than the controls (Figures 4(a) and 4(b) and Supplementary Figure S2D). Aberrant endings of bipolar cell axonal projections were found at the GCL (arrowheads in Figure 4(b) and Supplementary Figure S2B). The dendrites of bipolar cells were found at the ONL at different depth (arrows in Figure 4(b), Supplementary Figure S2B), a phenomenon which was also found in old-aged retina (arrows in Figure 1(d)). To test if the aberrant dendritic tips were active, we performed CtBP2 and Psd95 staining and found positive signals for both proteins at the extended dendritic tips of *Tsc1*-cKO bipolar cells

(Supplementary Figures S2B), suggesting that they were likely active in electro-signal transduction. In addition, hypertrophy of horizontal cells, amacrine, and ganglion cells were also observed (Figures 4(c)–4(h)).

Next we analyzed the effect of mTORC1 activation on glial cells. CRALBP staining showed that Müller glial cells traversed the entire thickness of the *Tsc1*-cKO retina, indicating cell hypertrophy (Figures 4(i) and 4(j)). We observed positive GFAP staining in 6-week-old *Tsc1*-cKO retina (Supplementary Figure S2C). As the *Tsc1*-cKO grew older, the staining of GFAP became stronger, suggesting persistent Müller glial cell activation (Figures 4(k) and 4(l)). Iba-1 staining revealed increased number of microglial cells in the IPL of 6-week-old *Tsc1*-cKO retina (Supplementary Figure S2C). As the *Tsc1*-cKO grew older, more microglial cells with bigger cell soma, shorter and thicker processes, and less ramification were found at the IPL and INL. In 7-month-old *Tsc1*-cKO mice, activated microglial cells were found in the subretinal space, a phenomenon which was a hallmark of retina degeneration (Figures 4(m) and 4(n)).

While the inner retina of the *Tsc1*-cKO mice showed progressive thickening, the ONL became thinner with age. Cone-arrestin staining revealed progressive decrease of cone cell density with age in the *Tsc1*-cKO retina (Figures 4(o) and 4(p), and Supplementary Figures S3A and S3B). It was reported that the thinning of ONL in normal old mouse retina was the result of expanded retina surface [36]. Even though the KO mice were bigger than the control, the percentage of retinal surface increase between *Tsc1*-cKO and control mice was similar; therefore, the thinning of the ONL in the *Tsc1*-cKO retina most likely represented the loss of photoreceptor cells.

**3.4. Expression of Senescence-Associated Proteins and SA- $\beta$ -Gal Staining in *Tsc1*-cKO Mouse Retina.** To test if the activation of mTORC1 accelerated the development of age-related changes in the *Tsc1*-cKO mouse retina, we compared the expression of p16<sup>Ink4a</sup> and p21 proteins among 5-month-old *Tsc1*-cKO, age-matched control, and 24-month-old C57BL/6. Western blot analysis showed that both proteins were significantly upregulated in 5-month-old *Tsc1*-cKO and 24-month-old C57BL/6 retina compared to controls (Figures 5(a) and 5(b)). SA- $\beta$ -Gal staining revealed strong positive signals in ganglion cells of the 5-month-old *Tsc1*-cKO retina (Figure 5(c)). No distinctive signal was found in cells of the INL or photoreceptor cells. These findings were similar to what we have observed in 24-month-old C57BL/6 mouse retina (Figure 1(f)). The results suggested that mTORC1 activation stimulated ganglion cell senescence.

**3.5. Increased Oxidative Stress in *Tsc1*-cKO Retina.** An important feature of aging retina is the increase of oxidative stress, which often leads to the oxidation of protein, DNA, and lipid [37]. To analyze the level of reactive oxygen species, we performed DHE staining on 5-month-old *Tsc1*-cKO and compared that to age-matched control and 24-month-old C57BL/6 mouse retina. The *Tsc1*-cKO retina showed significantly stronger fluorescent signal than both control and old-aged retina, suggesting higher level of



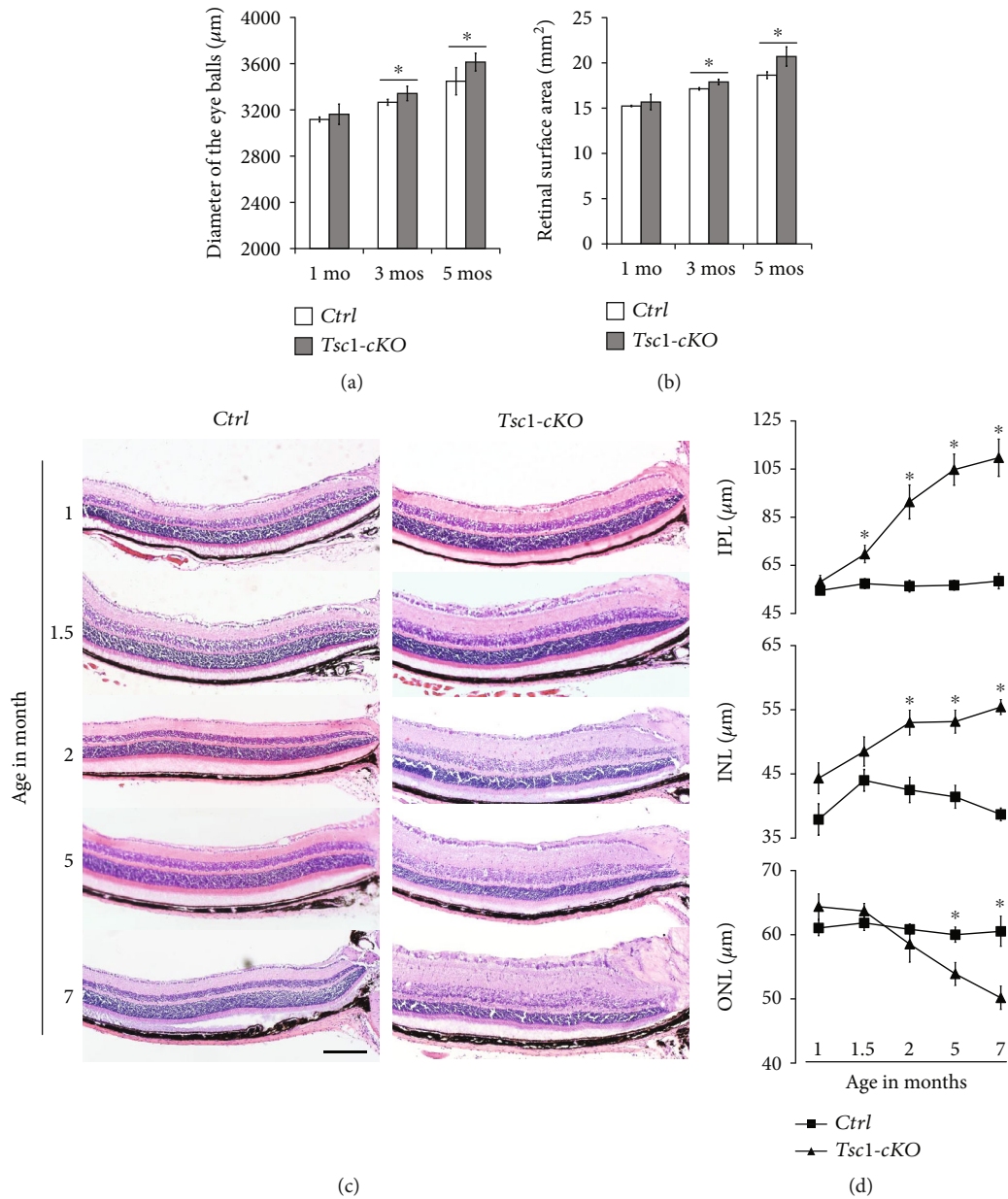


FIGURE 3: Histological changes of Tsc1-cKO retina. (a) The diameters of eye balls of 1-, 3-, and 5-month-old Tsc1-cKO and age-matched control mice. (b) Retinal surface area of 1-, 3-, and 5-month-old Tsc1-cKO and control mice. (c) H&E staining of 1-, 1.5-, 2-, 5-, and 7-month-old Tsc1-cKO and control mouse retina showing progressive thickening of the INL and IPL starting at 1.5 months and the thinning of the ONL starting at 3 months of age. (d) The average thickness of IPL, INL, and ONL of Tsc1-cKO and control retina. The thickness was measured on micrographs of H&E staining at about  $500\ \mu\text{m}$  away from the center of the optic nerve head. At least 5 eye balls from 5 different animals in each age group of Tsc1-cKO and control were measured, and the results were averaged. Error bars represented SE. \* $p < 0.05$  by unpaired Students'  $t$ -test between Tsc1-cKO and control group. Scale bar:  $200\ \mu\text{m}$ .

superoxide (Figures 6(a)–6(d)). Next, we compared the amount of MDA in retinal extracts of 5-month-old Tsc1-cKO, age-matched control, and 24-month-old C57BL/6 mice and found that the Tsc1-cKO retina had the highest level of MDA (Figure 6(e)). The difference between Tsc1-cKO and controls was statistically significant ( $p = 0.048$ , unpaired Students'  $t$ -test). Collectively, the data demonstrated that there was increased oxidative stress buildup in Tsc1-cKO retina.

**3.6. Tsc1-cKO Retina Showed Gene Expression Features Which Resembles Old-Aged Retina.** To further explore the overall characteristics of the Tsc1-cKO retina and changes related to aging, we compared gene expression of 5-month-old Tsc1-cKO, age-matched controls, and 24-month-old C57BL/6 mouse retina using Agilent SurePrint G3 mouse gene expression microarray. The all-sample average detection rate was 76.9%. Using the cutoff of 2-fold change and  $p < 0.05$  as criteria to select for differentially expressed genes (DEGs), we

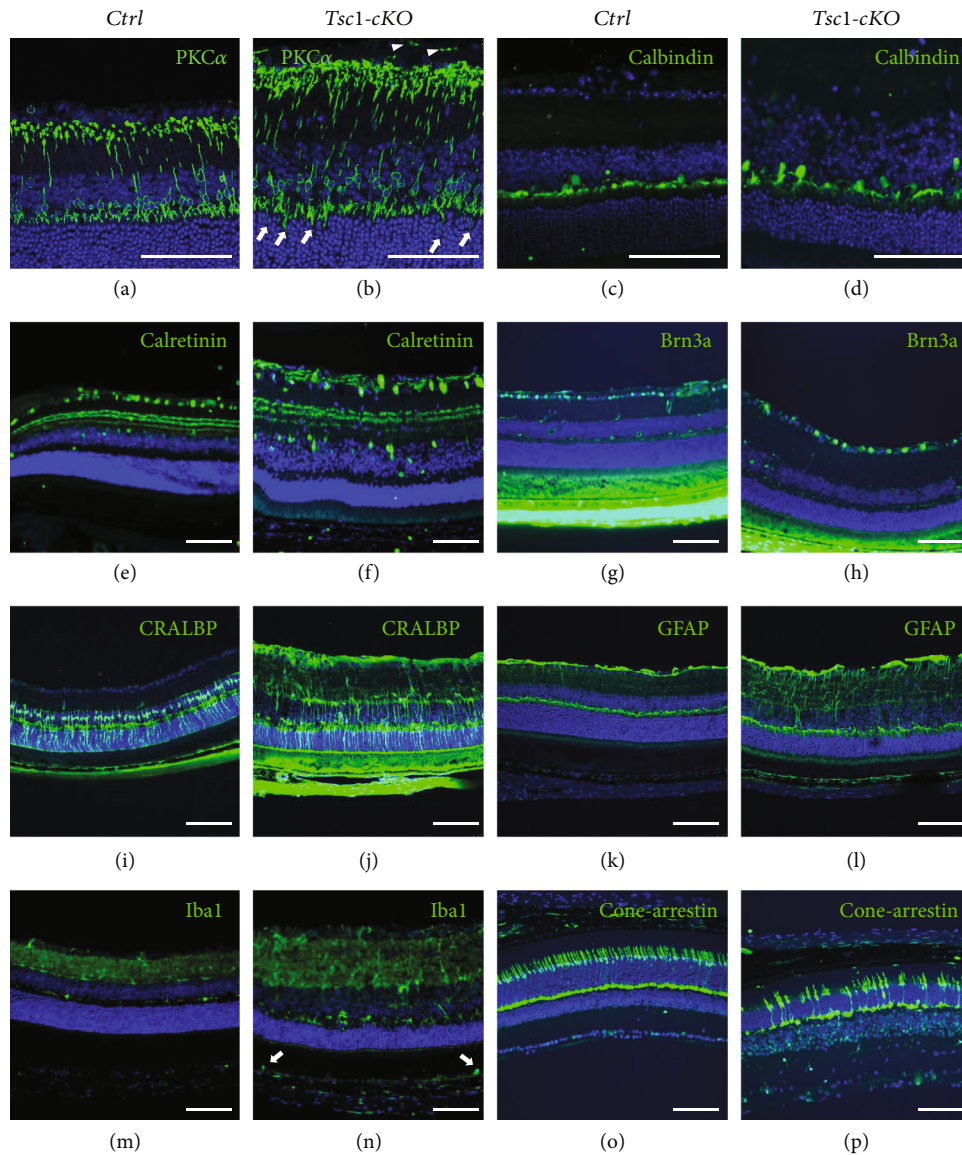


FIGURE 4: Morphological changes of the *Tsc1*-cKO retina. (a–l) Immunofluorescent staining of retina from 3-month-old *Tsc1*-cKO and control mice using antibodies against PKC $\alpha$  for rod bipolar cells (a, b), calbindin for horizontal cells (c, d), calretinin for amacrine cells (e, f), Brn3a for retinal ganglion cells (g, h), CRALBP (i, j), and GFAP (k, l) for Müller glia cells. White arrowheads and arrows in (a) indicated aberrant axon endings and dendritic tips in bipolar cells, respectively. (m–p) Immunofluorescent staining of Iba-1 and cone-arrestin of 7-month-old *Tsc1*-cKO and control retina to show activated microglia cells (m, n) and dramatically reduced cone photoreceptor cells (o, p). White arrows in (m) indicated Iba1-positive microglia cells in subretinal space. Scale bar: 100  $\mu$ m.

found 2210 upregulated and 1580 downregulated genes in the *Tsc1*-cKO retina compared to the age-matched controls. Between 24-month-old C57BL/6 and the controls, we found 929 upregulated and 1249 downregulated genes (Figures 7(a) and 7(b)). Some of the most up- and downregulated protein-encoding genes in two groups were denoted. The reliability of the microarray results was validated by real-time PCR analysis of selective gene expression using RNA extracted from different *Tsc1*-cKO, old-aged, and control mouse retina (Figure 7(c)). The microarray analysis showed that *Tsc1* expression in *Tsc1*-cKO retina was 28.6% of control, which was similar to the real-time PCR results. The DEG for old vs. control and cKO vs. control were plotted against one

another in Figure 7(d). The number of DEGs between old-aged and control mice was more than previous report using 20- and 3-month-old C57BL/6 [38], while most of the DEGs reported in the previous study were also identified here. The difference was likely because the control we used here was *Chx10-Cre;Tsc1<sup>+/+</sup>* mice. It is also possible that more genes showed altered expression between 20- and 24-month-old retinas.

GSEA analysis of DEGs in the *Tsc1*-cKO retina showed statistically significant enrichment of aging, microglia activity, immune system, chemokine activity, chemokine-mediated signaling pathway, and lysosome in *Tsc1*-cKO compared to control retina (Figure 8(a)). Next we identified 941 common DEGs between the *Tsc1*-cKO and old-aged

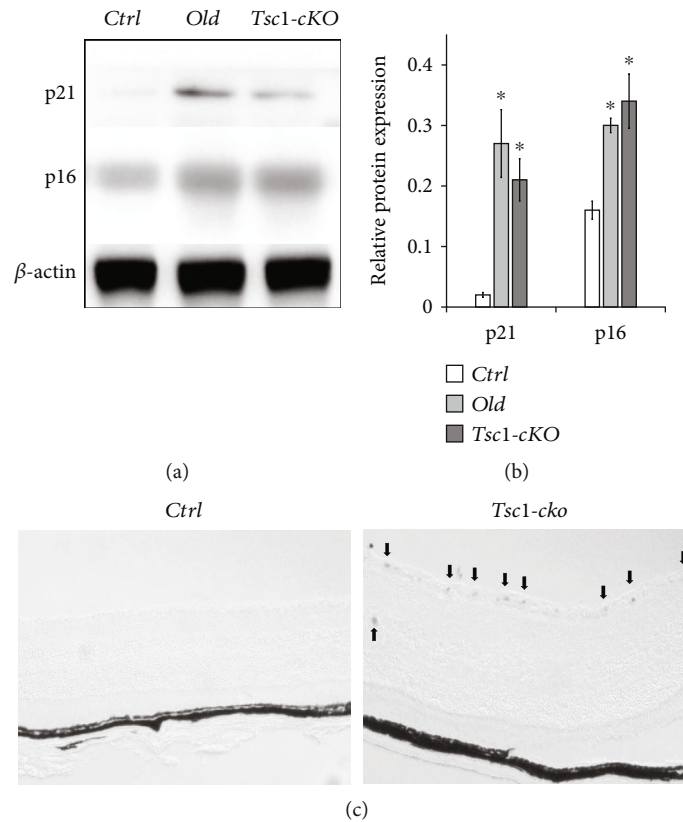


FIGURE 5: Expression of senescence-related markers in *Tsc1*-cKO retina. (a, b) Western blot analysis showed the upregulation of p21 and p16Ink4a protein in 5-month-old *Tsc1*-cKO and 24-month-old C57BL/6 (old) retina compared to age-matched control (Ctrl). The experiment was repeated twice with two different samples in each group. \* $p < 0.05$  by unpaired Students' *t*-test between groups. (c) SA- $\beta$ -gal staining of the 5-month-old *Tsc1*-cKO retina and age-matched control. Strong positive signals were found in GCL and INL (arrows in (c)) of the *Tsc1*-cKO retina. No distinctive signal was found in photoreceptor cells. Scale bar: 100  $\mu$ m.

groups (Figure 8(b)). The hierarchical clustering analysis of all DEGs (5027 genes in total) was shown in Figure 8(c). The top 5 most upregulated genes in *Tsc1*-cKO retina which were also significantly upregulated in the old-aged group compared to control were *Gpx3* (71-fold in *Tsc1*-cKO; 5.4-fold in old-aged), *Ccl12* (56.8-fold in *Tsc1*-cKO; 14.9-fold in old-aged), *Opticin* (40.2-fold in *Tsc1*-cKO; 3.1-fold in old-aged), *Glycam1* (23.3-fold in *Tsc1*-cKO; 7.1-fold in old-aged), and *Lilrb4* (22.6-fold in *Tsc1*-cKO; 8.4-fold in old-aged). They were involved in redox homeostasis and chemotactic responses. Among the downregulated genes, *Pttg1*, which encodes Securin, a protein which is involved in chromosome stability, was most downregulated in both groups (-93.7-fold in *Tsc1*-cKO; -48.5 fold in old-aged).

Gene Ontology (GO) analysis on the DEGs of the *Tsc1*-cKO and old-aged groups also revealed significant similarity. We used the FDR  $< 0.01$  as cutoff threshold to select for significant GO terms and found 49 and 12 terms enriched in *Tsc1*-cKO and old-aged groups, respectively (Supplementary Table S3). Among these terms, 10 were in common. The enrichment scores of the 10 common terms in each group were plotted in Figures 8(d) and 8(e). The GO terms and representative genes included immune system process (GO:0002376; *Ccl12*, *Agtr1a*, *Cfb*, *C3*, *Cd163*, etc.), extracellular region (GO:0005576; *Gpx3*, *Optc*, *Defb9*, *Glycam1*, *Ltbp2*, etc.), and calcium ion

binding (GO:0005509; *Tnnt2*, *Adgre1*, *Mctp1*, *Tgm2*, *S100a6*, etc.). A number of the GO terms which were found significantly involved only in *Tsc1*-cKO mice were also related to inflammation/immune responses (GO:0006954; *Thr1*, *Oasl1*, *Ccl4*, *Nlr5*, *Cd55*, etc.), chemotaxis (GO:0006935; *Pf4*, *Ccl5*, *Cxcl13*, *Ccl4*, *Ccl2*, etc.), and extracellular matrix (GO:0031012; *Gpx6*, *Wif1*, *Scrg1*, *Colec10*, *Crisp1*, etc.). In addition, there were alterations in the regulation of cell apoptosis (GO:0042981; *Tnfsf10*, *Casp1*, *Bcl2a1c*, *Bid*, *Casp12*, etc.), oxidoreductase activity (GO:0016491; *Frrs1*, *Ptgs1*, *Ncf1*, *Hmox1*, *Pyroxd2*, etc.), and aging (GO:007568; *Agtr1a*, *Pttg1*, *B2m*, *Apoe*, *Apod*, etc.) in *Tsc1*-cKO mice. Collectively, the data suggested that the activation of mTORC1 signaling caused disruption in retinal homeostasis.

**3.7. Progressive Reduction of ERG Responses with Age in *Tsc1*-cKO Mice.** Retina aging contributes to the deterioration of visual function [1]. To evaluate the function of *Tsc1*-cKO mouse retina, we conducted full-field scotopic and photopic ERG on *Tsc1*-cKO and control mice (Figures 9(a) and 9(b)). At 1 month, there was no significant difference in scotopic or photopic ERG responses between *Tsc1*-cKO and controls. At 2 months, the *Tsc1*-cKO exhibited smaller b-wave amplitude than the littermate controls at 1 and 1.3 log cd $\cdot$ s/m $^2$  under scotopic conditions, suggesting abnormal bipolar cell activity. The reduction in b-wave amplitude progressed as

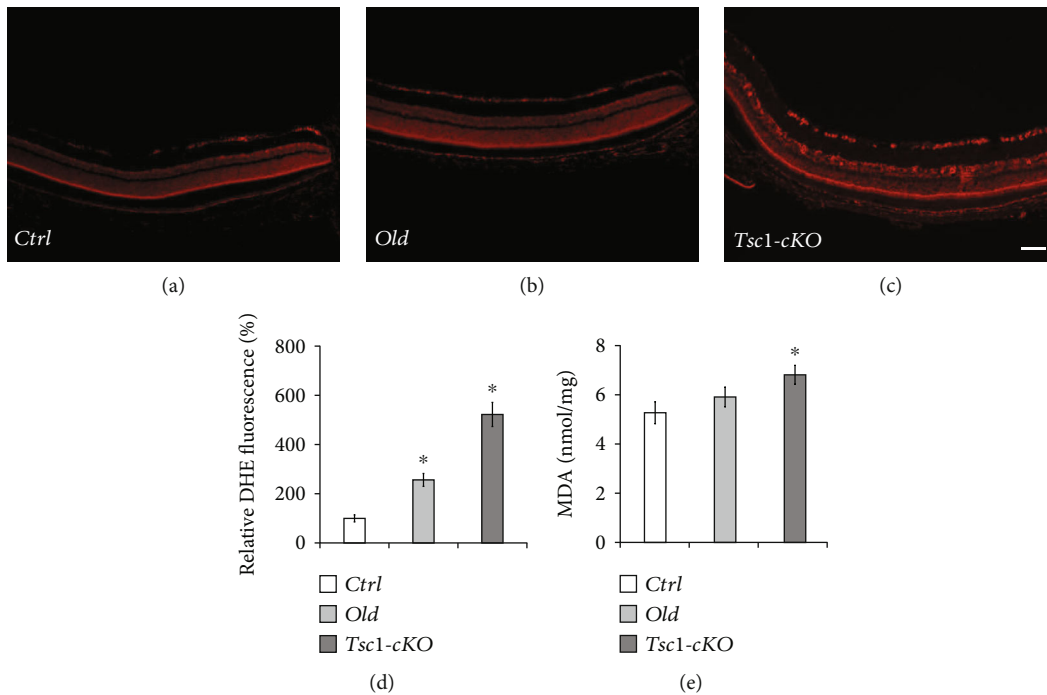


FIGURE 6: Increased oxidative stress in *Tsc1*-cKO retina. In vivo detection of ROS production via intraperitoneal injection of DHE revealed that retina sections from 5-month-old *Tsc1*-cKO mice (c) and 24-month-old C57BL/6 (old) (b) produced more ROS than age-matched control (Ctrl) mice (a). The staining was repeated on three different animals in each group. (d) The average DHE fluorescent signal intensities in *Tsc1*-cKO, old-aged, and control retina. The fluorescent intensity was quantified using ImageJ. The averaged signal intensity of the control group was set as 100%. Error bar represented SE. (e) Quantification of MDA in the retina of *Tsc1*-cKO, control, and old C57BL/6 group. Three retina samples of each group were analyzed, and the results were averaged. Error bar represented SE. Scale bar: 100  $\mu$ m. \* $p < 0.05$  by unpaired Students' *t*-test between experimental group and controls.

the *Tsc1*-cKO became older. At the age of 5 months, differences between *Tsc1*-cKO and control were seen at lower flash unit of luminance. In addition, the decrease of a-wave amplitude in *Tsc1*-cKO became significant. To better isolate the activities of photoreceptor cells in the ERG [39], we also compared the amplitudes at 8 ms after the flash to exclude the potential contribution from the inner retina cells and found that the *Tsc1*-cKO had significantly reduced amplitudes than controls (Supplementary Figure S3C). At the age of 7 months, the maximal a- and b-wave amplitudes of *Tsc1*-cKO were about 36% ( $p = 0.034$ ) and 24.3% ( $p = 0.009$ ) of those of the control mice, respectively. A similar decrease in the amplitudes at 8 ms after the flash was also observed in the *Tsc1*-cKO mice.

Consistent with the reduced scotopic responses, decreased b-wave amplitude was also observed in *Tsc1*-cKO under photopic conditions. As comparison, we also measured ERG responses in 24-month-old C57BL/6 mice. The results showed that the ERG responses of the 5-month-old *Tsc1*-cKO were comparable to those of the 24-month-old C57BL/6 mice (Figure 9(b)).

**3.8. Rapamycin Treatment Largely Reverted the Abnormalities Observed in *Tsc1*-cKO Retina.** To verify that the abnormalities observed in *Tsc1*-cKO retina were indeed due to mTORC1 activation, we used rapamycin to inhibit mTORC1 signaling in *Tsc1*-cKO mice. Intraperitoneal injection of rapamycin effectively reduced the phosphorylation of mTOR, 4E-BP1,

and S6K in the retina of *Tsc1*-cKO mice (Figures 10(a) and 10(b)). When we treated young *Tsc1*-cKO mice with rapamycin before they developed significant morphological abnormalities, we found that rapamycin effectively prevented the thickening of INL and IPL (data not shown). We then treated 3-month-old *Tsc1*-cKO mice (which already showed significantly thicker INL and IPL than the age-matched controls) with rapamycin and found that it effectively reversed the thickened INL and IPL. At the end of the treatment, the INL and IPL layers were significantly thinner than the PBS-treated *Tsc1*-cKO mice (Figures 10(c) and 10(d)). On the other hand, rapamycin treatment had no significant effect on the retinal thickness of control animal (Figure 10(c)). PKC $\alpha$  and Vimentin staining revealed shortened bipolar and Müller glia in *Tsc1*-cKO retina after rapamycin treatment (Figure 10(e)), suggesting that the thinning of the INL and IPL was most likely due to the shortening of the secondary neurons. However, improper dendritic tip arborization of bipolar cells at ONL remained (Figure 10(e), white arrows).

The rapamycin-treated *Tsc1*-cKO mice also showed less Iba-1 positive cells than the PBS-treated retina (Figure 10(e)), suggesting reduced microglial cell activation in *Tsc1*-cKO retina after rapamycin treatment. We further compared the RNA expression profile of the rapamycin-treated *Tsc1*-cKO retina to that of control and 5-month-old *Tsc1*-cKO retina without treatment. We used 4-month-old *Tsc1*-cKO for rapamycin treatment because the retina already showed signs of old-aged animal. The results showed that the RNA expression

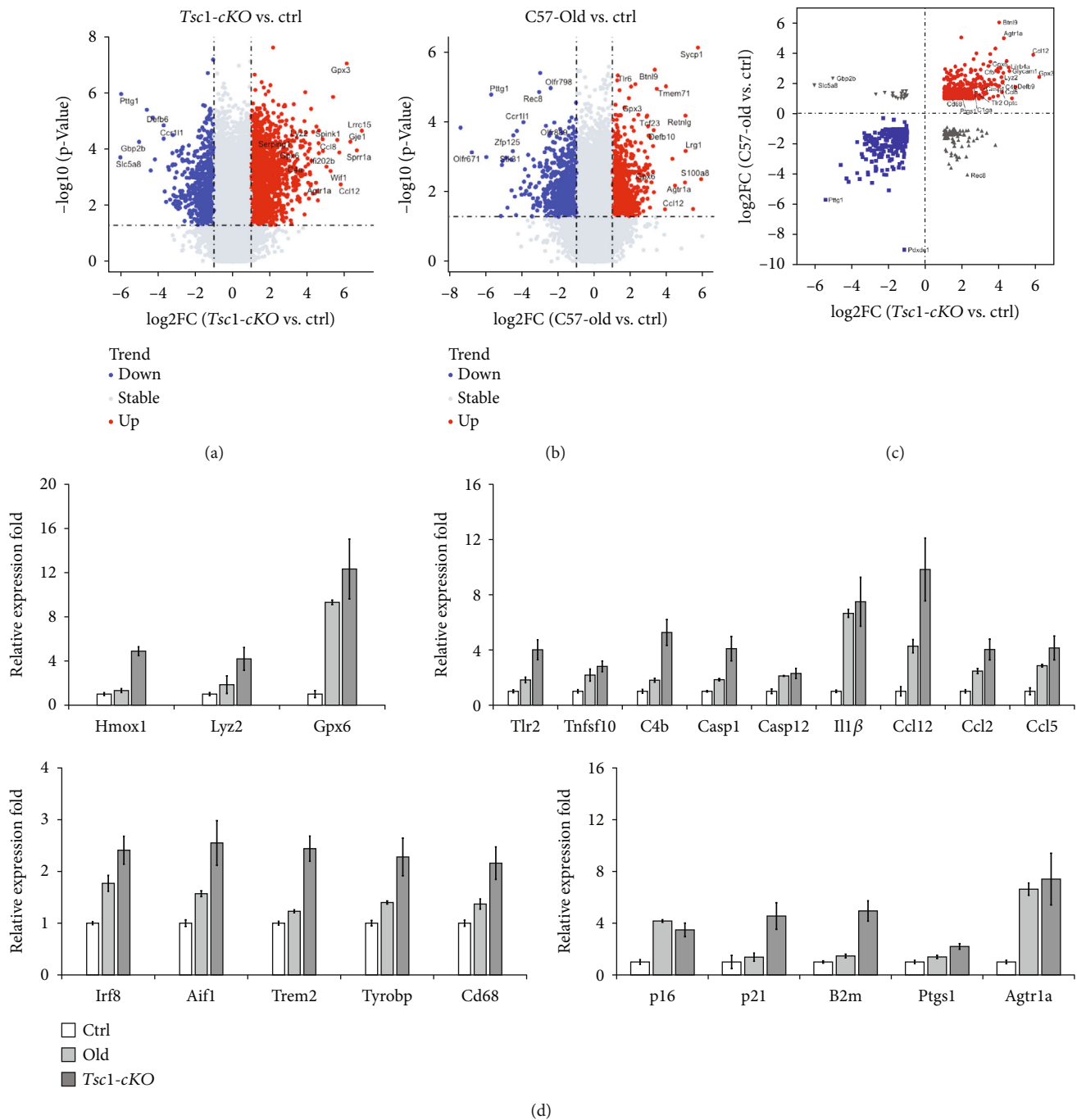


FIGURE 7: Gene expression profiles of *Tsc1*-cKO and 24-month-old C57BL/6 mouse retina. (a–c) Volcano plot showed the fold change of genes (log<sub>2</sub> scale) and significance (log<sub>10</sub> scale) between *Tsc1*-cKO and age-matched control mouse retina (a) and between 24-month-old C57BL/6 (old) and control (b). The vertical dotted lines indicated the threshold of fold change (log<sub>2</sub> > 1). The horizontal dotted line indicated the threshold of the statistical significance ( $p < 0.05$ ). The DEG for old vs. control and cKO vs. control were plotted against one another in (c). (d) Validation of microarray results with real-time PCR analysis. Fold change was relative to control and calculated as means  $\pm$  SE. Each PCR was performed using two different samples and in duplicates each time, and the fold change was averaged.

profile of the rapamycin-treated retina was similar to that of controls and very different from that of the *Tsc1*-cKO (Figure 10(f)). Furthermore, the expression of inflammation-related genes was significantly reduced in rapamycin-treated *Tsc1*-cKO retina compared to *Tsc1*-cKO without treatment (Figure 10(g)).

However, the ERG responses of the rapamycin-treated 4-month-old *Tsc1*-cKO were slightly reduced than that of the PBS-treated *Tsc1*-cKO mice, but the differences were not statistically significant (Figure 10(h)). Interestingly, rapamycin also caused small reduction of ERG responses in control mice. We speculated that the lack of ERG

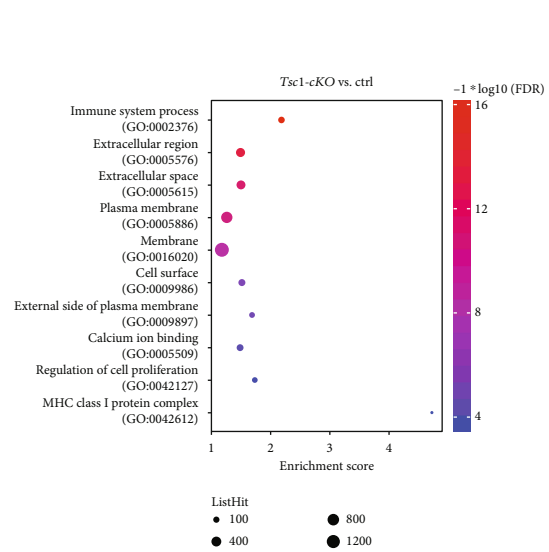
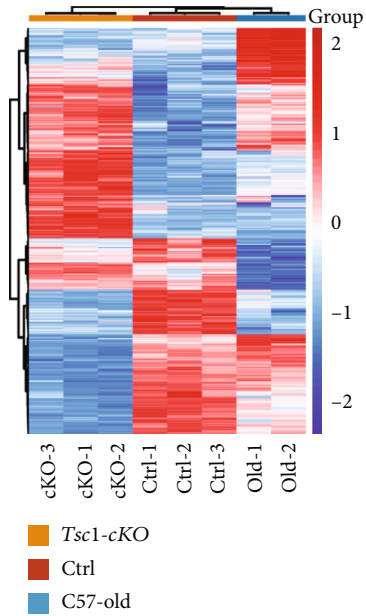
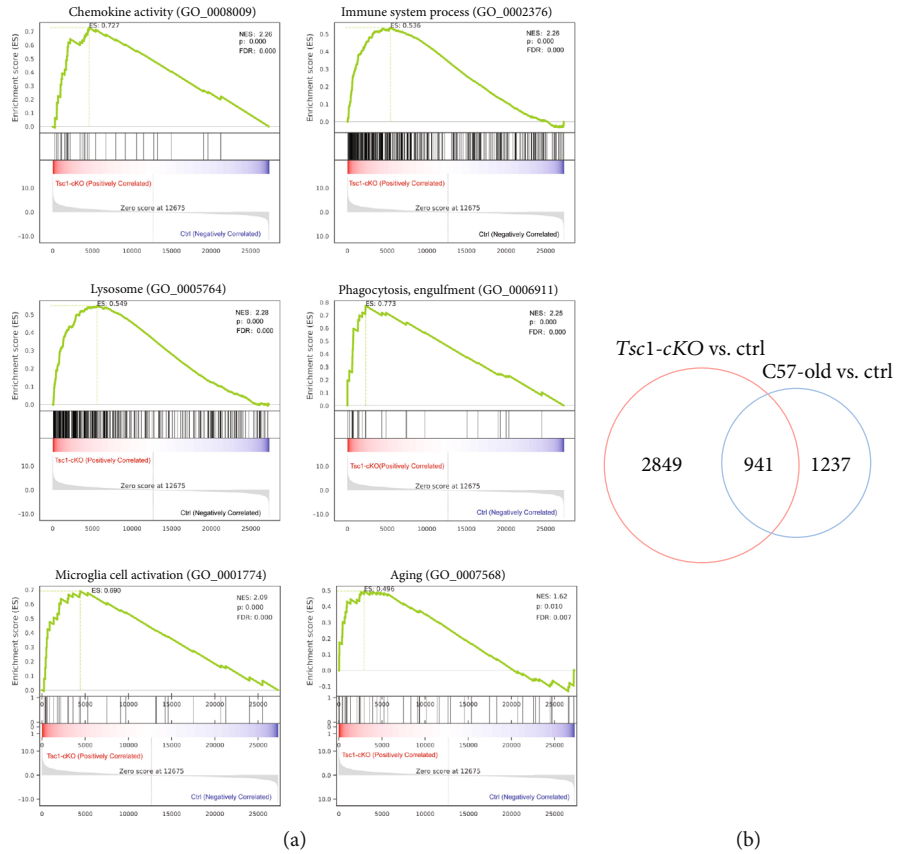


FIGURE 8: Continued.

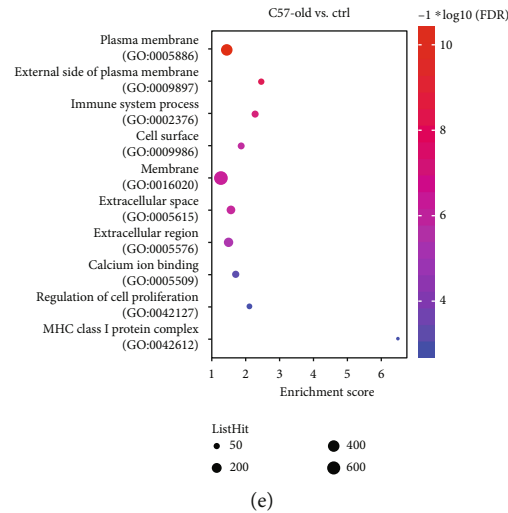


FIGURE 8: The 5-month-old *Tsc1*-cKO retina showed gene expression profile characteristic of old-aged retina. (a) Gene set enrichment analysis (GSEA) of DEGs between *Tsc1*-cKO mice and control mice. Diagrams represented selected gene sets enriched in *Tsc1*-cKO retina. (b) The Venn diagram of overlap in DEGs between *Tsc1*-cKO mice and control and old-aged C57BL/6 and control. (c) Hierarchical clustering analysis of all DEGs from *Tsc1*-cKO mice and control and old-aged C57BL/6 and control. (d) Gene Ontology (GO) analysis showing enrichment of the ten common GO terms in *Tsc1*-cKO (top) and 24-month-old (bottom).

improvement was associated with the remaining of aberrant dendritic tip endings at the ONL of the rapamycin-treated retina. In another study using the knockout of *Pten* to activate mTORC1 signaling, the authors found that rapamycin treatment could not reverse the aberrant migration of granule cells at dentate gyrus [40]. It is also possible that the toxic effect of rapamycin as previously reported in rabbit eye was responsible for the lack of rescuing effect here [41].

**3.9. Inhibition of Microglial Cell Activity by Minocycline Prevented Photoreceptor Cell Loss and Partially Restored ERG Function in the *Tsc1*-cKO Mice.** Activated microglial cell is believed to stimulate retina aging [42]. Compared to old-aged retina, the *Tsc1*-cKO retina showed a higher degree of microglial cell activation as indicated by *Iba-1* staining (Figures 1(e) and 4(m)). To determine the role of activated microglial cells in the development of the abnormalities observed in *Tsc1*-cKO retina, we treated 4-months-old *Tsc1*-cKO mice with minocycline for 4 weeks. The minocycline-treated *Tsc1*-cKO retina showed less microglial cell accumulation at the IPL and OPL than the PBS-treated *Tsc1*-cKO retina, and the cells were also more ramified (Figures 11(a) and 11(b)), indicating successful inhibition of microglial cell activation. Furthermore, cone-arrestin staining showed that the minocycline-treated *Tsc1*-cKO retina had higher cone cell density than the PBS-treated ones, suggesting that minocycline treatment prevented the loss of photoreceptor cells in the *Tsc1*-cKO retina (Figures 11(c) and 11(d)). ERG analysis showed that the minocycline-treated *Tsc1*-cKO had significantly bigger a-wave and b-wave amplitudes than the PBS-treated *Tsc1*-cKO under scotopic conditions (Figure 11(e)). Measurement of responses at 8 ms after the flash also revealed a bigger amplitude in minocycline-treated *Tsc1*-cKO mice.

Next we compared the expression of selective oxidative stress- and inflammation-related genes in minocycline and PBS-treated *Tsc1*-cKO retina to control retina and found that the oxidative stress-associated genes such as *Homx1* and *Pyroxd2* and inflammation-related genes such as *Aif1*, *C4b*, *Ccl2*, *Ccl5*, and *Il1 $\beta$*  were significantly downregulated in the minocycline-treated group (Figure 11(f)). Collectively, these results suggested that the activation of microglial cells was at least partially responsible for the functional loss of *Tsc1*-cKO retina.

## 4. Discussion

This study investigated the role of mTORC1 signaling in retina aging in old-aged C57BL/6 and *Tsc1*-cKO mice. We showed that mTORC1 signaling was upregulated in naturally aged C57BL/6 retina, and the upregulation of mTORC1 signaling in *Chx10*-expression retinal cells accelerated the aging process and caused retinal degeneration. This was evidenced by selective cell senescence, accumulation of oxidative stress, activation of microglial cells, a gene expression profile which bears signatory features of aging retina, and profound decline in retinal function.

We found that mTORC1 activation was most noticeable in ganglion cells of naturally aged retina and mTORC1 activation accelerated ganglion cell aging. The results were consistent with previous study which showed prominent expression of typical senescence-related proteins in ganglion cells, less in cells of the INL, such as amacrine, and Müller glial cells and limited in rod photoreceptor cells [4]. Single-cell RNA sequencing of primate retina also showed that RGC cells had most DEGs between old-aged and young animals [43]. Other studies have shown that the activation of mTORC1 was required for axonal regrowth after ganglion

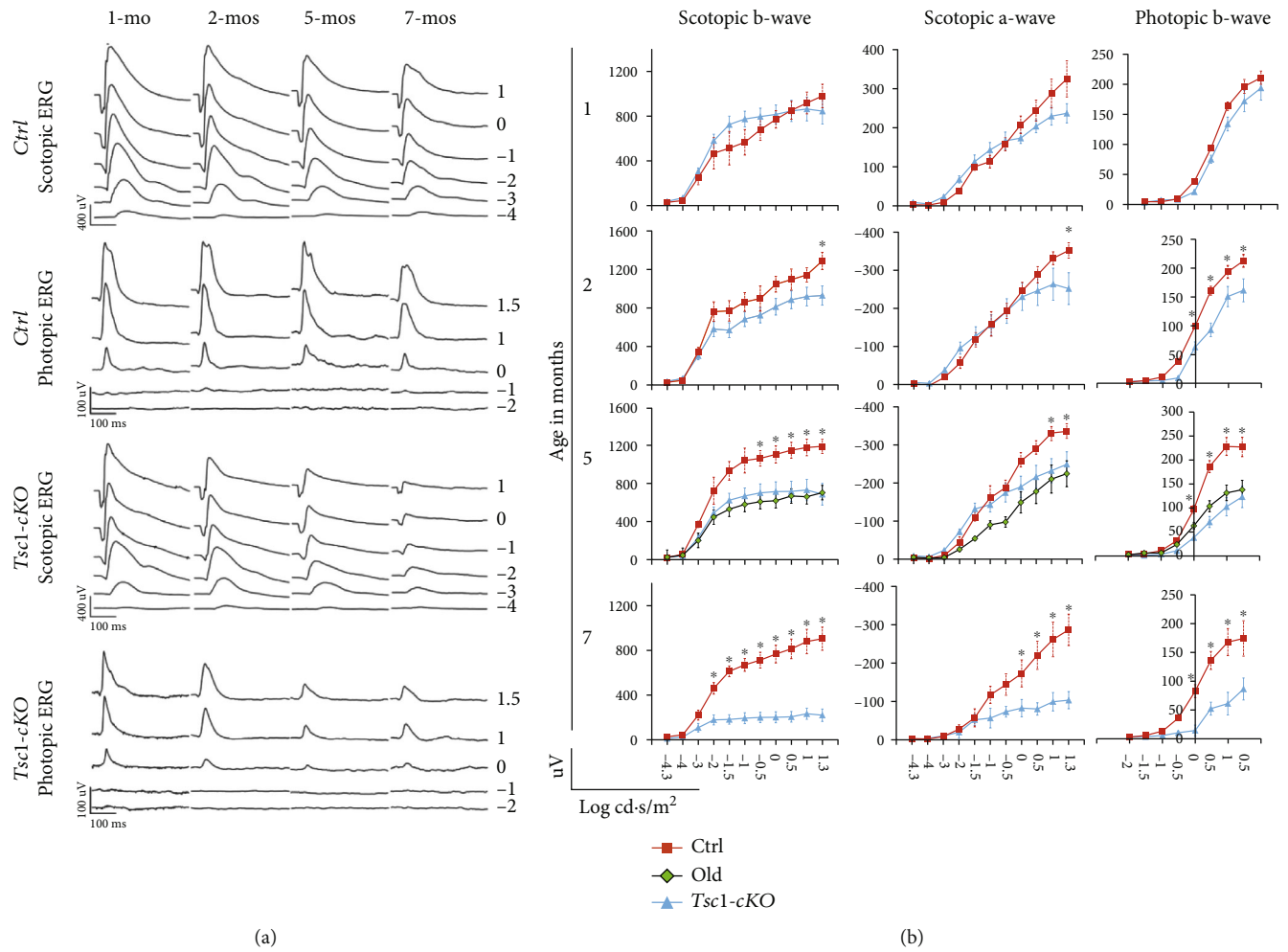


FIGURE 9: ERG responses of *Tsc1-cKO*, age-matched control, and 24-month-old C57BL/6 mice. (a) Representative full-field scotopic and photopic ERG responses of the *Tsc1-cKO* and control mice at 1, 2, 5, and 7 months of age. Rapid decrease of both scotopic and photopic responses was observed in the *Tsc1-cKO* mice. (b) Average a- and b-wave amplitudes at different units of luminance in *Tsc1-cKO* and control mice by age. The age of each group was indicated at the left side. The responses of 24-month-old C57BL/6 (old) were compared to that of the 5-month-old *Tsc1-cKO* and control. At least 6 mice in each age group of each genotype were tested. The error bars represented the SE. \* $p < 0.05$  by unpaired Students'  $t$ -test between *Tsc1-cKO* and control.

cell trauma [9, 13]. In fact, the optic nerve fiber of the *Chx10-cre* mice was also thicker than that of the controls (data not shown). Collectively, these results demonstrated an important role of mTORC1 signaling in ganglion cell homeostasis and aging.

Our study also suggested that mTORC1 activation is involved in age-related changes of bipolar cells. In 24-month-old C57BL/6 mouse retina, we found that the dendritic tips of the PKC $\alpha$ -positive rod bipolar cells extended to the ONL, a phenomenon which was also reported in an earlier study [31]. This phenomenon was replicated in *Tsc1-cKO* retina with significant cell hypertrophy. Abnormal extension of the bipolar cell dendritic tips to the ONL was found when there were photoreceptor cell contraction or defective synaptic protein synthesis [44–47]. In these circumstances, the extension of bipolar cell processes was likely an adaptive response to restore visual signal transduction. However, this is not likely the case in *Tsc1-cKO* retina, since

photoreceptor cells were not the primary affected cells and the thinning of ONL layer occurred at a much later stage. Therefore, it is tentative to propose that activation of mTORC1 stimulated the growth of bipolar cell processes which resulted in abnormal positioning of the dendritic endings and contributed to defective visual-signal transduction.

Despite the expression of *Chx10* in significant number of Müller glial cells, we observed very faint p-S6 staining in Müller glial cells of the *Tsc1-cKO* retina. The result suggested limited mTORC1 activation and was consistent with a previous report which showed that mouse Müller glia predominantly express mTORC2 [12]. However, Müller glial cell hypertrophy and activation was evident in *Tsc1-cKO* retina starting at 6 weeks of age, at the same time when bipolar cells start showing hypertrophy. At the present time, we were not able to tell if Müller gliosis were the direct consequence of altered mTORC1 signaling or the response to the hypertrophy of bipolar and other intermediate neurons.



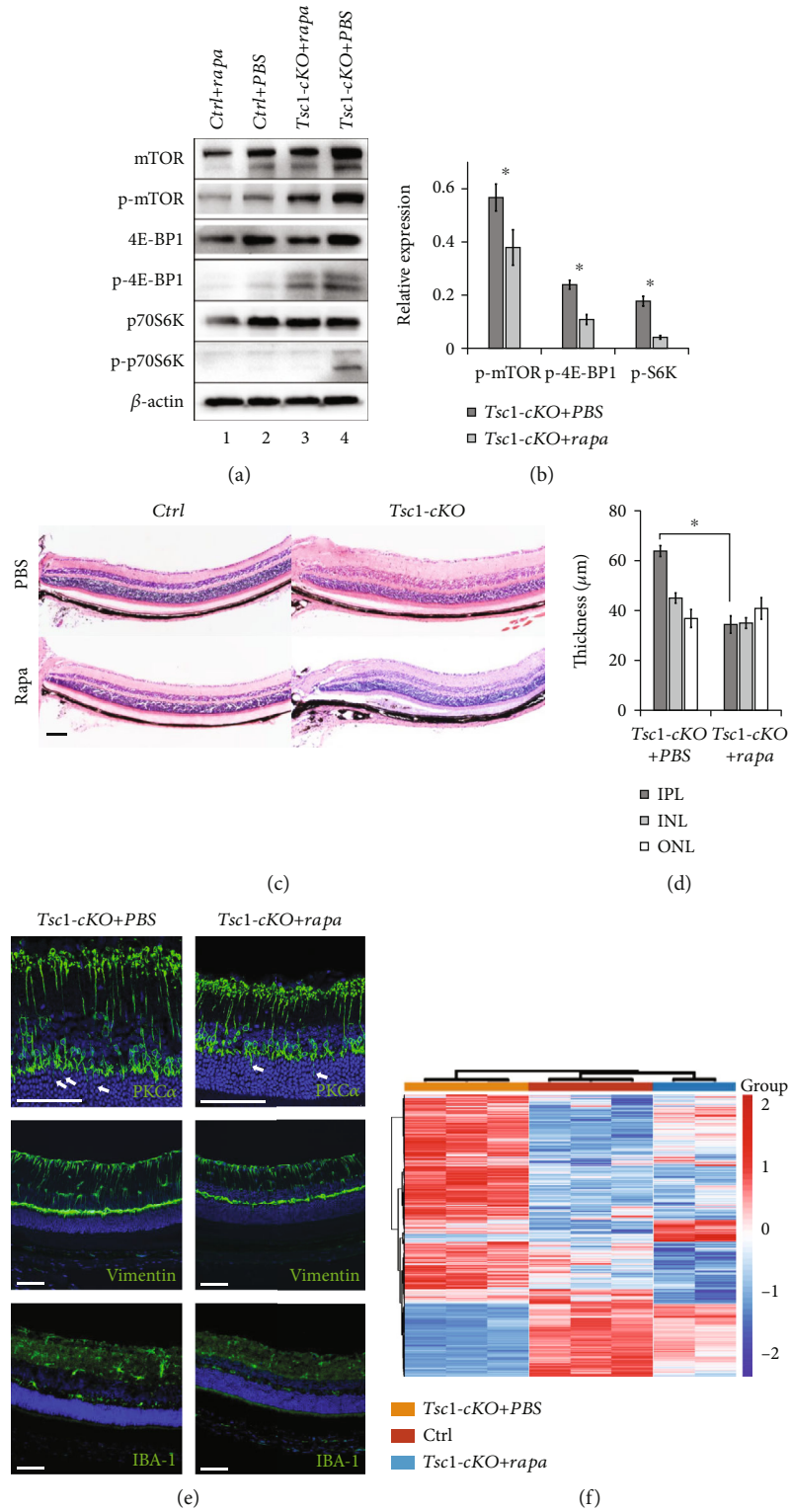


FIGURE 10: Continued.

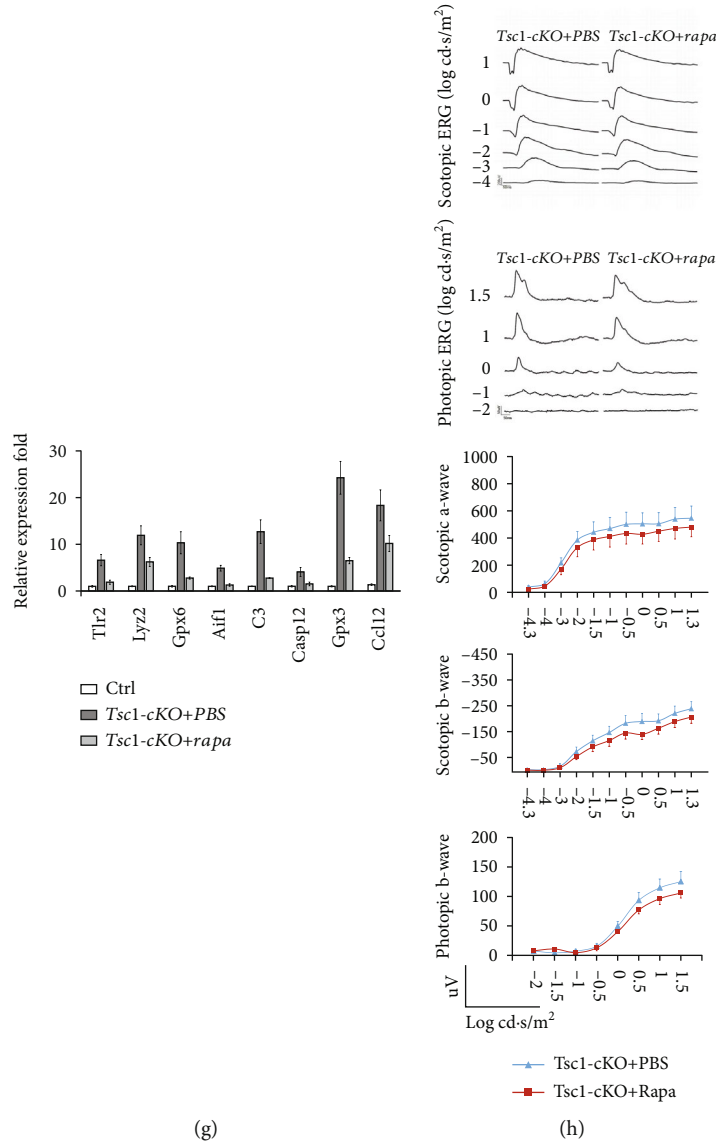
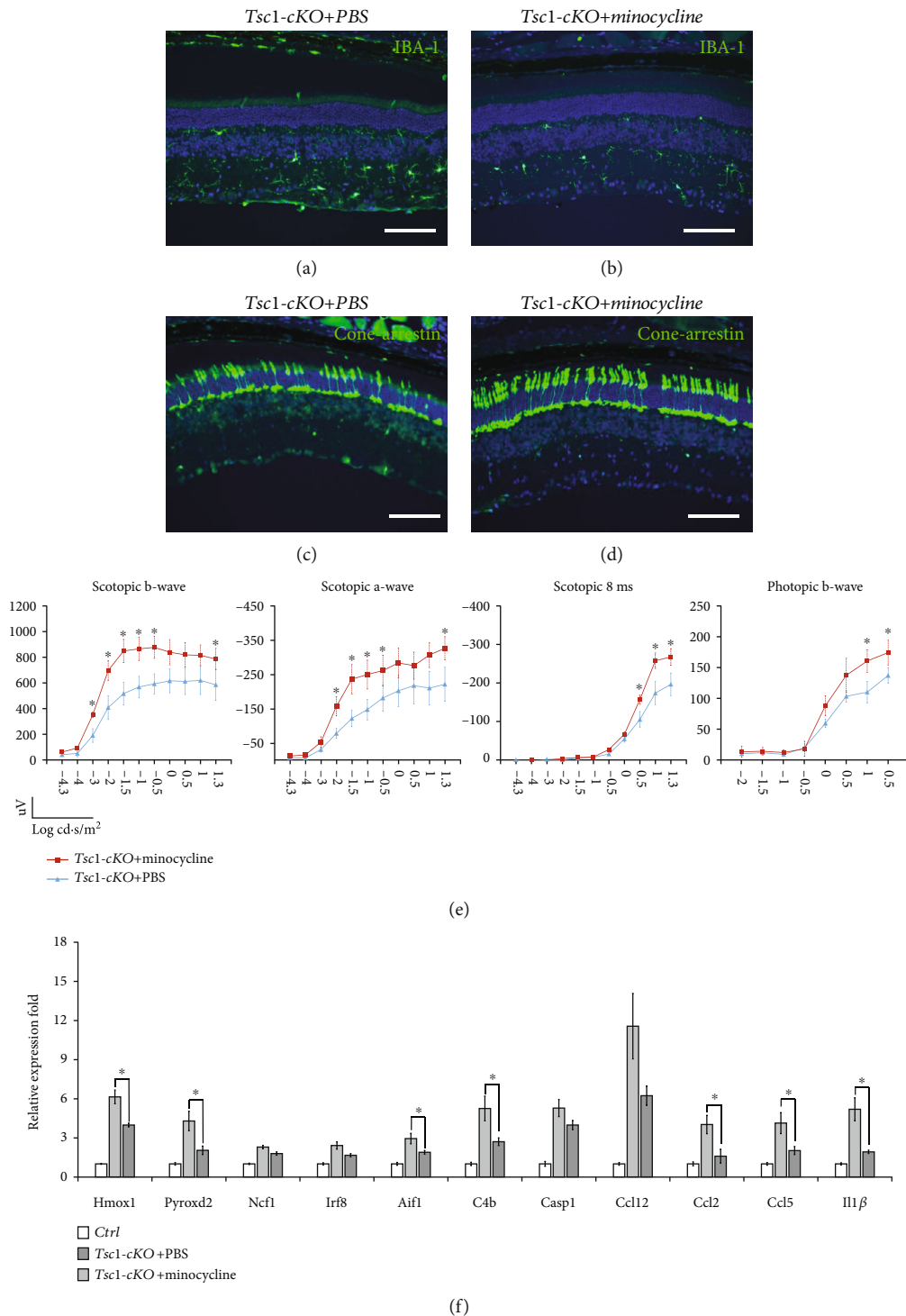


FIGURE 10: The effect of rapamycin on Tsc1-cKO retina. (a) Representative Western blot analysis of total and phosphorylated form of mTOR, 4E-BP1, and p70S6K in total retinal extracts of Tsc1-cKO and control mice after rapamycin (Rapa) or PBS treatment for 1 month. Rapamycin treatment successfully downregulated mTORC1 signaling in the Tsc1-cKO retina. (b) Relative quantification of protein expression. The density of the bands was normalized as described above. \* $p < 0.05$  by unpaired Students'  $t$ -test between Tsc1-cKO and control group. The experiments were repeated three times with one pair of samples at each time. (c) Representative H&E staining of 3-month-old Tsc1-cKO and control mouse retina after rapamycin- or PBS-treatment. (d) The average thickness of INL, IPL, and ONL of Tsc1-cKO mice after rapamycin or PBS treatment. The thickness was measured as described in Figure 3. Data represented the average reading from 4 animals in each group. Error bars represented SE. \* $p < 0.05$  by unpaired Students'  $t$ -test between PBS and rapamycin-treated group. Scale bar: 200  $\mu\text{m}$ . (e) Immunofluorescent staining of PKC $\alpha$  (top panel), Vimentin (middle panel), and Iba-1 (bottom panel) on Tsc1-cKO retina after rapamycin (right column) or PBS (left column) treatment. (f) Hierarchical clustering analysis of gene expression profiles of control, Tsc1-cKO, and rapamycin-treated Tsc1-cKO retina. (g) Expression of representative genes in rapamycin-treated and untreated Tsc1-cKO retina. Fold change was relative to control and calculated as means  $\pm$  SE. (h) Representative full field ERG responses of Tsc1-cKO mice after PBS or rapamycin treatment. The a-wave and b-wave amplitudes in response to increasing flash intensity were presented at the lower part of the panel. The data represented the averaged readings from 4 animals in each group. Error bars represented SE. Unpaired Students'  $t$ -test was performed to compare the differences between PBS- and rapamycin-treated animals at each light intensity; no significant differences were found.

In zebrafish and chicken eyes, mTOR activation promoted the dedifferentiation of Müller glial cells and the formation of Müller glia-derived progenitor cells and subsequent retina regeneration [48, 49]. In human retina of old age, heterogeneous groups of glial cells were

found by single cell transcriptomic analysis [50]. However, no significant changes of Müller glia function in old-aged retina were reported. Therefore, the role of mTORC1 signaling in Müller glia aging remains to be explored.



**FIGURE 11:** The effect of minocycline on *Tsc1-cKO* mouse retina. (a, b) Retina sections of *Tsc1-cKO* retina with or without minocycline treatment were stained with Iba-1 to show the inhibition of microglial cells after minocycline treatment. (c, d) Cone-arrestin staining of the *Tsc1-cKO* retina with and without minocycline treatment. The minocycline-treated retina showed more arrestin-positive cells, suggesting that the inhibition of microglial cells prevented photoreceptor cell loss. The staining was performed on 6 retina from 6 different animals, 3 in each group. (e) ERG responses of *Tsc1-cKO* mice with or without minocycline treatment. Three animals in each group were subjected to ERG analysis, and the a-wave, b-wave, and responses at 8 ms after the flash were averaged. Error bars represented SE. \* marked significant differences of  $p < 0.05$  by unpaired Students' *t*-test at the indicated luminance. (f) Real-time PCR analysis of genes associated with oxidative stress (Hmox1, Pyroxd2, Ncf1), microglia activity (Irf8, Aif1, C4b), chemotaxis activity (Ccl12, Ccl2, Ccl5), and inflammatory response (Casp1, Il1 $\beta$ ) in *Tsc1-cKO* retina with or without minocycline treatment. The fold change was relative to untreated- and age-matched control. Six total RNA samples, 3 in each group, were used for PCR analysis. \* $p < 0.05$  by unpaired Students' *t*-test between minocycline- and PBS-treated groups.

One of the most interesting findings of this study was the contribution of microglial cells in retinal aging and degeneration. Microglial cells play important roles in developmental, physiological, and pathophysiological processes of retina [51]. A previous study showed that the activation of microglial cells and the severity of inflammation attributed to the susceptibility of retinal degeneration in different mouse strains [52]. It was speculated that the activated microglial cells participated in the aging of retina [42, 53]. Microglial cell activation in *Tsc1*-cKO retina followed bipolar and Müller glial cell hypertrophy. In response to *Tsc1* ablation-induced mTORC1 activation, the microglia cells of the *Tsc1*-cKO retina showed more profound activation than the naturally aged retina, which correlated with more intense oxidative stress buildup and upregulation of a broad range of redox- and inflammation-related genes. Inhibition of microglial cells by minocycline in the *Tsc1*-cKO mice prevented the decrease of ERG responses and photoreceptor cell loss. The role of microglia cell in accelerating the retinal aging and degeneration represented a noncell autonomous effect of mTORC1 activation in neuronal retinal cells.

Finally, our study complemented a previous study which also used *Tsc1*-cKO mice and showed that mTORC1 activation accelerated retinal development by shorten the cell cycle time of the affected retinal progenitor cells [10]. Our results suggested that in adult *Tsc1*-cKO mice, mTORC1 activation accelerated senescence of the postmitotic, fully differentiated neuroretinal cells and ultimately led to retinal degeneration.

## 5. Conclusions

In summary, our study showed that mTORC1 activation participated in retinal aging via both cell autonomous (as in retinal ganglion cells) and nonautonomous mechanisms (largely by activated microglia cells). Our study further highlighted the role of microglia cells in driving the functional decline of the retina. Finally, we showed that the *Tsc1*-cKO mice represented an animal model of retinal degeneration and aging.

## Data Availability

The datasets supporting the conclusions of this article are available in the GEO repository (GSE177039: <https://www.ncbi.nlm.nih.gov/geo/query/acc.cgi?acc=GSE177039>). The datasets used and/or analyzed during the current study are available from the corresponding author on reasonable request.

## Ethical Approval

The animal study was reviewed and approved by Institutional Animal Care and Use Committee of Xinhua Hospital affiliated to Shanghai Jiao Tong University School of Medicine. No human studies are presented in this manuscript. No potentially identifiable human images or data is presented in this study.

## Conflicts of Interest

All authors declare that the research was conducted in the absence of any commercial or financial relationships that could be construed as a potential conflict of interest.

## Acknowledgments

We would like to thank Drs. Qiao Zhengdong and Xing Fengying for the assistance in animal husbandry. This work was supported by grants from the National Natural Science Foundation of China to JL (grant number: 81873679) and the National Key Research and Development Program of China to JL (grant number: 2018YFA0800801).

## Supplementary Materials

Supplementary Table S1: antibodies used for immunofluorescent staining and Western blot. Supplementary Table S2: sequences of primers used in the study. Supplementary Table S3: GO terms significantly upregulated in 5-month-old *Tsc1*-cKO retina compared to age-matched controls. Supplementary Figure S1: identification of *Chx10*-expressing cells in postnatal mouse retina. Supplementary Figure S2: histological and morphological changes in *Tsc1*-cKO retina. Supplementary Figure S3: progressive loss of cone photoreceptor cells and the associated decrease in ERG responses in *Tsc1*-cKO mice. (*Supplementary Materials*)

## References

- [1] J. B. Lin, K. Tsubota, and R. S. Apte, "A glimpse at the aging eye," *NPJ aging and mechanisms of disease*, vol. 2, no. 1, 2016.
- [2] J. Luu and K. Palczewski, "Human aging and disease: lessons from age-related macular degeneration," *Proceedings of the National Academy of Sciences of the United States of America*, vol. 115, no. 12, pp. 2866–2872, 2018.
- [3] B. C. Chauhan, J. R. Vianna, G. P. Sharpe et al., "Differential effects of aging in the macular retinal layers, neuroretinal rim, and peripapillary retinal nerve fiber layer," *Ophthalmology*, vol. 127, no. 2, pp. 177–185, 2020.
- [4] M. López-Luppo, J. Catita, D. Ramos et al., "Cellular senescence is associated with human retinal microaneurysm formation during aging," *Investigative Ophthalmology & Visual Science*, vol. 58, no. 7, pp. 2832–2842, 2017.
- [5] J. Kim and K. L. Guan, "mTOR as a central hub of nutrient signalling and cell growth," *Nature Cell Biology*, vol. 21, no. 1, pp. 63–71, 2019.
- [6] R. A. Saxton and D. M. Sabatini, "mTOR signaling in growth, metabolism, and disease," *Cell*, vol. 169, no. 2, pp. 361–371, 2017.
- [7] M. Wataya-Kaneda, "Mammalian target of rapamycin and tuberous sclerosis complex," *Journal of Dermatological Science*, vol. 79, no. 2, pp. 93–100, 2015.
- [8] I. S. Liu, J. D. Chen, L. Ploder et al., "Developmental expression of a novel murine homeobox gene (*Chx10*): Evidence for roles in determination of the neuroretina and inner nuclear layer," *Neuron*, vol. 13, no. 2, pp. 377–393, 1994.
- [9] S. Rowan and C. L. Cepko, "Genetic analysis of the homeodomain transcription factor *Chx10* in the retina using a novel

- multifunctional BAC transgenic mouse reporter,” *Developmental Biology*, vol. 271, no. 2, pp. 388–402, 2004.
- [10] J. H. Choi, H. S. Jo, S. Lim et al., “mTORC1 accelerates retinal development via the immunoproteasome,” *Nature Communications*, vol. 9, no. 1, 2018.
- [11] I. Jones, A. C. Hägglund, G. Törnqvist, C. Nord, U. Ahlgren, and L. Carlsson, “A novel mouse model of tuberous sclerosis complex (TSC): eye-specific Tsc1-ablation disrupts visual pathway development,” *Disease Models & Mechanisms*, vol. 8, no. 12, pp. 1517–1529, 2015.
- [12] M. Losiewicz, L. Elghazi, D. C. Fingar et al., “mTORC1 and mTORC2 expression in inner retinal neurons and glial cells,” *Experimental Eye Research*, vol. 197, 2020.
- [13] X. Duan, M. Qiao, F. Bei, I. J. Kim, Z. He, and J. R. Sanes, “Subtype-specific regeneration of retinal ganglion cells following axotomy: effects of osteopontin and mTOR signaling,” *Neuron*, vol. 85, no. 6, pp. 1244–1256, 2015.
- [14] P. Morgan-Warren, J. O’Neill, F. de Cogan et al., “siRNA-mediated knockdown of the mTOR inhibitor RTP801 promotes retinal ganglion cell survival and axon elongation by direct and indirect mechanisms,” *Investigative Ophthalmology & Visual Science*, vol. 57, no. 2, pp. 429–443, 2016.
- [15] K. Park, K. Liu, Y. Hu et al., “Promoting axon regeneration in the adult CNS by modulation of the PTEN/mTOR pathway,” *Science*, vol. 322, no. 5903, pp. 963–966, 2008.
- [16] F. Sun, K. K. Park, S. Belin et al., “Sustained axon regeneration induced by co-deletion of PTEN and SOCS3,” *Nature*, vol. 480, no. 7377, pp. 372–375, 2011.
- [17] P. Teotia, M. J. van Hook, D. Fischer, and I. Ahmad, “Human retinal ganglion cell axon regeneration by recapitulating developmental mechanisms: effects of recruitment of the mTOR pathway,” *Development*, vol. 146, no. 13, 2019.
- [18] S. Cheng, J. Cipi, S. Ma et al., “Altered photoreceptor metabolism in mouse causes late stage age-related macular degeneration-like pathologies,” *Proceedings of the National Academy of Sciences of the United States of America*, vol. 117, no. 23, pp. 13094–13104, 2020.
- [19] S. Ma, A. Venkatesh, F. Langellotto et al., “Loss of mTOR signaling affects cone function, cone structure and expression of cone specific proteins without affecting cone survival,” *Experimental Eye Research*, vol. 135, pp. 1–13, 2015.
- [20] A. Venkatesh, S. Ma, and C. Punzo, “TSC but not PTEN loss in starving cones of retinitis pigmentosa mice leads to an autophagy defect and mTORC1 dissociation from the lysosome,” *Cell Death & Disease*, vol. 7, no. 6, article e2279, 2016.
- [21] S. C. Johnson, P. S. Rabinovitch, and M. Kaerberlein, “mTOR is a key modulator of ageing and age-related disease,” *Nature*, vol. 493, no. 7432, pp. 338–345, 2013.
- [22] Y. Chen, J. Wang, J. Cai, and P. Sternberg, “Altered mTOR signaling in senescent retinal pigment epithelium,” *Investigative Ophthalmology & Visual Science*, vol. 51, no. 10, pp. 5314–5319, 2010.
- [23] N. G. Kolosova, N. A. Muraleva, A. A. Zhdankina, N. A. Stefanova, A. Z. Fursova, and M. V. Blagosklonny, “Prevention of age-related macular degeneration-like retinopathy by rapamycin in rats,” *The American Journal of Pathology*, vol. 181, no. 2, pp. 472–477, 2012.
- [24] N. Tanimoto, V. Sothilingam, and M. W. Seeliger, “Functional phenotyping of mouse models with ERG,” *Methods in Molecular Biology*, vol. 935, pp. 69–78, 2012.
- [25] A. Subramanian, P. Tamayo, V. K. Mootha et al., “Gene set enrichment analysis: a knowledge-based approach for interpreting genome-wide expression profiles,” *Proceedings of the National Academy of Sciences of the United States of America*, vol. 102, no. 43, pp. 15545–15550, 2005.
- [26] N. Fan, S. M. Silverman, Y. Liu et al., “Rapid repeatable *in vivo* detection of retinal reactive oxygen species,” *Experimental Eye Research*, vol. 161, pp. 71–81, 2017.
- [27] R. Hosoi, S. Sato, M. Shukuri et al., “A simple *ex vivo* semi-quantitative fluorescent imaging utilizing planar laser scanner: detection of reactive oxygen species generation in mouse brain and kidney,” *Molecular Imaging*, vol. 18, 2019.
- [28] R. Selvarani, S. Mohammed, and A. Richardson, “Effect of rapamycin on aging and age-related diseases-past and future,” *Geroscience*, vol. 43, no. 3, pp. 1135–1158, 2021.
- [29] A. Bosco, D. M. Inman, M. R. Steele et al., “Reduced retinal microglial activation and improved optic nerve integrity with minocycline treatment in the DBA/2J mouse model of glaucoma,” *Investigative Ophthalmology & Visual Science*, vol. 49, no. 4, pp. 1437–1446, 2008.
- [30] H. Levkovitch-Verbin, M. Kalev-Landoy, Z. Habet-Wilner, and S. Melamed, “Minocycline delays death of retinal ganglion cells in experimental glaucoma and after optic nerve transection,” *Archives of Ophthalmology*, vol. 124, no. 4, pp. 520–526, 2006.
- [31] L. Liets, K. Eliasieh, D. A. van der List, and L. M. Chalupa, “Dendrites of rod bipolar cells sprout in normal aging retina,” *Proceedings of the National Academy of Sciences of the United States of America*, vol. 103, no. 32, pp. 12156–12160, 2006.
- [32] Q. Lu, E. Ivanova, T. H. Ganjawala, and Z. H. Pan, “Cre-mediated recombination efficiency and transgene expression patterns of three retinal bipolar cell-expressing Cre transgenic mouse lines,” *Molecular Vision*, vol. 19, pp. 1310–1320, 2013.
- [33] W. Yan, M. A. Laboulaye, N. M. Tran, I. E. Whitney, I. Benhar, and J. R. Sanes, “Mouse retinal cell atlas: molecular identification of over sixty amacrine cell types,” *The Journal of Neuroscience*, vol. 40, no. 27, pp. 5177–5195, 2020.
- [34] Y. Zhang, I. J. Kim, J. R. Sanes, and M. Meister, “The most numerous ganglion cell type of the mouse retina is a selective feature detector,” *Proceedings of the National Academy of Sciences of the United States of America*, vol. 109, no. 36, pp. E2391–E2398, 2012.
- [35] A. Venkatesh, S. Ma, Y. Z. le, M. N. Hall, M. A. Rüegg, and C. Punzo, “Activated mTORC1 promotes long-term cone survival in retinitis pigmentosa mice,” *The Journal of Clinical Investigation*, vol. 125, no. 4, pp. 1446–1458, 2015.
- [36] M. Samuel, Y. Zhang, M. Meister, and J. R. Sanes, “Age-related alterations in neurons of the mouse retina,” *The Journal of Neuroscience*, vol. 31, no. 44, pp. 16033–16044, 2011.
- [37] I. Liguori, G. Russo, F. Curcio et al., “Oxidative stress, aging, and diseases,” *Clinical Interventions in Aging*, vol. Volume 13, pp. 757–772, 2018.
- [38] M. Chen, E. Muckersie, J. V. Forrester, and H. Xu, “Immune activation in retinal aging: a gene expression study,” *Investigative Ophthalmology & Visual Science*, vol. 51, no. 11, pp. 5888–5896, 2010.
- [39] J. Robson, S. M. Saszik, J. Ahmed, and L. J. Frishman, “Rod and cone contributions to thea-wave of the electroretinogram of the macaque,” *The Journal of Physiology*, vol. 547, no. 2, pp. 509–530, 2003.

- [40] R. A. Miller, D. E. Harrison, C. M. Astle et al., "Rapamycin, but not resveratrol or simvastatin, extends life span of genetically heterogeneous mice," *The Journals of Gerontology. Series A, Biological Sciences and Medical Sciences*, vol. 66A, no. 2, pp. 191–201, 2011.
- [41] R. Manzano, G. A. Peyman, P. Khan, M. Kivilcim, P. Chevez-Barrios, and W. Takahashi, "Testing intravitreal toxicity of rapamycin in rabbit eyes," *Arquivos Brasileiros de Oftalmologia*, vol. 72, no. 1, pp. 18–22, 2009.
- [42] W. Ma and W. T. Wong, "Aging changes in retinal microglia and their relevance to age-related retinal disease," *Advances in Experimental Medicine and Biology*, vol. 854, pp. 73–78, 2016.
- [43] S. Wang, Y. Zheng, Q. Li et al., "Deciphering primate retinal aging at single-cell resolution," *Protein Cell*, vol. 12, pp. 889–898, 2021.
- [44] S. Ball and R. Gregg, "Using mutant mice to study the role of voltage-gated calcium channels in the retina," *Advances in Experimental Medicine and Biology*, vol. 514, pp. 439–450, 2002.
- [45] C. Beier, A. Hovhannisyan, S. Weiser et al., "Deafferented adult rod bipolar cells create new synapses with photoreceptors to restore vision," *The Journal of Neuroscience*, vol. 37, no. 17, pp. 4635–4644, 2017.
- [46] O. Dick, S. tom Dieck, W. D. Altmann et al., "The presynaptic active zone protein bassoon is essential for photoreceptor ribbon synapse formation in the retina," *Neuron*, vol. 37, no. 5, pp. 775–786, 2003.
- [47] N. Shen, B. Wang, F. Soto, and D. Kerschensteiner, "Homeostatic plasticity shapes the retinal response to photoreceptor degeneration," *Current Biology*, vol. 30, no. 10, pp. 1916–1926.e3, 2020, e3.
- [48] C. Zelinka, L. Volkov, Z. A. Goodman et al., "mTor-signaling is required for the formation of proliferating Müller glia-derived progenitor cells in the chick retina," *Development*, vol. 143, no. 11, pp. 1859–1873, 2016.
- [49] Z. Zhang, H. Hou, S. Yu et al., "Inflammation-induced mammalian target of rapamycin signaling is essential for retina regeneration," *Glia*, vol. 68, no. 1, pp. 111–127, 2020.
- [50] M. Menon, S. Mohammadi, J. Davila-Velderrain et al., "Single-cell transcriptomic atlas of the human retina identifies cell types associated with age-related macular degeneration," *Nature Communications*, vol. 10, no. 1, 2019.
- [51] M. Karlstetter, R. Scholz, M. Rutar, W. T. Wong, J. M. Provis, and T. Langmann, "Retinal microglia: just bystander or target for therapy?," *Progress in Retinal and Eye Research*, vol. 45, pp. 30–57, 2015.
- [52] D. Mustafi, T. Maeda, H. Kohno, J. H. Nadeau, and K. Palczewski, "Inflammatory priming predisposes mice to age-related retinal degeneration," *The Journal of Clinical Investigation*, vol. 122, no. 8, pp. 2989–3001, 2012.
- [53] M. Chen, C. Luo, J. Zhao, G. Devarajan, and H. Xu, "Immune regulation in the aging retina," *Progress in Retinal and Eye Research*, vol. 69, pp. 159–172, 2019.

## Research Article

# Trilobatin Alleviates Cognitive Deficits and Pathologies in an Alzheimer's Disease Mouse Model

Jiuyang Ding<sup>1</sup>, Jian Huang<sup>2</sup>, Dan Yin<sup>3</sup>, Ting Liu<sup>4</sup>, Zheng Ren<sup>1</sup>, Shanshan Hu<sup>5</sup>, Yuanliang Ye<sup>6</sup>, Cuiyun Le<sup>1</sup>, Na Zhao<sup>1</sup>, Hongmei Zhou<sup>1</sup>, Zhu Li<sup>1</sup>, Xiaolan Qi<sup>7</sup>, and Jiang Huang<sup>1</sup>

<sup>1</sup>School of Forensic Medicine, Guizhou Medical University, Guiyang 550004, China

<sup>2</sup>School of Forensic Medicine, Southern Medical University, Guangzhou 510515, China

<sup>3</sup>Laboratory of Electron Microscopy, School of Basic Medicine, Guizhou Medical University, Guiyang 550004, China

<sup>4</sup>State Key Laboratory of Functions and Applications of Medicinal Plants, Key Laboratory of Pharmaceutics of Guizhou Province, Guizhou Medical University, Guiyang 550004, China

<sup>5</sup>Good Clinical Practice Center, Affiliated Hospital of Zunyi Medical University, Zunyi 563003, China

<sup>6</sup>Department of Neurosurgery, Liuzhou People's Hospital, Liuzhou, China

<sup>7</sup>Key Laboratory of Endemic and Ethnic Diseases, Ministry of Education, Guizhou Medical University, Guiyang 550004, China

Correspondence should be addressed to Jiang Huang; [mmm\\_hj@126.com](mailto:mmm_hj@126.com)

Received 9 August 2021; Accepted 26 October 2021; Published 5 November 2021

Academic Editor: Xu Wu

Copyright © 2021 Jiuyang Ding et al. This is an open access article distributed under the Creative Commons Attribution License, which permits unrestricted use, distribution, and reproduction in any medium, provided the original work is properly cited.

Alzheimer's disease (AD) is the most common neurodegenerative disease nowadays that causes memory impairments. It is characterized by extracellular aggregates of amyloid-beta ( $A\beta$ ), intracellular aggregates of hyperphosphorylated Tau (p-Tau), and other pathological features. Trilobatin (TLB), a natural flavonoid compound isolated from *Lithocarpus polystachyus* Rehd., has emerged as a neuroprotective agent. However, the effects and mechanisms of TLB on Alzheimer's disease (AD) remain unclear. In this research, different doses of TLB were orally introduced to 3×FAD AD model mice. The pathology, memory performance, and Toll-like receptor 4- (TLR4-) dependent inflammatory pathway protein level were assessed. Here, we show that TLB oral treatment protected 3×FAD AD model mice against the  $A\beta$  burden, neuroinflammation, Tau hyperphosphorylation, synaptic degeneration, hippocampal neuronal loss, and memory impairment. The TLR4, a pattern recognition immune receptor, has been implicated in neurodegenerative disease-related neuroinflammation. We found that TLB suppressed glial activation by inhibiting the TLR4-MYD88-NF $\kappa$ B pathway, which leads to the inflammatory factor TNF- $\alpha$ , IL-1 $\beta$ , and IL-6 reduction. Our study shows that TLR4 might be a key target of TLB in AD treatment and suggests a multifaceted target of TLB in halting AD. Taken together, our findings suggest a potential therapeutic effect of TLB in AD treatment.

## 1. Introduction

Alzheimer's disease (AD) is the most common neurodegenerative disease in the elderly [1]. The AD patient number will reach 100 million worldwide by 2050, which creates an enormous burden on societies and families [2]. Evidence shows that amyloid- $\beta$  ( $A\beta$ ), oxidative stress, synaptic degeneration, and neuroinflammation play central roles in AD progression [3, 4]. However, drugs that target  $A\beta$  deposition or Tau phosphorylation would not efficiently halt AD

progression in recent years [5, 6]. Besides synthetic drugs, many traditional Chinese medicines and natural products are found available for AD management [7–12]. These research studies shed new light on the discovery of natural products to alleviate AD pathologies.

Recently, there has been increasing evidence showing that the immune system function alters in AD cases [13]. In AD patients, chronic neuroinflammation is remarkable and leads to immune system dysfunction [14]. Toll-like receptors (TLRs) are a class of highly conserved receptors

that modulate innate immune responses [15]. Among the 13 TLRs in mammals, the Toll-like receptor 4 (TLR4) has been well studied in neurodegenerative disease. TLR4 can activate downstream signals through MYD88 and non-MYD88 pathways [16]. The nuclear factor kappa B (NF $\kappa$ B) promoter, which transcribes inflammatory factors including TNF- $\alpha$ , interleukin 1 $\beta$  (IL-1 $\beta$ ), and interleukin 6 (IL-6), is the downstream protein of TLR4 [17]. In the central nervous system, TLR4 is mainly expressed in glial cells with very low-level expression in neurons [18]. TLR4 is seen upregulated in the brains of AD patients and AD model mice [19]. The toxic A $\beta$  leads to glial activation and enhances the phagocytosis function of glial cells through TLR4 [20]. Given that the TLR4 alters in AD progression, targeting TLR4 is a promising direction in halting AD. It has been demonstrated that suppressing TLR4 shows a protective effect in AD pathology through an anti-inflammatory mechanism [21, 22].

Trilobatin (TLB), isolated from *Lithocarpus polystachyus* Rehd., has been shown to alleviate neuroinflammation and oxidative stress in an ischemia/reperfusion brain injury mouse model [23]. In this model, TLB exerts neuroprotective effects through the Nrf2/Kelch-like ECH-associated protein 1 (Keap-1) signaling pathway. A recent study shows that TLB can delay aging through an antioxidative mechanism in *Caenorhabditis elegans* [24]. Moreover, TLB was found to modulate TLR4 function in the ischemia/reperfusion brain injury mouse model [23]. Thus, we hypothesize that TLB can alleviate AD-related neuroinflammation through the TLR4 pathway and attenuate AD pathology. To address this hypothesis, we treated 3 $\times$ FAD AD model mice with TLB and evaluated the effects of TLB on AD-related pathology and memory function. We found that TLB attenuated memory deficits, alleviated Tau and A $\beta$  pathology, modulated spine plasticity, protected neuronal loss, and inhibited gliosis in the 3 $\times$ FAD AD mouse model. We think that TLB might alleviate glial activation through the TLR4 pathway. Our results uncovered a natural compound TLB that might halt AD progression through multiple pathways. It might provide a potential therapeutic approach involving TLR4 inhibition in AD treatment.

## 2. Materials and Methods

**2.1. Animals.** C57BL/6J mice (male, 18~26 g, 6~8 weeks old) were purchased from the Laboratory Animal Center of Guizhou Medical University (Guizhou, China). 3 $\times$ FAD transgenic AD mice (APP Swedish, MAPT P301L, and PSEN1 M146V) were purchased from Beijing iBio Logistics Co., Ltd. (Beijing, China). Mice were kept under a 12 h light-dark cycle with full access to food and water. All procedures involving animals were preapproved by the Institutional Animal Care and Use Committee of Guizhou Medical University.

**2.2. Drug Treatment and Experimental Groups.** Four-month-old wild-type (WT) mice and 3 $\times$ FAD transgenic AD mice were used for all experiments. TLB was dissolved in saline for gavage. The 10 mg/kg or 20 mg/kg dose of TLB (10 mg/kg and 20 mg/kg) was given as reported in earlier studies [23]. Mice were divided into five groups:

WT: saline was administered by gavage in place of TLB solution.

WT+TLB<sub>H</sub>: WT mice were treated with TLB (high dose) by gavage at a dose of 20 mg/kg once a day for 12 weeks.

3 $\times$ FAD: the 3 $\times$ FAD transgenic AD mice were treated with saline by gavage in place of TLB.

3 $\times$ FAD+TLB<sub>L</sub>: the 3 $\times$ FAD transgenic AD mice were treated with TLB (low dose) by gavage at a dose of 10 mg/kg once a day for 12 weeks.

3 $\times$ FAD+TLB<sub>H</sub>: the 3 $\times$ FAD transgenic AD mice were treated with TLB (high dose) by gavage at a dose of 20 mg/kg once a day for 12 weeks.

After 12 weeks of TLB gavage, the mice were humanely killed with an overdose of sodium pentobarbital (80 mg/kg, i.p.). Then, samples were perfused with 0.9% saline transcardially for 5 min. Mouse brains were removed. One hemisphere of each brain was used for biochemical analysis, and the other hemisphere was fixed in 4% paraformaldehyde for morphological analysis.

**2.3. Morris Water Maze (MWM) Test.** The effect of TLB on the memory performance of mice was analyzed by the MWM test [25]. The maze (110 cm in diameter) was filled with ~20°C opacified water. Before the test, mice were trained to habituate the maze. During training, the mice were allowed to swim for 60 s to find the platform (10 cm in side length) in the second quadrant. The platform was set 1 cm beneath the water surface. The mice were reset at the platform when they failed to find the platform in 60 s. The mice were trained twice a day with a 30 min interval between training sessions. The platform was removed one day after the training. The mice were left in the fourth quadrant and allowed to swim. The swimming trials were recorded using a camera set above the maze. The time spent in the target quadrant (second quadrant) and times of crossing the platform were analyzed as an indicator of memory performance. The test of each mouse was repeated 3 times, and the average time of these three trials was recorded.

**2.4. Congo Red Staining.** Congo red staining was conducted using a Congo red amyloid stain kit (G1532, Solarbio Life Science, Beijing, China). Paraffin-embedded brains were sectioned using a microtome (RM2235, Leica, Germany), immersed in Congo red solution for 25 min, and then washed with 0.1 M PBS. After being stained with hematoxylin for 30 sec, the sections were dehydrated in gradient alcohol. Pictures were acquired using a microscope (CX23, Olympus, Japan). Six mice per group were included in the experiment. Three separate serial sections per mouse were processed for Congo red staining analysis.

**2.5. Immunohistochemical (IHC) Staining.** Brain tissues were sectioned using a microtome (RM2235, Leica, Germany). After antigen recovery using sodium citrate, the sections were incubated with primary antibodies mouse anti-GFAP (3670s, 1:200, Cell Signaling Technology, USA), A $\beta$  (ab201060, 1:200, Abcam, USA), phosphor-Tau (ab32057, 1:150, Abcam, USA), and rabbit anti-NeuN (ab128886, 1:200, Abcam, USA). The sections were developed with



3,3'-diaminobenzidine (DAB) kits (Cat#CW2069, CWBio, China) according to the manufacturer's protocol. Images were obtained using a microscope (CX23, Olympus, Japan). Six mice per group were included in the experiment. Three separate serial sections per mouse were processed for immunostaining analysis.

For immunofluorescence labeling, frozen sections (25  $\mu$ m) were cut using a freezing microtome (CM1950, Leica, Wetzlar, Germany). After blocking with 5% BSA containing 0.5% Triton X-100 for 40 min, the floating sections were incubated with primary antibodies A $\beta$  (ab201060, 1:200, Abcam, USA) and Iba1 (ab178846, 1:200, Abcam, USA). After being rinsed in water, the sections were incubated in the secondary antibody Alexa Fluor 488 (A-21206, Thermo Fisher Scientific, MA, USA). Nuclei were labeled using DAPI (H-1020, Vector Labs, CA, USA). Images were acquired using a confocal microscope (LSM 900, Carl Zeiss, Germany). Six mice per group were included in the experiment. Three separate serial sections per mouse were processed for immunostaining analysis.

**2.6. Nissl Staining.** The Nissl staining was conducted using a Nissl staining kit (G1434, Solarbio Life Science, Beijing, China) according to the manufacturer's protocol. Paraffin-embedded brain tissues were sectioned using a microtome (RM2235, Leica, Germany). Then, the sections were dewaxed and rehydrated before being immersed into methylene blue stain solution for 10 min. After being immersed into the Nissl differentiation solution for 3 sec, the sections were rinsed in water. At last, the sections were dehydrated in pure alcohol. Pictures were acquired using a microscope (CX23, Olympus, Japan). Six mice per group were included in the experiment. Three separate serial sections per mouse were processed for Nissl staining analysis.

**2.7. Western Blot.** Hippocampal tissue was homogenized in the protein extraction buffer containing protease and phosphatase inhibitors. After centrifugation, the protein supernatant was collected. Protein concentration was measured with a Protein Quantitative Analysis Kit (Biocolors, Shanghai, China). The supernatant was then mixed with the loading buffer and boiled at 99°C for 10 min. The samples were separated by SDS-PAGE and transferred to PVDF membranes (Millipore, Billerica, MA, USA). The membranes were blocked in 5% nonfat milk at room temperature for 1 h, then incubated overnight at 4°C with the following primary antibodies: A $\beta$  (ab217153, 1:1000, Abcam, USA), BACE1 (ab108394, 1:1000, Abcam, USA), sAPP $\beta$  (ab32136, 1:1000, Abcam, USA), p-GSK3 $\beta$  Y216 (ab68476, 1:1000, Abcam, USA), GSK3 $\beta$  (ab93926, 1:1000, Abcam, USA), p-Ser396 Tau (9632S, 1:1000, Cell Signaling Technology, USA), p-Ser202 Tau (39357S, 1:1000, Cell Signaling Technology, USA), Tau (ab80579, 1:1000, Abcam, USA), PSD95 (ab2723, 1:1000, Abcam, USA), SNAP25 (ab109105, 1:1000, Abcam, USA), Syn1 (ab254349, 1:1000, Abcam, USA), SYP (ab32127, 1:1000, Abcam, USA), VAMP1 (ab151712, 1:1000, Abcam, USA), TLR4 (ab13556, 1:1000, Abcam, USA), MYD88 (ab219413, 1:1000, Abcam, USA), TRAF6 (ab33915, 1:1000, Abcam,

USA), p-NF $\kappa$ B (ab76302, 1:1000, Abcam, USA), NF $\kappa$ B (ab32536, 1:1000, Abcam, USA), TNF- $\alpha$  (ab66579, 1:1000, Abcam, USA), IL-1 $\beta$  (ab200478, 1:1000, Abcam, USA), IL-6 (ab208113, 1:1000, Abcam, USA), and  $\beta$ -actin (ab8226, 1:1000, Abcam, USA). After incubating with the secondary antibody at room temperature for 1 h, the membranes were interacted with electrochemiluminescence reagents (Bio-Rad, Hercules, CA, USA) to visualize the immunoblot signals. ImageJ software was used to measure band densities, and protein expression levels were normalized to  $\beta$ -actin intensity.

**2.8. Dendritic Spine Analysis.** Brain tissues were fixed in 4% PFA for 4 hrs. Sections of 250  $\mu$ m were made using a vibratome (VT1200S, Leica, Germany) and were mounted on glass slides. Lucifer yellow fluorescent dye (4% in lithium chloride, L453, Thermo Fisher Scientific) was loaded into a pipette and injected into the neurons in the hippocampal area. Briefly, the dye was injected into a neuron with a  $\sim$ 2 nA current for 20 min until the whole dendritic branches were visualized under a fluorescent microscope. The 3D  $z$ -stack dendritic spine images were obtained using a confocal microscope (LSM 880, Carl Zeiss, Germany). The number of dendritic spines was analyzed using Imaris software (Oxford instruments). Six mice per group were included in the experiment. Three separate serial sections per mouse were processed for dendritic spine analysis.

**2.9. Statistical Analysis.** Results were collected from three independent experiments. The data were presented as mean  $\pm$  SD and were analyzed using SPSS 25.0 (IBM Corporation, Armonk, NY, USA) and GraphPad Prism 7.0 (GraphPad Software, Inc., CA, USA). The differences were assessed by one-way analysis of variance.  $p < 0.05$  was defined as statistically significant.

### 3. Results

**3.1. TLB Ameliorated Cognitive Deficits in 3 $\times$ FAD Mice.** The MWM test was conducted to determine whether the cognitive impairments of 3 $\times$ FAD AD mice were rescued by TLB. The MWM test showed that the escape latency was progressively decreased from day 1 to day 5 (Figure 1(d)). However, the 3 $\times$ FAD mice showed an elevated escape latency compared to WT mice on day 5. In contrast, 3 $\times$ FAD AD mice treated with a low level of TLB (10 mg/kg) showed a decreased escape latency compared to 3 $\times$ FAD mice (Figure 1(e)). Moreover, the 3 $\times$ FAD mice treated with a high dose of TLB (20 mg/kg) showed a significantly lower escape latency compared to 3 $\times$ FAD mice treated with a low dose of TLB (Figure 1(e)). It is noteworthy that the escape latency in 3 $\times$ FAD mice treated with a high dose of TLB has no differences compared to that in WT mice. Furthermore, we compared the time spent in the target quadrant from each mouse group. The 3 $\times$ FAD mice showed a shorter time in the target quadrant than WT mice. And the 3 $\times$ FAD mice treated with low-dose TLB showed a longer swimming time in the target quadrant compared to 3 $\times$ FAD mice. The 3 $\times$ FAD mice treated with high-dose

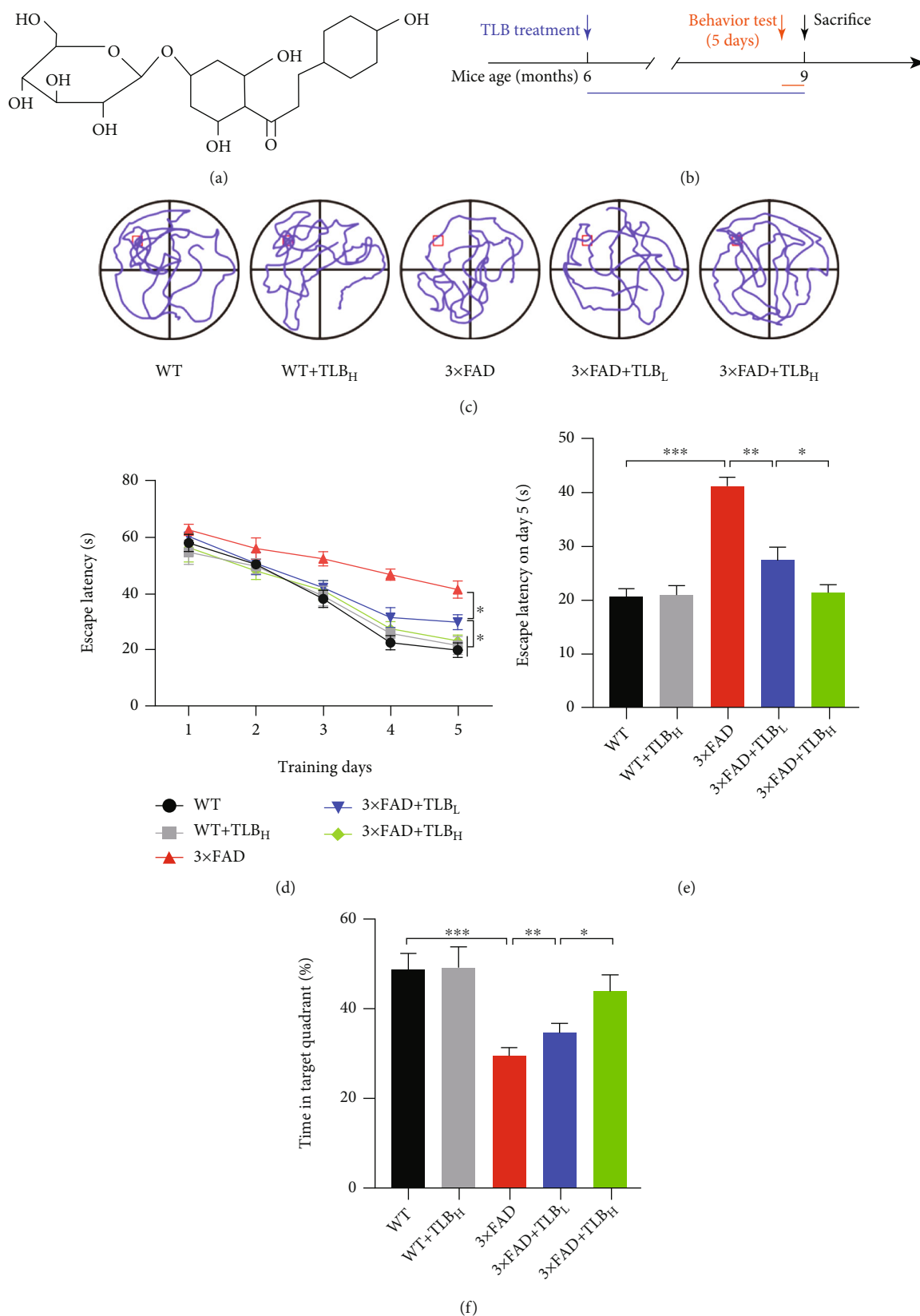
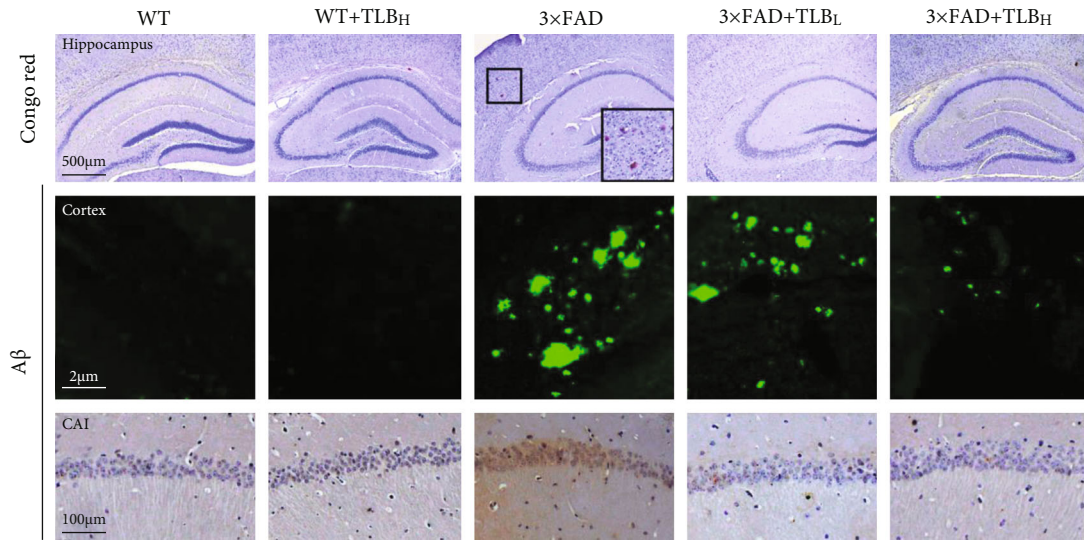
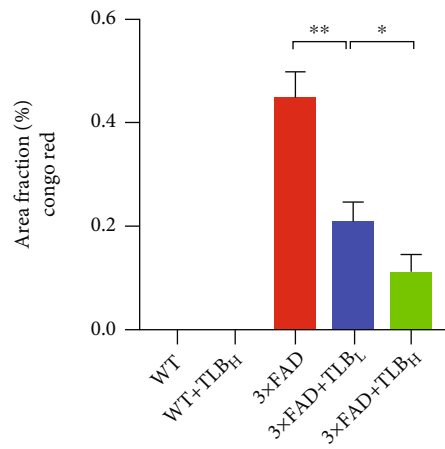


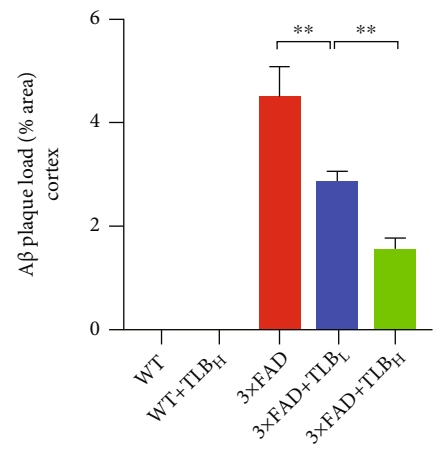
FIGURE 1: TLB ameliorated cognitive deficits in 3×FAD mice. (a) Chemical structure of TLB ( $C_{21}H_{24}O_{10}$ , molecular weight = 436.4). (b) Experimental design. (c) Representative paths in the MWM test. (d) The escape latency of each mouse group tested from day 1 to day 5. (e) The escape latency on day 5. (f) Time spent in the target quadrant in the MWM test.  $n = 6$  per group. \* $p < 0.05$ ; \*\* $p < 0.01$ ; \*\*\* $p < 0.001$ .



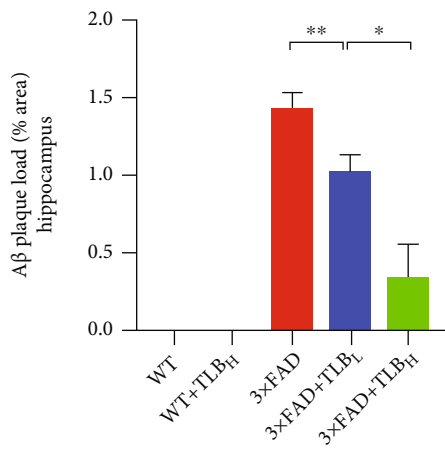
(a)



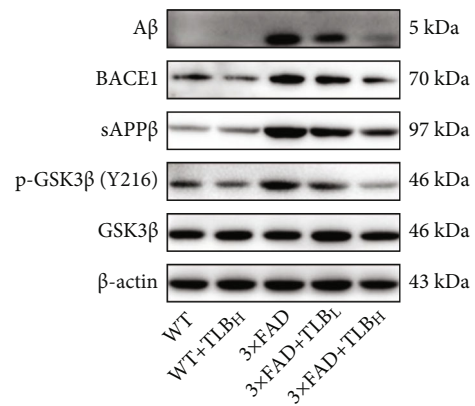
(b)



(c)



(d)



(e)

FIGURE 2: Continued.

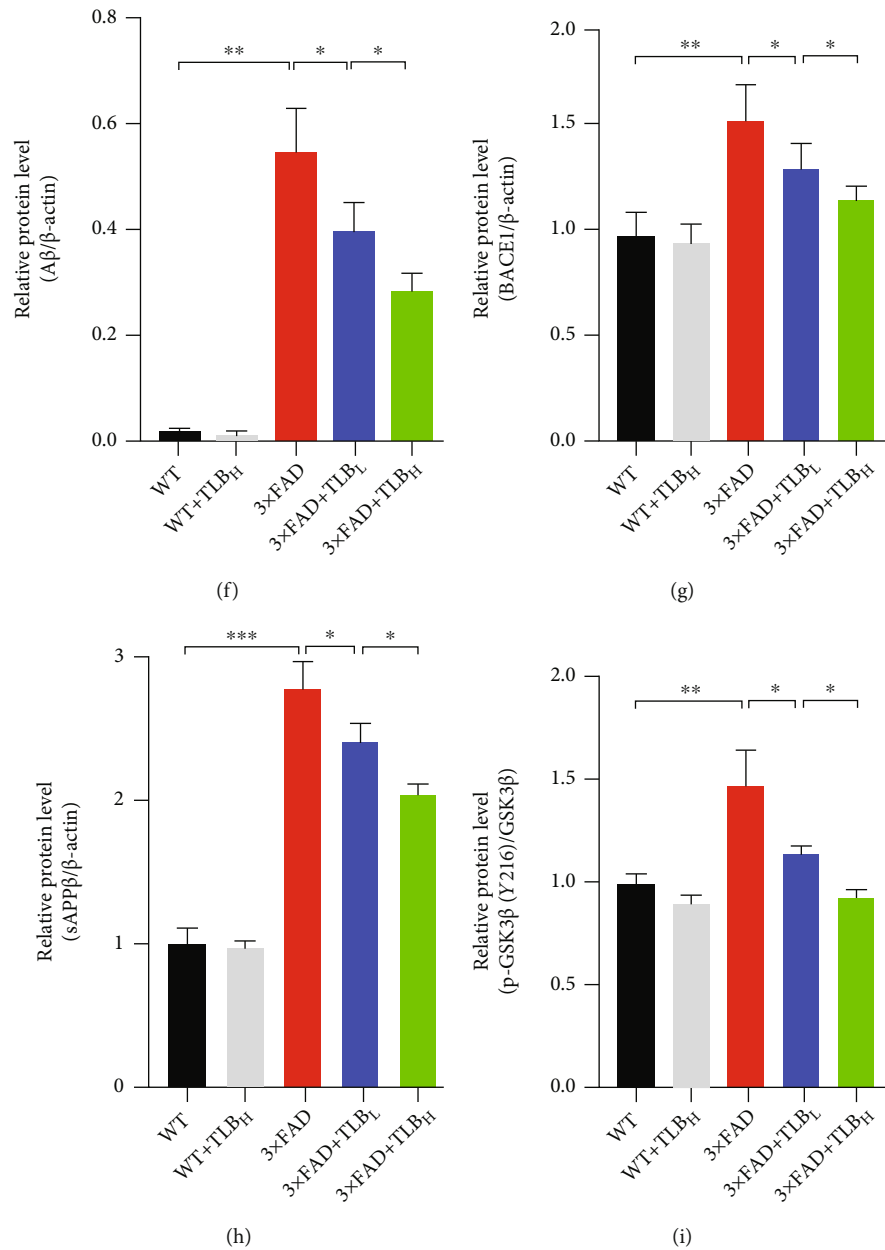


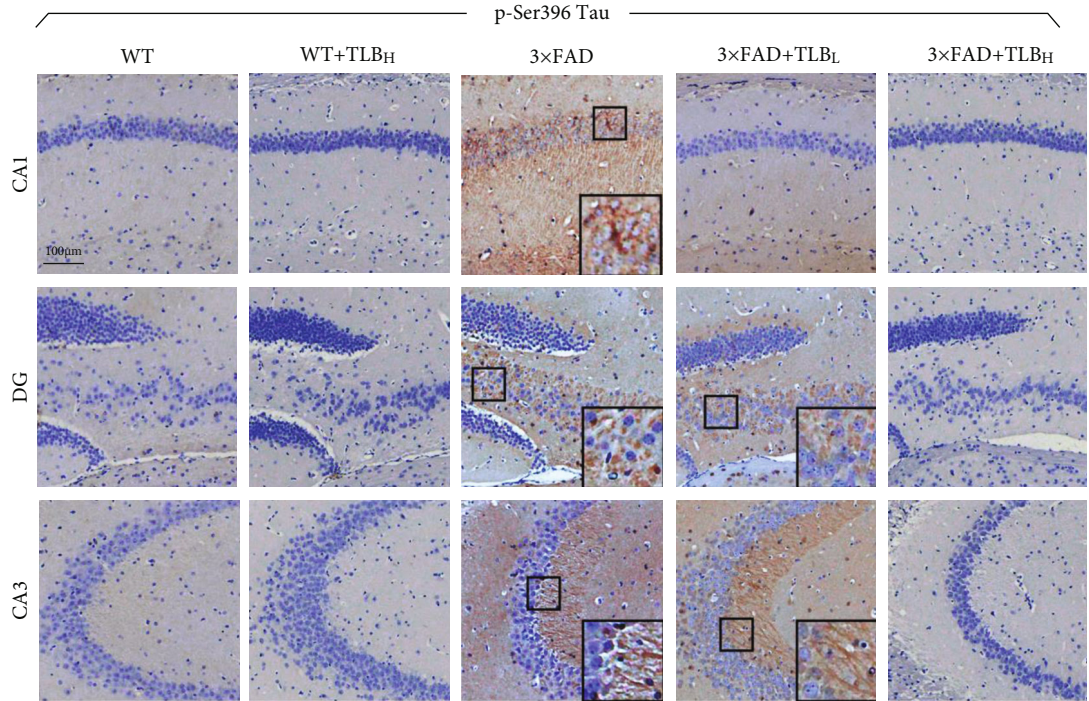
FIGURE 2: TLB alleviated A $\beta$  deposition in 3 $\times$ FAD mice. (a) Congo red staining and A $\beta$  IHC staining in the hippocampal area and cortex. (b) Comparison of Congo red staining analysis in the hippocampal area. (c) Comparison of A $\beta$ -positive plaque in the cortex. (d) A $\beta$  plaque load in the hippocampal CA1 area. (e–i) Western blot and quantitative analysis of A $\beta$ , BACE1, sAPP $\beta$ , p-GSK3 $\beta$ , and GSK3 $\beta$  in hippocampal tissues.  $n = 6$  per group. \* $p < 0.05$ ; \*\* $p < 0.01$ ; \*\*\* $p < 0.001$ .

TLB showed a longer swimming time in the target quadrant compared to low-dose TLB-treated mice (Figure 1(f)).

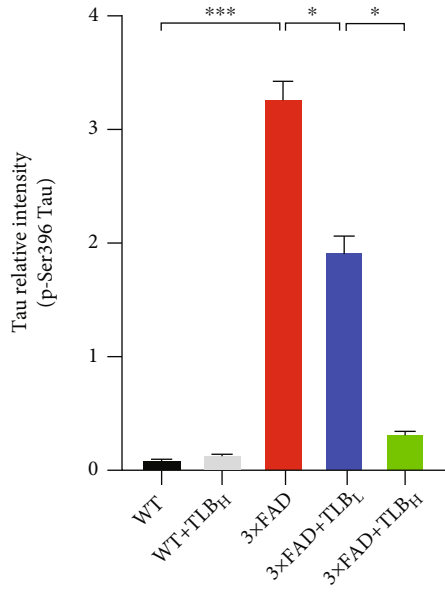
**3.2. TLB Alleviated A $\beta$  Deposition in 3 $\times$ FAD Mice.** To investigate the effect of TLB on A $\beta$  deposition, the Congo red staining and A $\beta$  IHC staining were performed. Both revealed that the A $\beta$  plaque load is significantly increased in 3 $\times$ FAD AD mice. Compared to the 3 $\times$ FAD mice, the mice treated with a low dose of TLB showed a significant decrease of the A $\beta$  plaque load in the cortex and hippocampus. Furthermore, a high dose of TLB showed a remarkable A $\beta$  load alleviation effect than a low dose of TLB in 3 $\times$ FAD

mice (Figures 2(a)–2(d)). Next, we examined the effect of TLB on amyloidogenic processing in 3 $\times$ FAD mice. We found that the BACE1 and sAPP $\beta$  protein levels were increased in 3 $\times$ FAD mice compared to WT mice. And both a low dose and a high dose of TLB decreased the BACE1 and sAPP $\beta$  levels in 3 $\times$ FAD mice. Furthermore, TLB reversed the phosphorylation of GSK3 $\beta$  levels in 3 $\times$ FAD mice (Figures 2(e)–2(i)).

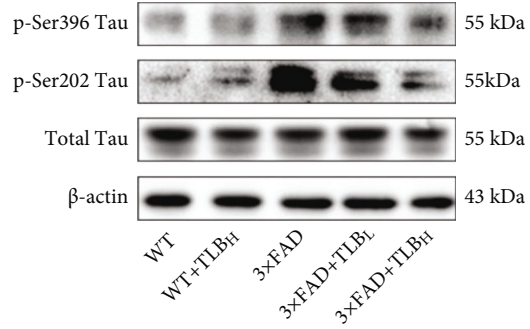
**3.3. TLB Inhibited Tau Phosphorylation in the AD Mouse Model.** The Tau pathology was assessed in the 3 $\times$ FAD AD mouse model. Tau IHC staining showed that p-Ser396 Tau



(a)



(b)



(c)

FIGURE 3: Continued.

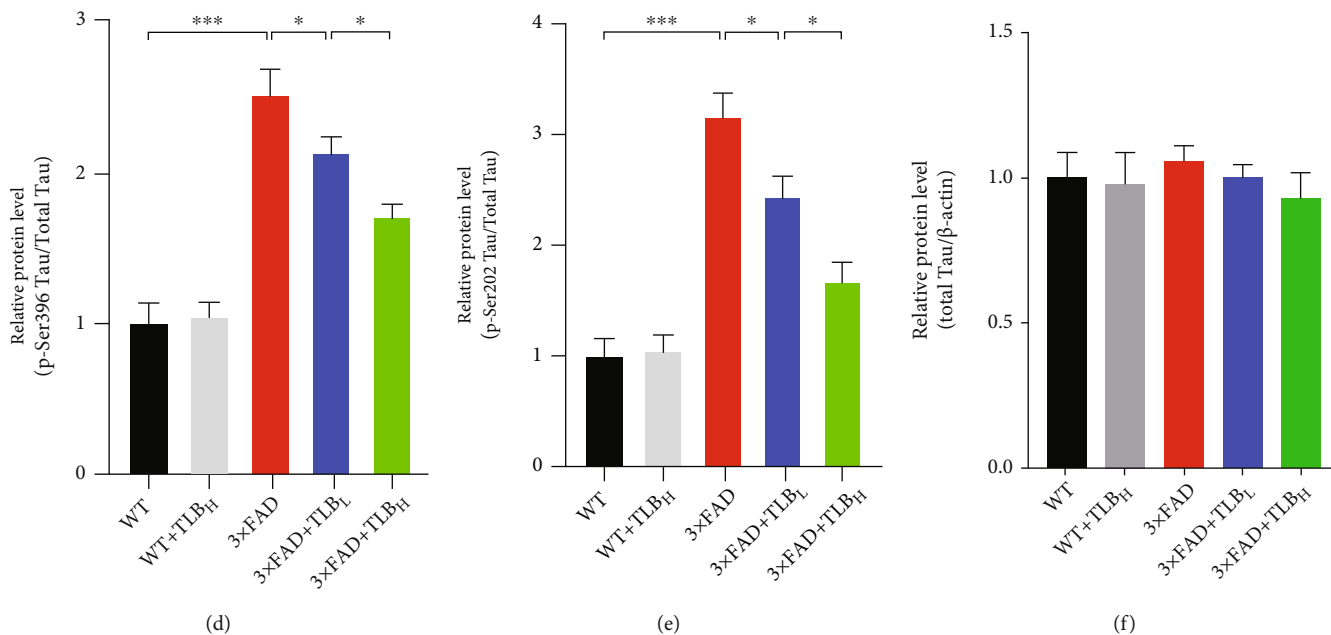


FIGURE 3: TLB inhibited Tau phosphorylation in the AD mouse model. (a) Representative images of p-Ser396 Tau IHC staining. (b) Relative intensity of p-Ser396 Tau in hippocampal subregions. (c–f) Western blot and quantification for phosphorylated Tau at Ser396 and Ser202 sites and total Tau in the hippocampus.  $n = 6$  per group. \* $p < 0.05$ ; \*\* $p < 0.01$ ; \*\*\* $p < 0.001$ .

pathology was remarkable in 3x FAD mice. The intensity of p-Ser396 Tau was significantly lower in hippocampal subregions of low-dose TLB-treated AD model mice than in those of WT mice. And a high dose of TLB showed a much stronger Tau pathology alleviation effect than a low dose of TLB (Figures 3(a) and 3(b)). Western blots further revealed that Tau phosphorylation at Ser396 and Ser202 sites was remarkably decreased in 3x FAD+TLBL and 3x FAD+TLBH mice compared to 3x FAD mice (Figures 3(c)–3(f)).

**3.4. TLB Reduced Neuronal Loss and Synaptic Degeneration in 3x FAD Mice.** In order to assess whether oral administration of TLB affects the neuronal number in 3x FAD mice, we performed neuronal marker NeuN IHC staining and Nissl staining in the cortex and hippocampus. We found a remarkable reduction of the NeuN-positive cell number in the cortex and hippocampus of 3x FAD mice compared to WT mice. Consistently, Nissl staining showed that the Nissl-positive cell number was suppressed in 3x FAD mice compared to WT mice. In contrast, treatment with low and high doses of TLB clearly increased the NeuN- and Nissl-positive cell number in the AD mouse model. Note that the neuronal number in the 3x FAD+TLBH group was higher than that in the 3x FAD+TLBL group (Figure 4).

To further test the effect of TLB on synaptic density, we conducted spine morphology analysis. The total spine number and mushroom spine number were suppressed in 3x FAD AD model mice compared to WT mice. However, low and high doses of TLB oral treatment reduced the total and mushroom spine density loss in hippocampal areas of AD model mice (Figures 5(a)–5(c)). Western blot further revealed that the synapse-associated protein including PSD95, SNAP25, Syn1, SYP, and VAMP1 expression was

suppressed in 3x FAD AD model mice. In contrast, low and high doses of TLB treatment reversed the synapse-associated protein loss in 3x FAD AD model mice (Figures 5(d)–5(i)).

**3.5. TLB Alleviated Glial Activation in AD Model Mice.** In order to test the effect of TLB on glial activation, hippocampal sections were immunostained with antibodies including astrocyte marker GFAP and microglial marker Iba1. A significant increase of the GFAP- and Iba1-positive cell number was detected in the 3x FAD mouse brains compared with WT mice. And a remarkable reduction of the GFAP- and Iba1-positive cell number was detected in the hippocampal CA1 area of the 3x FAD mice compared with the vehicle-treated mice. Furthermore, a significant difference of the GFAP- and Iba1-positive cell number was noticed between the low- and high-dose TLB-treated 3x FAD AD mice (Figure 6).

**3.6. TLB Ameliorated Neuroinflammation through Reducing TLR4 in AD Model Mice.** To further study the potential mechanism underlying the effect of TLB on AD pathology-related neuroinflammation, we tested the TLR4 signaling pathway proteins. We found that TLR4, MYD88, TRAF6, p-NFκB/NFκB, TNF-α, IL-1β, and IL-6 were elevated in 3x FAD mice compared to WT mice. And TLB treatment induced a reduction of TLR4, MYD88, TRAF6, p-NFκB/NFκB, TNF-α, IL-1β, and IL-6 levels compared to the vehicle-treated 3x FAD mice. Furthermore, a significant difference was observed between the low and high-dose TLB-treated mice.

## 4. Discussion

In the present study, we identified that TLB might alleviate Aβ deposition, Tau pathology, synaptic degeneration, glial

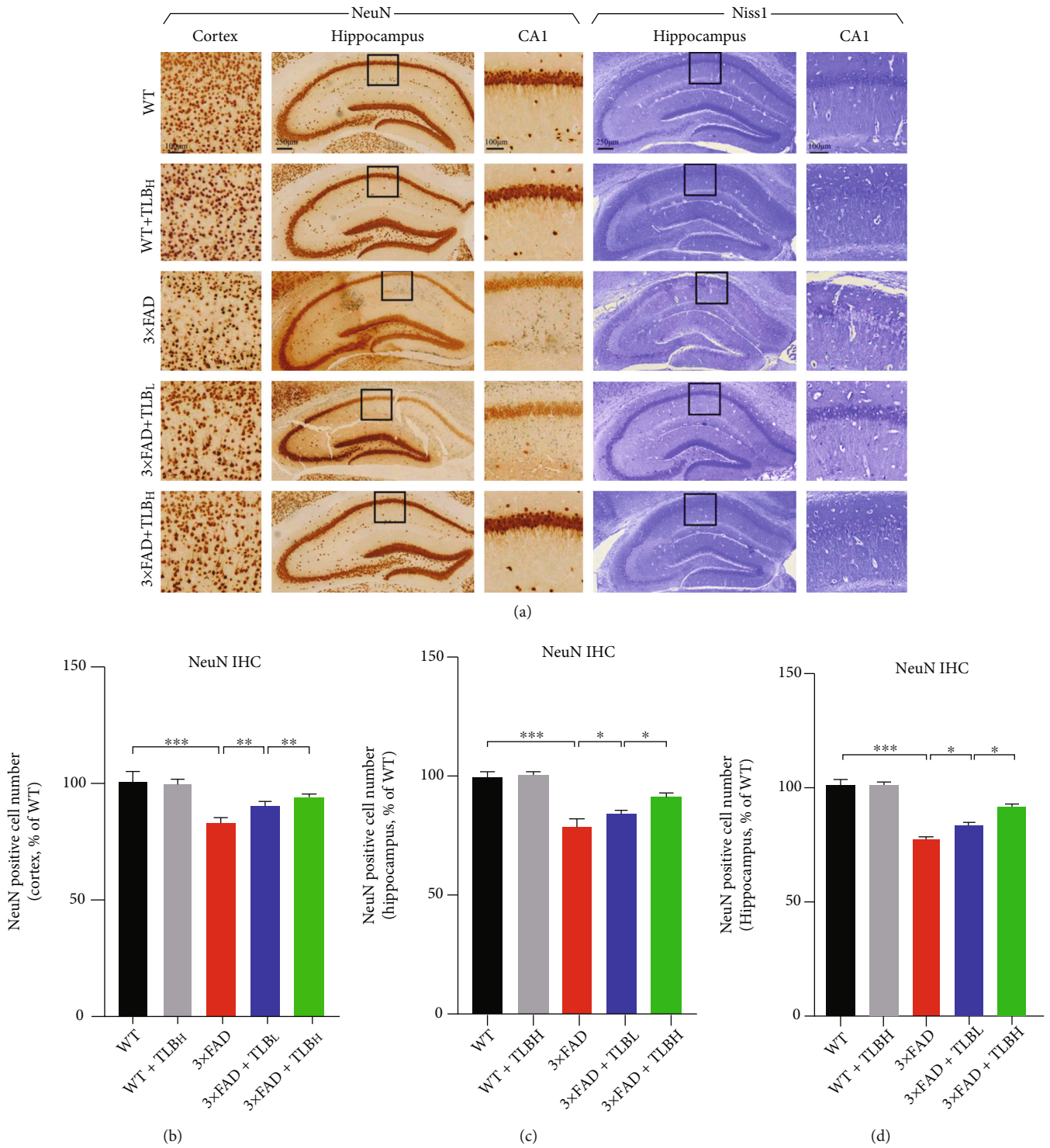


FIGURE 4: TLB reduced neuronal loss in 3x FAD mice. (a) Representative figures of NeuN staining in the cortex and hippocampus and Nissl staining in hippocampal regions. (b, c) Quantification of neuronal content in the cortex and hippocampus from NeuN IHC staining results. (d) Quantitative analysis of the surviving neuron number in the hippocampus from Nissl staining results.  $n = 6$  per group. \*  $p < 0.05$ ; \*\*  $p < 0.01$ ; \*\*\*  $p < 0.001$ .

activation, and memory impairment in the AD mouse model. And the TLR4-MYD88-NK $\kappa$ B pathway might be involved in the anti-neuroinflammatory effect in the process. We show for the first time that TLB reverses AD pathology

and memory impairment in 3x FAD mice, indicating a promising drug candidate for halting AD progression.

In a recent study, Chen et al. [26] showed that TLB protects HT22 cell death induced by A $\beta_{25-35}$  through the

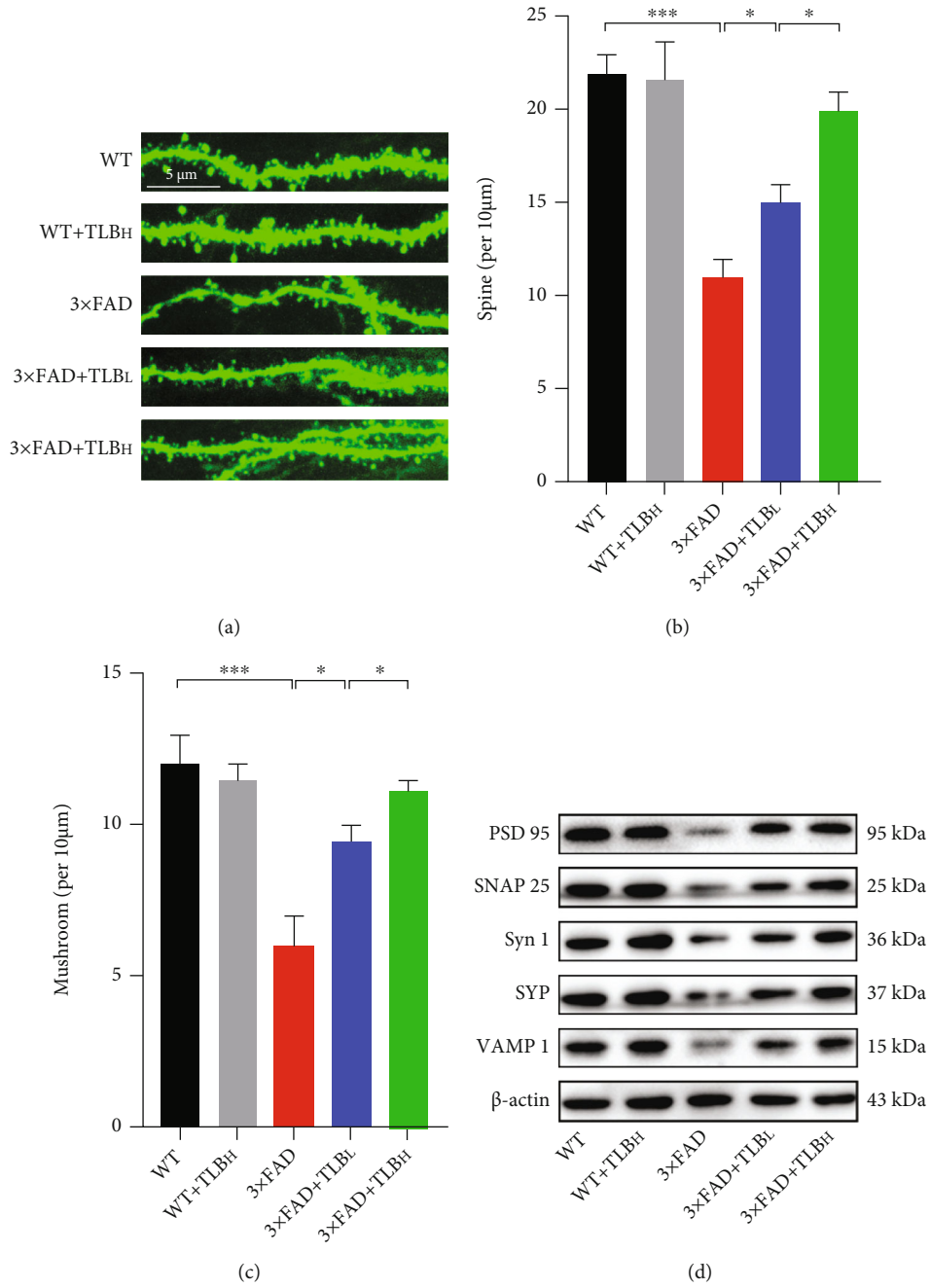


FIGURE 5: Continued.



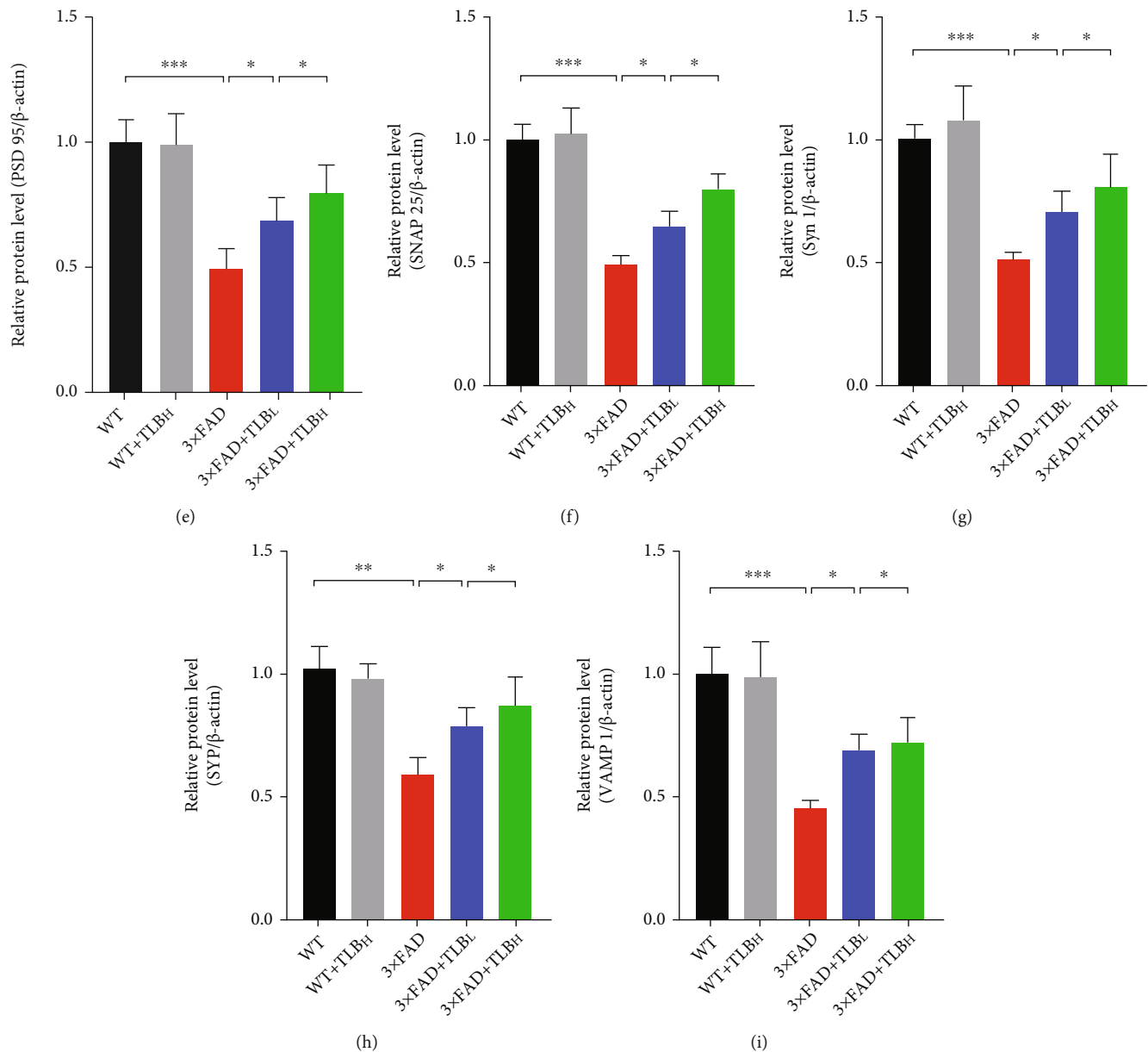


FIGURE 5: TLB alleviated synaptic degeneration in AD model mice. (a) Representative images of spine morphology in each group. (b, c) Quantitative analysis of total spine density and mushroom-type spine density. (d) The representative blots of PSD95, SNAP25, Syn1, SYP, and VAMP1 in each group. (e–i) Quantitative analysis of PSD95, SNAP25, Syn1, SYP, and VAMP1 protein levels.  $n = 6$  per group. \* $p < 0.05$ ; \*\* $p < 0.01$ ; \*\*\* $p < 0.001$ .

ROS/p38/caspase 3 pathway. However, the study has not shown the effect of TLB in the AD *in vivo* model. In the present study, we showed that TLB has reversed the memory impairment phenotype in the 3x FAD AD mouse model using the MWM test. Notably, the high dose of TLB improved the memory function of 3x FAD mice to the level of WT mice (Figures 1(c)–1(f)).

Since AD is a neurodegenerative disease characterized by  $A\beta$  deposition and p-Tau aggregation, we therefore tested the effect of TLB on  $A\beta$  and p-Tau pathology. Specifically, we applied Congo red and  $A\beta$  IHC staining in hippocampal and cortical regions. We found that TLB dramatically reduced the  $A\beta$  burden (Figures 2(a)–2(d)). More impor-

tantly, we observed that TLB inhibited the expression of BACE1 and sAPP $\beta$ , suggesting that TLB can break the loop of the BACE1-mediated amyloidogenesis. And TLB also suppressed the hyperphosphorylation of GSK3 $\beta$ , which acts as a Tau kinase (Figures 2(e)–2(i)). As we know, GSK3 $\beta$  modulates BACE1 expression, and  $A\beta$  can drive the BACE1 level to increase. Thus, it is likely that the reduced amyloid deposition by TLB might be through breaking the vicious cycle of the  $A\beta$  burden,  $A\beta$ -induced GSK3 $\beta$  activation, and GSK3 $\beta$ -induced BACE1 expression. Moreover, TLB inhibited the Tau hyperphosphorylation at Ser396 and Ser202 sites, as evidenced by western blot and IHC staining (Figures 3). TLB may also suppress the activation of GSK3 $\beta$ ,

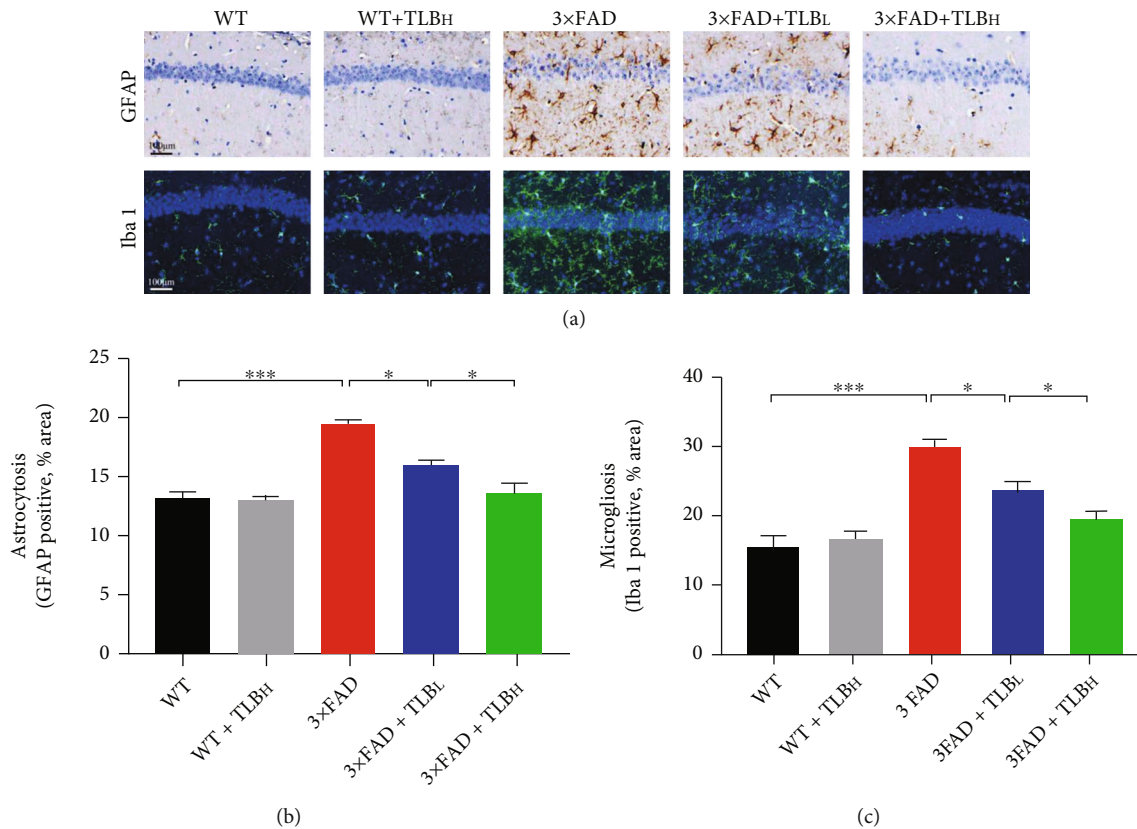


FIGURE 6: TLB alleviated glial activation in AD model mice. (a) Representative images of GFAP and Iba1 staining in the hippocampal area. (b) Quantification of GFAP staining in each group. (c) Quantification of Iba1 staining in each group.  $n = 6$  per group. \* $p < 0.05$ ; \*\* $p < 0.01$ ; \*\*\* $p < 0.001$ .

which is characterized by GSK3 $\beta$  hyperphosphorylation. This finding suggests that TLB ameliorates Tau hyperphosphorylation by inhibiting GSK3 $\beta$  activation.

The neuronal loss in the hippocampal region accounts for memory deficits in AD [27]. We examined the effect of TLB on neuronal density in the hippocampus and cortex. We found that a low dose and high dose of TLB treatment rescued the neuronal loss in 3×FAD AD mice, as examined by NeuN IHC and Nissl staining methods (Figure 4). This neuroprotective effect of TLB is consistent with the finding in an earlier study of oxygen deprivation and reoxygenation on primary cortical neurons [23].

Given that synaptic degeneration is also involved in the process of AD-related memory impairment [28], we then tested the effect of TLB on synaptic pathological plasticity. Spine density analysis unexpectedly revealed synaptic pathology in the 3×FAD AD mouse hippocampal area (Figures 5(a)–5(c)). Our finding of rescued total spine density and mushroom spine density in TLB-treated 3×FAD mice showed a synaptic protective effect of TLB. Additionally, western blot analysis revealed that the loss of synaptic proteins in 3×FAD mice was attenuated by orally treated TLB (Figures 5(d)–5(i)). It is likely that the memory improvement by TLB was due to the spine density increase and synaptic protein upregulation. In line with this, preserving dendritic spine density leads to cognitive improvement

and memory loss attenuation in the 5×FAD AD mouse model [29].

Extracellular A $\beta$  deposition and intracellular p-Tau aggregation might trigger reactive gliosis which leads to inflammatory factors [30]. And reactive gliosis has been proved to drive the pathogenic cascades of AD [31]. Previous studies of anti-inflammatory strategies showed improvements in neurodegenerative disease models [32]. Thus, we applied GFAP and Iba1 immunostaining analysis to observe the number of astrocytes and microglia. Increased astrocytosis and microgliosis were observed in 3×FAD mouse brains, whereas reduced gliosis was observed in the TLB-treated AD model brain samples, suggesting a strong anti-inflammatory effect of TLB (Figure 6). The data from Gao et al. [23] are consistent with ours in that TLB exerts an inactivation effect on glial cells. Studies have shown that, in AD, glial cells' phagocytosis function is impaired, which leads to the toxic A $\beta$  burden [33]. Thus, we reckoned that the glial phagocytosis function is enhanced after TLB treatment, and the A $\beta$  burden is reduced finally.

Although we found that TLB can inhibit reactive gliosis in AD mouse brains, the molecular mechanisms responsible for this inhibition remained unknown. Earlier studies revealed that the anti-inflammatory effect of TLB correlates with inhibiting NF $\kappa$ B phosphorylation *in vivo* and *in vitro* [34]. Based on this notion, we detected the TLR4-MYD88-

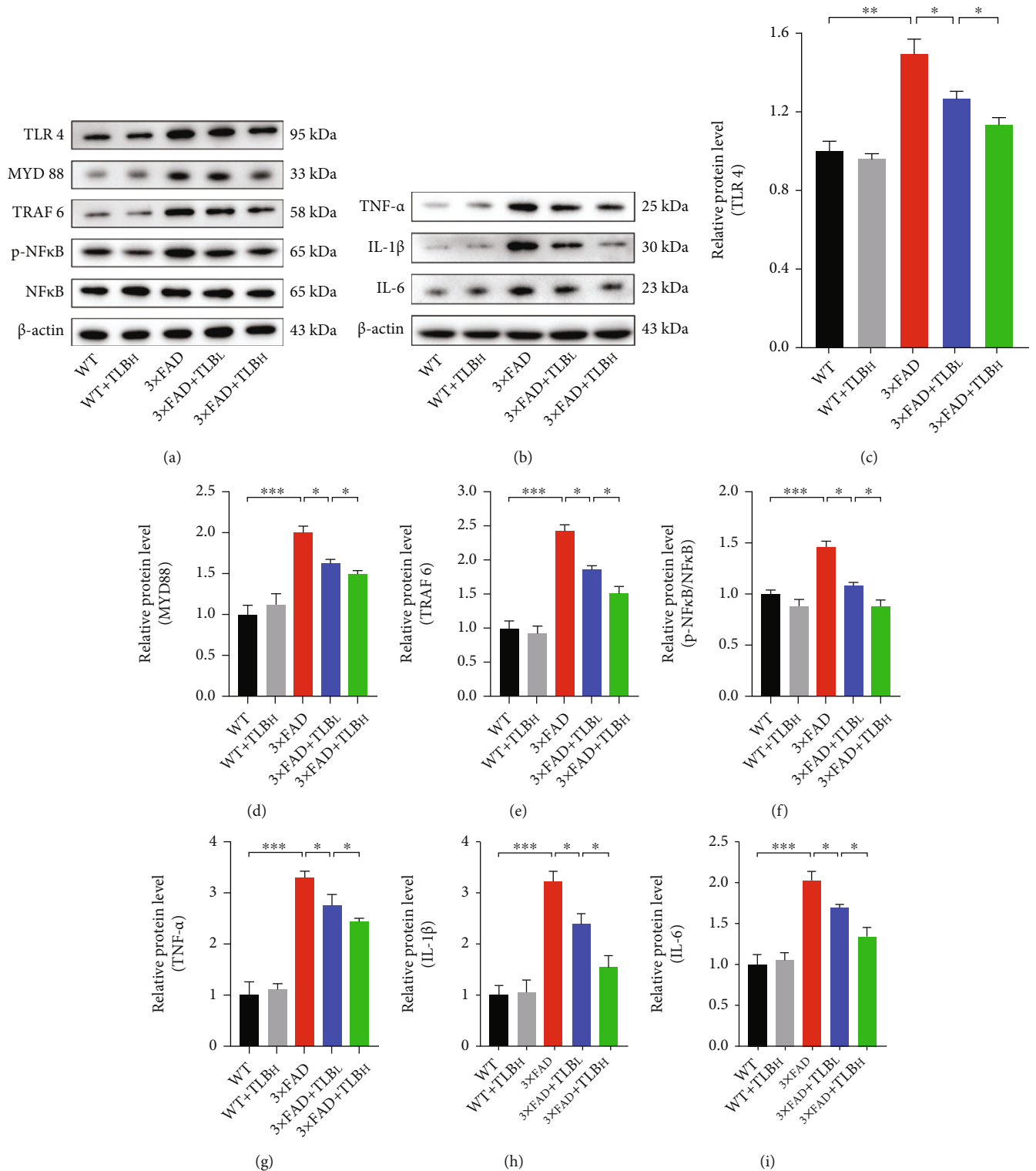


FIGURE 7: TLB ameliorated neuroinflammation through reducing TLR4 in AD model mice. (a) Representative western blots of TLR4, MYD88, TRAF6, p-NFκB, and NFκB. (b) Representative western blots of TNF-α, IL-1β, and IL-6. (c-f) Quantification of TLR4, MYD88, TRAF6, and p-NFκB/NFκB levels in each group. (g-i) Quantification of TNF-α, IL-1β, and IL-6 levels in each group.  $n = 6$  per group. \* $p < 0.05$ ; \*\* $p < 0.01$ ; \*\*\* $p < 0.001$ .

NFκB pathway proteins. As expected, we found that, in 3x FAD mouse brains, TLR4-MYD88 pathway proteins were overexpressed, accompanied by NFκB hyperphosphoryla-

tion. TLB reversed the changes in this AD mouse model, suggesting that the anti-inflammatory effect might be TLR4-MYD88-NFκB pathway-dependent (Figure 7).

Moreover, we demonstrated that TLB reduces the inflammatory factors which are regulated by NF $\kappa$ B phosphorylation. In line with this, studies have found that the loss of function or inhibition of TLR4 suppresses AD progression in the mouse model [35, 36]. Moreover, previous studies showed that inhibiting the TLR4 pathway alleviated motor impairment and dopaminergic neuron death in the Parkinson's disease mouse model [37]. And Kwilas et al. showed that TLR4 antagonists prevented the production of proinflammatory factors and motor dysfunction in the experimental autoimmune encephalomyelitis mouse model [38]. All these studies have shown that TLR4 might be a promising target in neuroinflammation treatment. Given the fact that inflammatory factors contribute to neuronal loss, synaptic loss, and behavior impairments in AD progression, we think that the TLR4-MYD88-NF $\kappa$ B-dependent anti-inflammatory effect of TLB might be accountable for its neuroprotective effect.

Due to the complicated pathophysiological changes in AD progression, drugs targeting A $\beta$  failed in halting AD-related memory deficits and pathological changes. We think that targeting multiple pathways for AD intervention, such as anti-inflammation, A $\beta$  reduction, and Tau hyperphosphorylation inhibition, might be an effective treatment plan. According to the experiments above, we have a reason to consider that TLB seems to have multiple targets on halting AD progression.

## 5. Conclusion

In summary, we uncovered TLB for AD therapy by exploring multiple pathway mechanisms including A $\beta$  burden reduction, Tau hyperphosphorylation inhibition, and anti-inflammation. TLB was effective in reducing neuronal loss, alleviating synaptic degeneration, and ameliorating memory deficits in the AD mouse model. More studies and further clinical trials to test its efficacy would be necessary.

## Data Availability

All processed data and models used during the study are available from the corresponding authors by request. But the raw data required to reproduce these findings cannot be shared at this time as the data also forms part of an ongoing study.

## Conflicts of Interest

The authors declare there are no conflicts of interest.

## Authors' Contributions

Jiang Huang and Jiuyang Ding conceived and designed the experiments. Jiuyang Ding, Dan Yin, and Jian Huang performed the behavioral test experiments. Jiuyang Ding and Zheng Ren performed the IHC experiments. Jian Huang, Shanshan Hu, and Cuiyun Le conducted the western blot analysis. Yuanliang Ye, Na Zhao, and Hongmei Zhou performed the dendritic spine analysis. Jiuyang Ding and Ting Liu wrote the manuscript. Dan Yin and Zhu Li helped Jiuyang Ding analyze the data. Jiuyang Ding, Jian Huang, and Dan Yin are co-first authors.

## Acknowledgments

This work was supported by the Research Foundation for Advanced Talents of Guizhou Medical University (Grant No. University Contract of Doctors J [2021] 014), Natural Science Foundation of Guizhou Medical University Incubation Program (Grant No. 20NSP084) (to Jiuyang Ding), Guizhou Province Engineering Technology Research Centre Project (Qian High-Tech of Development and Reform Commission No. [2016] 1345), Guizhou Scientific Support Project (Qian Science Support [2019] 2825), Guizhou "Hundred" innovative talents project (Qian Science Talent Platform [2020] 6012), Guizhou Scientific Support Project (Qian Science Support [2020] 4Y057), and Guizhou Science Project (Qian Science Foundation [2020] 1Y353) (to Jiang Huang).

## References

- [1] S. Hoscheidt, A. H. Sanderlin, L. D. Baker et al., "Mediterranean and Western diet effects on Alzheimer's disease biomarkers, cerebral perfusion, and cognition in mid-life: a randomized trial," *Alzheimer's & Dementia*, vol. 17, 2021.
- [2] A. Alzheimer's, "2016 Alzheimer's disease facts and figures," *Alzheimers Dement*, vol. 12, no. 4, pp. 459–509, 2016.
- [3] A. Singleton and J. Hardy, "The evolution of genetics: Alzheimer's and Parkinson's diseases," *Neuron*, vol. 90, no. 6, pp. 1154–1163, 2016.
- [4] O. Zolochovska and G. Tagliatalata, "Selected microRNAs increase synaptic resilience to the damaging binding of the Alzheimer's disease amyloid beta oligomers," *Molecular neurobiology*, vol. 57, no. 5, pp. 2232–2243, 2020.
- [5] J. M. Long and D. M. Holtzman, "Alzheimer disease: an update on pathobiology and treatment strategies," *Cell*, vol. 179, no. 2, pp. 312–339, 2019.
- [6] J. M. Schott, P. S. Aisen, J. L. Cummings, R. J. Howard, and N. C. Fox, "Unsuccessful trials of therapies for Alzheimer's disease," *The Lancet*, vol. 393, no. 10166, p. 29, 2019.
- [7] R. Y. Pan, J. Ma, X. X. Kong et al., "Sodium rutin ameliorates Alzheimer's disease-like pathology by enhancing microglial amyloid- $\beta$  clearance," *Science advances*, vol. 5, no. 2, article eaa6328, 2019.
- [8] S. S. Jiao, X. Q. Yao, Y. H. Liu et al., "Edaravone alleviates Alzheimer's disease-type pathologies and cognitive deficits," *Proceedings of the National Academy of Sciences*, vol. 112, no. 16, pp. 5225–5230, 2015.
- [9] W. Yang, K. Zhou, Y. Zhou et al., "Naringin dihydrochalcone ameliorates cognitive deficits and neuropathology in APP/PS1 transgenic mice," *Frontiers in aging neuroscience*, vol. 10, p. 169, 2018.
- [10] J. H. Lee, N. H. Ahn, S. B. Choi, Y. Kwon, and S. H. Yang, "Natural products targeting amyloid beta in Alzheimer's disease," *International Journal of Molecular Sciences*, vol. 22, no. 5, p. 2341, 2021.
- [11] K. Rajasekhar, S. Samanta, V. Bagoband, N. A. Murugan, and T. Govindaraju, "Antioxidant berberine-derivative inhibits multifaceted amyloid toxicity," *iScience*, vol. 23, no. 4, p. 101005, 2020.
- [12] S. Samanta, K. Rajasekhar, M. Ramesh et al., "Naphthalene Monoimide Derivative Ameliorates Amyloid Burden and Cognitive Decline in a Transgenic Mouse Model of

- Alzheimer's Disease," *Advanced Therapeutics*, vol. 4, no. 4, article 2000225, 2021.
- [13] A. Wiecekowska-Gacek, A. Mietelska-Porowska, M. Wydrych, and U. Wojda, "Western diet as a trigger of Alzheimer's disease: from metabolic syndrome and systemic inflammation to neuroinflammation and neurodegeneration," *Ageing research reviews*, vol. 70, article 101397, 2021.
- [14] J. Lutshumba, B. S. Nikolajczyk, and A. D. Bachstetter, "Dysregulation of systemic immunity in aging and dementia," *Frontiers in Cellular Neuroscience*, vol. 15, p. 652111, 2021.
- [15] N. A. Lind, V. E. Rael, K. Pestal, B. Liu, and G. M. Barton, "Regulation of the nucleic acid-sensing Toll-like receptors," *Nature Reviews Immunology*, vol. 21, 2021.
- [16] T. R. Kollmann, O. Levy, R. R. Montgomery, and S. Goriely, "Innate immune function by Toll-like receptors: distinct responses in newborns and the elderly," *Immunity*, vol. 37, no. 5, pp. 771–783, 2012.
- [17] H. A. Saleh, M. H. Yousef, and A. Abdelnaser, "The anti-inflammatory properties of phytochemicals and their effects on epigenetic mechanisms involved in TLR4/NF-kappaB-mediated inflammation," *Frontiers in immunology*, vol. 12, article 606069, 2021.
- [18] S. M. Kerfoot, E. M. Long, M. J. Hickey et al., "TLR4 contributes to disease-inducing mechanisms resulting in central nervous system autoimmune disease," *The Journal of Immunology*, vol. 173, no. 11, pp. 7070–7077, 2004.
- [19] M. E. Gambuzza, V. Sofo, F. M. Salmeri, L. Soraci, S. Marino, and P. Bramanti, "Toll-like receptors in Alzheimer's disease: a therapeutic perspective," *CNS & Neurological Disorders - Drug Targets*, vol. 13, no. 9, pp. 1542–1558, 2014.
- [20] S. E. Doyle, R. M. O'Connell, G. A. Miranda et al., "Toll-like receptors induce a phagocytic gene program through p38," *Journal of Experimental Medicine*, vol. 199, no. 1, pp. 81–90, 2004.
- [21] M. Rahimifard, F. Maqbool, S. Moeini-Nodeh et al., "Targeting the TLR4 signaling pathway by polyphenols: a novel therapeutic strategy for neuroinflammation," *Ageing Research Reviews*, vol. 36, pp. 11–19, 2017.
- [22] R. Chen, Z. Wang, Z. Zhi, J. Tian, Y. Zhao, and J. Sun, "Targeting the TLR4/NF- $\kappa$ B pathway in  $\beta$ -amyloid-stimulated microglial cells: A possible mechanism that oxysphoridine exerts anti-oxidative and anti-inflammatory effects in an in vitro model of Alzheimer's disease," *Brain Research Bulletin*, vol. 175, pp. 150–157, 2021.
- [23] J. Gao, N. Chen, N. Li et al., "Neuroprotective effects of trilobatin, a novel naturally occurring Sirt3 agonist from *Lithocarpus polystachyus* Rehd., mitigate cerebral ischemia/reperfusion injury: involvement of TLR4/NF-kappaB and Nrf2/Keap-1 signaling," *Antioxidants & redox signaling*, vol. 33, no. 2, pp. 117–143, 2020.
- [24] N. Li, X. Li, Y. L. Shi et al., "Trilobatin, a component from *Lithocarpus polystachyus* Rehd., increases longevity in *C. elegans* through activating SKN1/SIRT3/DAF16 signaling pathway," *Frontiers in Pharmacology*, vol. 12, article 655045, 2021.
- [25] C. V. Vorhees and M. T. Williams, "Morris water maze: procedures for assessing spatial and related forms of learning and memory," *Nature Protocols*, vol. 1, no. 2, pp. 848–858, 2006.
- [26] N. Chen, J. Wang, Y. He et al., "Trilobatin protects against A $\beta$ <sub>25–35</sub>-induced hippocampal HT22 cells apoptosis through mediating ROS/p38/caspase 3-dependent pathway," *Frontiers in pharmacology*, vol. 11, p. 584, 2020.
- [27] N. Mirzaei, B. C. Mota, A. M. Birch et al., "Imidazoline ligand BU224 reverses cognitive deficits, reduces microgliosis and enhances synaptic connectivity in a mouse model of Alzheimer's disease," *British Journal of Pharmacology*, vol. 178, no. 3, pp. 654–671, 2021.
- [28] B. Dejanovic, M. A. Huntley, A. de Mazière et al., "Changes in the synaptic proteome in tauopathy and rescue of Tau-induced synapse loss by C1q antibodies," *Neuron*, vol. 100, no. 6, pp. 1322–1336.e7, 2018, e1327.
- [29] P. Maiti, Z. Bowers, A. Bourcier-Schultz, J. Morse, and G. L. Dunbar, "Preservation of dendritic spine morphology and postsynaptic signaling markers after treatment with solid lipid curcumin particles in the 5xFAD mouse model of Alzheimer's amyloidosis," *Alzheimer's research & therapy*, vol. 13, no. 1, p. 37, 2021.
- [30] T. Wisniewski and F. Goni, "Immunotherapeutic approaches for Alzheimer's disease," *Neuron*, vol. 85, no. 6, pp. 1162–1176, 2015.
- [31] C. K. Glass, K. Saijo, B. Winner, M. C. Marchetto, and F. H. Gage, "Mechanisms underlying inflammation in neurodegeneration," *Cell*, vol. 140, no. 6, pp. 918–934, 2010.
- [32] C. Scassellati, A. C. Galoforo, C. Esposito, M. Ciani, G. Ricevuti, and C. Bonvicini, "Promising intervention approaches to potentially resolve neuroinflammation and steroid hormones alterations in Alzheimer's disease and its neuropsychiatric symptoms," *Ageing and Disease*, vol. 12, no. 5, pp. 1337–1357, 2021.
- [33] M. E. Tremblay, M. R. Cookson, and L. Civiero, "Glial phagocytic clearance in Parkinson's disease," *Molecular neurodegeneration*, vol. 14, no. 1, p. 16, 2019.
- [34] X. Fan, Y. Zhang, H. Dong, B. Wang, H. Ji, and X. Liu, "Trilobatin attenuates the LPS-mediated inflammatory response by suppressing the NF-kappaB signaling pathway," *Food Chemistry*, vol. 166, pp. 609–615, 2015.
- [35] B. Cameron, W. Tse, R. Lamb, X. Li, B. T. Lamb, and G. E. Landreth, "Loss of interleukin receptor-associated kinase 4 signaling suppresses amyloid pathology and alters microglial phenotype in a mouse model of Alzheimer's disease," *Journal of Neuroscience*, vol. 32, no. 43, pp. 15112–15123, 2012.
- [36] J. Yang, L. Wise, and K. I. Fukuchi, "TLR4 cross-talk with NLRP3 inflammasome and complement signaling pathways in Alzheimer's disease," *Frontiers in immunology*, vol. 11, p. 724, 2020.
- [37] Z. Zhao, F. Li, J. Ning et al., "Novel compound FLZ alleviates rotenone-induced PD mouse model by suppressing TLR4/MyD88/NF- $\kappa$ B pathway through microbiota-gut-brain axis," *Acta pharmaceutica Sinica B*, vol. 11, no. 9, pp. 2859–2879, 2021.
- [38] A. J. Kwilas, S. M. Fulgham, J. C. Duran-Malle et al., "Toll-like receptor 2 and 4 antagonism for the treatment of experimental autoimmune encephalomyelitis (EAE)-related pain," *Brain, Behavior, and Immunity*, vol. 93, pp. 80–95, 2021.

## Review Article

# Food-Origin Mycotoxin-Induced Neurotoxicity: Intend to Break the Rules of Neuroglia Cells

Xingyao Pei <sup>1</sup>, Wenjuan Zhang,<sup>2</sup> Haiyang Jiang <sup>1</sup>, Dingkuo Liu,<sup>3</sup> Xinyu Liu,<sup>2</sup> Liuan Li,<sup>2</sup> Cun Li,<sup>2</sup> Xilong Xiao,<sup>1</sup> Shusheng Tang <sup>1</sup> and Daowen Li <sup>2,3,4</sup>

<sup>1</sup>Department of Pharmacology and Toxicology, College of Veterinary Medicine, China Agricultural University, Yuanmingyuan West Road No. 2, Haidian District, Beijing 100193, China

<sup>2</sup>Tianjin Key Laboratory of Agricultural Animal Breeding and Healthy Husbandry, College of Animal Science and Veterinary Medicine, Tianjin Agricultural University, Jinjing Road No. 22, Xiqing District, Tianjin 300384, China

<sup>3</sup>Tianjin Key Laboratory of Biological Feed Additive Enterprise, S&E Burgeoning Biotechnology (Tianjin) Co., Ltd, Tianjin 300383, China

<sup>4</sup>State Key Laboratory of Medicinal Chemical Biology and Tianjin Key Laboratory of Molecular Drug Research, College of Pharmacy, Nankai University, Haihe Education Park, Tongyan Road No. 38, Tianjin 300353, China

Correspondence should be addressed to Shusheng Tang; [tssfj@cau.edu.cn](mailto:tssfj@cau.edu.cn) and Daowen Li; [lidaowen@tjau.edu.cn](mailto:lidaowen@tjau.edu.cn)

Received 7 March 2021; Revised 29 June 2021; Accepted 14 September 2021; Published 28 September 2021

Academic Editor: Xu Wu

Copyright © 2021 Xingyao Pei et al. This is an open access article distributed under the Creative Commons Attribution License, which permits unrestricted use, distribution, and reproduction in any medium, provided the original work is properly cited.

Mycotoxins are key risk factors in human food and animal feed. Most of food-origin mycotoxins could easily enter the organism and evoke systemic toxic effects, such as aflatoxin B1 (AFB1), ochratoxin A (OTA), T-2 toxin, deoxynivalenol (DON), zearalenone (ZEN), fumonisin B1 (FB1), and 3-nitropropionic acid (3-NPA). For the last decade, the researches have provided much evidences in vivo and in vitro that the brain is an important target organ on mycotoxin-mediated neurotoxic phenomenon and neurodegenerative diseases. As is known to all, glial cells are the best regulator and defender of neurons, and a few evaluations about the effects of mycotoxins on glial cells such as astrocytes or microglia have been conducted. The fact that mycotoxin contamination may be a key factor in neurotoxicity and glial dysfunction is exactly the reason why we reviewed the activation, oxidative stress, and mitochondrial function changes of glial cells under mycotoxin infection and summarized the mycotoxin-mediated glial cell proliferation disorders, death pathways, and inflammatory responses. The purpose of this paper is to analyze various pathways in which common food-derived mycotoxins can induce glial toxicity and provide a novel perspective for future research on the neurodegenerative diseases.

## 1. Introduction

Mycotoxins spontaneously produce in food and feed, which have threatened human and animal health around the world. The thorny issue is not just their toxicity but their high prevalence in agriculture and strong connection with human diet and animal life [1]. Mycotoxins are the most likely toxins to invade human body due to the changes in the natural environment or improper manual handling which may facilitate the occurrence and spread of mycotoxins among food crops and their derivative products [2]. The mycotoxins enter the human body primarily along with plant-based foods in a

direct route, and they also come from various food of mycotoxin infected animal origin in an indirect aspect with secondary contamination [3–6]. Thus, mycotoxins could enter every stage of the food chain and every step of food handling through contaminated source to infect final consumers and users. According to official statistics, more than 25% of the global crops are growing fungi and contaminated with mycotoxins [7]. In addition, an increasingly volatile global climate as a force majeure factor may also aggravate the intensity of mycotoxins growth [8]. Early studies have shown that large quantities of cereal-based products were contaminated with fusarium toxin particularly in a long

period of rainy years [9]. In addition, sugarcane has also been proved to be a carrier of mycotoxins in humid environments. For instance, sugarcane was harvested in the south of China and transported to northern regions for sale: during transport and storage, damp conditions favor growth of *Arthrinium* spp., which secrete the mycotoxin 3-NPA. The above process has resulted in the established CNS disease known as Mildewed Sugarcane-induced Dystonia, a disease that has been prevalent in eastern regions of China (including Beijing) among children who have eaten sugarcane purchased from street vendors [10, 11]. More remarkably, the extent to which crops are contaminated with mycotoxins has been more unpredictable as the global warming. Also, note that human behavior of contemporary lifestyle like plant hybridization is reducing the stress tolerance of crops and making food and feed more susceptible to mycotoxin exposure, not to mention the high stability of mycotoxins [12].

Mycotoxins are all secondary metabolites of different fungi [13]. Although the mycotoxins have a large population of more than 300 species, the most common mycotoxins in human food and animal feed are aflatoxin B1 (AFB1), ochratoxin A (OTA), T-2 toxin, deoxynivalenol (DON), zearalenone (ZEN), fumonisin B1 (FB1), and 3-nitropropionic acid (3-NPA), which are the protagonist in this paper [14]. Available literatures have listed out acute or chronic toxicity including hepatotoxicity, nephrotoxicity, dermal toxicity, reproductive toxicity, and immunotoxicity in humans and food-producing animals caused by an excessive number of food-origin mycotoxins [15, 16]. As research continues, mycotoxins have been regarded as the typical food-related exogenous toxin which could attack the brain, and some of them have been known to cross the blood-brain barrier (BBB), which could accumulate in the brain and disrupt the normal function of central nervous system (CNS) [17–20]. So far, the neurotoxicity of mycotoxins involved in the predisposing factors of nerve diseases is becoming better recognized by researchers. In general, the AFB1, DON, T-2, OTA, FB1, and 3-NPA, which have strong affinity with brain, could enter the systemic circulation through consumption or contact, and some of their metabolites could easily cross the BBB and reach in the nerve cells via transporters [21–23]. It was important to note that after neurotoxin 3-NPA was absorbed by the stomach and intestines, the BBB was rapidly and extensively destroyed [24]. Furthermore, the fact for mycotoxins to enter the brain and develop toxic effects has been highlighted in recent literatures. For instance, 3-NPA is a mitochondrial neurotoxin that shuts down energy transformation in nerve system, resulting in brain damage that appears clinically in the form of persistent (lifelong) dystonia and ballism [25]. Furthermore, experimental animal models of 3-NPA-induced neurotoxicity have been used to help find therapeutic strategy for Huntington's disease [26, 27]. OTA is a neurotoxin that has a high affinity with the brain; the mice treated with OTA showed acute depletion of both dopamine and metabolites in the striatum with excessive OTA in the brain [26, 27]. OTA also caused male-specific autism in vivo and in vitro by combining the microRNA and X-chromosome in the brain [28]. Recently

published studies have revealed that the metallothionein (MTs) gene in the fetal brain could be upregulated by T-2 toxin accumulated in the brain of female mice, demonstrating that the regulation of mycotoxins on antioxidant-related genes could be two-way transmitted between mother brain and fetus brain [22]. However, researchers also found that AFB1 affected neurons potentially by activating immune cells in the bloodstream of mice, causing neurodevelopmental and function abnormalities, in addition to causing brain damage directly [29–31]. Besides, the ability of AFB1 to indirectly affect neurons by affecting the function of glial cells has also been demonstrated [32]. Most importantly, mycotoxins have been demonstrated to increase the occurrence of global neurological diseases. It has been reported that the concentration of T-2 toxin in the serum of 182 residents with a history of mycotoxin exposure was significantly increased, neurodevelopment was hindered, and exercise balance, visual function, reaction speed, cognitive ability, and emotional management ability were all weakened. In addition, the decrease in frontal cortex activity was detected by quantitative EEG [33]. Through individual neuropsychological data and symptom observation, mycotoxins were also suspected to be one of the triggers of autism spectrum disorders, consistent with recent epidemiological research reports on mycotoxins and autism spectrum disorders [34]. A neurophysiological test for children showed that the evoked potentials of brainstem, visual, and somatosensory were abnormal after long-term exposure to mycotoxins [35]. The cognitive impairment of 277 children in Poland was proved by a 6-year mycotoxin exposure test, indicating that the exposure time was negatively related to the IQ of participants. Similarly, the concentration of ochratoxin in urine and serum of 52 autistic patients was significantly higher than that of the control groups. Additionally, the upregulation of microRNA-132 mediated by OTA in vitro has been verified, which was connected with depression-related genes PTEN and MeCP2. Conversely, the way of adsorbing or removing OTA could rescue autism symptoms [36]. Based on the characteristics of these common mycotoxins about their easy passage through the BBB and their potential threat to the central nervous system, exploring the interconnections between their neurotoxic mechanisms and the nerve-associated diseases is becoming more urgent for us.

A large number of records indicated that glial cells especially astrocytes and microglia play irreplaceable central roles in brain homeostasis, neural information transmission, neuronal survival, and neuroinflammation [37–40]. Furthermore, astrocytes and microglia are not only the most abundant glial cells to protect CNS but also the crucial participants in both brain injury and neurodegenerative disorders, particularly in the Alzheimer's, Parkinson's, and Huntington's diseases [41]. Although the amount of available information about the mycotoxin-induced gliocytotoxicity are still limited and lack complete integration and analysis, the neurotoxicity through altering the survival status and function of the glia cells have been demonstrated in mycotoxin [42]. Previous research proved that the oxidative stress and gene expression of ZEN-

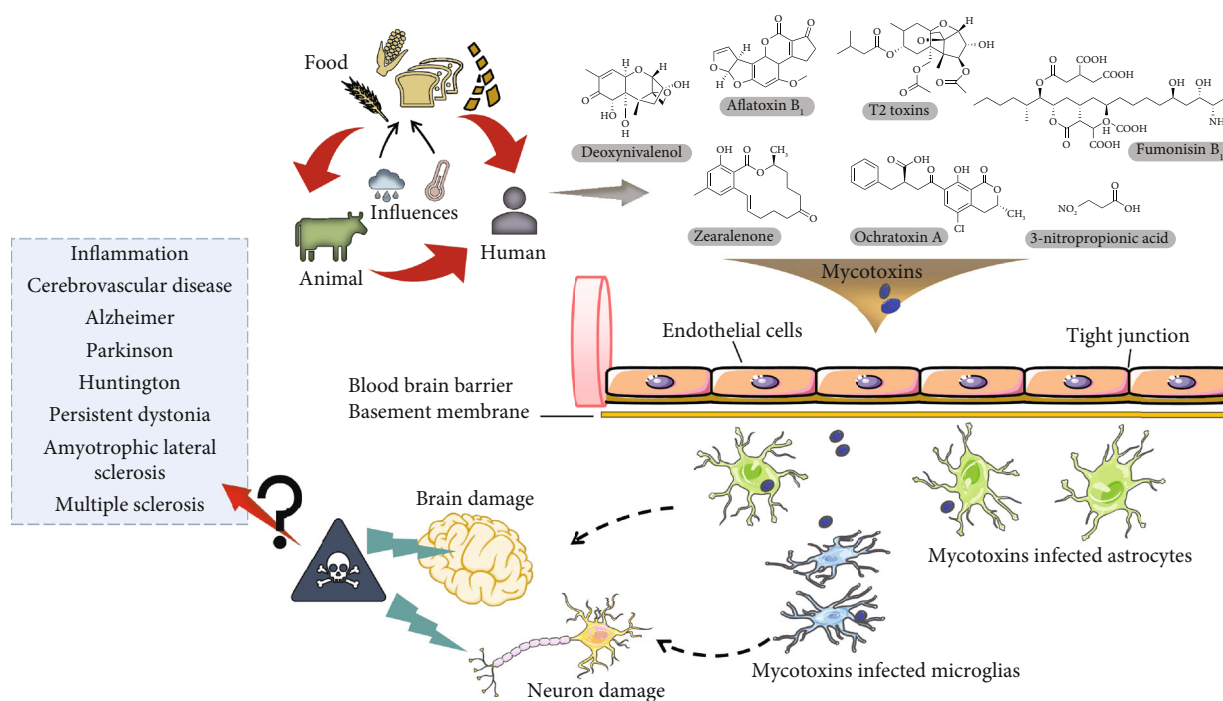


FIGURE 1: Food-origin mycotoxins cause neuronal and brain damage by infecting astrocytes and microglia. Mycotoxins including aflatoxin B1 (AFB1), ochratoxin A (OTA), T-2 toxins, deoxynivalenol (DON), zearalenone (ZEN), fumonisin B1 (FB1), and 3-nitropropionic acid (3-NPA) enter the body mainly through food crops and animal-origin foods (meat, eggs, milk, sugarcane, and edible viscera). Mycotoxins and its metabolites can easily cross the blood-brain barrier (BBB) and infect astrocytes and microglia, which eventually leading to neuronal damage and brain damage. Whether mycotoxins cause neurodegenerative diseases, such as Alzheimer, Parkinson, Huntington, and amyotrophic lateral sclerosis need further research.

treated neurons were strictly regulated by glial cells with the evidence that the presence or absence of glial cells affected the expression of thyroid receptors  $\alpha$  and  $\beta$  [43]. Another report about typical neurotoxin FB1 suggested that the primary and mature neurons of the mice were not the primary targets of FB1 (50  $\mu\text{mol/L}$ ) neurotoxicity in vitro; on the contrary, the immune active cells such as astrocytes showed both obvious cytotoxicity and cell death after 8-day exposure. In addition, the obvious microglial cytotoxicity mediated by FB1 (20  $\mu\text{mol/L}$ ) was also observed in mice at the 4th day. Therefore, increasing evidences have indicated that the neurotoxicity of mycotoxins was secondary to the complex roles of glial cells, potentially promoting the development of neurodegenerative diseases [44]. Considering the indispensable roles of glial cells in CNS diseases, as well as the inevitable mycotoxins in feed and food, we now comprehensively describe the essential connection between mycotoxins and glial cells from the perspective of astrocytes and microglia cells (Figure 1). Despite the evidence that ZEN causes glial toxicity is limited, the interferences of other mycotoxins on glial cells were summarized in this report, so as to systematically explain how the mycotoxins stimulate the glial cell status related to the nerve injury. The long-term purpose is to provide necessary information for protecting CNS against the threat of exogenous factors and find an effective way to delay neurodegenerative diseases.

## 2. The Dual Role of Glial Cell Activation

During external stimulus, astrocytes and microglia would transform resting state into activation state, undergo changes in morphology, proliferation, and migration [45]. It has been known that glial cells could play the dual roles of protection and damage depending on different activation levels, which can not only protect and repair the brain but also cause damage to the CNS [46, 47]. The activation and proliferation of glial cells have been proven to affect the microenvironment of nerve tissue repair after injury or ischemia: excessive activation of astrocytes and microglial cells, on the one hand, forms a glial scar and oppresses the microvessels, on the other hand, tends to secrete harmful cytokines, which affect nerve regeneration. Meanwhile, activated glial cells produce a large amount of nitric oxide, which affects DNA modification and lead to neuron injury [48, 49]. Rapid and severe overactivation of glial cells caused by neurotoxic substances could lead to a metabolic disturbance in the interactions between neurons and astrocytes and result in severe brain disease [50]. Related literatures have confirmed that this process has been implicated in the course of Alzheimer, Huntington's dance, demyelinating disease, and brain trauma [51].

**2.1. Mycotoxin-Mediated Astrocyte Activation.** The activation and immune responses of astrocytes have been suspected of



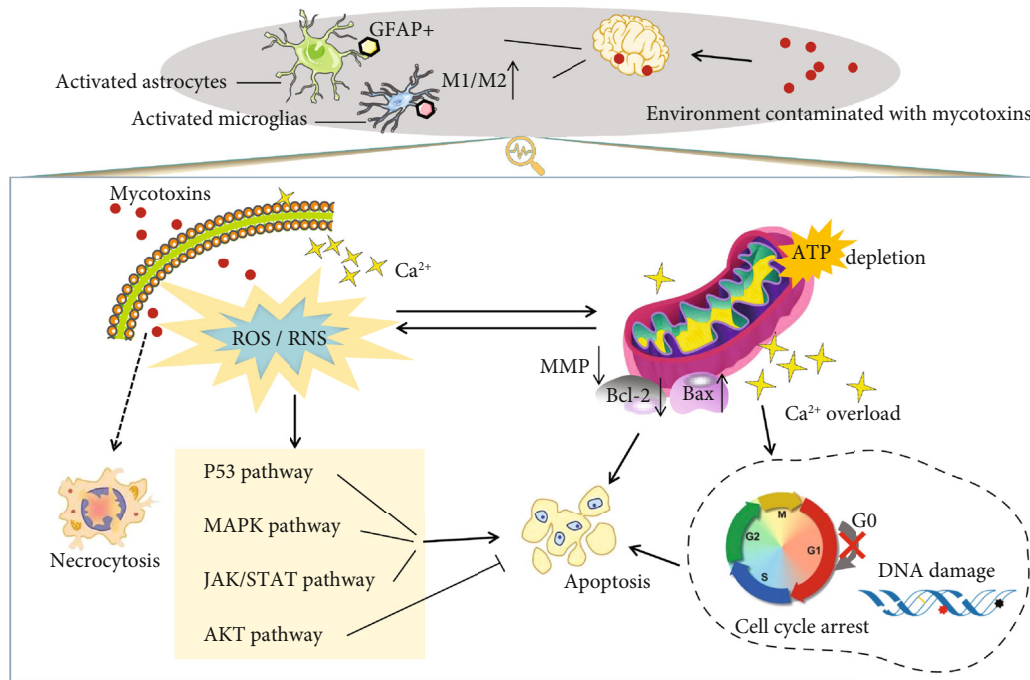


FIGURE 2: Main pathways of mycotoxin-induced neurotoxicity in astrocytes and microglia. Mycotoxins could cross the blood–brain barrier (BBB) and activated astrocytes and microglia. Mycotoxins stimulate the generation of reactive oxygen species (ROS) and reactive nitrogen species (RNS), lead to mitochondrial dysfunction (decrease of mitochondrial membrane potential (MMP), increase the ratio of Bax/Bcl-2, ATP depletion, and Ca<sup>2+</sup> overload), DNA damage, cell cycle arrest, and apoptosis. The activation of the p53 pathway, MAPK pathway, JAK/STAT pathway, and AKT pathway is involved in mycotoxin-induced apoptosis. In addition, mycotoxin can directly induce necrocytosis.

augmenting proinflammation, calcium imbalance, mitochondrial damage, and the accumulation of oxidative stress products such as reactive oxygen species (ROS), which tend to expand neuronal deterioration and contribute neuronal death [52, 53]. Glial fibrillary acidic protein (GFAP) generated in cell body of astrocytes has been recognized as the activation marker protein of astrocytes (Figure 2) [54]. Previous evidence has suggested that another protein, matrix metalloproteinase 2 (MMP2) with different specific expression pattern [55], played protective role against heavy metals or drug toxicity in astrocytes [56]. During the process of chemical, degenerative, or mechanical injury repair in the brain, the activity, proliferation, and function of astrocytes were influenced by the changes of the expression of GFAP and MTs. Therefore, GFAP and MTs were not only important factors for the stabilization and tight junctions of BBB but also represented the severity of astrocyte activation directly and indirectly, respectively [57]. It has been confirmed that the activation of astrocytes could protect neurons against oxidative stress which occurred in neural stem cells (NSCs) in early progenitor cells of weaned mice infected with T-2 toxin and reduced transient neural disconnection in the hippocampus tissue. Relevant research has observed a significant increase in the number of MT-I/II+ positive astrocytes in various brain regions, and this protective mechanism was suggested as a toxic target of T-2 toxin [58]. Early experiments have shown that astrocyte activation was rapidly initiated in neurodegenerative injury, accompanied by increasing GFAP expression. Similar findings showed that GFAP activity in the cerebellum of rodents was rapidly

enhanced by AFB1, promoting the proliferation of astrocytes and the release of inflammatory factors and neurotoxic substances [59]. After long-term oral administration of 0.025 mg/kg AFB1, the GFAP area percentage in hippocampal CA1 area of male rats was significantly increased compared with that of the control group, due to the activation of the nitric oxide (NO) produced by AFB1. As an endothelial relaxation factor, NO initiated the activation of microvascular endothelial cells, with a subsequent activation of astrocytes. Therefore, as the AFB1 administration went on for 90 days, astrocyte toxicity and damage were induced more severely [60]. Previous published studies have suggested that the increased number of astrocytes could also be a repair mechanism during the brain injury and the number of neurons in hippocampal CA1 region, which was rescued by astrocytes. In contrast, both in vivo and in vitro testing results showed that once aflatoxin was freed, the total number of glial cells and neurons in the frontal cortex would decline [61].

**2.2. Mycotoxin-Mediated Microglia Activation.** Microglia, the resident inflammatory sensors in the brain, have been thought to play a key role in the survival and homeostasis of neurons. Activated microglial cells were inclined to show two phenotypes, including the classic M1 phenotypes with the nerve inflammation and the M2 phenotypes focusing on nerve repair [62]. A growing number of evidences have shown that the changed ratio of M1 to M2 due to the excessive activation of microglia could break the balance between inflammation and repair, causing

immune disorders, mediate neuroinflammatory injury, and accelerate the neurodegenerative diseases [63, 64]. 24-hour long exposure to 20 ng/mL AFB1 activated the astrocytes as well as human microglial cells in the form of M1 phenotype; subsequent microglia-mediated inducible nitric oxide synthase (iNOS) upregulation promoted the arising of oxidative stress. Gene expression results indicated that the increasing of mRNA expression levels of TLRs, MyD88, and NF $\kappa$ B was evident under the stimulus of AFB1. The secretion of the proinflammatory factors (TNF- $\alpha$ , IL6), as well as granulocyte-macrophage colony stimulating factor (GM-CSF), was also promoted, which threatened other resting microglia cells. Nitric oxide has been verified to be one of signals for microglia to switch from M1 to M2 phenotype, but AFB1 only caused a slight increase in NO and had no tendency to activate M2 phenotype of microglia which explained the critical phenotype M1 [32]. Researchers also found that 48 hours of OTA exposure resulted in upregulation of proinflammatory factors such as IL-1 $\beta$  and IL-6, and the positive results of macrophage cells ED1/CD68 markers and microglia M1 activation markers were increased, which in turn intensified the release of proinflammatory cytokines. Moreover, anti-inflammatory factors such as IL-4 and IL-10 activated M2 phenotype of microglia. It has been reported that different types of activated glial cells probably interact with each other. For example, MTI and MTII proteins were downregulated by OTA, and it is noteworthy that the inflammatory response of microglia was rescued by the artificially treatment on MTI and MTII proteins in astrocytes, further indicating that the astrocytes might be able to adjust the trends of the activation microglia [65].

### 3. Oxidative Stress in Mycotoxin-Infected Glial Cells

In vivo and in vitro studies have shown that cellular oxidative stress is the direct mechanism of cytotoxicity caused by mycotoxins and their metabolites. ROS are increased by mycotoxins, causing oxidative stress, and then proteins, lipids, and chromosomes are attacked by ROS. Cell membrane is damaged or even lytic end with the increased lipid peroxidation (LPO) and decreased antioxidants [66]. Not only that, brain cells are vulnerable to oxidative stress injury induced by mycotoxins such as AFB1, OTA, T-2 toxins, DON, and FB1 in food and environment because of numerous oxygen consumption, energy expenditure, and peroxide fatty acids in brain tissue [67]. Furthermore, excessive ROS expression and ion imbalance in brain will be further increased with the injury of glial cells, thus damaging the function of the whole CNS [52, 53].

Mycotoxin-mediated oxidative stress in neuroglial cells has been described in related literatures, suggesting that the imbalance between ROS accumulation and elimination is the major neurotoxic mechanism of T-2 toxin among glial cells. The astrocytes of male pups are able to sense the presence of T-2 toxin infection in mice maternal environment and produce oxidative stress response in vivo, which is proved to be regulated by the significantly increased expression of metallothionein in fetal astrocytes [68]. In addition,

an increasing number of experiments has been evidenced that oxidative stress is also crucial to the cytotoxicity of microglia, indicating that microglia exposed to microorganisms can not only promote the generation of ROS but also stimulate the expression of NO synthase to promote the production of RNS, which is also considered as a universal indicator of oxidative stress in astrocytes and microglia [69, 70]. It was known from previous studies that ROS and lipid peroxidation were gradually accumulated over time in the cytoplasm of human astrocytes treated with aflatoxin B1. As a consequent of oxidative stress, mitochondrial permeability and DNA molecule are impaired [71]. In addition, aspartate aminotransferase (AST), alanine aminotransferase (ALT), and lactate dehydrogenase (LDH) were significantly released in the brain after oral administration of 20 ng/mL AFB1 for 30 days, and the connectivity of the BBB was completely destructed after 90 days. The findings of neuronal cell apoptosis, nuclear condensation, cellular vacuolization, neuroinflammation, and spongiform necrosis were also systematically recorded in the late stage of oxidative stress [60, 72]. It has been reported that iNOS mRNA of human microglia was upregulated after 3 hours exposure to AFB1, which further confirmed the role of AFB1 in promoting oxidation on CNS [73]. However, the observations of free radical assessment in recent literature showed that the increase of the total amount of free radicals and ROS was not obvious after AFB1 treatment, which reflecting that iNOS was not only a prooxidant molecule but also an important indicator in the process of oxidative stress of glial cells [74]. The oxidative stress of normal astrocytes was initiated by 48-hour exposure to OTA, characterized by a reduction of regulatory factors of oxidative stress response [65]. Several researchers treated the serum-free aggregating brain cells with noncytotoxic concentrations of OTA and analyze the results of the quantitative reverse transcription polymerase chain reaction (QRT-PCR). They found that peroxisome proliferator-activated receptor- $\gamma$ , heme oxygenase-1, and iNOS in astrocytes were significantly upregulated, while expressions of glial fibrillary acidic proteins were attenuated [75]. In vitro investigation, oxidative stress was also found to promote FB1-induced neural death pathway because of the role in inducing the cytotoxicity of human U-118MG glioblastoma through the production of ROS, the initiation of lipid peroxidation, and the reduction of glutathione [76]. Despite the evidence that the oxidative stress depends on more than 100  $\mu$ M FB1 and 2 to 6 days of exposure and may require some stimulation of indirect mechanism, the oxidative stress damage in glial cells will clearly be evoked by certain dose and duration of exposure. The metabolic changes of sphingomyelin (SL) caused by FB1 can be able to coordinate with oxidative stress to promote cell death and carcinogenesis on this basis [77].

### 4. Mitochondrial Dysfunction Mediated by Mycotoxins

Turning enough adenosine triphosphate (ATP) into chemical energy is essential for cell survive. While mitochondria, the "cellular energy plant" in the brain provides a constant

supply of ATP via oxidative phosphorylation (OXPHOS) [78]. Mitochondria can also prevent excessive calcium accumulation in nerve cells and play an important role in the regulation of apoptosis. It has been proved that the regulation of ATP and calcium in glial cells was disrupted as a consequence of mitochondrial dysfunction triggered by mycotoxins, which was also vastly involved in the free radicals, DNA damage, cell apoptosis, and necrosis (Figure 2) [79]. The ability of trichothecenes to inhibit mitochondrial protein translation directly has been exposed. For instance, T-2 toxin-mediated oxidative stress and apoptosis of nerve cells both associated with mitochondrial disorders has been shown in previous studies [80]. Recently, through the 3(4,5-dimethylthiazolyl-2)2,5-diphenyl tetrazolium bromide (MTT) assay signal, scientists found a dose-dependent decrease in mitochondrial activity of mouse microglia (BV-2) after the FB1 (8 mM to 50 mM) infection, and the active numerical value was significantly lower than the control group [81]. It was also found that the ROS produced by the primary mouse astrocytes derived from the impaired mitochondrial function perturbed by FB1. Furthermore, the mitochondrial electron transport chain suppression, mitochondrial membrane decline, and cellular respiratory inhibition eventually induced ROS explosion, measured by real-time imaging and specific inhibitor tests [82]. The oxidative phosphorylation defects of mitochondria have been investigated in AFB1-related tests, and the results showed that DNA damage was parallel to alteration of mitochondrial activity and function. ATP depletion caused by mitochondrial maladjustment was involved in glial cytotoxicity induced by AFB1. For example, in the process of apoptosis in human microglia induced by AFB1 (20 ng/mL) at 24 postexposure hours (PEH), the decreased level of ATP was demonstrated by using firefly luciferase assay [32].

Through the balance between intracellular and extracellular calcium ion ( $\text{Ca}^{2+}$ ) signals, astrocytes recycle and release various neurotransmitters such as glutamate and  $\gamma$ -aminobutyric acid (GABA) and ensure synaptic stability [83]. It is known that  $\text{Ca}^{2+}$  depends on ion pumps and  $\text{Ca}^{2+}$  channels (transient receptor potential channels, L type calcium channel, inositol triphosphate receptor,  $\text{Ca}^{2+}$ -ATP) to enter the neurocyte, and mitochondrial dysfunction-mediated  $\text{Ca}^{2+}$  migration is accomplished by mitochondrial calcium uniporter [84]. Therefore, the injured astrocyte, depolarized mitochondrion, and the decline of mitochondrial membrane potential (MMP) induced calcium overload, which occurs in the process of AFB1-mediated astrocyte proliferation testing. Interestingly, the proliferation of astrocytes was subsequently rescued after the inhibition of  $\text{Ca}^{2+}$  levels by chelating agents and inhibitors [85]. An imaging of astrocytes exposed to 3-NPA in vitro has showed an excessive  $\text{Ca}^{2+}$  overload that caused astrocyte destruction [86]. Furthermore, OTA decreased MMP in human astrocytes, increased the concentration of  $\text{Ca}^{2+}$  in mitochondria and cytosol, upregulated the proapoptotic factors Bax and P53, and increased the expression level of urokinase plasminogen activator receptor (PLAUR) mRNA [87]. The literature has shown that the calcium influx was in accordance with oxidative stress. For example, transient receptor

potential channels and mitochondrial calcium transporters in the astrocytes were activated by excessive ROS, exhibiting the inhibition of the cell survival [88].

## 5. The Inhibition of Glial Cell Viability Caused by Mycotoxins

Mycotoxins have been identified in recent studies as reducing the survival of glial cells in the CNS. The results of neurotoxic correlation assessment of AFB1 suggested that high dose of AFB1 significantly reduced microglial activity in a dose- and time-dependent manner. Treatment with 40  $\mu\text{g}/\text{mL}$  AFB1 caused about 50% loss of living glial cells in mice, while AFB1 infection with 1  $\mu\text{M}$  reduced the viability of zebrafish embryos by 66% [85]. The sensitivity of astrocyte viability to mycotoxins has also been demonstrated in previous literatures. For example, murine microglia and astrocytes developed cell necrosis and a decreased number of living cells as a result of in vitro stimulation with FB1 at doses higher than 25 mM [81]. Continuous infection of FB1 in the concentration range of 1-40 mM induced a decrease in astrocyte maturation and survival rate during 25-35 d [89], with significant DNA damage at 48 h, 72 h, and 6 d posttreatment [90]. In addition, about 35% of rat C6 glioma cells died after being treated with FB1 (9  $\mu\text{mol}$ ) and incubated for 24 h [91]. In addition, 30% of mice with 3-NPA injection produced abnormal gait, tremor, and somnolence. The swollen and disintegrated striatal astrocytes were observed by electron microscopy [86]. Furthermore, 10 nM T-2 toxin reduced the viability of the astrocyte population by 70% at 24 hours after incubation, and 24 nM T-2 toxin inhibited 50% of cells at 48 hours after exposure, determining the  $\text{IC}_{50}$  value. It should be emphasized that the comparison of the  $\text{IC}_{50}$  values of primary astrocytes with those of other primary cells indicated that CNS was susceptible to the toxicity of T-2 toxin [23]. Recently, the sensitivity of different nerve-related cells to mycotoxins has been compared and recognized. The  $\text{LC}_{50}$  of NPCs, microglia, and astrocytes in 24-hour AFB1 exposure was 75,000 ng/mL, 50,000 ng/mL, and 40,000 ng/mL, respectively, indicating that the cytotoxic priority of the three types of cells was different [73]. In the test of DON interfered with primary enriched cultures, different glial cells had different response degrees to DON. The  $\text{IC}_{50}$  of astrocytes was 31  $\mu\text{M}$ , 119 times higher than the value of 0.259 of microglia. Similarly, human astrocyte  $\text{IC}_{50}$  (50  $\mu\text{M}$ ) was more than 12 times that of human microglia  $\text{IC}_{50}$  (4.1  $\mu\text{M}$ ). The microglial cells were also found higher sensitivity in the mixed glia cells coculture system. Immunofluorescence and MTT results showed that DON with a concentration less than 25  $\mu\text{M}$  was resisted by astrocytes. Nevertheless, microglia (ox-42 positive cells) were selectively killed when DON was less than 10  $\mu\text{M}$  [92].

Studies related to cell cycle arrest have also revealed the reasons for the decreased survival rate of glial cells after continuous exposure to mycotoxin. Flow cytometry analysis showed that proliferation of human astrocytes treated with AFB1 was inhibited at the sub G0/G1 stage, which was correlated with the upregulated Bax, Bak, and cytochrome c (Cyt-c), and the proliferation activity of astrocytes was also

regulated by the AKT and MAPK signaling pathways [85]. In addition, the sub G0/G1 cell cycle arrest characterized by mRNA downregulation of CCND1, CCNE1, CDK4, and MYC was also observed in OTA infected astrocytes, accompanied by the reduced secretion of neurotransmitters such as norepinephrine, dopamine, and serotonin [87, 93]. Unexpectedly, there was no correlation between the antiproliferation effect of FB1 at a concentration of 2.5 mM on mouse microglia and the cell cycle arrest. Although FB1 has previously been reported to inhibit the proliferation of other cell types through cell cycle arrest, in mouse microglia, it exhibited a unique feature independent of cell cycle arrest [94, 95].

## 6. Apoptosis and Necrosis in Mycotoxin-Treated Glial Cells

So far, apoptosis and necrosis have been explained as the two main indicators of mycotoxin-mediated glial toxicity in vitro (Figure 2). The necrosis and hyperplasia occurred in brain according to immunohistochemical results with the action of AFB1 [96]. It has been reported that AFB1 initiated human astrocytes mitochondrial-dependent apoptosis pathway by inducing a dose-dependent decrease of MMP, an overexpression in proapoptotic proteins such as Bax, Bak, and Cyt-c and a decrease in the expression of phosphorylated Bcl-2 [85]. Microglial apoptosis mediated by low doses of AFB1 (20 ng/mL) was also demonstrated by bioluminescence-based methods. The expression of caspase-3 and caspase-7 increased at 24 PEH, the apoptosis-related genes such as p21 and p53 were significantly elevated, and the phosphatidylserine transferred to the outer surface of the plasma membrane. Simultaneously, apoptotic bodies were formed, and the proportion of apoptosis (annexin V+) increased [97]. Besides, abnormal fluctuations in the expression of Cxcr4 gene were found at different time points in response to AFB1 [98]. It has been reported that the treatment of 1  $\mu$ M T-2 toxin for 24 h significantly enhanced the activity of caspase-3 in astrocytes, activated the JAK/STAT3 pathway, and eventually triggered apoptosis [68]. In addition, previous detections have revealed that T-2 toxin was time-dependently accumulated in T-2 incubated glial cells. For example, the cumulative concentration of T-2 toxin in astrocytes reached 200  $\mu$ M after treated with 10  $\mu$ M T2 toxin for 15 minutes. Subsequently, the absorption of T-2 toxin by human astrocytes reached a peak at 320  $\mu$ M after 1-hour long incubation, which was about 30 times of the concentration of T-2 toxin in the peripheral medium. Likewise, it was also found that HT-2, the main metabolite of T-2 toxin, also generated in human astrocytes and reached the maximum concentration of 150  $\mu$ M after 6 hours of exposure, indicating that the apoptotic pathway of primary astrocytes was produced by cooperation of T-2 and HT-2 toxins [23]. Moreover, researchers have determined the apoptosis in 3-NPA treated primary astrocytes and BV2 cells, and simultaneously, these cells expressed huntingtin. In turn, 0.5 mg/kg  $\alpha$ -melanocyte stimulating hormone ( $\alpha$ -MSH) could protect cells via promoting brain derived-neurotrophic factor (BDNF) and peroxisome proliferator-activated receptor- $\gamma$  (PPAR- $\gamma$ ) expression [99]. In addition, researchers found

that OTA triggered astrocytotoxicity through mitochondria-dependent apoptosis which was related to the increased phosphorylation of proteins in AKT and MAPK signal transduction pathway (e.g., JNK and ERK) [100]. In the other side, the role of mycotoxins in inducing direct or secondary glial cell necrosis, which was another way of non-neuronal cell death, has been speculated. For example, the death of nonapoptotic necrotizing cells occurred 8 days after 50  $\mu$ M FB1 infection in BV-2 and murine precursor astrocytes, as confirmed by lactate dehydrogenase release assay and annexin V/PI staining observations [81]. Based on the evidence of necrosis caused by FB1 and the past data on FB1 infected hamster ovarian cell test, researchers mechanistically speculated that the proapoptotic signals of such cells were possibly not vulnerable to boost by FB1. Instead, the necrotic death mode was involved in cell loss triggered by FB1 [101].

## 7. Inflammation/Immune Deregulatory in Glial Cells

Activated microglia cells and astrocytes both normally have the ability to release soluble factors for neuroinflammation, and their immune response has been considered to be essential for neuroinflammation [102, 103]. In general, inflammation could be produced and developed with injury, infection, and toxin stimulation. Although transient neuroinflammation may contribute to the elimination of pathogenic microorganisms, repair of brain infections, and protection of the nerve tissue, the chronic neuroinflammatory signal transduction could also potentially translate to the development of neurodegenerative disease, suggesting that inflammatory activation of glial cells could have biphasic effects [13, 104]. For example, astrocytes tend to maintain the homeostasis of brain function under normal physiological conditions, but they could be abnormally activated with injury or pathological interference, releasing various inflammatory factors and promoting the course of neurological diseases [105]. In addition, the immune effector cells of the CNS, microglia, normally played an important role in immune regulation, including sensing harmful stimuli in the environment, swallowing debris and abnormal proteins, digesting apoptotic neurons, and performing antigen-presenting function. On the other hand, microglia have also been recognized as an internal cause of pathologic neuroinflammation, exacerbating a variety of neurodegenerative diseases, including Parkinson's disease, Alzheimer's disease, amyotrophic lateral sclerosis, and multiple sclerosis [106–108]. In the latest literature, activation and proinflammatory response/immune dysregulation of murine microglia exposed to low quantity of AFB1 have been evaluated. Functional toll-like receptors (TLRs), as a key immunosensor of the CNS, have been known as one of the characteristics of the immune activity of glial cells, as well as the proinflammatory events in the brain in the stimulation of the external environment. TLR2 was overexpressed in 20 ng/mL AFB1-exposed microglia after 1 hour and triggered a prophase cascade, including MyD88, NF $\kappa$ B2, TNF- $\alpha$ , IL-6, chemokine receptor (CxCr4), and caspase-3/7, which were upregulated at gene and protein

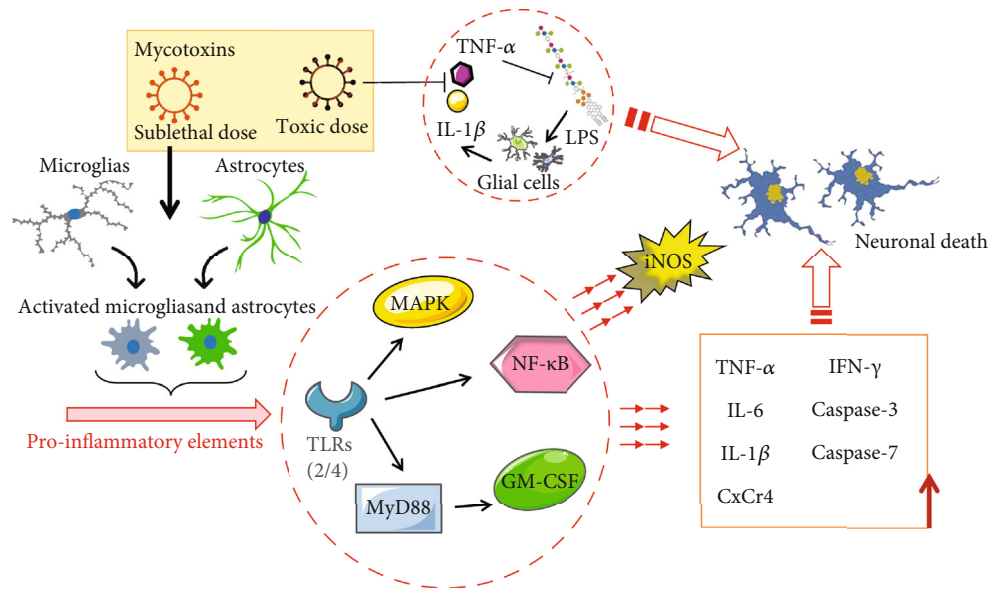


FIGURE 3: Mycotoxin-induced inflammation/immune deregulatory in glial cells. Sublethal dose of mycotoxins can activate microglia and astrocytes and promote proinflammatory element release. Mycotoxin activates MAPK, NF- $\kappa$ B, and MYD88/GM-CSF pathways through toll-like receptors (TLRs) to promote the release of iNOS and inflammatory cytokines, including TNF- $\alpha$ , IL-6, IL-1 $\beta$ , CxCr4, IFN- $\gamma$ , caspase-3, and caspase-7, and ultimately leads to death of neuronal cells. On the other hand, toxic dose of mycotoxin can reduce microglia's sensing for LPS through cytotoxic effects, leading to the risk of decreased anti-infection efficiency with the downregulation of TNF- $\alpha$  and IL-1 $\beta$ .

levels. The level of TLR4 then increased after 5 hours, further triggering the secretion of iNOS and NF- $\kappa$ B [73]. GM-CSF could aggravate inflammatory cell infiltration in mammalian brain, glial cell proliferation, and central nervous system immune disorder. *In vitro* evaluation indicated that MyD88 and TLRs stimulated the secretion of IFN- $\gamma$  and GM-CSF in activated microglia following exposure to AFB1, thus recruiting other resting microglia [32]. In AFB1-initiated proinflammatory microenvironment, astrocytes also increased the loads of TNF- $\alpha$ , IL-1, and IL-6 through TLR expression (IL-6 was the most upregulated) to exacerbate inflammation and injury, which was confirmed by cytokine expression profiles [73]. In addition to AFB1, repetitive OTA-derived stimulation has been believed to enhance neuroinflammation as visualized by an increase of activating glial cells and proinflammatory signals, such as iNOS, IL-1 $\beta$ , TNF- $\alpha$ , and IL-6, which were increased after 24 hours of exposure. M1 microglial cells were fully activated on day 10 of exposure, and ED1/CD68 positive cells and isolectin B4-labeled cells were significantly increased. Under the same conditions, GFAP, MTI, and MTII in astrocytes, that were known to be normally elevated in injury, were downregulated in the AFB1 environment, and the expression of vimentin in astrocytes was atypically increased [65]. Furthermore, the mechanism of 3-NPA-induced TNF- $\alpha$ , IL-1 $\beta$ , and IL-6 in mRNA levels was related to Nrf2 expression, which was the therapeutic target in the treatment of Huntington's disease [27]. OTA was also suspected to influence the expression of brain inflammation-related genes through astrocytic cytoskeletal changes in another study, and MTI/MTII was also suggested to be involved in the regulation of OTA-induced

neuroinflammation [109]. It has been well documented that microglia could be activated by bacterial lipopolysaccharides (LPS), then release proinflammatory factors and produce ROS and reactive nitrogen (RNS), causing damage and loss of peripheral neurons and glial cells. Therefore, the inhibition or promotion of above process could be sense for the study of degenerative neurological diseases and pathologic neuroinflammation [110]. Remarkably, DON possibly has a double side on the secretion of TNF- $\alpha$  and iNOS in microglia treated with LPS. For example, DON (sublethal dose) of less than 100 nM promoted the inflammatory effects through MAPK and NF- $\kappa$ B pathways, thereby increasing neuronal damage caused by infection, while DON (toxic dose) of IC<sub>50</sub> reduced microglial sensing for LPS through cytotoxic effects, leading to the risk of decreased anti-infection efficiency [92, 111]. Similarly, PCR results demonstrated that the expression of proinflammatory molecules including TNF- $\alpha$  and IL-1 $\beta$  was downregulated in the mixed culture of glial cells incubated with FB1 for 6 h or 24 h [81, 112]. Judging from the available evidence, mycotoxins have been suggested to enhance or inhibit the production of proinflammatory factors in glial cells at the mRNA and protein levels, which in turn provide the possibility of brain instabilities, neuroimmune disturbances, and neurodegenerative diseases (Figure 3).

## 8. Failure of Glutamate Clearance in Glial Cells

It has been known that the survival of neurons depends on astrocytes, partly because the latter responds to an overdose of neurotransmitters through their receptors and reabsorb some of the neurotransmitters to end the synaptic process

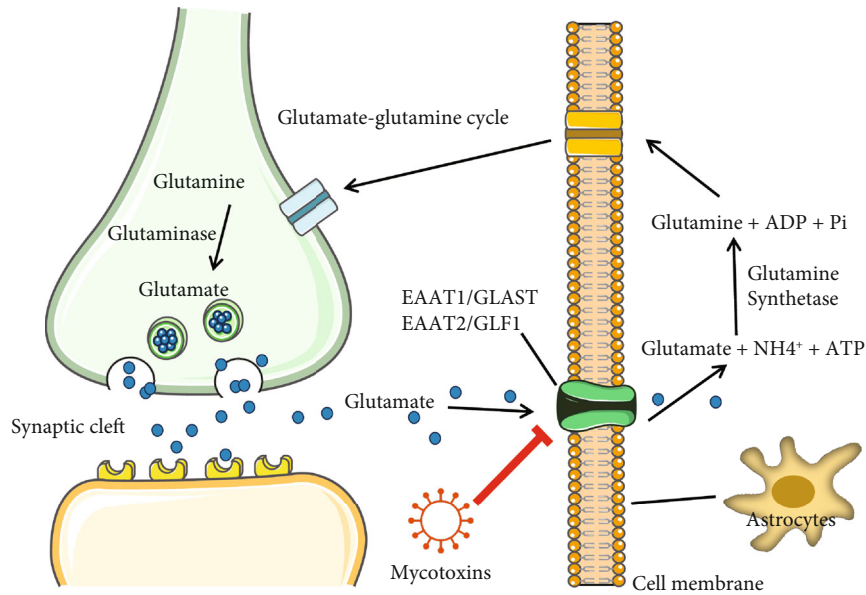


FIGURE 4: Mycotoxins inhibit glutamate clearance in glial cells. Mycotoxin-mediated astrocyte injury inhibits glutamate uptake and leads to a large accumulation of extracellular glutamate, which eventually induced excitotoxicity, functional impairment, or death of nerve cells.

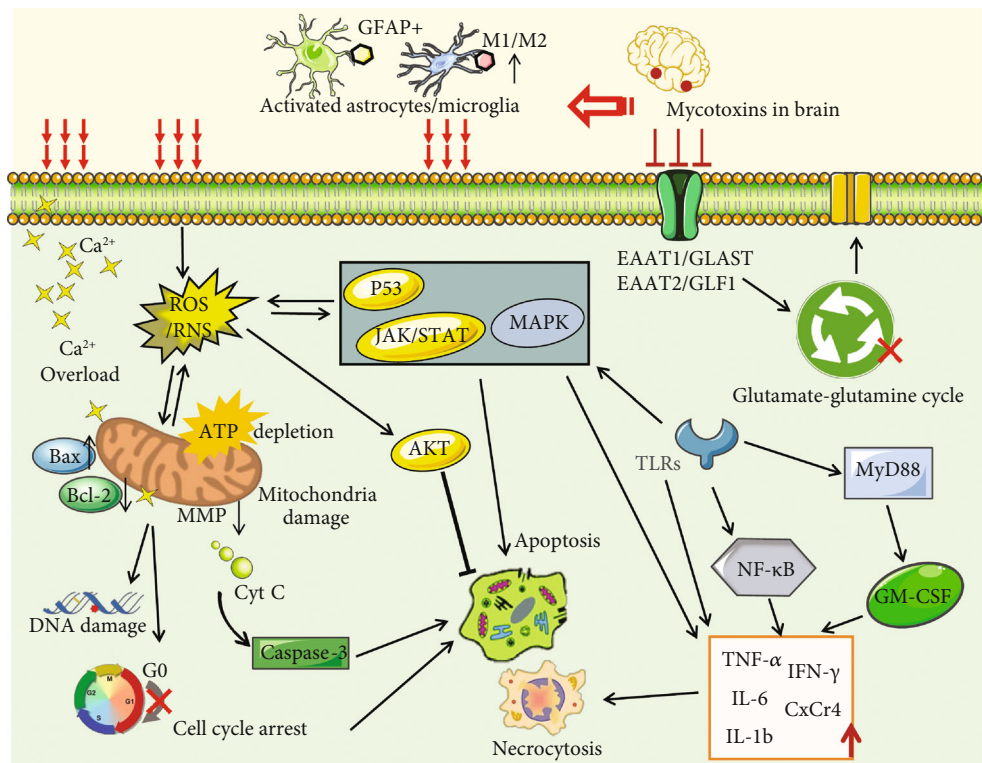


FIGURE 5: Molecular mechanisms of mycotoxin-induced neurotoxicity in neuroglia cells: (i) ROS and RNS were accumulated in oxidative stress damage; (ii) mitochondrial function was impaired, aggravating ATP depletion and calcium imbalance; (iii) the ability to buffer transmitters such as glutamate was inhibited, inducing neural defects; (iv) the viability of glial cells was decreased, cell proliferation was inhibited at the G0/G1 stage, and the release of proinflammatory factors changed dramatically, resulting in apoptosis or necrosis; (v) the activation of the p53 pathway, MAPK pathway, JAK/STAT pathway, and AKT pathway is involved in mycotoxin-induced apoptosis.

in time [113]. The “glutamate-glutamine cycle” has been known as the main metabolic coupling pathway between astrocytes and neurons. The glutamate has been considered

both as the primary excitatory neurotransmitter in the CNS of mammals and a potential neurotoxin whose excitatory toxicity may lead to the death of nerve cells. To remain

the sensitivity of the synaptic transmission, astrocytes timely ingest and buffer glutamate through high-sodium-dependent excitatory amino acid transporters (EAAT) including EAAT1/GLAST and EAAT2/GLT-1. Glutamate is then converted into glutamine by the enzyme glutamine synthetase (GS) in astrocytes and released extracellular, where it will be reabsorbed by neurons into a new cycle [114]. In addition to terminating synaptic transmission, glutamate clearance by astrocytes could also prevent excitotoxicity, functional impairment, or neuron death due to high level of glutamate [115, 116]. In the early stage, researchers selectively inhibited the expression of glutamate vector in astrocytes by using antisense nucleic acid technology, leading to astroglial reactivity characterized by dramatically increased concentration of extracellular glutamate, and the neurons eventually deteriorated due to excitotoxicity. In addition, it has been verified that neurons release large amounts of glutamate during cerebral anemia, and astrocytes subsequently absorb glutamate to protect neurons from damage. In infection, inflammation, hypoxia, ischemia, trauma, and various pathologies like Alzheimer, the ability of GS to recover and convert glutamate was suppressed, leading to neuroexcitatory toxicity and neuronal death [116, 117]. Similarly, mycotoxin-mediated astrocyte injury also inhibited the uptake of glutamate and induced a large accumulation of extracellular glutamate. For example, DON decreased the expression of EAAT on the plasma membrane of astrocytes in time-dependent manner at 1 and 10  $\mu\text{M}$ , thereby inhibiting the function of taking in L-glutamate from the synaptic gap. The  $\text{IC}_{50}$  of this inhibition was 50 nM, which had no correlation with the DON toxic-mediated decline in astrocyte activity [92]. In recent reports, OTA affected the membrane insertion state of EAATs in cell surface of primary astrocytes, and the expression of glutamate transporter 1 (GLT1) was also downregulated by OTA infection, resulting in the failure of L-glutamate capture in the nervous system [118]. Now we know that these mycotoxins could inhibit manipulation of neurotransmitters in limited findings, suggesting that all neural activity associated with information transmission could be regulated by mycotoxins in our environment through the glial cells (Figure 4).

## 9. Conclusions

On the basis of existing studies in regard to mammalian nervous system diseases, the important position of glial cells in the CNS has been increasingly recognized. The homeostasis of the brain environment, the transmission of synaptic information, the integrity of the BBB, and the survival of neurons are all maintained and monitored by glial cells, including microglia and astrocytes. Once the viability and function of glial cells were lost, neurological diseases and neuronal death characterized by abnormal glial cells would be triggered. It is tempting to liken the glial cells, led by astrocytes and microglia, to the umbrella of the CNS, where exogenous stimuli with neurotoxic effects could more or less destroy these guardian, causing neurological damage. In view of the more frequent occurrence of mycotoxin overdose and

poisoning in the consumption of substandard food and feed, mycotoxins have been gradually included in the research of potential neurotoxins. Recent studies have found that mycotoxins such as AFB1, DON, T-2, OTA, FB1, and 3-NPA could cross the BBB, accumulate in the brain, and disrupt the normal order of CNS. In addition, glial cells, especially astrocytes and microglia, have been found to be significantly affected by the toxicity of mycotoxins, which possibly because they are themselves immunosensors and inflammatory effector cells. Compared with other neural accessory cells, these two glial cells tend to be more sensitive to mycotoxins and exhibit toxic effects more obviously.

As illustrated in Figure 5, astrocytes and microglial cells were activated by mycotoxins in different forms; the expression of GFAP and MMP2 in the former was adjusted, and the ratio of M1 and M2 activation phenotypes in the latter was changed. Whatever, excessive activation of glial cells could bring out subsequent glial cell toxicity effect: (i) ROS and RNS were accumulated in oxidative stress damage; (ii) mitochondrial function was impaired, aggravating ATP depletion and calcium imbalance; (iii) the ability to buffer transmitters such as glutamate was inhibited, inducing neural defects; (iv) the viability of glial cells was decreased, cell proliferation was inhibited at the G0/G1 stage, and the release of proinflammatory factors changed dramatically, resulting in apoptosis or necrosis of the cells eventually; (v) the activation of the p53 pathway, MAPK pathway, JAK/STAT pathway, and AKT pathway is involved in mycotoxin-induced apoptosis. According to the related research, we can analyze that even low-dose food-derived mycotoxins could mediate brain damage and neuronal death through glial cytotoxicity and promote the occurrence of pathological neuroinflammation and neurodegenerative diseases. It is important to note that the incidence of neurodegenerative diseases is increasing, which affects the normal neurogenic behaviour of human beings. Neurodegenerative diseases are closely related to environmental changes, and in fact, mycotoxin contamination has been one of the major problems caused by environmental changes. Therefore, mycotoxin-induced nerve damage is expected to become the key to deal with to the trend of neurodegenerative diseases. Of course, these evidences could further guide researchers to explore the connections between glial cells and other important components in the common microenvironment of CNS, such as the complex regulatory mechanisms between glial cells and various neurons that are simultaneously exposed to mycotoxin. In addition, the combined neurotoxicity of different mycotoxins in vivo and in vivo may also be the next research target, given that their synergistic mutagenesis has been demonstrated in other cells. Most importantly, the glial toxicity of mycotoxins reminds us to develop neuroprotective agents targeting glial cells in order to effectively respond to neurological diseases, such as Alzheimer's, Parkinson's, and Huntington's diseases. In conclusion, understanding the link between mycotoxins and glial injury could help us more comprehensively and effectively assess the risks of animal feed and food and also provide data support for drug new targets in CNS, so as to overcome more clinical troubles. Given the difficulty in completely avoiding

mycotoxins in food crops and the absence of visible warning labels on raw materials and consumer goods, real-time and efficient supervision on food security remains the primary tasks of ensuring human and animal health.

## Conflicts of Interest

The authors declare that there is no conflict of interest regarding the publication of this paper.

## Acknowledgments

This review article was funded by the Research Project of Tianjin Education Commission (2019KJ034), the National Natural Science Foundation of China (31972740), the Major Science and Technology Innovation Project of Shandong Province (2019JZZY010735), and the Talent Cultivation Program of China Agricultural University.

## References

- [1] J. Pleadin, J. Frece, and K. Markov, "Mycotoxins in food and feed," *Advances in Food and Nutrition Research*, vol. 89, pp. 297–345, 2019.
- [2] R. Coffey, E. Cummins, and S. Ward, "Exposure assessment of mycotoxins in dairy milk," *Food Control*, vol. 20, no. 3, pp. 239–249, 2009.
- [3] D. T. Asefa, C. F. Kure, R. O. Gjerde et al., "A HACCP plan for mycotoxigenic hazards associated with dry-cured meat production processes," *Food Control*, vol. 22, no. 6, pp. 831–837, 2011.
- [4] S. Cavret and S. Lecoecur, "Fusariotoxin transfer in animal," *Food and Chemical Toxicology*, vol. 44, no. 3, pp. 444–453, 2006.
- [5] F. Fleurat-Lessard, "Integrated management of the risks of stored grain spoilage by seedborne fungi and contamination by storage mould mycotoxins - An update," *Journal of Stored Products Research*, vol. 71, pp. 22–40, 2017.
- [6] J. Pleadin, J. Frece, N. Kudumija et al., "Citrinin in cereals and feedstuffs coming from Croatia and Bosnia & Herzegovina," *Food Additives & Contaminants Part B, Surveillance*, vol. 9, no. 4, pp. 268–274, 2016.
- [7] WHO, *Food Irradiation: A Technique for Preserving and Improving the Safety of Food*, World Health Organization, Geneva, 1988, October 2018, <http://www.who.int/iris/handle/10665/38544>.
- [8] E. M. Binder, L. M. Tan, L. J. Chin, J. Handl, and J. Richard, "Worldwide occurrence of mycotoxins in commodities, feeds and feed ingredients," *Animal Feed Science and Technology*, vol. 137, no. 3–4, pp. 265–282, 2007.
- [9] J. Pleadin, N. Vahčić, N. Perši, D. Švelj, K. Markov, and J. Frece, "Fusarium\_ mycotoxins' occurrence in cereals harvested from Croatian fields," *Food Control*, vol. 32, no. 1, pp. 49–54, 2013.
- [10] Y. Fu, F. He, S. Zhang, and X. Jiao, "Consistent striatal damage in rats induced by 3-nitropropionic acid and cultures of arthrinium fungus," *Neurotoxicology and Teratology*, vol. 17, no. 4, pp. 413–418, 1995.
- [11] L. Ming, "Moldy sugarcane poisoning—a case report with a brief review," *Journal of Toxicology Clinical Toxicology*, vol. 33, no. 4, pp. 363–367, 1995.
- [12] L. B. Bullerman and A. Bianchini, "Stability of mycotoxins during food processing," *International Journal of Food Microbiology*, vol. 119, no. 1–2, pp. 140–146, 2007.
- [13] IARC, "Some naturally occurring and synthetic food components, furocoumarins and ultraviolet radiation," in *IARC Monographs on the Evaluation of the Carcinogenic Risk of Chemicals to Humans*, vol. 40, pp. 1–415, IARC Working Group, Lyon, 1986.
- [14] CAST, *Mycotoxins: Risk in Plant, Animal and Human Systems*, Council for Agricultural Science and Technology. Task Force Report No, Ames, Iowa, USA, 2003.
- [15] J. W. Bennett and M. Klich, "Mycotoxins," *Clinical Microbiology Reviews*, vol. 16, no. 3, pp. 497–516, 2003.
- [16] E. E. Creppy, "Update of survey, regulation and toxic effects of mycotoxins in Europe," *Toxicology Letters*, vol. 127, no. 1–3, pp. 19–28, 2002.
- [17] A. Belmadani, P. S. Steyn, G. Tramu, A. M. Betbeder, I. Baudrimont, and E. E. Creppy, "Selective toxicity of ochratoxin A in primary cultures from different brain regions," *Archives of Toxicology*, vol. 73, no. 2, pp. 108–114, 1999.
- [18] A. Bruinink, T. Rasonyi, and C. Sidler, "Differences in neurotoxic effects of ochratoxin A, ochracin and ochratoxin-alpha in vitro," *Natural Toxins*, vol. 6, no. 5, pp. 173–177, 1998.
- [19] K. N. Corps, Z. Islam, J. J. Pestka, and J. R. Harkema, "Neurotoxic, inflammatory, and mucosecretory responses in the nasal airways of mice repeatedly exposed to the macrocyclic trichothecene mycotoxin roridin A: dose-response and persistence of injury," *Toxicologic Pathology*, vol. 38, no. 3, pp. 429–451, 2010.
- [20] J. Zhang, L. You, W. Wu et al., "The neurotoxicity of trichothecenes T-2 toxin and deoxynivalenol (DON): current status and future perspectives," *Food and Chemical Toxicology*, vol. 145, article 111676, 2020.
- [21] R. H. ElMazouy and A. A. Attia, "Endocrine-disrupting and cytotoxic potential of anticholinesterase insecticide, diazinon in reproductive toxicity of male mice," *Journal of Hazardous Materials*, vol. 209–210, pp. 111–120, 2012.
- [22] J. Ravindran, M. Agrawal, N. Gupta, and P. V. Rao, "Alteration of blood brain barrier permeability by T-2 toxin: role of MMP-9 and inflammatory cytokines," *Toxicology*, vol. 280, no. 1–2, pp. 44–52, 2011.
- [23] M. Weidner, M. Lenczyk, G. Schwerdt, M. Gekle, and H. U. Humpf, "Neurotoxic potential and cellular uptake of T-2 toxin in human astrocytes in primary culture," *Chemical Research in Toxicology*, vol. 26, no. 3, pp. 347–355, 2013.
- [24] X. Jin, T. R. Riew, H. L. Kim, S. Kim, and M. Y. Lee, "Spatio-temporal expression of GRP78 in the blood vessels of rats treated with 3-nitropropionic acid correlates with blood-brain barrier disruption," *Frontiers in Cellular Neuroscience*, vol. 12, p. 434, 2018.
- [25] A. Ayala, J. L. Venero, J. Cano, and A. Machado, "Mitochondrial toxins and neurodegenerative diseases," *Frontiers in Bioscience*, vol. 12, no. 1, pp. 986–1007, 2007.
- [26] J. Duran-Vilaregut, V. J. Del, G. Manich et al., "Role of matrix metalloproteinase-9 (MMP-9) in striatal blood-brain barrier disruption in a 3-nitropropionic acid model of Huntington's disease," *Neuropathology and Applied Neurobiology*, vol. 37, no. 5, pp. 525–537, 2011.
- [27] M. Jang, J. H. Choi, Y. Chang, S. J. Lee, S. Y. Nah, and I. H. Cho, "Gintonin, a ginseng-derived ingredient, as a novel therapeutic strategy for Huntington's disease: Activation of the



- Nrf2 pathway through lysophosphatidic acid receptors,” *Brain, Behavior, and Immunity*, vol. 80, pp. 146–162, 2019.
- [28] A. Mezzelani, M. E. Raggi, A. Marabotti, and L. Milanesi, “Ochratoxin A as possible factor triggering autism and its male prevalence via epigenetic mechanism,” *Nutritional Neuroscience*, vol. 19, no. 1, pp. 43–46, 2016.
- [29] A. M. Malvandi, J. Mehrzad, and M. Saleh-moghaddam, “Biologically relevant doses of mixed aflatoxins B and G up-regulate MyD88, TLR2, TLR4 and CD14 transcripts in human PBMCs,” *Immunopharmacology and immunotoxicology*, vol. 35, no. 4, pp. 528–532, 2013.
- [30] J. Mehrzad, M. Milani, and M. Mahmoudi, “Naturally occurring level of mixed aflatoxins B and G stimulate toll-like receptor-4 in bovine mononuclear cells,” *The Veterinary Quarterly*, vol. 33, no. 4, pp. 186–190, 2013.
- [31] A. Mohammadi, J. Mehrzad, M. Mahmoudi, and M. Schneider, “Environmentally relevant level of aflatoxin B1 dysregulates human dendritic cells through signaling on key toll-like receptors,” *International Journal of Toxicology*, vol. 33, no. 3, pp. 175–186, 2014.
- [32] J. Mehrzad, S. Hosseinkhani, and A. M. Malvandi, “Human microglial cells undergo proapoptotic induction and inflammatory activation upon in vitro exposure to a naturally occurring level of aflatoxin B<sub>1</sub>,” *Neuroimmunomodulation*, vol. 25, no. 3, pp. 176–183, 2018.
- [33] B. R. Crago, M. R. Gray, L. A. Nelson, M. Davis, L. Arnold, and J. D. Thrasher, “Psychological, neuropsychological, and electrocortical effects of mixed mold exposure,” *Archives of Environmental Health*, vol. 58, no. 8, pp. 452–463, 2003.
- [34] A. M. Ratnaseelan, I. Tsilioni, and T. C. Theoharides, “Effects of mycotoxins on neuropsychiatric symptoms and immune processes,” *Clinical Therapeutics*, vol. 40, no. 6, pp. 903–917, 2018.
- [35] E. C. Anyanwu, A. W. Campbell, and A. Vojdani, “Neurophysiological effects of chronic indoor environmental toxic mold exposure on children,” *Scientific World Journal*, vol. 3, pp. 281–290, 2003.
- [36] B. De Santis, C. Brera, A. Mezzelani et al., “Role of mycotoxins in the pathobiology of autism: a first evidence,” *Nutritional Neuroscience*, vol. 22, no. 2, pp. 132–144, 2019.
- [37] S. T. Dheen, C. Kaur, and E. A. Ling, “Microglial activation and its implications in the brain diseases,” *Current Medicinal Chemistry*, vol. 14, no. 11, pp. 1189–1197, 2007.
- [38] C. Farina, F. Aloisi, and E. Meinl, “Astrocytes are active players in cerebral innate immunity,” *Trends in Immunology*, vol. 28, no. 3, pp. 138–145, 2007.
- [39] M. Machado-Pereira, T. Santos, L. Bernardino, and R. Ferreira, “Vascular inter-regulation of inflammation: molecular and cellular targets for CNS therapy,” *Journal of Neurochemistry*, vol. 140, no. 5, pp. 692–702, 2017.
- [40] H. Wake, A. J. Moorhouse, and J. Nabekura, “Functions of microglia in the central nervous system—beyond the immune response,” *Neuron Glia Biology*, vol. 7, no. 1, pp. 47–53, 2011.
- [41] R. Medzhitov, “Origin and physiological roles of inflammation,” *Nature*, vol. 454, no. 7203, pp. 428–435, 2008.
- [42] R. Franco, S. Li, H. Rodriguez-Rocha, M. Burns, and M. I. Panayiotidis, “Molecular mechanisms of pesticide-induced neurotoxicity: Relevance to Parkinson’s disease,” *Chemico-Biological Interactions*, vol. 188, no. 2, pp. 289–300, 2010.
- [43] D. S. Kiss, E. Ioja, I. Toth et al., “Comparative analysis of zearalenone effects on thyroid receptor alpha (TR $\alpha$ ) and beta (TR $\beta$ ) expression in rat primary cerebellar cell cultures,” *International Journal of Molecular Sciences*, vol. 19, no. 5, p. 1440, 2018.
- [44] A. M. Domijan, “Fumonisin B (1): a neurotoxic mycotoxin,” *Arhiv za Higijenu Rada i Toksikologiju*, vol. 63, no. 4, pp. 531–544, 2012.
- [45] Y. Dong and E. N. Benveniste, “Immune function of astrocytes,” *Glia*, vol. 36, no. 2, pp. 180–190, 2001.
- [46] D. R. Li, T. Ishikawa, D. Zhao et al., “Histopathological changes of the hippocampus neurons in brain injury,” *Histology and Histopathology*, vol. 24, no. 9, pp. 1113–1120, 2009.
- [47] F. Monnet-Tschudi, M. G. Zurich, and P. Honegger, “Neurotoxicant-induced inflammatory response in three-dimensional brain cell cultures,” *Human & Experimental Toxicology*, vol. 26, pp. 339–346, 2007.
- [48] Z. Cai, C. Q. Wan, and Z. Liu, “Astrocyte and Alzheimer’s disease,” *Journal of Neurology*, vol. 264, no. 10, pp. 2068–2074, 2017.
- [49] M. J. Webster, J. O’Grady, J. E. Kleinman, and C. S. Weickert, “Glial fibrillary acidic protein mRNA levels in the cingulate cortex of individuals with depression, bipolar disorder and schizophrenia,” *Neuroscience*, vol. 133, no. 2, pp. 453–461, 2005.
- [50] H. Turkez and F. Geyikoglu, “Boric acid: a potential chemoprotective agent against aflatoxin b (1) toxicity in human blood,” *Cytotechnology*, vol. 62, no. 2, pp. 157–165, 2010.
- [51] L. F. Eng and R. S. Ghirnikar, “GFAP and astrogliosis,” *Brain Pathology*, vol. 4, no. 3, pp. 229–237, 1994.
- [52] P. R. Angelova and A. Y. Abramov, “Interaction of neurons and astrocytes underlies the mechanism of A $\beta$ -induced neurotoxicity,” *Biochemical Society Transactions*, vol. 42, no. 5, pp. 1286–1290, 2014.
- [53] S. Gupta, P. Goswami, J. Biswas et al., “6-Hydroxydopamine and lipopolysaccharides induced DNA damage in astrocytes: involvement of nitric oxide and mitochondria,” *Mutation Research, Genetic Toxicology and Environmental Mutagenesis*, vol. 778, pp. 22–36, 2015.
- [54] N. L. Johnston-Wilson, C. D. Sims, J. P. Hofmann et al., “Disease-specific alterations in frontal cortex brain proteins in schizophrenia, bipolar disorder, and major depressive disorder,” *Molecular Psychiatry*, vol. 5, no. 2, pp. 142–149, 2000.
- [55] J. Hidalgo, M. Aschner, P. Zatta, and M. Vasak, “Roles of the metallothionein family of proteins in the central nervous system,” *Brain Research Bulletin*, vol. 55, no. 2, pp. 133–145, 2001.
- [56] H. Takano, K. Inoue, R. Yanagisawa et al., “Protective role of metallothionein in acute lung injury induced by bacterial endotoxin,” *Thorax*, vol. 59, no. 12, pp. 1057–1062, 2004.
- [57] Q. Pan, C. He, H. Liu et al., “Microvascular endothelial cells-derived microvesicles imply in ischemic stroke by modulating astrocyte and blood brain barrier function and cerebral blood flow,” *Molecular Brain*, vol. 9, no. 1, p. 63, 2016.
- [58] T. Tanaka, H. Abe, M. Kimura et al., “Developmental exposure to T-2 toxin reversibly affects postnatal hippocampal neurogenesis and reduces neural stem cells and progenitor cells in mice,” *Archives of Toxicology*, vol. 90, pp. 2009–2024, 2016.
- [59] N. G. Bahey, E. H. Abd, and K. K. Gadalla, “Toxic effect of aflatoxin B1 and the role of recovery on the rat cerebral cortex and hippocampus,” *Tissue & Cell*, vol. 47, no. 6, pp. 559–566, 2015.

- [60] A. Alsayyah, R. ElMazoudy, M. Al-Namshan, M. Al-Jafary, and N. Alaqeel, "Chronic neurodegeneration by aflatoxin B1 depends on alterations of brain enzyme activity and immunoeexpression of astrocyte in male rats," *Ecotoxicology and Environmental Safety*, vol. 182, article 109407, 2019.
- [61] R. S. Ashton, A. Conway, C. Pangarkar et al., "Astrocytes regulate adult hippocampal neurogenesis through ephrin-B signaling," *Nature Neuroscience*, vol. 15, no. 10, pp. 1399–1406, 2012.
- [62] K. A. Kigerl, J. C. Gensel, D. P. Ankeny, J. K. Alexander, D. J. Donnelly, and P. G. Popovich, "Identification of two distinct macrophage subsets with divergent effects causing either neurotoxicity or regeneration in the injured mouse spinal cord," *The Journal of Neuroscience*, vol. 29, no. 43, pp. 13435–13444, 2009.
- [63] D. Boche, V. H. Perry, and J. A. Nicoll, "Review: activation patterns of microglia and their identification in the human brain," *Neuropathology and Applied Neurobiology*, vol. 39, no. 1, pp. 3–18, 2013.
- [64] M. Schwartz, O. Butovsky, W. Bruck, and U. K. Hanisch, "Microglial phenotype: is the commitment reversible?," *Trends in Neurosciences*, vol. 29, no. 2, pp. 68–74, 2006.
- [65] J. S. Von Tobel, P. Antinori, M. G. Zurich et al., "Repeated exposure to ochratoxin A generates a neuroinflammatory response, characterized by neurodegenerative M1 microglial phenotype," *Neurotoxicology*, vol. 44, pp. 61–70, 2014.
- [66] H. Fang, Y. Wu, J. Guo et al., "T-2 toxin induces apoptosis in differentiated murine embryonic stem cells through reactive oxygen species-mediated mitochondrial pathway," *Apoptosis*, vol. 17, no. 8, pp. 895–907, 2012.
- [67] X. Y. Fu, M. F. Yang, M. Z. Cao et al., "Strategy to suppress oxidative damage-induced neurotoxicity in PC12 cells by curcumin: the role of ROS-mediated DNA damage and the MAPK and AKT pathways," *Molecular Neurobiology*, vol. 53, pp. 369–378, 2016.
- [68] K. Nakajima, T. Tanaka, Y. Masubuchi et al., "Developmental exposure of mice to T-2 toxin increases astrocytes and hippocampal neural stem cells expressing metallothionein," *Neurotoxicity Research*, vol. 35, no. 3, pp. 668–683, 2019.
- [69] G. C. Brown, "Mechanisms of inflammatory neurodegeneration: iNOS and NADPH oxidase," *Biochemical Society Transactions*, vol. 35, no. 5, pp. 1119–1121, 2007.
- [70] J. Saura, "Microglial cells in astroglial cultures: a cautionary note," *Journal of Neuroinflammation*, vol. 4, no. 1, p. 26, 2007.
- [71] D. Shi, S. Liao, S. Guo, H. Li, M. Yang, and Z. Tang, "Protective effects of selenium on aflatoxin B1-induced mitochondrial permeability transition, DNA damage, and histological alterations in duckling liver," *Biological Trace Element Research*, vol. 163, no. 1–2, pp. 162–168, 2015.
- [72] E. E. Golli-Bennour, B. Kouidhi, A. Bouslimi, S. Abid-Essefi, W. Hassen, and H. Bacha, "Cytotoxicity and genotoxicity induced by aflatoxin B1, ochratoxin A, and their combination in cultured Vero cells," *Journal of Biochemical and Molecular Toxicology*, vol. 24, no. 1, pp. 42–50, 2010.
- [73] J. Mehrzad, A. M. Malvandi, M. Alipour, and S. Hosseinkhani, "Environmentally relevant level of aflatoxin B<sub>1</sub> elicits toxic pro-inflammatory response in murine CNS-derived cells," *Toxicology Letters*, vol. 279, pp. 96–106, 2017.
- [74] S. A. Liddelow, K. A. Guttenplan, L. E. Clarke et al., "Neurotoxic reactive astrocytes are induced by activated microglia," *Nature*, vol. 541, no. 7638, pp. 481–487, 2017.
- [75] M. G. Zurich, S. Lengacher, O. Braissant, F. Monnet-Tschudi, L. Pellerin, and P. Honegger, "Unusual astrocyte reactivity caused by the food mycotoxin ochratoxin A in aggregating rat brain cell cultures," *Neuroscience*, vol. 134, no. 3, pp. 771–782, 2005.
- [76] H. Stockmann-Juvala, J. Mikkola, J. Naarala, J. Loikkanen, E. Elovaara, and K. Savolainen, "Fumonisin B<sub>1</sub>-induced toxicity and oxidative damage in U-118MG glioblastoma cells," *Toxicology*, vol. 202, no. 3, pp. 173–183, 2004.
- [77] S. Abel and W. C. Gelderblom, "Oxidative damage and fumonisin B<sub>1</sub>-induced toxicity in primary rat hepatocytes and rat liver in vivo," *Toxicology*, vol. 131, no. 2–3, pp. 121–131, 1998.
- [78] C. Dai, G. D. Ciccotosto, R. Cappai et al., "Curcumin attenuates colistin-induced neurotoxicity in N2a cells via anti-inflammatory activity, suppression of oxidative stress, and apoptosis," *Molecular Neurobiology*, vol. 55, no. 1, pp. 421–434, 2018.
- [79] M. T. Islam, S. K. Mishra, S. Tripathi et al., "Mycotoxin-assisted mitochondrial dysfunction and cytotoxicity: unexploited tools against proliferative disorders," *IUBMB Life*, vol. 70, no. 11, pp. 1084–1092, 2018.
- [80] X. V. Liu, V. Fielding-Singh, T. J. Iwashyna, J. Bhattacharya, and G. J. Escobar, "Reply: the timing of early antibiotics and hospital mortality in sepsis: playing devil's advocate," *American Journal of Respiratory and Critical Care Medicine*, vol. 196, no. 7, pp. 935–936, 2017.
- [81] M. F. Osuchowski and R. P. Sharma, "Fumonisin B<sub>1</sub> induces necrotic cell death in BV-2 cells and murine cultured astrocytes and is antiproliferative in BV-2 cells while N2A cells and primary cortical neurons are resistant," *Neurotoxicology*, vol. 26, no. 6, pp. 981–992, 2005.
- [82] A. M. Domijan and A. Y. Abramov, "Fumonisin B<sub>1</sub> inhibits mitochondrial respiration and deregulates calcium homeostasis—implication to mechanism of cell toxicity," *The International Journal of Biochemistry & Cell Biology*, vol. 43, no. 6, pp. 897–904, 2011.
- [83] M. Santello and A. Volterra, "Synaptic modulation by astrocytes via Ca<sup>2+</sup>-dependent glutamate release," *Neuroscience*, vol. 158, no. 1, pp. 253–259, 2009.
- [84] E. Shigetomi, S. Patel, and B. S. Khakh, "Probing the complexities of astrocyte calcium signaling," *Trends in Cell Biology*, vol. 26, no. 4, pp. 300–312, 2016.
- [85] S. Park, J. Y. Lee, S. You, G. Song, and W. Lim, "Neurotoxic effects of aflatoxin B1 on human astrocytes *in vitro* and on glial cell development in zebrafish *in vivo*," *Journal of Hazardous Materials*, vol. 386, p. 121639, 2020.
- [86] H. Nishino, M. Kumazaki, A. Fukuda et al., "Acute 3-nitropropionic acid intoxication induces striatal astrocytic cell death and dysfunction of the blood-brain barrier: involvement of dopamine toxicity," *Neuroscience Research*, vol. 27, no. 4, pp. 343–355, 1997.
- [87] S. Park, W. Lim, S. You, and G. Song, "Ochratoxin A exerts neurotoxicity in human astrocytes through mitochondria-dependent apoptosis and intracellular calcium overload," *Toxicology Letters*, vol. 313, pp. 42–49, 2019.
- [88] Q. Wang, L. Huang, and J. Yue, "Oxidative stress activates the TRPM2-Ca<sup>2+</sup>-CaMKII-ROS signaling loop to induce cell death in cancer cells," *Biochimica et Biophysica Acta (BBA)-Molecular Cell Research*, vol. 1864, no. 6, pp. 957–967, 2017.
- [89] F. Monnet-Tschudi, M. G. Zurich, O. Sorg, J. M. Matthieu, P. Honegger, and B. Schilter, "The naturally occurring food

- mycotoxin fumonisin B1 impairs myelin formation in aggregating brain cell culture,” *Neurotoxicology*, vol. 20, no. 1, pp. 41–48, 1999.
- [90] F. Galvano, A. Campisi, A. Russo et al., “DNA damage in astrocytes exposed to fumonisin B<sub>1</sub>,” *Neurochemical Research*, vol. 27, no. 4, pp. 345–351, 2002.
- [91] T. A. Mobio, R. Anane, I. Baudrimont et al., “Epigenetic Properties of Fumonisin B<sub>1</sub>: Cell Cycle Arrest and DNA Base Modification in C6 Glioma Cells,” *Toxicology and Applied Pharmacology*, vol. 164, no. 1, pp. 91–96, 2000.
- [92] H. Razafimanjato, A. Benzaria, N. Taieb et al., “The ribotoxin deoxynivalenol affects the viability and functions of glial cells,” *Glia*, vol. 59, no. 11, pp. 1672–1683, 2011.
- [93] I. Wilk-Zasadna and M. Minta, “Developmental toxicity of ochratoxin A in rat embryo midbrain micromass cultures,” *International Journal of Molecular Sciences*, vol. 10, no. 1, pp. 37–49, 2009.
- [94] M. A. Dombrink-Kurtzman, R. Gomez-Flores, and R. J. Weber, “Activation of rat splenic macrophage and lymphocyte functions by fumonisin B<sub>1</sub>,” *Immunopharmacology*, vol. 49, no. 3, pp. 401–409, 2000.
- [95] E. M. Schmelz, M. A. Dombrink-Kurtzman, P. C. Roberts, Y. Kozutsumi, T. Kawasaki, and A. J. Merrill, “Induction of Apoptosis by Fumonisin B<sub>1</sub> in HT29 Cells Is Mediated by the Accumulation of Endogenous Free Sphingoid Bases,” *Toxicology and Applied Pharmacology*, vol. 148, no. 2, pp. 252–260, 1998.
- [96] H. Li, L. Xing, M. Zhang, J. Wang, and N. Zheng, “The toxic effects of aflatoxin B1 and aflatoxin M1 on kidney through regulating L-proline and downstream apoptosis,” *BioMed Research International*, vol. 2018, Article ID 9074861, 11 pages, 2018.
- [97] X. J. Yang, H. Y. Lu, Z. Y. Li et al., “Cytochrome P450 2A13 mediates aflatoxin B1-induced cytotoxicity and apoptosis in human bronchial epithelial cells,” *Toxicology*, vol. 300, no. 3, pp. 138–148, 2012.
- [98] X. Wang, C. Li, Y. Chen et al., “Hypoxia enhances CXCR4 expression favoring microglia migration via HIF-1 $\alpha$  activation,” *Biochemical and Biophysical Research Communications*, vol. 371, no. 2, pp. 283–288, 2008.
- [99] J. Saba, L. Carniglia, D. Ramirez et al., “Melanocortin 4 receptor activation protects striatal neurons and glial cells from 3-nitropropionic acid toxicity,” *Molecular and Cellular Neurosciences*, vol. 94, pp. 41–51, 2019.
- [100] K. Szydłowska, A. Gozdz, M. Dabrowski, M. Zawadzka, and B. Kaminska, “Prolonged activation of ERK triggers glutamate-induced apoptosis of astrocytes: neuroprotective effect of FK506,” *Journal of Neurochemistry*, vol. 113, no. 4, pp. 904–918, 2010.
- [101] C. H. Yu, Y. M. Lee, Y. P. Yun, and H. S. Yoo, “Differential effects of fumonisin B1 on cell death in cultured cells: the significance of the elevated sphinganine,” *Archives of Pharmacal Research*, vol. 24, no. 2, pp. 136–143, 2001.
- [102] M. Aschner, “Astrocytes as mediators of immune and inflammatory responses in the CNS,” *Neurotoxicology*, vol. 19, no. 2, pp. 269–281, 1998.
- [103] W. J. Streit, J. R. Conde, S. E. Fendrick, B. E. Flanary, and C. L. Mariani, “Role of microglia in the central nervous system’s immune response,” *Neurological Research*, vol. 27, no. 7, pp. 685–691, 2005.
- [104] T. C. Frank-Cannon, L. T. Alto, F. E. McAlpine, and M. G. Tansey, “Does neuroinflammation fan the flame in neurodegenerative diseases?,” *Molecular Neurodegeneration*, vol. 4, no. 1, p. 47, 2009.
- [105] N. Janabi, S. Peudener, B. Heron, K. H. Ng, and M. Tardieu, “Establishment of human microglial cell lines after transfection of primary cultures of embryonic microglial cells with the SV40 large T antigen,” *Neuroscience Letters*, vol. 195, no. 2, pp. 105–108, 1995.
- [106] H. Lassmann, “Multiple sclerosis pathology,” *Cold Spring Harbor Perspectives in Medicine*, vol. 8, no. 3, 2018.
- [107] C. Venegas, S. Kumar, B. S. Franklin et al., “Microglia-derived ASC specks cross-seed amyloid- $\beta$  in Alzheimer’s disease,” *Nature*, vol. 552, no. 7685, pp. 355–361, 2017.
- [108] W. Zhang, T. Wang, Z. Pei et al., “Aggregated alpha-synuclein activates microglia: a process leading to disease progression in Parkinson’s disease,” *The FASEB Journal*, vol. 19, no. 6, pp. 533–542, 2005.
- [109] M. Penkowa, M. Caceres, R. Borup et al., “Novel roles for metallothionein-I + II (MT-I + II) in defense responses, neurogenesis, and tissue restoration after traumatic brain injury: insights from global gene expression profiling in wild-type and MT-I + II knockout mice,” *Journal of Neuroscience Research*, vol. 84, no. 7, pp. 1452–1474, 2006.
- [110] X. Wu, C. Liu, L. Chen et al., “Protective effects of tauroursodeoxycholic acid on lipopolysaccharide-induced cognitive impairment and neurotoxicity in mice,” *International Immunopharmacology*, vol. 72, pp. 166–175, 2019.
- [111] M. Maresca, N. Yahi, L. Younes-Sakr, M. Boyron, B. Caporiccio, and J. Fantini, “Both direct and indirect effects account for the pro-inflammatory activity of enteropathogenic mycotoxins on the human intestinal epithelium: Stimulation of interleukin-8 secretion, potentiation of interleukin-1 $\beta$  effect and increase in the transepithelial passage of commensal bacteria,” *Toxicology and Applied Pharmacology*, vol. 228, no. 1, pp. 84–92, 2008.
- [112] J. Szelenyi, “Cytokines and the central nervous system,” *Brain Research Bulletin*, vol. 54, no. 4, pp. 329–338, 2001.
- [113] V. Gallo and C. A. Ghiani, “Glutamate receptors in glia: new cells, new inputs and new functions,” *Trends in Pharmacological Sciences*, vol. 21, no. 7, pp. 252–258, 2000.
- [114] D. D. Wang and A. Bordey, “The astrocyte odyssey,” *Progress in Neurobiology*, vol. 86, no. 4, pp. 342–367, 2008.
- [115] K. A. Nave, “Myelination and support of axonal integrity by glia,” *Nature*, vol. 468, no. 7321, pp. 244–252, 2010.
- [116] A. Schousboe and H. S. Waagepetersen, “Role of astrocytes in glutamate homeostasis: implications for excitotoxicity,” *Neurotoxicity Research*, vol. 8, no. 3-4, pp. 221–225, 2005.
- [117] S. Tilleux and E. Hermans, “Neuroinflammation and regulation of glial glutamate uptake in neurological disorders,” *Journal of Neuroscience Research*, vol. 85, no. 10, pp. 2059–2070, 2007.
- [118] H. Razafimanjato, N. Garmy, X. J. Guo et al., “The food-associated fungal neurotoxin ochratoxin A inhibits the absorption of glutamate by astrocytes through a decrease in cell surface expression of the excitatory amino-acid transporters GLAST and GLT-1,” *Neurotoxicology*, vol. 31, no. 5, pp. 475–484, 2010.

## Research Article

# Mitochondrial Protection and Against Glutamate Neurotoxicity via Shh/Ptch1 Signaling Pathway to Ameliorate Cognitive Dysfunction by Kaixin San in Multi-Infarct Dementia Rats

Xiaoqiong Li <sup>1,2</sup>, Wen Wen <sup>1,2</sup>, Ping Li <sup>1,2</sup>, Ying Fu <sup>1,2</sup>, Hao Chen <sup>1,2</sup>,  
Fushun Wang <sup>3</sup>, Yuan Dai <sup>1,4</sup>, and Shijun Xu <sup>1,2,5</sup>

<sup>1</sup>Institute of Material Medica Integration and Transformation for Brain Disorders, Chengdu University of Traditional Chinese Medicine, Chengdu, Sichuan 611137, China

<sup>2</sup>School of Pharmacy, Chengdu University of Traditional Chinese Medicine, Chengdu, Sichuan 611137, China

<sup>3</sup>Institute of Brain and Psychological Science, Sichuan Normal University, Chengdu 610060, China

<sup>4</sup>School of Health Preservation and Rehabilitation, Chengdu University of Traditional Chinese Medicine, Chengdu, Sichuan 610075, China

<sup>5</sup>State Key Laboratory of Southwestern Chinese Medicine Resources, Chengdu, Sichuan 611137, China

Correspondence should be addressed to Yuan Dai; [daiyuan@cdutcm.edu.cn](mailto:daiyuan@cdutcm.edu.cn) and Shijun Xu; [xushijun@cdutcm.edu.cn](mailto:xushijun@cdutcm.edu.cn)

Received 19 February 2021; Accepted 17 June 2021; Published 9 July 2021

Academic Editor: Xu Wu

Copyright © 2021 Xiaoqiong Li et al. This is an open access article distributed under the Creative Commons Attribution License, which permits unrestricted use, distribution, and reproduction in any medium, provided the original work is properly cited.

Multi-infarct dementia (MID), a prominent subtype of vascular dementia (VD), is responsible for at least 15 to 20 percent of dementia in the elderly. Mitochondrial dysfunctions and glutamate neurotoxicity due to chronic hypoperfusion and oxidative stress were regarded as the major risk factors in the pathogenesis. *Kaixin San* (KXS), a classic prescription of *Beiji Qianjin Yaofang*, was applied to treatment for “amnesia” and has been demonstrated to alleviate the cognitive deficit in a variety of dementias, including MID. However, little is known whether mitochondria and glutamate are associated with the protection of KXS in MID treatment. The aim of this study was to investigate the role of KXS in improving the cognitive function of MID rats through strengthening mitochondrial functions and antagonizing glutamate neurotoxicity via the Shh/Ptch1 signaling pathway. Our data showed that KXS significantly ameliorated memory impairment and hippocampal neuron damage in MID rats. Moreover, KXS improved hippocampal mitochondrial functions by reducing the degree of mitochondrial swelling, increasing the mitochondrial membrane potential (MMP), and elevating the energy charge (EC) and ATP content in MID rats. As expected, the concentration of glutamate and the expression of p-NMDAR1 were significantly reduced by KXS in the brain tissue of MID rats. Furthermore, our results showed that KXS noticeably activated the Shh/Ptch1 signaling pathway which was demonstrated by remarkable elevations of Ptch1, Smo, and Gli1 protein levels in the brain tissue of MID rats. Intriguingly, the inhibition of the Shh signaling pathway with cyclopamine significantly inhibited the protective effects of KXS on glutamate-induced neurotoxicity in PC12 cells. To sum up, these findings suggested that KXS protected MID rats from memory loss by rescuing mitochondrial functions as well as against glutamate neurotoxicity through activating Shh/Ptch1 signaling pathway.

## 1. Introduction

Multi-infarct dementia (MID) is a prominent subtype of vascular dementia (VD) and is responsible for at least 15 to 20 percent of dementia in the elderly. It is widely known that

multiple lesions, infarction of small arteries in the cerebral gray-white matter, and neuronal degeneration are its characteristic lesion [1, 2]. MID is resulted from atherosclerotic disease in large arteries (e.g., carotid) with widespread thromboembolic events, accompanied with chronic cerebral

hypoperfusion, which leads to obvious brain pathological damage and cognitive impairment [3–5]. Cerebral ischemia caused by chronic hypoperfusion could induce cerebral hypoxic and result in the production of reactive oxygen species (ROS) and excitatory amino acid (EAA), such as glutamate [6], which directly impair mitochondrial homeostasis and energy production [4, 7]. Therefore, flawed energy metabolism and accumulated EAA in the brain are usually considered as the hallmarks in the pathogenesis of MID. The mitochondria are a cell's power packs and responsible for the energy supply of nerve cells as well as neurotoxicity through oxidative phosphorylation. The hippocampal structure in the brain is the core division for spatial cognitive activity, and its mitochondria are very sensitive to ROS and energy deficit, thus, hippocampal mitochondrial dysfunction plays a key role in cerebral ischemia-induced cognitive impairment [8]. In addition, glutamate outflow and excessive extracellular glutamate accumulation resulted from the death of nerve cells due to energy deficit in turn could also lead to ischemic neuronal death and cognitive disorder [9, 10]. Previous studies suggested that cognitive deficit could be alleviated by reversing brain mitochondrial dysfunction and reducing excessive glutamate content in MID rats [4, 11, 12].

The sonic hedgehog (Shh)/patched1 (Ptch1) pathway plays an important role in cell development, proliferation, pattern, and fate specification [13–15], which mainly includes Shh ligand, its receptor patched (Ptch1), and the pathway activator smoothened (Smo) receptors. Briefly, the binding of Shh to Ptch1 results in release of Smo, Smo activation, and subsequent activation of Gli transcription factors (Gli1, Gli2, and Gli3) [16]. Current investigations had suggested that activating Shh/Ptch1 signaling pathway could improve neurological function and alleviate vascular cognitive impairment [17–19] and protect brain tissue from cerebral ischemia injury [20]. Importantly, the improvement of mitochondrial function and the antagonism of glutamate neurotoxicity of hippocampal neurons via activating Shh signaling pathway had been reported [21, 22], which indicated that Shh/Ptch1-mediated mitochondrial function and glutamate neurotoxicity played a critical role in alleviating damage of chronic hypoperfusion in MID.

*Kaixin San* (KXS), a classic prescription of *Beiji Qianjin Yaofang*, was used to treat “amnesia” for thousand years in China and Southeast Asia. KXS is composed of *Panax ginseng* C.A. Meyer. (Renshen), *Poria cocos* (Schw.) Wolf (Fuling), *Polygala tenuifolia* Willd. (Yuanzhi), and *Acorus tatarinowii* Schott (Shichangpu). KXS had been reported to improve cognitive dysfunction in many animal models of Alzheimer's disease (AD). Increasing number of studies had also shown that these four herbs or combinations of them were frequently used to alleviate the cognitive deficit in dementia, such as VD and AD [23–25]. Our previous studies had shown that KXS could alleviate memory impairment through decreasing the content of  $\gamma$ -aminobutyric acid (GABA) and inducible nitric oxide synthase (iNOS) or elevating the ATP content of brain tissue in MID rats [26]. However, the underlying mechanisms of KXS treating MID remain unclear.

In this study, we investigated the effects of KXS on rescuing cognitive damage in MID rats based on its effects on regulating mitochondrial function and glutamate neurotoxicity via activating the Shh/Ptch1 signaling pathway. Our data showed that KXS provided a neuroprotective effect on cognitive impairment via improving mitochondrial function and inhibiting glutamate neurotoxicity by activating Shh/Ptch1 signaling pathway in MID rats. Furthermore, our data also proved that Shh/Ptch1 signaling pathway played a key role of against glutamate neurotoxicity of KXS *in vitro*.

## 2. Materials and Methods

**2.1. Animals and Cell Line.** 65 male Sprague-Dawley rats (200 ± 20 g, SPF) were purchased from Chengdu dashuo experimental animal Co., Ltd. (Chengdu, China) and used in this research. All rats were housed in an animal observation room of Chengdu University of Traditional Chinese Medicine (temperature: 22 ± 2°C, humidity: 65 ± 5%, 12-hour light/dark cycle) and were free to access water and food. The experimental procedure was approved by the Ethics Committee for Animal Experiments of the Institute of Material Medica Integration and Transformation for Brain Disorders (Chengdu University traditional Chinese medicine, No. IBD2017013) and carried out in accordance with the NIH Guide for the Care and Use of Laboratory Animals (NIH Publication No. 85-23, 1985, revised 1996). Rat pheochromocytoma-derived cell line PC12 cells (high differentiation) were obtained from the cell bank of the Chinese Academy of Sciences (Shanghai, China).

**2.2. Materials and Reagents.** Mesylate dihydroergotamine tablets (Lot No. 7C883T) were purchased from Tianjin Huajin Pharmaceutical Co., Ltd. (Tianjin, China). Adenosine triphosphate (ATP) disodium salt (Lot No. 1001665443), adenosine diphosphate (ADP) disodium salt (Lot No. 101606467), adenosine monophosphate (AMP) disodium salt (Lot No. 1001726877), and glutamate (Lot # SLCD3953) were obtained from Sigma-Aldrich (USA). Cyclopamine (Cyc, Cat.# HY-17024/CS-0633) was provided by Med Chem Express (MCE). The glutamic acid measurement kit (Cat.NoA07411) was supplied by Nanjing Jiancheng Bioengineering Institute (Nanjing, China). Tissue mitochondria isolation kit (Cat.NoC3606) was furnished by Beyotime Institute of Biotechnology (Shanghai, China). JC-1 kit (Cat. No 551302) was produced by Becton-Dickinson and Company (USA). Primary antibodies, including Smo (66851-1-Ig) and Gli1 (66905-1-Ig), were provided by Wuhan Sanying Biotechnology Co., Ltd., (Wuhan, China); NMDAR1 (5704S) and p-NMDAR1 (3384S) were obtained from Cell Signaling Technology (USA); Ptch1 (NBP1-71662) was provided by Novus (USA).

**2.3. Preparation and Analysis of KXS Extract.** *Panax ginseng* C.A. Meyer. (Renshen), *Poria cocos* (Schw.) Wolf (Fuling), *Polygala tenuifolia* Willd. (Yuanzhi), and *Acorus tatarinowii* Schott (Shichangpu) were purchased from the pharmacy of Affiliated Hospital of Chengdu University of Traditional Chinese Medicine (Chengdu, China). Renshen, Fuling,

Yuanzhi, and Shichangpu were mixed at a ratio of 3:3:2:2 as reported previously [23, 27]. The above four Chinese herbal pieces were soaked with 6 times of distilled water for 1 hour and then boiled 3 times for 1.5 h every time. The three decoctions were merged, filtered, and condensed to 0.6 g/mL at 80°C for animals administrated or 10 g/mL for high-performance liquid chromatography (HPLC) analysis. A moderate amount of KXS extracts was dissolved in methanol, centrifuged (13,000 rpm, 10 min), and filtered through 0.22  $\mu\text{m}$  filter before HPLC analysis. The Agilent 1260 Infinity High-Performance Liquid Chromatography instrument (Agilent Technologies, Inc.) was used to analyze the KXS extract solution, and chromatographic separation was performed using an Agilent C18 Column (4.6  $\times$  250 mm, 5  $\mu\text{m}$ ; Agilent Technologies, Inc.) with a column temperature of 25°C, flow rate of 1 mL/min, and injection volume of 10  $\mu\text{L}$ . A gradient elution was provided with 0.1% formic acid water as solvent A (80%~20%) and acetonitrile as solvent B (20%~80%), and the effluent absorbance was measured at 210 nm and 320 nm. The concentration of ginsenoside Rg1, ginsenoside Rd, ginsenoside Rb1, polygalaxanthone III, and 3,6'-disinapoyl sucrose were used as reference compounds to verify the main components of KXS extracts. For cell studies, the extracts were dried by a freeze dryer into powder for storage. Before the treatment, the powder was redissolved with water and filtered through a 0.22  $\mu\text{m}$  filter to obtain KXS extracts.

**2.4. Animal Model and Administration.** As previously reported, an animal model of MID was established by injecting homologous blood emboli into the right internal carotid artery of male Sprague-Dawley rats [28]. Briefly, rat microthrombus of 150-180  $\mu\text{m}$  fine particles was prepared in 20 mg/6 mL normal saline suspension early. After rats were anesthetized by pentobarbital sodium 40 mg/kg, the right internal carotid artery was exposed, and 0.4 mL microthrombus suspension was injected into the right internal carotid artery in each rat to induce MID. The same surgical procedure was implemented in the sham-operation group, but microthrombus suspension was replaced with 0.4 mL normal saline. Our previous study had proved that the dose (high-dose KXS, 2.12 g/kg and low-dose KXS, 1.06 g/kg) and the duration of treatment (once a day for 45 days) of KXS had great therapeutic effects on MID rats [26]. Therefore, we refer to the previous dose and time of administration of KXS in this experiment. Two weeks later, the survive rats ( $n = 50$ ) were randomly divided into model group ( $n = 10$ ), hydergine group (0.7 mg/kg,  $n = 10$ , hydergine is the most commonly used vasodilator in the treatment of MID, we used it as a positive control to evaluate rats model and effectiveness of KXS), high-dose KXS group (KXS H, 2.12 g/kg,  $n = 10$ ), and low-dose KXS group (KXS L, 1.06 g/kg,  $n = 10$ ) according to body weight. Besides, 10 sham-operated rats were used as control group. All animals were orally 10 mL/kg administered with respective drugs except the control group (administered with normal saline) once a day for 45 d.

**2.5. Morris Water Maze Test.** Eight rats in each group were tested in Morris Water Maze to assess the cognitive function.

The rats were placed in an EthoVision XT Morris water maze video tracking test system that can automatically record time for rats to find the platform. The procedure was performed as previously described [29]. On the 40th day of drug intervention, a 5-day hidden platform experiment started. The training time was 60 s, and all animals were trained twice a day. The time of finding the platform was recorded as the escape latency. Attentively, it needed to be artificially guided to stay on the platform for 10 s, and the escape latency was recorded as 60 s if the rat did not find the platform in the first five days. On the sixth day, the platform was removed to test the spatial search ability of the rats, following the frequency of rats passed through where the platform was initially placed was recorded [30], the percent of time staying in target quadrant and the time of first arrival at the platform zone within 60 s were calculated.

**2.6. Hematoxylin and Eosin Staining.** The left hemisphere of six rats in each group was fixed with 4% paraformaldehyde, dehydrated, and embedded, cut into 5  $\mu\text{m}$  slices, then stained by hematoxylin for 30 min and eosin for 5 min, vitrified with xylene, and sealed with neutral resin. The stained slices were observed and photographed under an optical microscope for examining the pathological changes in the hippocampal CA1 region.

**2.7. Measurement of the Mitochondrial Swelling and MMP.** Mitochondrial swelling and mitochondrial membrane potential (MMP) were measured with flow cytometry (FCM). The hippocampal mitochondria of three rats in each group were extracted strictly according to the tissue mitochondria isolation kit. The isolated mitochondria were resuspended with mitochondria storage buffer and adjusted to a concentration of  $1 \times 10^5$  cells/mL per tube, then detected with flow cytometry (Bio-Rad, ZE5) for mitochondrial swelling. The ratio of FSC/SSC reflects the degree of mitochondrial swelling. Similarly, hippocampal cell suspension of  $1 \times 10^5$  cells/mL was prepared, centrifuged, and resuspended with 500  $\mu\text{L}$  of JC-1 working solution. Then incubated at 37°C for 15 min, resuspended cells with PBS, then analyzed by flow cytometry for MMP. The ratio of red/green (PE /FITC) fluorescence intensity reflects the level of MMP.

**2.8. Detection of Hippocampus Energy Charge (EC) with HPLC.** A total of 70 mg of hippocampus tissue was collected, mixed with normal saline (weight of hippocampus : normal saline volume = 1 : 10), and then disrupted with a homogenizer. Then, 0.6 mL homogenate was needed, add an equal volume of 0.5 mol/L perchloric acid, and centrifuged for 10 min at 12000g at 4°C. Furthermore, 0.8 mL supernatant was collected, add 45  $\mu\text{L}$  NaOH (5 mol/L) to neutralize PH, and centrifuged for 10 min at 12000 g at 4°C after standing for 30 min. The supernatant was used for subsequent HPLC detection. The Agilent 1260 Infinity High-Performance Liquid Chromatography instrument (Agilent Technologies, Inc.) was used to detect the contents of AMP, ADP, and ATP, and chromatographic separation was performed using an Agilent C18 Column (4.6  $\times$  250 mm, 5  $\mu\text{m}$ ; Agilent Technologies, Inc.) with a column temperature of 25°C, flow rate

of 1 mL/min, and injection volume of 10  $\mu$ L. A gradient elution was provided with 0.05% phosphate buffer (PH = 6.5) as solvent A (98%~90%) and methanol as solvent B (2%~10%), and the effluent absorbance was measured at 254 nm. The energy charge (EC) was calculated by the following formula:  $EC = ([ATP] + 1/2[ADP]) / ([ATP] + [ADP] + [AMP])$ .

**2.9. Enzyme-Linked Immunosorbent Assay.** A total of 60 mg of brain tissue was weighed and mixed with PBS containing 1% PMSF. Then, the brain tissue was grounded with a homogenizer and then centrifuged for 10 min at 5000 g at 4°C. The supernatant was collected. Subsequently, supernatant (100  $\mu$ L/well) was used to determine the concentrations of glutamate strictly according to the kit instructions.

**2.10. Western Blot Analysis.** An appropriate amount of brain tissue was lysed in RIPA lysate containing 1% PMSF, 1% phosphatase inhibitor, and centrifuged at 4°C, 12000 g for 10 min. The supernatant was collected for detecting protein concentration and western blot analysis. The target protein was separated with SDS-PAGE, transferred to a PVDF membrane, sealed with 5% BSA at room temperature for 90 min, and incubated with the primary antibodies at 4°C overnight: anti-Ptch1 (1 : 1000), anti-Smo (1 : 1000), anti-Gli1 (1 : 1000), anti-NMDAR1 (1 : 1000), anti-p-NMDAR1 (1 : 1000), and anti-GAPDH (1 : 5000). Subsequently, the target protein was washed with TBST solution three times, incubated with the secondary antibody (1 : 5000) at room temperature for 90 min, washed with TBST solution three times again, and visualized by hypersensitive ECL kit. The relative expression of the target proteins was analyzed using the Quantity One software (Bio-Rad, USA).

**2.11. Cell Culture and Cell Viability Assay.** PC12 cells were maintained in DMEM containing 10% fetal bovine serum (FBS), 1% Penicillin streptomycin in a 5% CO<sub>2</sub> incubator at 37°C. PC12 cells were employed to investigate the effect of KXS on antigitamate neurotoxicity. To evaluate the effect of glutamate on the PC12 cell viabilities, cells were presented with glutamate at concentrations of 2.5, 5, 10, 20, and 40 mM for 24 h (37°C, 5% CO<sub>2</sub>). To evaluate the effect of KXS and hydergine on cell viability, KXS at the final concentrations of 31.25, 62.5, 125, 250, and 500  $\mu$ g/mL and hydergine at the final concentrations of 15.625, 31.25, 62.5, and 125  $\mu$ g/mL were added and cultured (37°C, 5% CO<sub>2</sub>) for 24 h. In addition, to evaluate the key role of KXS in antigitamate neurotoxicity via Shh/Ptch1 signaling pathway, PC12 cells were divided into control, model (glutamate, 5 mM), Glu+hydergine (100  $\mu$ g/mL), Glu+KXS L (freeze-dried powder, 50  $\mu$ g/mL), Glu+KXS H (freeze-dried powder, 100  $\mu$ g/mL), and Glu+KXS H+cyclopamine (100  $\mu$ g/mL, 5  $\mu$ M). The cells of Glu+hydergine, Glu+KXS L, Glu+KXS H, and Glu+KXS H+cyclopamine groups were pretreated with the corresponding concentration of drugs and were incubated for 2 h before stimulation with glutamate (5 mM) for 24 h. The cells of the model group were only stimulated with 5 mM glutamate for 24 h. Afterward, 10  $\mu$ L of MTT (5 mg/mL) was added to each well and incubated at 37°C for 4 h. The formazan crystals

were solubilized in 100  $\mu$ L of dimethylsulfoxide (DMSO), and the absorbance was measured at 540 nm using a microplate reader (Thermo Labsystems, Franklin, MA, USA). Cell viability was calculated as a percentage of the vehicle control group [31]. All of the absorption values were calculated by averaging the results of each sample in triplicate.

**2.12. Statistical Analysis.** Data were expressed as mean  $\pm$  standard error of the mean (SEM). Morris water maze escape latency data were analyzed with a two-way analysis of variance (ANOVA) with Tukey's multiple comparisons test. The other data were analyzed by one-way ANOVA followed by Dunnett's multiple comparison test. The significance of statistical differences was considered at  $p < 0.05$ .

### 3. Results

**3.1. Quality Control of KXS Extracts.** To control the quality of KXS extracts, we used HPLC to quantify the main components. A typical HPLC profile was developed for KXS extracts (Figure 1), which served as an index for the identification of KXS. Ginsenoside Rg1, ginsenoside Rb1, ginsenoside Rd, polygalaxanthone III, and 3,6'-disinapoyl sucrose are characteristic components of KXS and were detected by HPLC. The contents of those signature ingredients were  $0.444 \pm 0.003$   $\mu$ g/mg,  $0.330 \pm 0.001$   $\mu$ g/mg,  $0.877 \pm 0.001$   $\mu$ g/mg,  $0.745 \pm 0.0003$   $\mu$ g/mg, and  $1.142 \pm 0.0006$   $\mu$ g/mg, respectively.

**3.2. KXS Ameliorated Cognitive Impairment and Hippocampal CA1 Neuron Damage in MID Rats.** To evaluate whether KXS could ameliorate the memory dysfunction of MID rats, we conducted the Morris Water Maze test for these rats. As Figure 2(a) shows, the escape latency of each group (except for the model group) remarkably shortened constantly with the increased training days, and the model group exhibited longer escape latency than the sham group ( $F(1, 10) = 30.96$ ,  $p < 0.001$ ); administration of KXS-L ( $F(1, 10) = 33.9$ ,  $p < 0.001$ ) and KXS-H ( $F(1, 10) = 19.27$ ,  $p < 0.01$ ) significantly attenuated the increased latency to reach the platform. The results of the spatial search test are shown in Figures 2(b)–2(d), the frequency of crossing the platform and the percent of time staying in the target quadrant were decreased in the model group compared with the sham group ( $p < 0.05$  or  $p < 0.01$ ). The MID rats treated with KXS-L and KXS-H both increased the time staying in the target quadrant ( $p < 0.01$ ), and KXS-L can also increase the frequency of crossing the platform of MID rats ( $p < 0.01$ ). Besides, MID rats spent more time in arriving at the platform zone ( $p < 0.05$ ), which can be shorten by hydergine and high-dose KXS ( $p < 0.05$  or  $p < 0.01$ ). The above results showed that KXS could ameliorate the memory impairment of MID rats.

The hippocampal CA1 region is very sensitive to ischemic injury and closely related to cognitive function [32]. To further investigate the role of KXS in alleviating cognitive dysfunction, we detected the hippocampus pathology of MID rats. As Figure 2(f) shows, compared with the sham group, the pathology changes of hippocampus CA1 region such as nerve cells necrosis and cell degeneration (blue

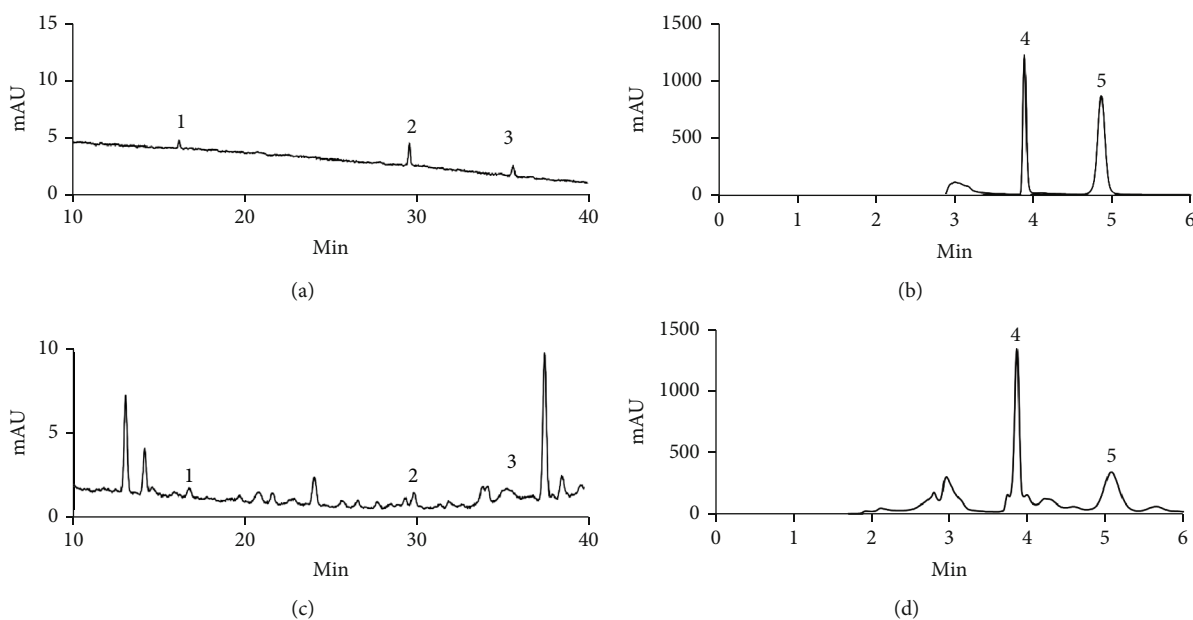


FIGURE 1: The main components of KXS extract were determined by HPLC. (a) Renshen standards liquid. (b) Yuanzhi standards liquid. (c and d) The KXS extracts. Peak 1: ginsenoside Rg1; peak 2: ginsenoside Rb1; peak 3: ginsenoside Rd; peak 4: polygalaxanthone III; peak 5: 3,6'-disinapoyl sucrose.

arrow), a decrease in the number of neurons (red arrow) and an enlarged gap (black arrow), the darkening of the nuclei (yellow arrow), were obvious in the model group while those pathological characteristics were markedly alleviated after treatment with KXS and hydergine. Subsequently, we counted the number of necrotic cells in the hippocampus CA1 region (Figure 2(g)). Our results showed that the number of necrotic cells in the model group was significantly increased compared with the sham group ( $p < 0.001$ ). In the rats treated with hydergine or KXS, the number of necrotic cells was significantly reduced ( $p < 0.001$ ). These results suggested KXS could protect against hippocampal histopathological alterations in MID rats.

**3.3. Effects of KXS on Hippocampal Mitochondrial Functions in MID Rats.** Hippocampal mitochondrial dysfunction plays a major role in the pathogenesis of VD [8, 11]. MMP and mitochondrial swelling are considered important parameters assessing mitochondrial bioenergy. To further investigate the role of KXS on mitochondrial functions, we detected MMP and mitochondrial swelling in the hippocampus of MID rats. As Figure 3(a) shows, MMP decreased significantly in the model group compared with the sham group ( $p < 0.01$ ). However, the above lesion was reversed both in KXS-L and KXS-H groups ( $p < 0.05$  or  $p < 0.01$ ). As Figure 3(b) shows, mitochondrial swelling was increased in the model group compared with the sham group ( $p < 0.01$ ), while the pathological changes were ameliorated both in KXS-L and KXS-H groups ( $p < 0.05$ ).

Mitochondria supply the necessary energy to support the survival and function of neurons. As Figures 3(c) and 3(d) shows, the ATP and EC were decreased in the model group ( $p < 0.05$ ); however, the content of ATP was significantly

increased in the KXS-L and KXS-H groups compared with the model group ( $p < 0.01$  or  $p < 0.05$ ). Besides, the brain EC was elevated in the KXS-L group ( $p < 0.01$ ). Given the findings mentioned above, we believed KXS has protective effects on hippocampal mitochondria.

**3.4. Effects of KXS on Glutamate Neurotoxicity.** Excessive extracellular glutamate can lead to the overactivation of post-synaptic glutamate receptors, like N-methyl-D-aspartate receptor 1 (NMDAR1), which evokes mitochondrial dysfunction and neuronal dysfunction [33, 34]. Considering the above factors, we wonder if KXS's protective effects on mitochondria and neurons are associated with reducing the content of glutamate and p-NMDAR1. As Figures 4(a)–4(c) shows, the concentration of glutamate and expression level of p-NMDAR1 were both increased in the model group compared with the sham group ( $p < 0.05$  or  $p < 0.001$ ). On the contrary, the concentration of glutamate was reduced in KXS H ( $p < 0.05$ ), and the expression level of p-NMDAR1 was significantly downregulated in both KXS L and KXS H groups ( $p < 0.001$ ) compared with the model group. This experiment showed KXS could decrease the concentration of glutamate and the level of p-NMDAR1 in MID rats.

To further study the against glutamate neurotoxicity of KXS, we used glutamate to induce neurotoxicity in PC12 cells and used this model to evaluate the antiglutamate neurotoxicity of KXS. The results of glutamate, KXS, and hydergine on the cell viabilities of PC12 cells were presented in Figures 4(d)–4(f). It could be found that KXS did not show any toxicity of up to the concentration of 500  $\mu\text{g}/\text{mL}$ , and hydergine did not show any toxicity of up to the concentration of 125  $\mu\text{g}/\text{mL}$ . However, glutamate at concentrations of 2.5–40 mM has significant toxicity on PC12 cells under 24 h



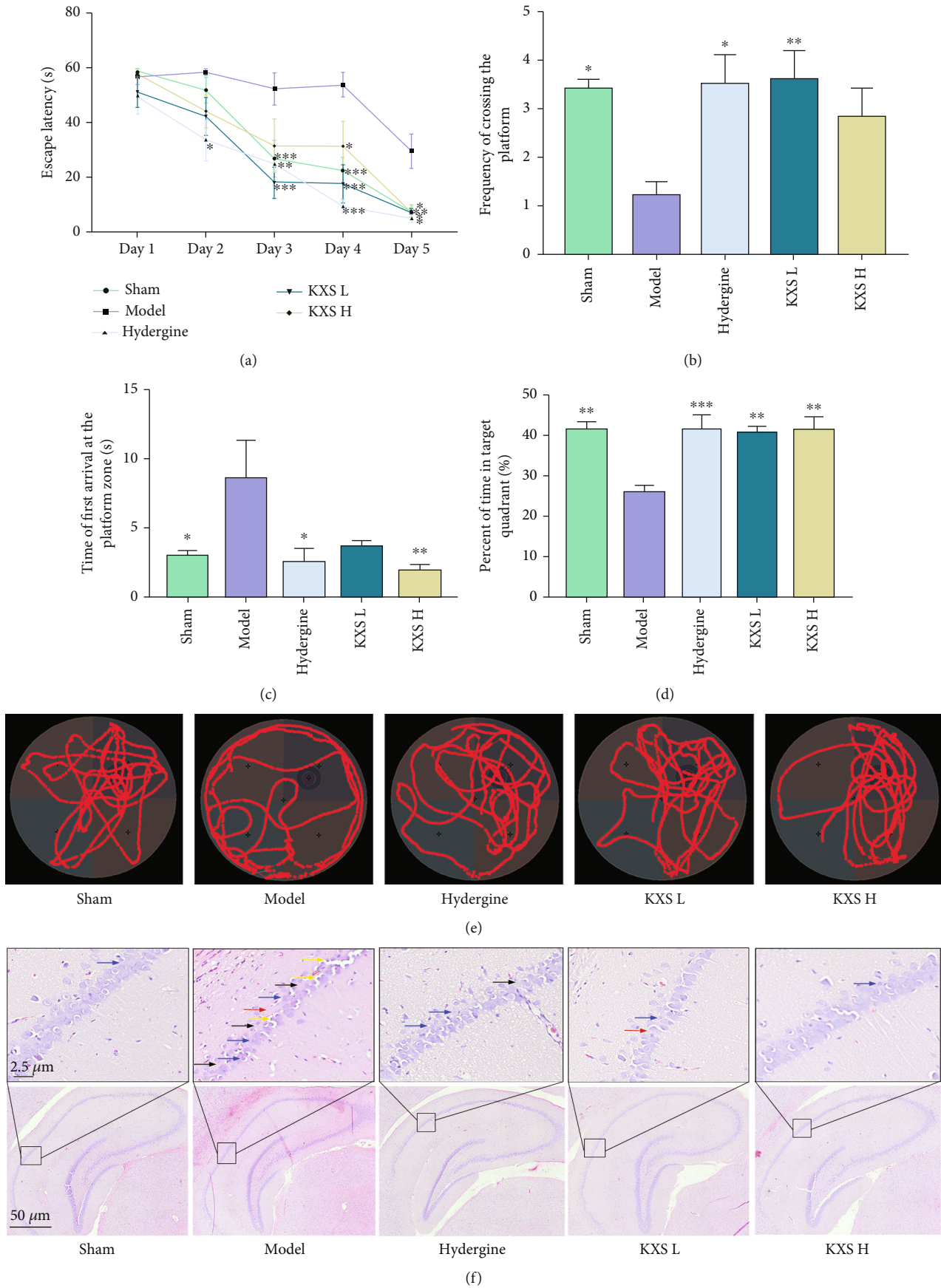


FIGURE 2: Continued.

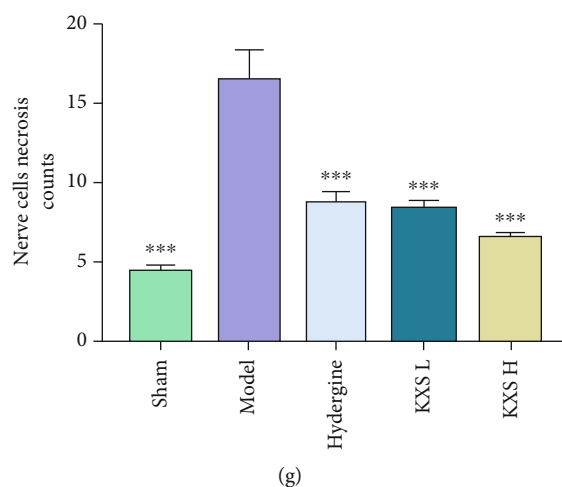


FIGURE 2: KXS alleviated cognitive impairment and hippocampal CA1 neuronal damage in MID rats. Escape latency (a,  $n = 8$ ), frequency of crossing the platform (b,  $n = 8$ ), time to first reach the platform zone (c,  $n = 8$ ), percent of time staying in the target quadrant (%), (d,  $n = 8$ ), representative traces of each group (e) in Morris Water Maze test. (f) Representative pictures of hematoxylin and eosin staining showed KXS extracts attenuated the damage to the hippocampus CA1 region in the MID rats (magnification: 200 $\times$ ). Nerve cell necrosis and cell degeneration (blue arrow), a decrease in the number of neurons (red arrow) and an enlarged gap (black arrow), the darkening of the nuclei (yellow arrow). (g) The necrotic cells count in the CA1 region ( $n = 6$ ). The above data were presented as mean  $\pm$  SEM. \* $p < 0.05$ , \*\* $p < 0.01$ , and \*\*\* $p < 0.001$  compared with the model group. The escape latency was performed by two-way ANOVA with Tukey's multiple comparisons test, and the others were performed by one-way ANOVA with Dunnett's multiple comparison test.

culture time, and the cell viability of PC12 cells was reduced to 60.71% after treated with 5 mM glutamate for 24 h. Thus, glutamate at the concentrations of 5 mM for 24 h was used to establish neurotoxicity. As shown in Figure 4(g), the cell viability was significantly increased by treatment with KXS and hydergine compared with the model group ( $p < 0.01$  or  $p < 0.001$ ). Consequently, these results indicated that KXS can effectively reduce the concentration of glutamate and level of p-NMDAR1 in MID rats and effectively inhibit the neurotoxicity induced by glutamate in PC12 cells.

**3.5. KXS Activated Shh/Ptch1 Pathway in MID Rats and against Glutamate Neurotoxicity in PC12 Cells via Shh/Ptch1 Pathway.** Recently, studies have shown that activating the Shh signaling pathway can increase mitochondrial activities and protect hippocampal neurons against glutamate-induced neurotoxicity [21]. To illuminate whether the effects of KXS on improving mitochondrial function and reducing glutamate neurotoxicity were related to Shh/Ptch1 signaling pathway, we detected the protein expression of Ptch1, Smo, and Gli1. As Figures 5(a)–5(d) show, the protein levels of Ptch1, Smo, and Gli1 were significantly decreased ( $p < 0.01$  or  $p < 0.001$ ) in the model group compared with the sham group. After treatment with KXS, the protein levels of Ptch1, Smo, and Gli1 were upregulated, respectively ( $p < 0.05$ ,  $p < 0.01$ , or  $p < 0.001$ ). To evaluate the key role of Shh/Ptch1 signaling pathway in antiglutamate neurotoxicity of KXS, we detected the cellular activity of PC12 under glutamate stimulation conditions. As Figure 5(e) shows, cyclopamine (a Shh pathway antagonist) could significantly inhibit the protective effect of KXS on glutamate neurotoxicity in PC12 cells ( $p < 0.05$ ).

## 4. Discussion

*Kaixin San* is a classic Chinese medicine prescription for forgetfulness and has been testified to improve cognitive impairment in many types of animal dementia models [23, 24, 35, 36]. Our present study demonstrates that treatment with KXS (i) improves cognitive dysfunction and alleviates hippocampal neuron damage of MID rats, (ii) rescues mitochondrial dysfunction through upregulating brain energy, alleviating mitochondrial swelling and improving MMP under chronic hypoperfusion conditions, (iii) inhibits glutamate neurotoxicity via decreasing the content of glutamate and the level of p-NMDAR1 in MID rats, and (iv) activates Shh/Ptch1 signaling pathway in MID rats and protects PC12 cells against glutamate neurotoxicity through Shh/Ptch1 signaling pathway. Collectively, improving mitochondrial quality and inhibiting glutamate neurotoxicity via activating Shh/Ptch1 signaling pathway constituted part of an essential mechanism of KXS to provide the neuroprotective effect on MID rats.

Multiple-infarct dementia (MID) is the most common type of vascular dementia (VD). MID's clinically pathological changes are common in atherosclerosis and hypertensive arteriole disease [37]. The thrombus fragments fall off and enter the blood circulation after arteriosclerosis. When thrombus fragments pass the small branches of the cerebral blood vessels form blockages, which results in brain tissue ischemia and hypoxia (chronic hypoperfusion) and then causes brain tissue damages and cognitive impairment [3, 38]. So chronic hypoperfusion is considered to contribute significantly to brain tissue damage and cognitive decline. Multiple infarcts and thromboembolism model are the

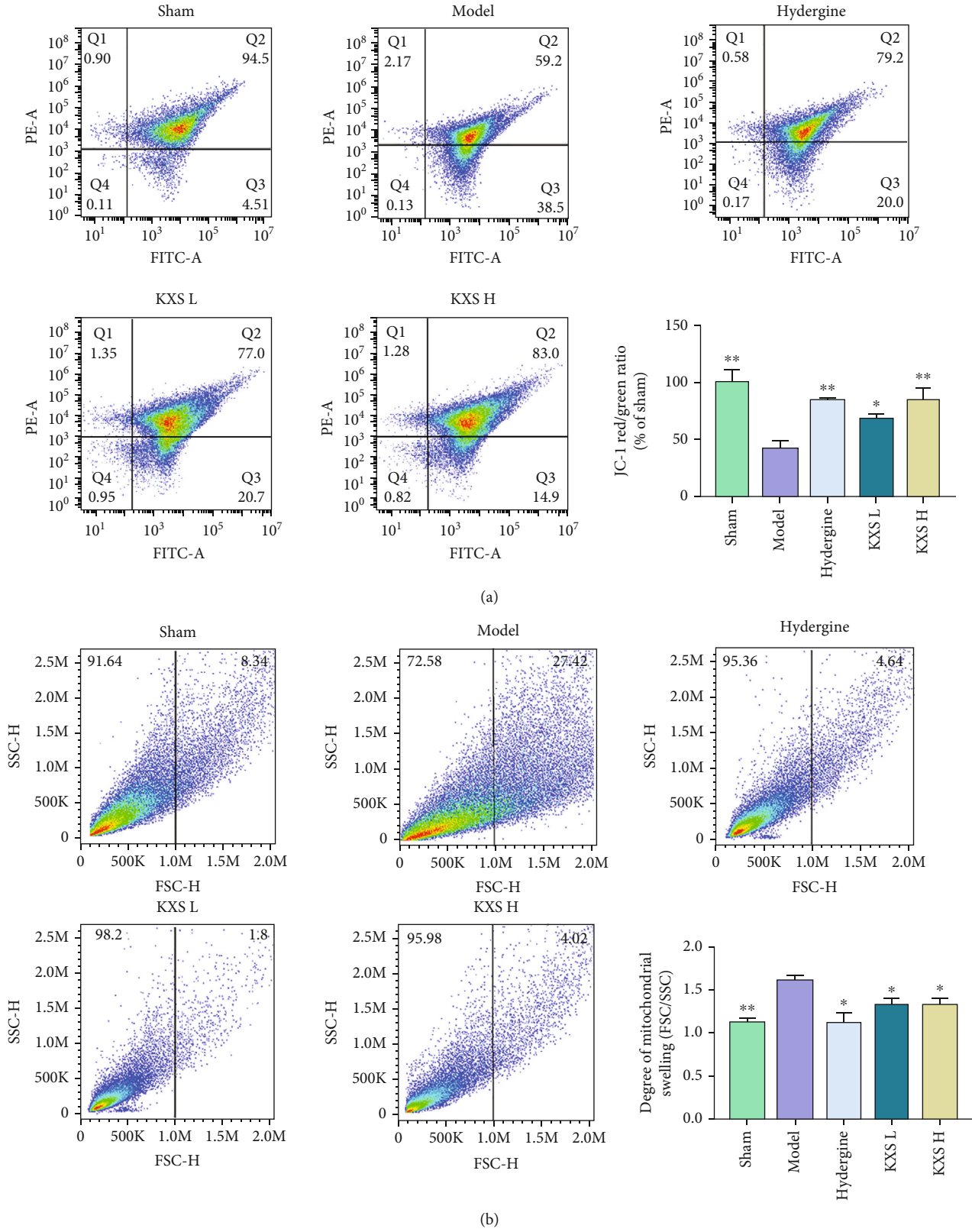


FIGURE 3: Continued.

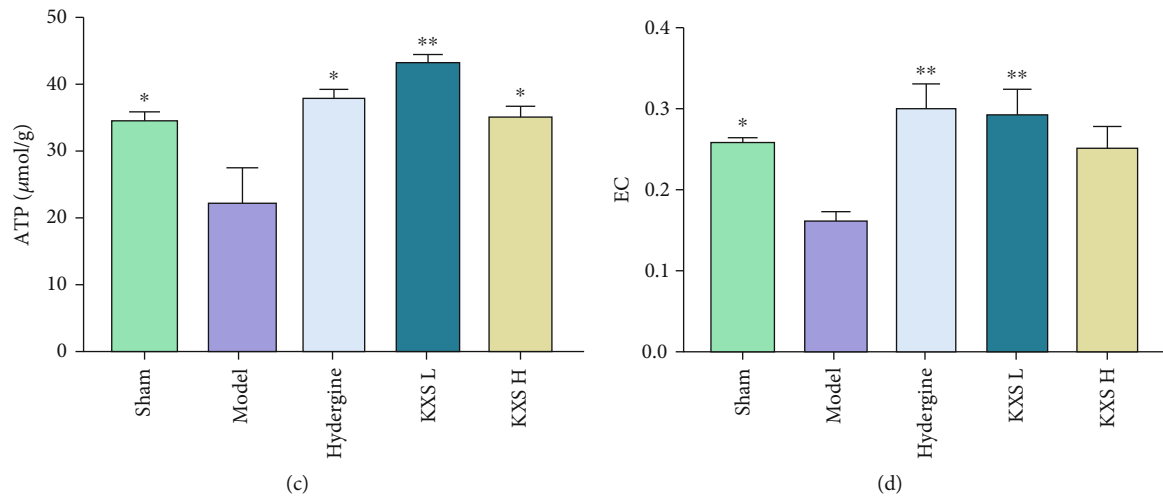


FIGURE 3: Effects of KXS on hippocampal mitochondrial functions in MID rats. (a) Flow cytometry analysis and quantification of mitochondrial membrane potential (MMP). (b) Flow cytometry analysis and quantification of mitochondrial swelling. (c) The content of ATP in MID rats. (d) The level of EC. The above data were presented as mean  $\pm$  SEM ( $n = 3$ ). \* $p < 0.05$ , \*\* $p < 0.01$ , and \*\*\* $p < 0.001$  compared with the model group. Comparisons were performed by one-way ANOVA with Dunnett's multiple comparison test.

most relevant model to VD [38]. In this study, the microthromboembolism-induced MID rats were used to simulate conditions of chronic cerebral hypoperfusion and utilized to evaluate the effects of KXS on cognitive dysfunction. As a vasodilator, clinical research had shown that hydergine could increase oxygen uptake as well as improve cerebral blood flow and decrease vascular resistance in patients with cerebrovascular disease, such as VD and MID [39]. So it is commonly used for treating patients with either dementia or “age-related” cognitive symptoms [40]. Like previous studies [41–43], we used hydergine as a positive control as well. Our results showed that the learning-memory ability was severely impaired in about 2 months after microthromboembolism surgery in rats, and these results were consistent with previous studies in MID model rats [4, 28]. Moreover, our data also showed that KXS could ameliorate the cognitive impairment of MID. It is widely known that the hippocampus CA1 region is an important area that is associated with learning and memory impairment [44]. Similar to the above results, the results of our study illuminated that nerve cell necrosis and cell degeneration were obvious in the model group rats while these changes dramatically reduced after KXS treatment. These results showed KXS alleviated cognitive impairment and hippocampal neuron injury in MID rats.

Glutamate plays an important role in neuronal development, axon guidance, brain development and maturation, learning and memory, and synaptic plasticity [45, 46]. But, excessive concentration of extracellular glutamate is neurotoxicity, known as glutamate excitotoxicity, which is the leading mechanism of neuronal death and cognitive disorder in cerebral ischemia disease [9, 47, 48]. It is reported that hypoperfusion (a main contributor to MID) can trigger hypoxia and glucose deprivation in nerve cells, which results in membrane depolarization and glutamate outflow [49]. Studies have reported that glutamate acts on glutamate receptors,

such as the N-methyl-D-aspartate receptors (NMDARs), specifically the NMDAR1 subunit, and leads to neuronal hyperexcitability and death [50, 51]. Consistent with previous studies, our study showed that MID-induced chronic cerebral hypoperfusion increased the content of glutamate and p-NMDAR1, while KXS reduced the levels of glutamate and p-NMDAR1. In addition, our results also showed KXS could effectively inhibit the neurotoxicity of glutamate in glutamate-induced PC12 cells. Therefore, it is reasonable to suspect that antiglutamate neurotoxicity plays an important role in the neuroprotective effect of KXS.

Hippocampus is key for spatial learning and memory, which is most sensitive to ischemic insult, and its mitochondrial damage plays an important role in the pathogenesis of VD [8]. Excessive glutamate can also induce mitochondrial dysfunction through activating NMDA receptors, which results in  $\text{Ca}^{2+}$  influx and MMP collapse [34]. Glutamate excitotoxicity can induce mitochondrial dysfunction, and mitochondrial damage can exacerbate glutamate excitotoxicity as well. For instance, energy failure, an early consequence of hypoxia-ischemia and the key sign of mitochondrial dysfunction, renders neurons vulnerable to excitotoxicity [52]. Mitochondrial energy metabolism, MMP, and mitochondrial swelling are major parameters to assess mitochondrial bioenergy [53, 54]. In our study, KXS increased ATP content and hippocampus MMP and decreased the degree of mitochondrial swelling in the MID rats, which revealed that KXS can improve mitochondrial quality and against glutamate excitotoxicity to ameliorate learning and memory impairment and neuron damage in MID rats.

Shh/Ptch1 signaling pathway is involved in cell development, survival, and differentiation in kinds of cells, including neurons [55]. Dysfunction or aberrant activation of the Shh signaling pathway is associated with developmental deformities and cancers [56]. Recently, beneficial actions

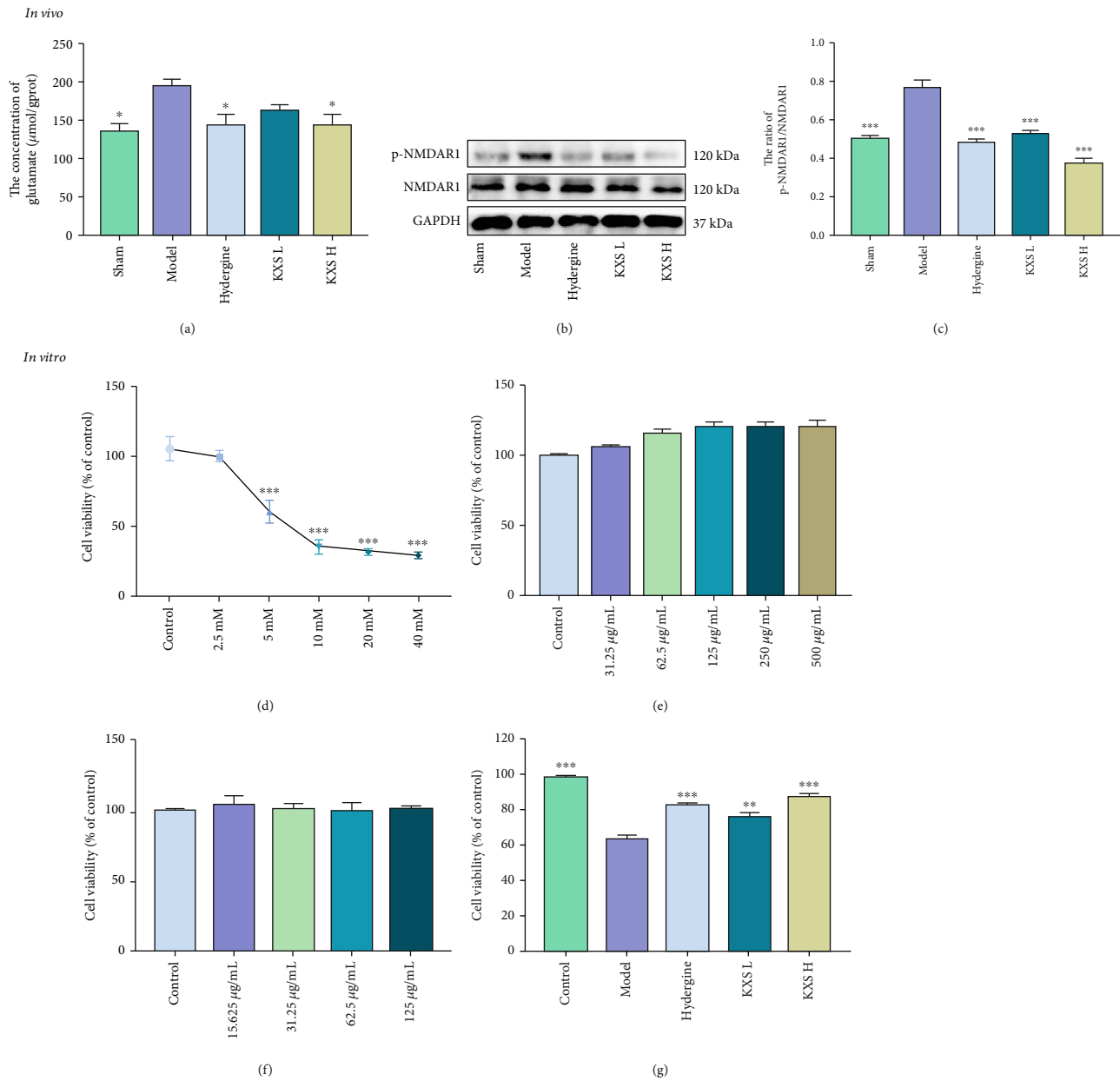


FIGURE 4: Effects of KXS on the concentration of glutamate and expression of p-NMDAR1 in MID rats and anti-glutamate neurotoxicity in vitro. (a) Concentration of glutamate in MID rats brain tissue (mean  $\pm$  SEM,  $n = 5$ ). (b) Representative western blot images of p-NMDAR1 and NMDAR1. (c) Quantification of p-NMDAR1/NMDAR1 ratio (mean  $\pm$  SEM,  $n = 3$ ). (d) The viability of the different doses of glutamate in PC12 cells (mean  $\pm$  SEM,  $n = 3$ ). (e) The viability of the different doses of KXS in PC12 cells (mean  $\pm$  SEM,  $n = 3$ ). (f) The viability of the different doses of hydergine in PC12 cells (mean  $\pm$  SEM,  $n = 3$ ). \* $p < 0.05$ , \*\* $p < 0.01$ , and \*\*\* $p < 0.001$  compared with the model group. Comparisons were performed by one-way ANOVA with Dunnett's multiple comparison test.

of activating canonical Shh/Ptch1 signaling pathway in cerebral ischemic injury have been reported, such as enhancing neurogenesis and white matter remodeling, antioxidation, antiexcitotoxicity, and antiapoptosis [18, 20, 57, 58]. Besides, a study reported the effects of activating the Shh/Ptch1 signaling pathway on reducing glutamate neurotoxicity by "nNOS-Sox2-Shh" axis, which functions as a novel feedback compensatory mechanism to protect neurons against the early excitotoxicity and ischemic injury [59]. Furthermore,

an increasing number of studies had shown that Shh/Ptch1 signaling pathway can also protect neurons against pathological stressors that cause or promote neuronal dysfunction by increasing mitochondrial mass and function [18, 21]. The Shh/Ptch1 signaling pathway mainly consists of Shh ligand, patched (Ptch1), and Smoothened (Smo) receptors, and Gli transcription factors (Gli1, Gli2, and Gli3). When the Shh ligand binds to Ptch1, it relieves the repression on Smo and ultimately activates Gli transcription factors

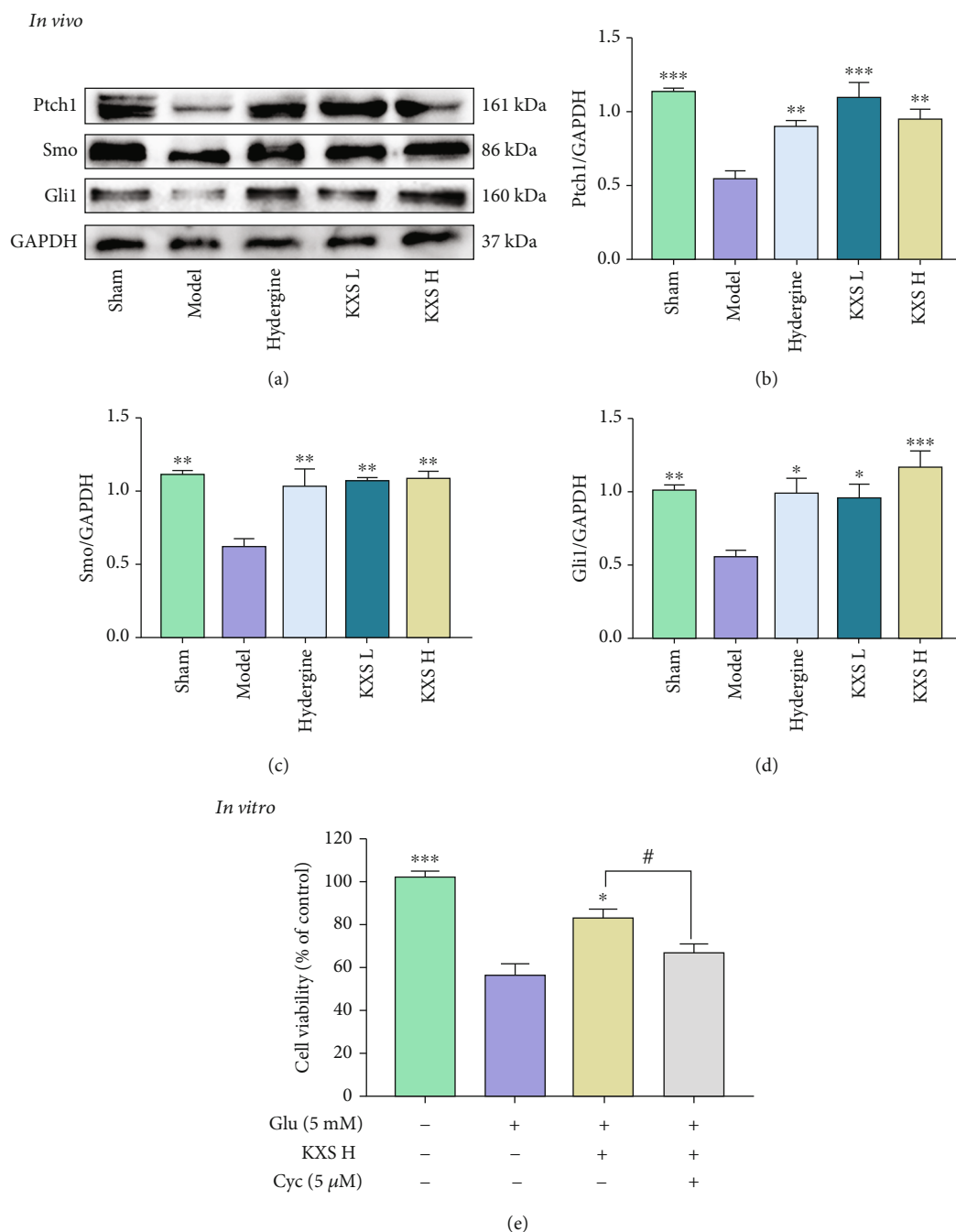


FIGURE 5: KXS activated Shh/Ptch1 pathway in MID rats and against glutamate neurotoxicity in PC12 cells via Shh/Ptch1 pathway. (a) Representative western blot images of Ptch1, Smo, and Gli1. Quantifications of Ptch1/GAPDH (b), Smo/GAPDH (c), and Gli1/GAPDH ratio (d). (e) The effect of KXS H and cyclopamine on glutamate-induced PC12 cells neurotoxicity. Above data were presented as mean ± SEM (n = 3). \*p < 0.05, \*\*p < 0.01, and \*\*\*p < 0.001 compared with the model group. #p < 0.05 compared with the Glu+KXS H group. Comparisons were performed by one-way ANOVA with Dunnett’s multiple comparison test.

[60]. Gli transcription factors, especially Gli1, are used as indicators of the activation of the Shh signaling pathway [61, 62]. In this experiment, we demonstrated that KXS could activate Shh/Ptch1 signaling pathway with upregulating the expression levels of Ptch1, Smo, and Gli1 in MID rats (Figures 5(a)–5(d)). Furthermore, cellular level experiment indicated that the inhibition of the Shh/Ptch1

signaling pathway by cyclopamine can inhibit the protective effect of KXS on glutamate-induced neurotoxicity in PC12 cells (Figure 5(e)). The above results suggested the neuroprotective effects of KXS (improved mitochondrial quality and inhibited glutamate neurotoxicity) in MID rats may work through activating the Shh/Ptch1 signaling pathway.

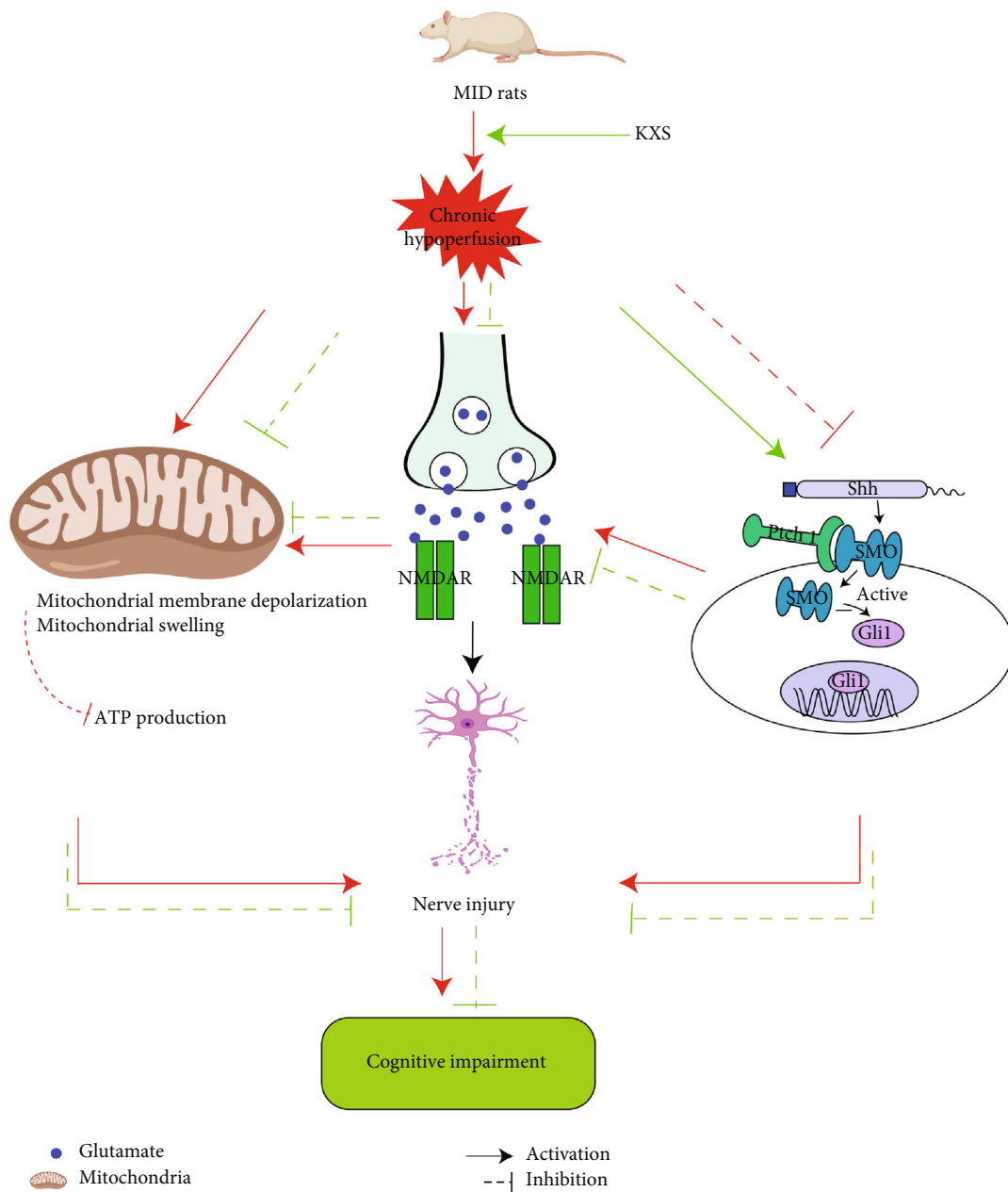


FIGURE 6: Schematic of the molecular mechanism of KXS protecting rats against MID via Shh/Ptch1 signaling pathway.

## 5. Conclusion

In summary, this study is the first to demonstrate that KXS could resist glutamate neurotoxicity and rescue mitochondrial function through activating the Shh/Ptch1 signaling pathway, thereby easing cognitive dysfunction and neurological deficits of MID (Figure 6). The present study may further offer basic information about the neuroprotective effect of KXS and indicate that KXS might be developed as an effective intervention drug of MID.

## Data Availability

The data used to support the findings of this study are available from the corresponding author upon request.

## Conflicts of Interest

The authors declare that there is no conflict of interest regarding the publication of this paper.

## Authors' Contributions

SJX conceived, designed the study, and critically reviewed, edited, and revised the paper. XQL and WW performed the research. XQL and PL wrote the original manuscript. YF, YD, and HC performed the western blot and prepared the figures. YD designed the study. FSW critically reviewed and revised the final manuscript. All authors read and approved the final manuscript. Xiaoqiong Li, Wen Wen, and Ping Li contribute equal contributions to this manuscript.

## Acknowledgments

The authors gratefully acknowledge the assistance of the Institute of Material Medica Integration and Transformation for Brain Disorders. This work was supported by the Sichuan Province Key R & D Project (Major Science and Technology Projects, No. 19ZDYF0600), the Chengdu Technological Innovation R & D Project (2019-YF05-01332-SN), the Special Project for Master of Traditional Chinese Medicine of Sichuan Provincial Administration of Traditional Chinese Medicine (2021MS0494), and the Xinglin Scholar Research Promotion Project of Chengdu University of TCM (No. XSGG2020011).

## References

- [1] C. Iadecola, "The pathobiology of vascular dementia," *Neuron*, vol. 80, no. 4, pp. 844–866, 2013.
- [2] E. H. Duthie Jr. and S. L. Glatt, "Understanding and treating multi-infarct dementia," *Clinics in Geriatric Medicine*, vol. 4, no. 4, pp. 749–766, 1988.
- [3] J. Kawamura, J. S. Meyer, Y. Terayama, and S. Weathers, "Cerebral hypoperfusion correlates with mild and parenchymal loss with severe multi-infarct dementia," *Journal of the Neurological Sciences*, vol. 102, no. 1, pp. 32–38, 1991.
- [4] X. Zhang, B. Wu, K. Nie, Y. Jia, and J. Yu, "Effects of acupuncture on declined cerebral blood flow, impaired mitochondrial respiratory function and oxidative stress in multi-infarct dementia rats," *Neurochemistry International*, vol. 65, pp. 23–29, 2014.
- [5] N. S. Jiwa, P. Garrard, and A. H. Hainsworth, "Experimental models of vascular dementia and vascular cognitive impairment: a systematic review," *Journal of Neurochemistry*, vol. 115, no. 4, pp. 814–828, 2010.
- [6] J. T. Coyle and P. Puttfarcken, "Oxidative stress, glutamate, and neurodegenerative disorders," *Science*, vol. 262, no. 5134, pp. 689–695, 1993.
- [7] J. L. Huang, S. T. Fu, Y. Y. Jiang et al., "Protective effects of Nicotiflorin on reducing memory dysfunction, energy metabolism failure and oxidative stress in multi-infarct dementia model rats," *Pharmacology, Biochemistry, and Behavior*, vol. 86, no. 4, pp. 741–748, 2007.
- [8] J. Du, M. Ma, Q. Zhao et al., "Mitochondrial bioenergetic deficits in the hippocampi of rats with chronic ischemia-induced vascular dementia," *Neuroscience*, vol. 231, pp. 345–352, 2013.
- [9] Z. V. Bakaeva, A. M. Surin, N. V. Lizunova et al., "Neuroprotective potential of peptides HFRWPGP (ACTH6–9PGP), KKRRPGP, and PyrRP in cultured cortical neurons at glutamate excitotoxicity," *Doklady. Biochemistry and Biophysics*, vol. 491, no. 1, pp. 62–66, 2020.
- [10] T. W. Lai, S. Zhang, and Y. T. Wang, "Excitotoxicity and stroke: identifying novel targets for neuroprotection," *Progress in Neurobiology*, vol. 115, pp. 157–188, 2014.
- [11] H. Li, Y. Liu, L. T. Lin et al., "Acupuncture reversed hippocampal mitochondrial dysfunction in vascular dementia rats," *Neurochemistry International*, vol. 92, pp. 35–42, 2016.
- [12] Y. Luo, H. P. Zhao, J. Zhang et al., "Effect of ferulic acid on learning and memory impairments of vascular dementia rats and its mechanism of action," *Yao Xue Xue bao = Acta Pharmaceutica Sinica*, vol. 47, no. 2, pp. 256–260, 2012.
- [13] P. Ma, T. An, L. Zhu et al., "RNF220 is required for cerebellum development and regulates medulloblastoma progression through epigenetic modulation of Shh signaling," *Development (Cambridge, England)*, vol. 147, 2020.
- [14] V. Palma, D. A. Lim, N. Dahmane et al., "Sonic hedgehog controls stem cell behavior in the postnatal and adult brain," *Development (Cambridge, England)*, vol. 132, no. 2, pp. 335–344, 2005.
- [15] C. Martínez, V. H. Cornejo, P. Lois et al., "Proliferation of murine midbrain neural stem cells depends upon an endogenous sonic hedgehog (Shh) source," *PLoS One*, vol. 8, no. 6, article e65818, 2013.
- [16] A. C. Alfaro, B. Roberts, L. Kwong, M. F. Bijlsma, and H. Roelink, "Ptch2 mediates the Shh response in Ptch1/-cells," *Development (Cambridge, England)*, vol. 141, no. 17, pp. 3331–3339, 2014.
- [17] X. L. Niu, X. Jiang, G. D. Xu et al., "DL-3-n-butylphthalide alleviates vascular cognitive impairment by regulating endoplasmic reticulum stress and the Shh/Ptch1 signaling-pathway in rats," *Journal of Cellular Physiology*, vol. 234, no. 8, pp. 12604–12614, 2019.
- [18] P. Yu, L. Wang, F. Tang et al., "Resveratrol pretreatment decreases ischemic injury and improves neurological function via sonic hedgehog signaling after stroke in rats," *Molecular Neurobiology*, vol. 54, no. 1, pp. 212–226, 2017.
- [19] O. V. Chechneva, F. Mayrhofer, D. J. Daugherty et al., "A smoothed receptor agonist is neuroprotective and promotes regeneration after ischemic brain injury," *Cell Death & Disease*, vol. 5, no. 10, article e1481, 2014.
- [20] L. Liu, B. Zhao, X. Xiong, and Z. Xia, "The neuroprotective roles of sonic hedgehog signaling pathway in ischemic stroke," *Neurochemical Research*, vol. 43, no. 12, pp. 2199–2211, 2018.
- [21] P. J. Yao, U. Manor, R. S. Petralia et al., "Sonic hedgehog pathway activation increases mitochondrial abundance and activity in hippocampal neurons," *Molecular Biology of the Cell*, vol. 28, no. 3, pp. 387–395, 2017.
- [22] W. He, L. Cui, C. Zhang et al., "Sonic hedgehog promotes neurite outgrowth of cortical neurons under oxidative stress: involving of mitochondria and energy metabolism," *Experimental Cell Research*, vol. 350, no. 1, pp. 83–90, 2017.
- [23] Y. M. Xu, X. C. Wang, T. T. Xu et al., "Kai Xin San ameliorates scopolamine-induced cognitive dysfunction," *Neural Regeneration Research*, vol. 14, no. 5, pp. 794–804, 2019.
- [24] B. Zhang, Y. Li, J. W. Liu et al., "Postsynaptic GluR2 involved in amelioration of A $\beta$ -induced memory dysfunction by KAIXIN-san through rescuing hippocampal LTP in mice," *Rejuvenation Research*, vol. 22, no. 2, pp. 131–137, 2019.
- [25] Y. Q. Wen, Y. Fu, J. P. Wei, H. Chen, Y. Dai, and S. J. Xu, "Based on the traditional Chinese medicine inheritance auxiliary platform to study the difference between the prescriptions for the treatment of senile dementia and vascular dementia," *Modernization of Traditional Chinese Medicine and Materia Medica-World Science and Technology*, vol. 20, pp. 2150–2155, 2018.
- [26] Y. Dai, C. Y. Sun, Y. Fu, Y. Q. Wen, and S. J. Xu, "Effects of Kai Xin San on learning and memory function and ATP/AMP in rats with multiple infarct dementia," *World Science and Technology/Modernization of Traditional Chinese Medicine and Materia Medica*, vol. 20, pp. 2180–2184, 2018.
- [27] S. Guo, J. Wang, Y. Wang et al., "Study on the Multitarget Synergistic Effects of Kai-Xin-San against Alzheimer's Disease



- Based on Systems Biology,” *Oxidative Medicine and Cellular Longevity*, vol. 2019, Article ID 1707218, 15 pages, 2019.
- [28] J. W. Yang, X. R. Wang, S. M. Ma, N. N. Yang, Q. Q. Li, and C. Z. Liu, “Acupuncture attenuates cognitive impairment, oxidative stress and NF- $\kappa$ B activation in cerebral multi-infarct rats,” *Acupuncture in Medicine: Journal of the British Medical Acupuncture Society*, vol. 37, no. 5, pp. 283–291, 2019.
  - [29] J.-P. Wei, W. Wen, Y. Dai et al., “Drinking water temperature affects cognitive function and progression of Alzheimer’s disease in a mouse model,” *Acta Pharmacologica Sinica*, vol. 42, 2021.
  - [30] C. V. Vorhees and M. T. Williams, “Morris water maze: procedures for assessing spatial and related forms of learning and memory,” *Nature Protocols*, vol. 1, no. 2, pp. 848–858, 2006.
  - [31] L. J. Gao, X. Q. Li, S. Meng, T. Y. Ma, L. H. Wan, and S. J. Xu, “Chlorogenic acid alleviates A $\beta_{25-35}$ -Induced autophagy and cognitive impairment via the mTOR/TFEB signaling Pathway,” *Drug Design, Development and Therapy*, vol. 14, pp. 1705–1716, 2020.
  - [32] R. Schmidt-Kastner and T. F. Freund, “Selective vulnerability of the hippocampus in brain ischemia,” *Neuroscience*, vol. 40, no. 3, pp. 599–636, 1991.
  - [33] M. Busse, R. Kunschmann, H. Dobrowolny et al., “Dysfunction of the blood-cerebrospinal fluid-barrier and N-methyl-D-aspartate glutamate receptor antibodies in dementias,” *European Archives of Psychiatry and Clinical Neuroscience*, vol. 268, no. 5, pp. 483–492, 2018.
  - [34] S. J. Yang, A. R. Han, E. A. Kim et al., “KHG21834 attenuates glutamate-induced mitochondrial damage, apoptosis, and NLRP3 inflammasome activation in SH-SY5Y human neuroblastoma cells,” *European Journal of Pharmacology*, vol. 856, article 172412, 2019.
  - [35] Q. Wang, Y. L. Zhang, Y. H. Li et al., “The memory enhancement effect of Kai Xin San on cognitive deficit induced by simulated weightlessness in rats,” *Journal of Ethnopharmacology*, vol. 187, pp. 9–16, 2016.
  - [36] C. Lu, Z. Shi, X. Sun et al., “Kai Xin San aqueous extract improves A $\beta_{1-40}$ -induced cognitive deficits on adaptive behavior learning by enhancing memory-related molecules expression in the hippocampus,” *Journal of Ethnopharmacology*, vol. 201, pp. 73–81, 2017.
  - [37] J. Gooch and D. M. Wilcock, “Animal models of vascular cognitive impairment and dementia (VCID),” *Cellular and Molecular Neurobiology*, vol. 36, no. 2, pp. 233–239, 2016.
  - [38] P. Venkat, M. Chopp, and J. Chen, “Models and mechanisms of vascular dementia,” *Experimental Neurology*, vol. 272, pp. 97–108, 2015.
  - [39] M. Ditch, F. J. Kelly, and O. Resnick, “An ergot preparation (hydergine) in the treatment of cerebrovascular disorders in the geriatric patient: double-blind study,” *Journal of the American Geriatrics Society*, vol. 19, no. 3, pp. 208–217, 1971.
  - [40] J. Olin, L. Schneider, A. Novit, and S. Luczak, “Hydergine for dementia,” *Cochrane Database of Systematic Reviews*, no. 3, article CD000359, 2000.
  - [41] X. Y. Ren, Y. Hu, J. P. Wei, W. J. Fu, S. J. Xu, and Y. Y. Wang, “Effects of Tongluo Xingnao effervescent tablets on blood rheology, iNOS, VEGF and LDH-5 in MID rats,” *Zhongguo Zhong Yao za Zhi = Zhongguo Zhongyao Zazhi = China Journal of Chinese Materia Medica*, vol. 41, no. 6, pp. 1119–1123, 2016.
  - [42] J. Cai, J. du, Z. H. Ge, F. Zhou, L. Y. Zhou, and L. Y. Chen, “Effect of Kangxin Capsule on the expression of nerve growth factors in parietal lobe of cortex and hippocampus CA1 area of vascular dementia model rats,” *Chinese Journal of Integrative Medicine*, vol. 12, no. 4, pp. 292–296, 2006.
  - [43] L. Zhang and H. T. Wang, “Effect of huadai xingshen decoction on cerebral somatostatin, arginine vasopressin and somatostatin mRNA expression in vascular dementia rat model,” *Zhongguo Zhong xi yi Jie he zhi Zhongguo Zhongxiyi Jiehe Zazhi = Chinese Journal of Integrated Traditional and Western Medicine*, vol. 21, no. 8, pp. 608–610, 2001.
  - [44] I. Soltesz and A. Losonczy, “CA1 pyramidal cell diversity enabling parallel information processing in the hippocampus,” *Nature Neuroscience*, vol. 21, no. 4, pp. 484–493, 2018.
  - [45] R. Cachepe and A. E. Pereda, “Regulatory roles of metabotropic glutamate receptors on synaptic communication mediated by gap junctions,” *Neuroscience*, vol. 456, pp. 85–94, 2021.
  - [46] G. Riedel and K. G. Reymann, “Metabotropic glutamate receptors in hippocampal long-term potentiation and learning and memory,” *Acta Physiologica Scandinavica*, vol. 157, no. 1, pp. 1–19, 1996.
  - [47] W. Zhang, J. Yu, M. Guo et al., “Dexmedetomidine attenuates glutamate-induced cytotoxicity by inhibiting the mitochondrial-mediated apoptotic pathway,” *Medical Science Monitor*, vol. 26, article e922139, 2020.
  - [48] X. X. Dong, Y. Wang, and Z. H. Qin, “Molecular mechanisms of excitotoxicity and their relevance to pathogenesis of neurodegenerative diseases,” *Acta Pharmacologica Sinica*, vol. 30, no. 4, pp. 379–387, 2009.
  - [49] E. L. Ashby, M. Kierzkowska, J. Hull, P. G. Kehoe, S. M. Hutson, and M. E. Conway, “Altered expression of human mitochondrial branched chain aminotransferase in dementia with lewy bodies and vascular dementia,” *Neurochemical Research*, vol. 42, no. 1, pp. 306–319, 2017.
  - [50] Z. Zhang, J. Liu, C. Fan et al., “The GluN1/GluN2B NMDA receptor and metabotropic glutamate receptor 1 negative allosteric modulator has enhanced neuroprotection in a rat subarachnoid hemorrhage model,” *Experimental Neurology*, vol. 301, Part A, pp. 13–25, 2018.
  - [51] C. Wahlestedt, E. Golanov, S. Yamamoto et al., “Antisense oligodeoxynucleotides to NMDA-R1 receptor channel protect cortical neurons from excitotoxicity and reduce focal ischemic infarctions,” *Nature*, vol. 363, no. 6426, pp. 260–263, 1993.
  - [52] M. P. Mattson, “Excitotoxic and excitoprotective mechanisms: abundant targets for the prevention and treatment of neurodegenerative disorders,” *Neuromolecular Medicine*, vol. 3, no. 2, pp. 65–94, 2003.
  - [53] Y. Tsujimoto, T. Nakagawa, and S. Shimizu, “Mitochondrial membrane permeability transition and cell death,” *Biochimica et Biophysica Acta*, vol. 1757, no. 9–10, pp. 1297–1300, 2006.
  - [54] J. Li, X. Ma, W. Yu et al., “Reperfusion promotes mitochondrial dysfunction following focal cerebral ischemia in rats,” *PLoS One*, vol. 7, no. 9, article e46498, 2012.
  - [55] J. E. Hooper and M. P. Scott, “Communicating with hedgehogs,” *Nature Reviews Molecular Cell Biology*, vol. 6, no. 4, pp. 306–317, 2005.
  - [56] A. M. Skoda, D. Simovic, V. Karin, V. Kardum, S. Vranic, and L. Serman, “The role of the hedgehog signaling pathway in cancer: a comprehensive review,” *Bosnian Journal of Basic Medical Sciences*, vol. 18, no. 1, pp. 8–20, 2018.
  - [57] L. Zhang, M. Chopp, D. H. Meier et al., “Sonic hedgehog signaling pathway mediates cerebrolysin-improved neurological

- function after stroke,” *Stroke*, vol. 44, no. 7, pp. 1965–1972, 2013.
- [58] S. S. Huang, H. Cheng, C. M. Tang et al., “Anti-oxidative, anti-apoptotic, and pro-angiogenic effects mediate functional improvement by sonic hedgehog against focal cerebral ischemia in rats,” *Experimental Neurology*, vol. 247, pp. 680–688, 2013.
- [59] D. Zhang, H. Wang, H. Liu, T. Tao, N. Wang, and A. Shen, “nNOS translocates into the nucleus and interacts with Sox2 to protect neurons against early excitotoxicity via promotion of Shh transcription,” *Molecular Neurobiology*, vol. 53, no. 9, pp. 6444–6458, 2016.
- [60] P. W. Ingham, Y. Nakano, and C. Seger, “Mechanisms and functions of hedgehog signalling across the metazoa,” *Nature Reviews Genetics*, vol. 12, no. 6, pp. 393–406, 2011.
- [61] M. Varjosalo and J. Taipale, “Hedgehog: functions and mechanisms,” *Genes & Development*, vol. 22, no. 18, pp. 2454–2472, 2008.
- [62] A. R. Altaba, C. Mas, and B. Stecca, “The Gli code: an information nexus regulating cell fate, stemness and cancer,” *Trends in Cell Biology*, vol. 17, no. 9, pp. 438–447, 2007.

## Research Article

# Downregulation of ATP6V1A Involved in Alzheimer's Disease via Synaptic Vesicle Cycle, Phagosome, and Oxidative Phosphorylation

Zhike Zhou,<sup>1</sup> Jun Bai,<sup>2</sup> Shanshan Zhong,<sup>3</sup> Rongwei Zhang,<sup>1</sup> Kexin Kang,<sup>1</sup> Xiaoqian Zhang,<sup>3</sup> Ying Xu,<sup>2,4</sup> Chuansheng Zhao <sup>3</sup> and Mei Zhao <sup>5</sup>

<sup>1</sup>Department of Geriatrics, The First Affiliated Hospital, China Medical University, Shenyang, 110001 Liaoning, China

<sup>2</sup>Cancer Systems Biology Center, The China-Japan Union Hospital, Jilin University, Changchun, 130033 Jilin, China

<sup>3</sup>Department of Neurology, The First Affiliated Hospital, China Medical University, Shenyang, 110001 Liaoning, China

<sup>4</sup>Computational Systems Biology Lab, Department of Biochemistry and Molecular Biology and Institute of Bioinformatics, The University of Georgia, USA

<sup>5</sup>Department of Cardiology, The Shengjing Affiliated Hospital, China Medical University, Shenyang, 110004 Liaoning, China

Correspondence should be addressed to Chuansheng Zhao; [cszhao@cmu.edu.cn](mailto:cszhao@cmu.edu.cn) and Mei Zhao; [zhaom1@sj-hospital.org](mailto:zhaom1@sj-hospital.org)

Received 23 January 2021; Revised 2 March 2021; Accepted 24 March 2021; Published 20 April 2021

Academic Editor: Daniele Vergara

Copyright © 2021 Zhike Zhou et al. This is an open access article distributed under the Creative Commons Attribution License, which permits unrestricted use, distribution, and reproduction in any medium, provided the original work is properly cited.

**Objective.** The objective of this study was to investigate the potential molecular mechanisms of ATPase H<sup>+</sup> transporting V1 subunit A (ATP6V1A) underlying Alzheimer's disease (AD). **Methods.** Microarray expression data of human temporal cortex samples from the GSE118553 dataset were profiled to screen for differentially expressed genes (DEGs) between AD/control and ATP6V1A-low/high groups. Correlations of coexpression modules with AD and ATP6V1A were assessed by weight gene correlation network analysis (WGCNA). DEGs strongly interacting with ATP6V1A were extracted to construct global regulatory network. Further cross-talking pathways of ATP6V1A were identified by functional enrichment analysis. Diagnostic performance of ATP6V1A in AD prediction was evaluated using area under the curve (AUC) analysis. **Results.** The mean expression of ATP6V1A was significantly downregulated in AD compared with nondementia controls. A total of 1,364 DEGs were overlapped from AD/control and ATP6V1A-low/high groups. Based on these DEGs, four coexpression modules were predicted by WGCNA. The blue, brown, and turquoise modules were significantly correlated with AD and low ATP6V1A, whose DEGs were enriched in phagosome, oxidative phosphorylation, synaptic vesicle cycle, focal adhesion, and gamma-aminobutyric acidergic (GABAergic) synapse. Global regulatory network was constructed to identify the cross-talking pathways of ATP6V1A, such as synaptic vesicle cycle, phagosome, and oxidative phosphorylation. According to the AUC value of 74.2%, low ATP6V1A expression accurately predicted the occurrence of AD. **Conclusions.** Our findings highlighted the pleiotropic roles of low ATP6V1A in AD pathogenesis, possibly mediated by synaptic vesicle cycle, phagosome, and oxidative phosphorylation.

## 1. Introduction

Alzheimer's disease (AD), referring to a progressive neurodegenerative disease, is pathologically characterized by extracellular senile plaques composed of amyloid beta (A $\beta$ ), neurofibrillary tangles composed of hyperphosphorylated tau, and neuron loss [1, 2]. In brain parenchyma of AD, A $\beta$  peptide is derived from continuous cleavage of amyloid precursor proteins (APP) by  $\beta$ - and  $\gamma$ -secretases,

with its deposition depending on the balance between production and removal [3, 4]. As the major processing compartment for A $\beta$ , lysosomes rely on an acidic environment of pH less than 5.0 to activate proteases for A $\beta$  degradation [4, 5]. This gradient of acidification is potentially mediated by vacuolar H<sup>+</sup>-ATPase (V-ATPase), a multisubunit enzyme consisting of V0 and V1 sectors that pumps protons into the lysosomal lumen by ATP consumption [6]. Dysfunction of V-ATPase-dependent acidification disrupts the trafficking

of substrates between endolysosomal compartments, which may facilitate molecular steps for neuronal degeneration, such as AD [7].

ATPase H<sup>+</sup> transporting V1 subunit A (ATP6V1A) encoding a peripheral subunit in V1 sector of V-ATPase constitutes ATP-binding interface and catalyzes ATP hydrolysis [8]. The resultant energy is then coupled with a ring of proteolipid subunits in V0 sector, giving rise to proton translocation across the membrane [9]. For instance, ATP6V1A assembles with V0 subunits to form the glucose-dependent complex of V1/Vo sectors that drives proton transport; simultaneously, this process can be interrupted by reversible dissociation of the complex into component V0 and V1 [10]. Several lines of evidence have demonstrated that misrouting V0 subunit-induced proton translocation contributed to defective lysosomal acidification, a devastating manifestation in virtually all lysosomal storage and neurodegenerative diseases [11–13]. However, the pathophysiological mechanism of AD due to dysfunction of V1 subunits (e.g., ATP6V1A) remains elusive and is difficult to be verified by traditional biological methods. Accordingly, we sought to perform a comprehensive bioinformatics analysis of ATP6V1A based on gene expression data and functional annotations, aiming to elucidate the molecular functions of ATP6V1A underlying the pathogenesis of AD.

## 2. Materials and Methods

**2.1. Data Resources.** The RNA microarray data of human postmortem temporal cortex samples, including 45 AD patients and 24 nondementia controls, were downloaded from the GSE118553 dataset of Gene Expression Omnibus (GEO, <https://www.ncbi.nlm.nih.gov/geo/>) [14]. This dataset was analyzed using Illumina HumanHT-12 V4.0 expression beadchip on the platform of GPL10558. Taking the average expression of ATP6V1A as the cut-off line, enrolled samples were dichotomized into two groups: the ATP6V1A-low group and the ATP6V1A-high group. Similarly, samples were divided into age-low/high groups according to the cut-off line of the mean age. The odds ratio (OR) was calculated by logistics regression analysis to detect the potential predictors of AD (Table 1). Low-expressed probes were removed to retain the highest one if a gene corresponded to multiple probes. Gene expression profiles were preprocessed by normalization adopting the *normalizeBetweenArrays* function in the *limma* package of R software version 3.6.2 [15].

**2.2. Gene Set Enrichment Analysis (GSEA).** GSEA analysis was conducted to screen out the biological processes (BP) of gene ontology terms that were significantly enriched in phenotypes of AD and low ATP6V1A expression [16, 17]. The number of permutations was set to 1000 and normalized  $P < 0.05$  was considered for significant enrichment. The results of GSEA were visualized by using *ClusterProfiler*, *enrichplot*, *ggplot2*, and *GSEABase* packages.

**2.3. Differential Expression Analysis.** The *lmFit* and *eBayes* functions in *limma* packages were used to filtrate differentially expressed genes (DEGs) between AD/control and

ATP6V1A-low/high groups. Analyses of two-dimensional hierarchical clustering and volcano plot were conducted employing the *limma* package in R. Threshold of statistical significance was defined as fold change (FC)  $\geq 1.5$  and a false discovery rate- (FDR-) adjusted  $P < 0.05$  [15, 18, 19].

**2.4. Coexpression Network Analysis.** Data of DEGs overlapped from AD/control and ATP6V1A-low/high groups were processed by weight gene correlation network analysis (WGCNA). Outlier samples were eliminated in clustering dendrogram to ensure the reliable outcome of coexpression network using the *hclust* function. The soft thresholding power of 6 was selected by *pickSoftThreshold* function to make the network conform to the power-law distribution and close to the real state of biological network [20]. Clustering tree was dissected into branches to construct coexpression modules of at least 30 genes, which were visualized by different color labels [21, 22]. The *labeledHeatmap* function was used to display the correlation values within a heatmap plot of module-trait relationships. Functional enrichment analysis of Kyoto Encyclopedia of Genes and Genomes (KEGG) pathways were performed using *clusterProfiler* package.

**2.5. Construction of Global Regulatory Network and Cross-Talking Pathways of ATP6V1A.** The intramodular connectivity and genetic phenotype were measured by module membership (MM) and gene significance (GS), respectively. Scatter diagram of the relationship between MM and GS was plotted using *verboseScatterplot* function [23]. According to the empirical criteria of  $MM > 0.4$  and  $GS > 0.5$ , DEGs strongly interacting with ATP6V1A expression were extracted, thus to construct global regulatory network of proteins based on the STRING database (Search Tool for the Retrieval of Interacting Genes, <https://www.string-db.org/>) [24]. The cross-talking pathways of ATP6V1A were identified by functional enrichment analysis of KEGG pathways. Visualization of global regulatory network and cross-talking pathways of ATP6V1A was accomplished adopting *cytoscape* software [25].

**2.6. Signature Genes of a Pathway.** The correlation between genes was quantitatively determined by Pearson correlation coefficient (PCC) analysis [26]. For each cross-talking pathway, the five genes with the highest PCC were designated as signature genes, whose expression was most strongly correlated with other genes of the pathway [27]. If the signature genes of a pathway were significantly correlated with ATP6V1A expression, ATP6V1A was recognized to modulate or mediate the pathway.

**2.7. Analysis of Area under the Curve (AUC).** The *pROC* function was used to estimate diagnostic performance of ATP6V1A in distinguishing AD from nondementia. Under continuous threshold conditions, classification performance was displayed via receiver operating characteristic (ROC) curves, and the discrimination was quantified by measuring AUC. As a method widely applied in medical diagnostics, AUC analysis estimated the probability of a model that could accurately differentiate the occurrence of events among

TABLE 1: Logistics regression analysis to detect AD predictors.

Characteristics	AD ( $n = 45$ )	Control ( $n = 24$ )	Logistics regression analysis		
			OR	SE	$P$ value
Gender (female/male)	25/20	10/14	1.058	0.618	0.928
Age (low/high)	$82.7 \pm 9.8$	$71.5 \pm 16.9$	0.246	0.628	0.026*
ATP6V1A (low/high)	$8.04 \pm 0.41$	$8.42 \pm 0.46$	5.831	0.586	0.003**

\* $P < 0.05$ ; \*\* $P < 0.01$ ; AD: Alzheimer's disease; OR: odds ratio; SE: standard error.

randomly selected individuals [28]. An AUC value of 100% was for complete prediction and 50% for random selection. All  $P$  values were bilateral, and statistical significance at  $P < 0.05$  was selected.

**2.8. Cell-Type Proportion Analysis.** To assess the proportion of cell types in the bulk tissue RNA-seq data in our study, a cell-type deconvolution on each sample was conducted by the brain cell-type marker signatures provided by the *BRETIGEA* R package [29]. Each cell type (e.g., neurons, endothelial cells, oligodendrocytes, microglia, astrocytes, and oligodendrocyte precursor cells (OPCs)) using 1000 marker genes from the human brain cell marker gene set was computed to generate an estimate of all surrogate cell-type proportion values (SPVs). Adopting the default parameters and the SPVs calculated above, the bulk RNA-seq data was normalized by *BRETIGEA* function.

**2.9. Cell-Type Specificity Plot.** To generate the cell-type specificity plot, each squared expression was calculated as a vector and plotted from the center on a polar coordinate system based on the mean cell-type gene expression from Zhang et al. [30]. Thereafter, the vector sum of expression values for each gene were measured and multiplied by a scaling coefficient to form a final point as an estimate of the cell-type specificity for any gene under consideration.

### 3. Results

**3.1. Baseline Characteristics of Samples and Identification of DEGs.** The flowchart of study design was shown in Figure 1. The mean expression of ATP6V1A in the temporal cortex of AD ( $8.04 \pm 0.41$ ) was significantly lower than that of nondementia controls ( $8.42 \pm 0.46$ ;  $P = 0.001$ ) (Figure 2(a)). This was consistent with western blot (Supplementary Figures 1A and 1B) and qRT-PCR (Supplementary Figure 1C) analyses of ATP6V1A expression between Mount Sinai Brain Bank (MSBB) Brodmann area 36 parahippocampal gyrus (BM36-PHG) samples of AD and normal controls [31]. Logistics regression analysis revealed that old age (OR = 0.246;  $P = 0.026$ ) and low ATP6V1A expression (OR = 5.831;  $P = 0.003$ ) were causally related to AD (Table 1). After removing unannotated and duplicate genes, 20,759 background genes were included for differential expression analysis. There were 3,416 DEGs (1,675 up- and 1,741 downregulated genes) filtrated in AD versus nondementia controls (Figure 2(b)). Whilst 5,303 DEGs (1,820 up- and 3,483 downregulated genes) were differentially expressed in ATP6V1A-low compared with high cohort (Figure 2(c)).

Finally, 1,364 DEGs (577 up- and 787 downregulated genes) were overlapped from AD/control and ATP6V1A-low/high groups. Heatmap of the DEGs between AD and nondementia controls was plotted in Figure 2(d).

**3.2. Coexpression Modules and Functional Enrichment Analysis.** All samples passed the cut-off line with a height of 25 and were hierarchically clustered by the average linkage (Figure 3(a)). Four coexpression modules (Figure 3(b)) were established by WGGNA, among which the grey module composed of noncoexpressed genes was regarded as the invalid module. Heatmap of module-trait relationships (Figure 3(c)) showed that blue module was positively correlated with AD (correlation coefficient = 0.65,  $P = 1e - 09$ ) and negatively associated with ATP6V1A (correlation coefficient = -0.63,  $P = 5e - 09$ ), whereas brown and turquoise modules had a negative correlation with AD (brown: correlation coefficient = -0.58,  $P = 2e - 07$ ; turquoise: correlation coefficient = -0.57,  $P = 3e - 07$ ) and positive association with ATP6V1A (brown: correlation coefficient = 0.59,  $P = 1e - 07$ ; turquoise: correlation coefficient = 0.92,  $P = 3e - 28$ ). Annotation of KEGG pathway (Figure 3(d)) was accomplished by functional enrichment analysis, showing that the DEGs in blue module were involved in proteoglycans in cancer and focal adhesion; the DEGs of brown module participated in biosynthesis of amino acids, dopaminergic synapse, and synaptic vesicle cycle; the DEGs in turquoise module were enriched in phagosome, dopaminergic synapse, oxidative phosphorylation, synaptic vesicle cycle, and gamma-aminobutyric acidergic (GABAergic) synapse.

**3.3. Global Regulation Network and AUC Analysis of ATP6V1A.** As shown in Figure 4(a), scatter diagram between MM and GS (Figure 4(a)) showed a significant correlation between intramodular connectivity and genetic phenotypes in the blue, brown, and turquoise modules (blue: correlation coefficient = 0.71,  $P = 9.2e - 27$ ; brown: correlation coefficient = 0.54,  $P = 6.9e - 12$ ; turquoise: correlation coefficient = 0.94,  $P = 1e - 200$ ), but not in the grey module (correlation coefficient = -0.31,  $P = 0.2$ ). Thereafter, DEGs strongly interacting with ATP6V1A (MM > 0.4 and GS > 0.5) were extracted and displayed in the global regulation network (Figure 4(b)). Further cross-talking pathways of ATP6V1A, including phagosome, oxidative phosphorylation, and synaptic vesicle cycle, were identified (Figure 4(c)). The result of AUC analysis (AUC = 74.2%) exhibited a good diagnostic performance of low ATP6V1A expression in AD onset (Figure 4(d)).

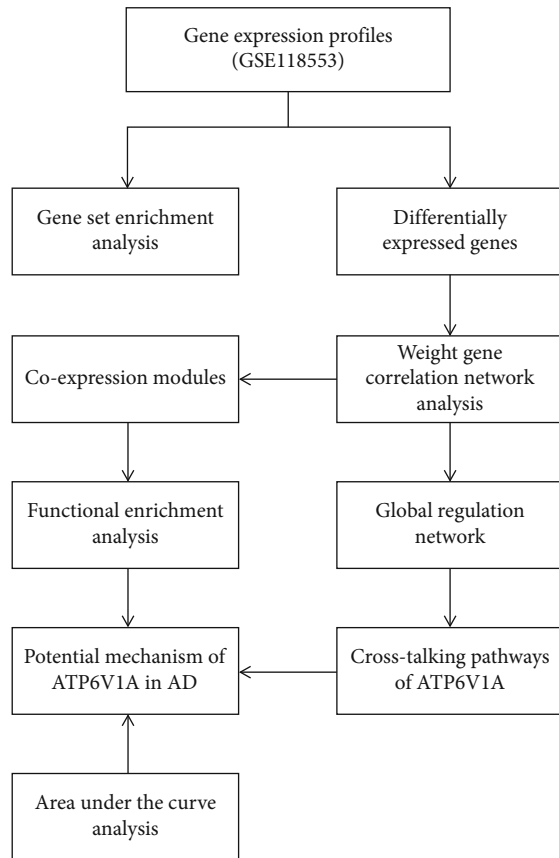


FIGURE 1: The flowchart of study design. AD: Alzheimer's disease.

**3.4. Verification of ATP6V1A-Mediated Pathway and GSEA in BP.** Five signature genes in each cross-talking pathway were determined by PCC analysis (Supplementary Table 1). As shown in Figure 5(a), each signature gene was significantly positively correlated with ATP6V1A expression ( $P < 0.05$ ). In the AD group, the major enrichment of BP involved memory, neurotransmitter secretion, regulation of synaptic plasticity, signal release from synapse, and synaptic vesicle cycle (Figure 5(b)). In the ATP6V1A-low group, the primary enrichment of BP consisted of cellular respiration, neurotransmitter secretion, oxidative phosphorylation, signal release from synapse, and synaptic vesicle cycle (Figure 5(c)).

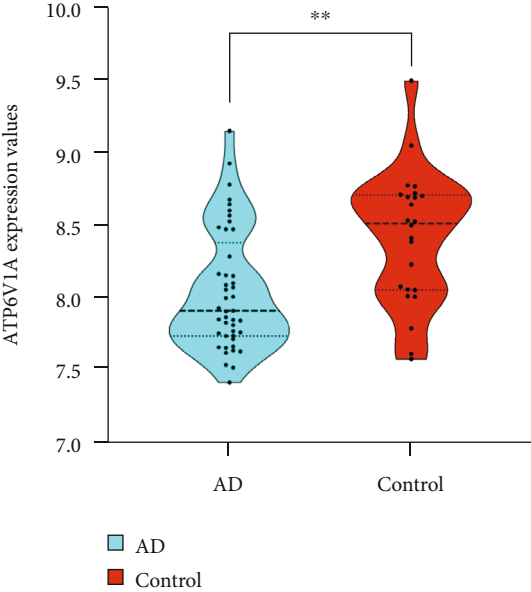
**3.5. Cell-Type Specificity of Signature Genes.** As shown in Supplementary Figure 1D, a decrease in neurons combined with an increase of OPCs, oligodendrocytes, astrocytes, and endothelial cells were observed, indicating the significant and unique changes in the cell-type composition in AD. As shown in Supplementary Figure 1E, the cell-type specificity of signature genes (including ATP6V1A) was examined by using RNA-seq data derived from different types of cultured brain cells, such as neurons, astrocytes, microglia, endothelial cells, and oligodendrocytes, which presented the downregulation of signature genes in neurons (ATP6V1A, SYT1, SNAP25, NDUFB5, NDUFS3, ATP6V1E1, NSF, and ATP6V1G1), oligodendrocytes (ATP6V1B2), and astrocytes (TUBB2A, TUBA4A, and TUBB3).

## 4. Discussion

In this study, the comparison of ATP6V1A expression was assessed between AD and nondementia controls. Intriguingly, we found downregulation of ATP6V1A in the temporal cortex of AD, a preferential region susceptible to AD neurodegeneration [32]. Further analyses of GSEA involving 20,759 background genes demonstrated that DEGs in AD and ATP6V1A-low cohorts were enriched in neurotransmitter secretion, signal release from synapse, and synaptic vesicle cycle. Of particular note was that these biological processes were possibly related to AD as well as low ATP6V1A expression. In secretory vesicles, V-ATPase was observed to drive neurotransmitter uptake by establishing proton and membrane potential gradients, hence linking the V-ATPase to neurosecretion of synaptic vesicles [33]. Herein, we constructed global regulatory network and co-expression modules of DEGs interacting with ATP6V1A to illustrate the genome-scale mechanism of ATP6V1A in AD pathophysiology.

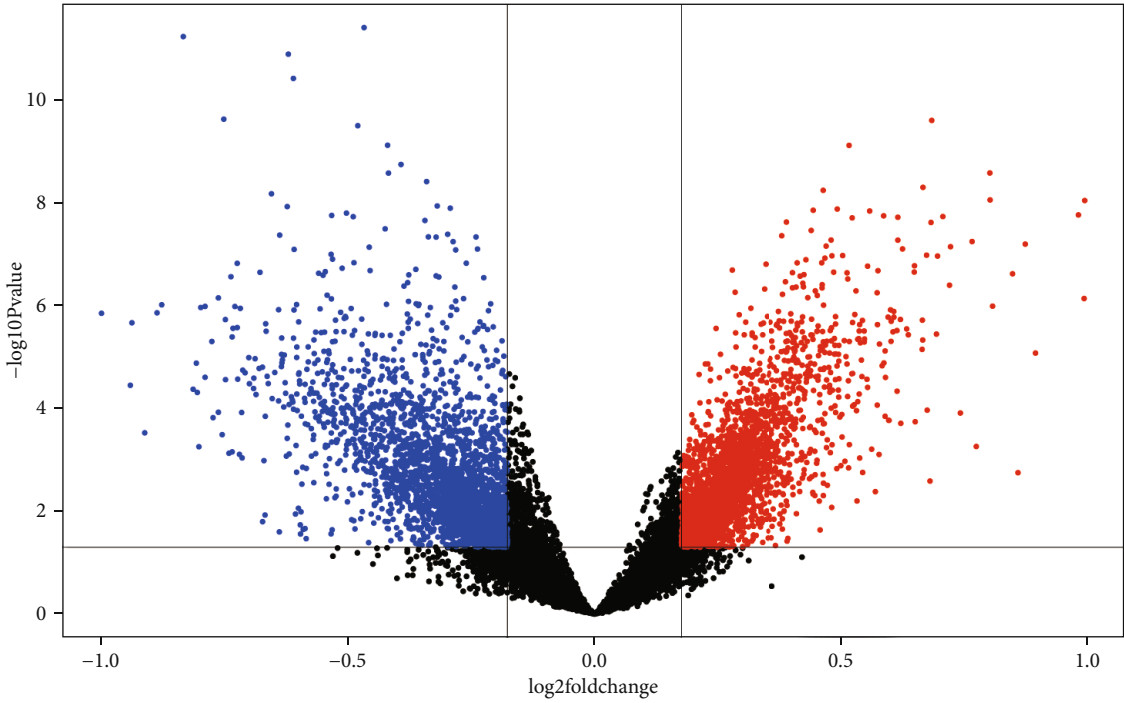
The results emerging from WGCNA revealed that the blue, brown, and turquoise modules were significantly correlated with AD and ATP6V1A, which were involved in phagosome, oxidative phosphorylation, synaptic vesicle cycle, focal adhesion, and GABAergic synapse. Among them, synaptic vesicle was found to tightly pack and store quanta of neurotransmitter molecules in nerve terminals [34]. Progressive dementia of AD was largely attributed to synaptic defects that were not functioning optimally even before structural deterioration [35]. Both biochemical and stereological evidence of AD presented a better correlation of cognitive decline with reduced synapse density than either A $\beta$  or NFT aggregates, highlighting the fundamental role of synaptic vesicle in AD pathogenesis [36, 37]. Notably, loading of neurotransmitters into synaptic vesicle required a proton gradient, which was precisely dependent on the multisubunit V-ATPase [38]. By contrast, abolishment of proton gradient has dramatic consequences for neurotransmitter release in synaptic vesicle, which should be taken into account when assessing the effects of molecular perturbation of ATP6V1A. Indeed, the effects of V-ATPase on synaptic vesicle were not only restricted to proton pumping and neurosecretion but also implicated in filling downstream and synaptic vesicle fusion [39, 40]. Genomic studies in mice and flies have shown that knockout of ATPase caused impaired presynaptic transmission, along with alterations in the amount and morphology of synapses [41, 42]. These were important processes of V-ATPase deficiency contributing to cognitive impairment and neuronal degeneration [7], consistent with our findings of the participation of low ATP6V1A-mediated synaptic vesicle cycle in AD pathogenesis.

Apart from synaptic vesicle cycle, functional enrichment analysis revealed that ATP6V1A was involved in phagosome and oxidative phosphorylation in AD. In terms of phagosome pathway, it was a step in the degradation processes for lysosome, an acidic and degradative organelle in cells that received and digested all sorts of macromolecules via endocytosis, phagocytosis, and autophagy [43]. During phagocytosis, the particle remained compartmentalized in



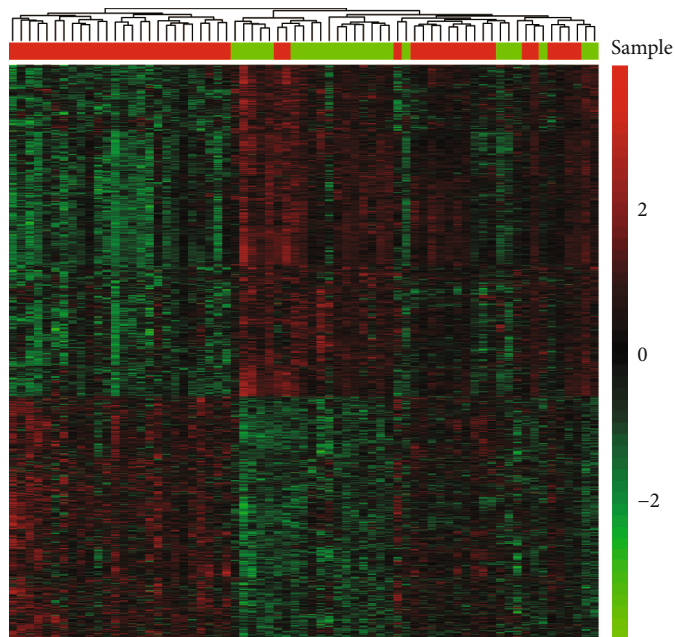
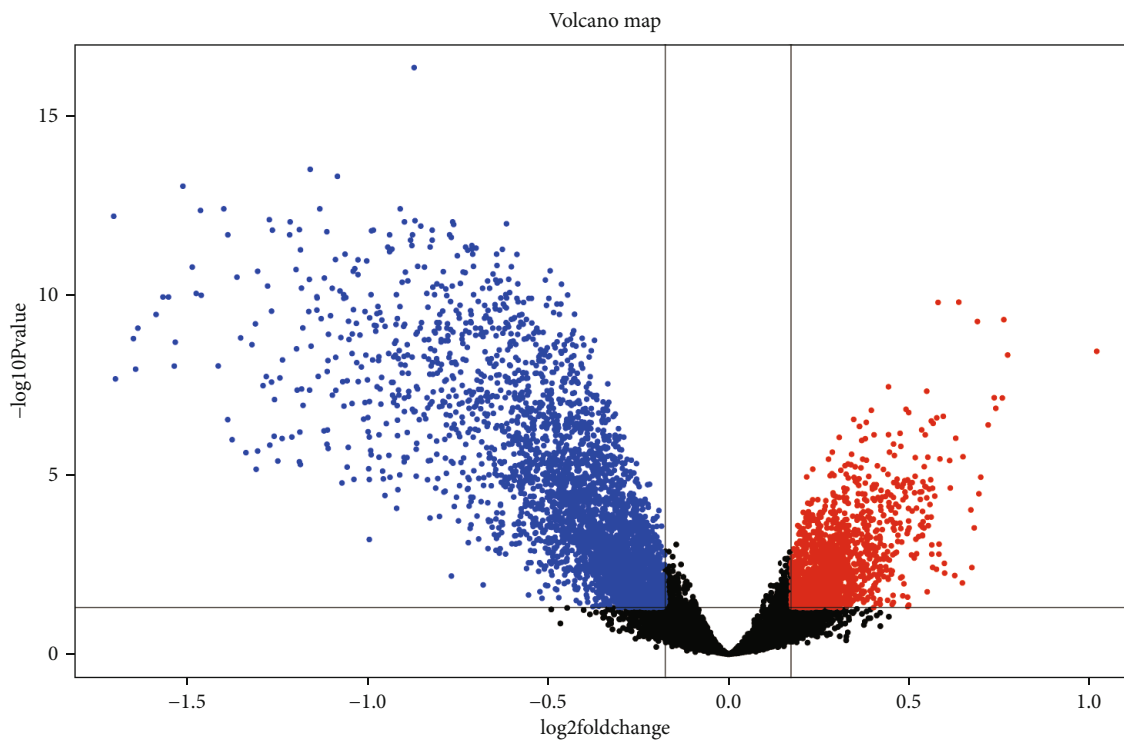
(a)

Volcano map



(b)

FIGURE 2: Continued.

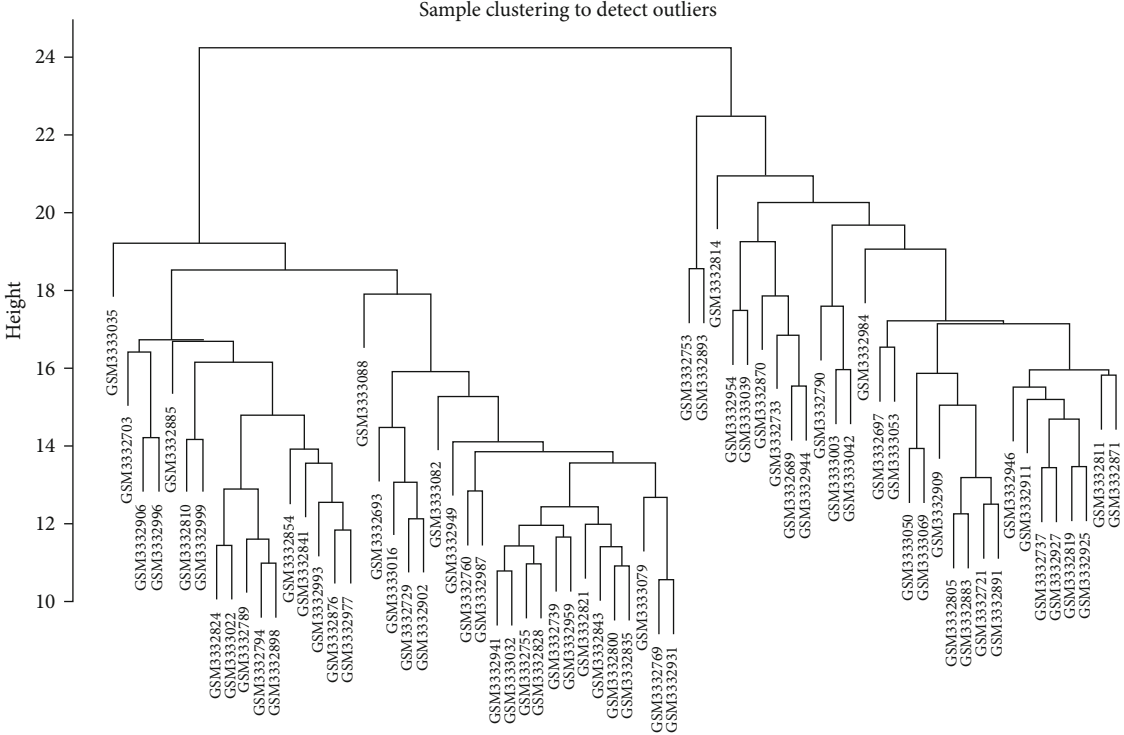


Sample  
■ AD  
■ Control

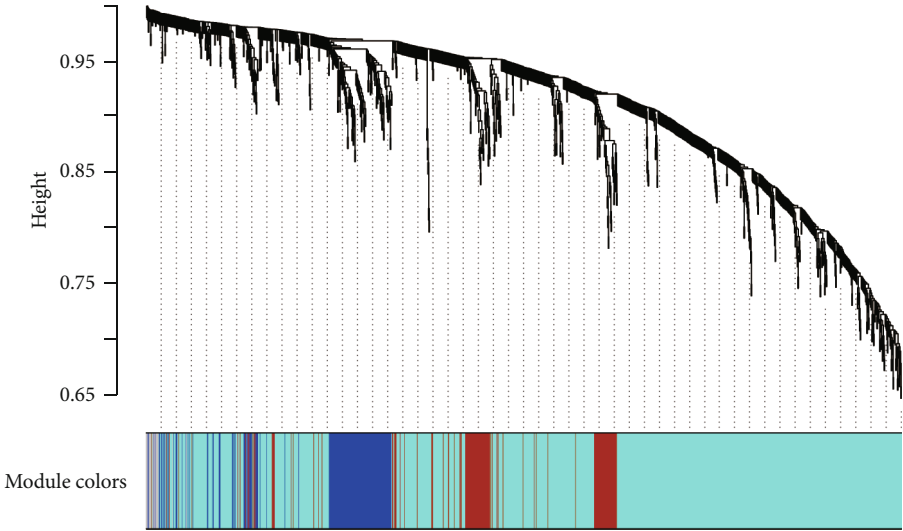
(d)

FIGURE 2: Differential expression gene analysis. ATP6V1A expression between AD and nondementia controls (a). Volcano plot of DEGs in the AD/control (b) and ATP6V1A-low/high groups (c): red represents upregulated and blue indicates downregulated. Heatmap of the DEGs in AD/control groups (d): green to red indicates the progression of gene expression from downregulated to upregulated.  $**P < 0.01$ ; AD: Alzheimer's disease; DEGs: differentially expression genes.





(a)  
Cluster dendrogram



(b)

FIGURE 3: Continued.

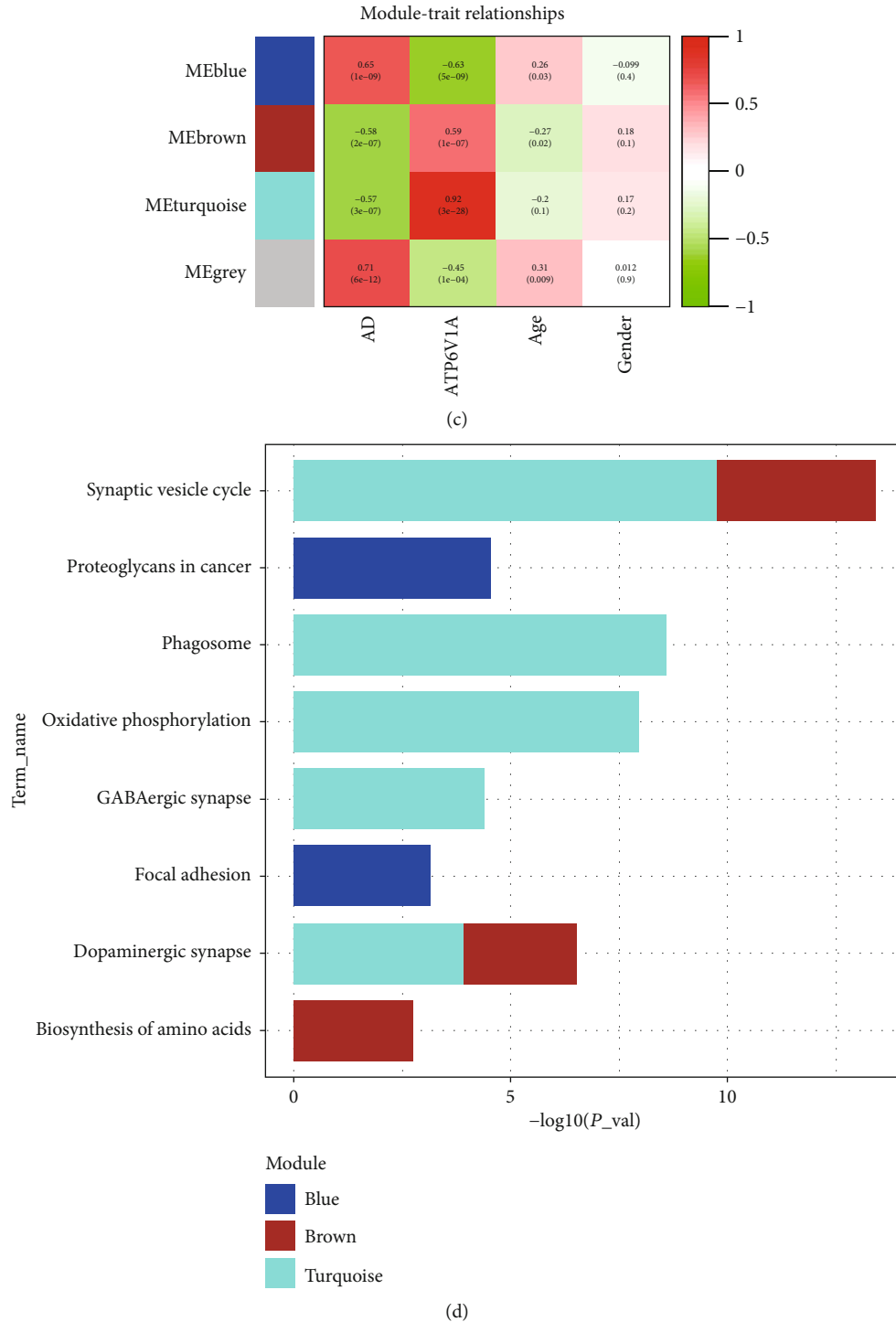
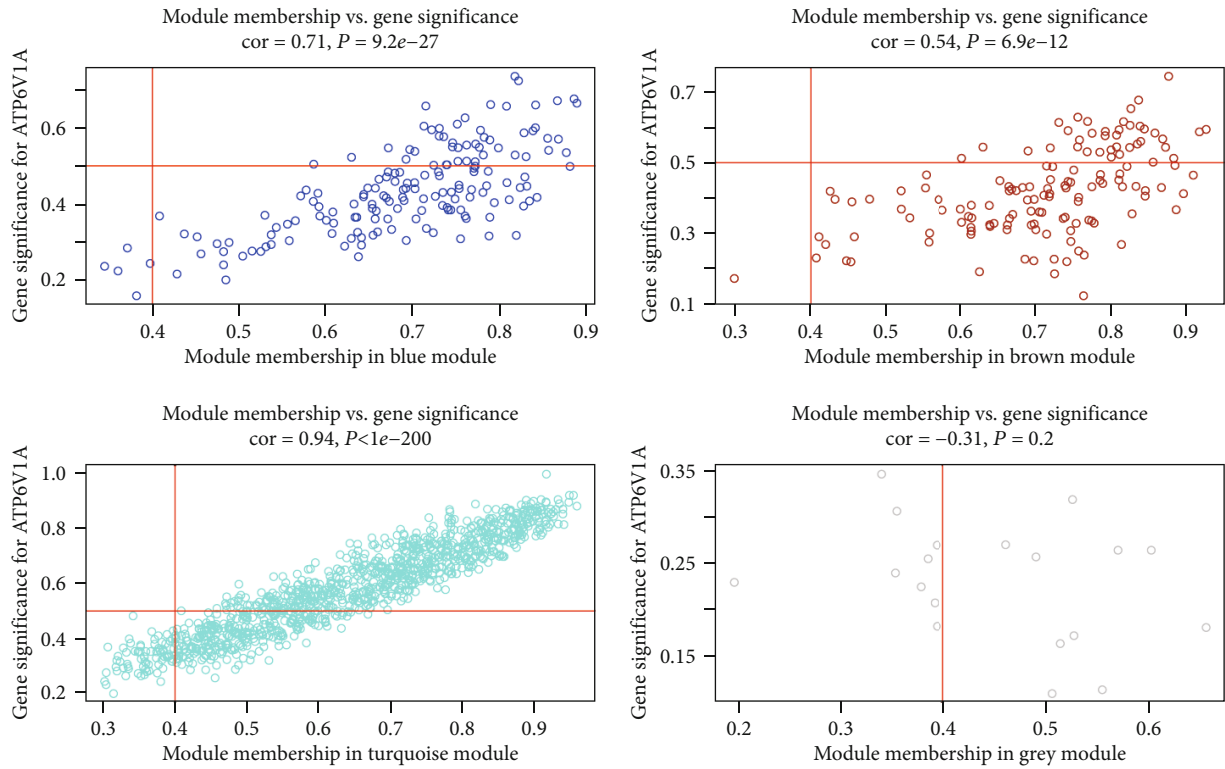


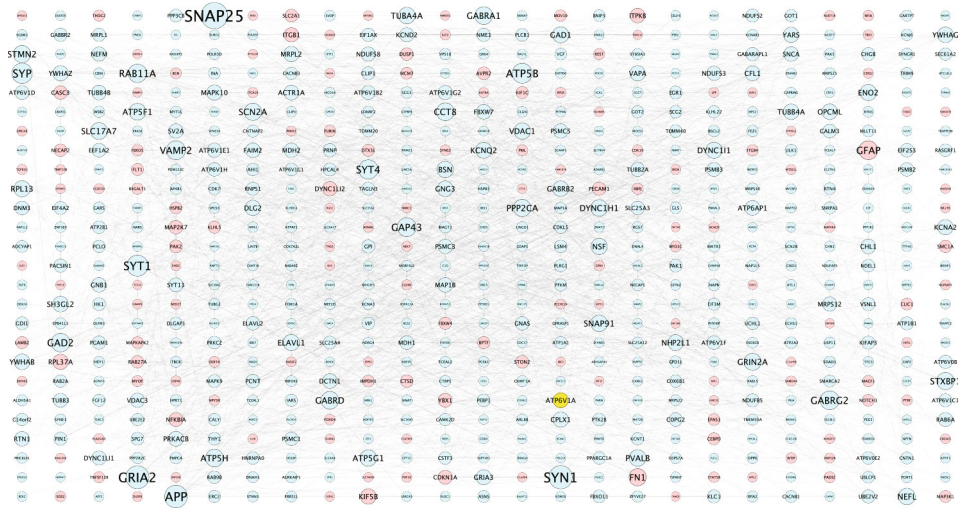
FIGURE 3: Weighted correlation network analysis. Clustering plot of samples (a). Cluster dendrogram of DEGs for distributing module colors (b): grey indicates nonclustering genes. Module-trait relationships of each module (c): green to red represents the correlation of modules from negative to positive with phenotypes. KEGG pathways of DEGs in each module (d). AD: Alzheimer’s disease; KEGG: Kyoto Encyclopedia of Genes and Genomes.

phagosomes and eventually underwent lysosomal degradation through the phagosome pathway, an important cause of neuronal loss in AD neuropathology [44, 45]. Previous studies showed that  $A\beta$  potentially activated the phagocytic capacity, by which neurons were eliminated before they died

[45, 46]. The results obtained here were supported by inhibition of phagocytosis using cytochalasin D and cyclo-(RGDfV), both of which prevented neuronal loss and unexpectedly increased survival cells in pathologically affected regions of AD [47]. Much evidence has underscored the

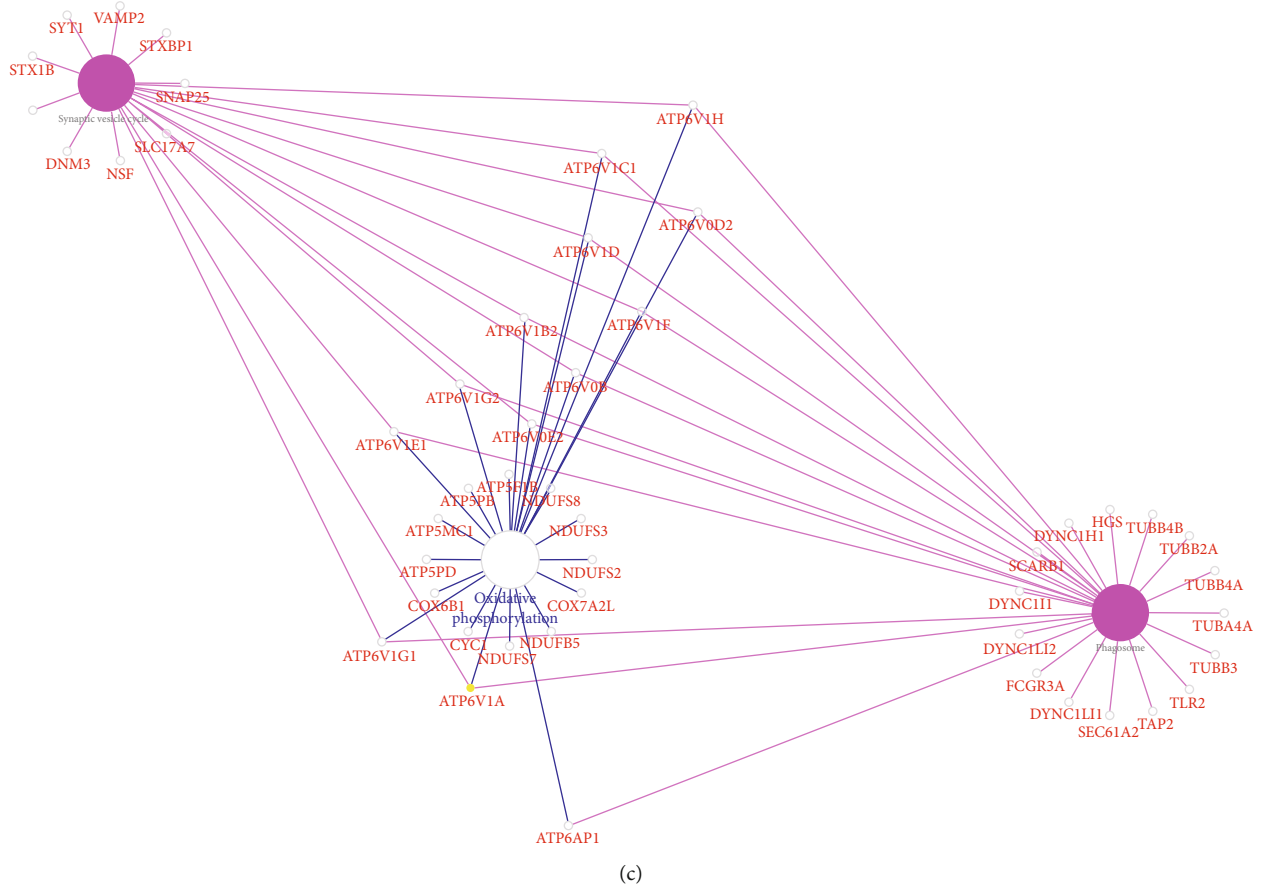


(a)

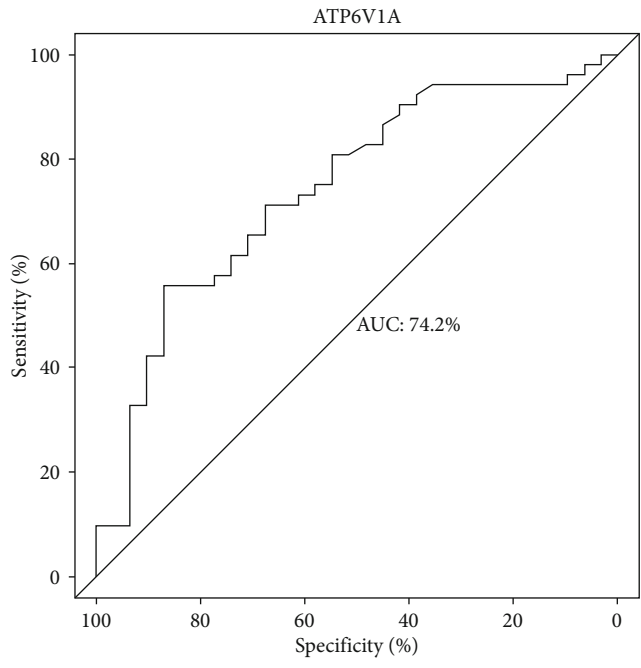


(b)

FIGURE 4: Continued.



(c)



(d)

FIGURE 4: Module-pathway regulatory network and AUC analysis. Scatter diagram of module membership versus gene significance (a). Global regulatory network on DEGs interacting with ATP6V1A (b): red represents high expression; blue and yellow indicate low expression; the size of nodes reflects the degree of gene connectivity. Identification of cross-talking pathways of ATP6V1A (c): yellow indicates the low ATP6V1A expression. AUC analysis in AD prediction (d). AD: Alzheimer’s disease; AUC: area under the curve.



(a)

FIGURE 5: Continued.

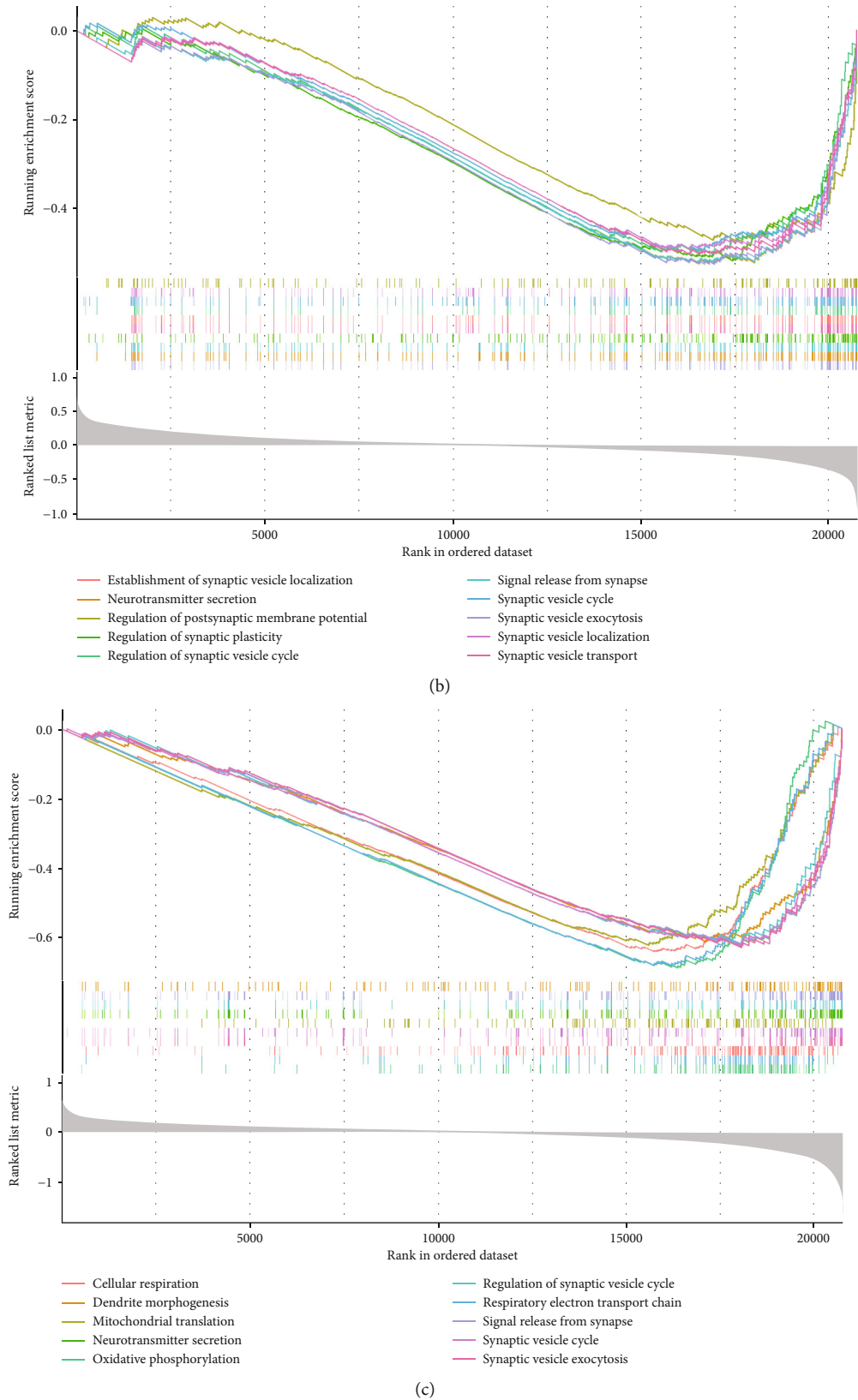


FIGURE 5: Correlation among genes and gene set enrichment analysis. Correlation of ATP6V1A with signature genes (a):  $*P < 0.05$ ; blue indicates positive correlation. BP terms of gene set enrichment analysis enriched in AD (b) and ATP6V1A-low (c) groups. AD: Alzheimer's disease; BP: biological processes.

viewpoint of bioenergetic failure and mitochondrial malfunction in preclinical and established AD [48, 49]. In addition, oxidative phosphorylation has important roles in mitochondrial ATP production and is modulated by respiratory enzyme complexes I–V [50, 51]. In AD model of triple transgenic mice, deregulations of complexes I and IV were tau- and A $\beta$ -dependent, respectively, which was implicated in reduction of mitochondrial proteins [52]. This provided support for the synergistic role of A $\beta$  and tau in perishing mitochondria, leading to reactive oxidative species (ROS) production, bioenergetic exhaustion, and neuronal apoptosis [53, 54]. There was also evidence that mitochondrial DNA mutation in V-ATPase contributed to various defects of oxidative phosphorylation [55, 56]. Inhibition of V-ATPase by Bafilomycin impaired decoupling of oxidative phosphorylation and thus to insufficient energy of neurons [57, 58]; meanwhile, energy could be supplemented by return of oxidative phosphorylation upon reoxygenation, which in turn activated V-ATPase [59]. Likewise, our findings supported the likelihood that low expression of ATP6V1A participated in oxidative phosphorylation and that enhancement of ATP6V1A could be neuroprotective in AD.

The results of logistics regression analysis revealed a causal relationship of AD with elder age and lower ATP6V1A expression, suggesting that either downregulation of ATP6V1A or increase of age might be a pathogenic factor of AD. Evidence in transgenic APP/PS1 model of mice showed that defects of V-ATPase and axonal transport were early pathogenic events deteriorated with age, leading to accumulation of APP and synaptic A $\beta$  [60, 61]. On basis of DEGs that were strongly interacting with ATP6V1A, global regulatory network was constructed to identify the cross-talking pathways of ATP6V1A, including synaptic vesicle cycle, phagosome, and oxidative phosphorylation. The analysis of PCC showed significantly positive correlation of ATP6V1A with signature genes of each cross-talking pathway, which provided computational statistical evidence for the involvement of low ATP6V1A in AD pathogenesis via synaptic vesicle cycle, phagosome, and oxidative phosphorylation. The AUC analysis showed that low ATP6V1A expression accurately predicted AD onset, also implying ATP6V1A to be a potential biomarker of AD. Cell-type proportion analysis exhibited a decrease in neurons along with an increase of OPCs, oligodendrocytes, astrocytes, and endothelial cells, in line with the significant and unique changes in response to misfolded or polymerized A $\beta$  in AD [62]. As supported by experiments using Western blot and qRT-PCR, downregulation of ATP6V1A was identified in MSBB BM36-PHG samples of AD relative to normal controls [31]. Cell-type specific analysis presented the downregulation of signature genes in neurons (ATP6V1A, SYT1, SNAP25, NDUFB5, NDUFS3, ATP6V1E1, NSF, and ATP6V1G1), oligodendrocytes (ATP6V1B2), and astrocytes (TUBB2A, TUBA4A, and TUBB3), supporting the linkage of low ATP6V1A with phagosome of astrocytes, neuronal synaptic vesicle cycle, and oxidative phosphorylation. Further *in vivo* or *in vitro* experiments are encouraged to verify the low ATP6V1A-mediated pathways underlying AD proposed in the current study.

## 5. Conclusions

Overall, the work undertaken in this study suggests that bioinformatics analysis is a promising approach to investigate the complex pathways of ATP6V1A in AD occurrence. Based on our findings, low expression of ATP6V1A was involved in the pathogenesis of AD, which might be mediated via synaptic vesicle cycle, phagosome, and oxidative phosphorylation.

## Data Availability

The datasets generated and/or analyzed during the current study are available in the GSE118553 repository, <https://www.ncbi.nlm.nih.gov/geo/query/acc.cgi?acc=GSE118553>.

## Conflicts of Interest

The authors declare that they have no conflicts of interest.

## Authors' Contributions

CSZ, MZ, and ZKZ conceived and designed the study. JB, KXK, RWZ, SSZ, XQZ, and ZKZ conducted the experiments and analyzed the data. MZ and ZKZ wrote the original draft. CSZ, YX, and ZKZ reviewed and edited the paper. All authors read and approved the final manuscript. Chuansheng Zhao and Mei Zhao contributed equally to this work.

## Acknowledgments

The research is supported by the National Natural Science Foundation of China (No. 81372104), the Natural Science Foundation of Liaoning Province (No. 20180540150), the Shenyang Population and Health Technical Critical Special Project (No. F16-206-9-01), the Program of the Distinguished Professor of Liaoning Province (Chuansheng Zhao), and Guidance Plan for Key Research and Development Plans of Liaoning Province (No. 2019JH8/10300002).

## Supplementary Materials

*Supplementary 1.* Supplementary Table 1: signature genes for each cross-talking pathway.

*Supplementary 2.* Supplementary Figure 1: expression changes of ATP6V1A and cell-type specificity of signature genes. ATP6V1A expression changes in MSBB BM36-PHG samples using Western blot (A and B) and qRT-PCR (C) analyses ([31]; available from doi:10.1016/j.neuron.2020.11.002). Mean change of cell-type proportion by computing the SPV average for the samples after cell-type deconvolution using *BRETIGEA* (D): blue to red indicates the change from a decrease to an increase. Vector addition of squared expression levels of signature genes across five different cell types in AD (E): yellow indicates downregulated expression. BM36-PHG: Brodmann area 36 parahippocampal gyrus; MSBB: Mount Sinai Brain Bank; NL: normal control; SPV: surrogate proportion value; ast: astrocytes; end: endothelial cells; mic: microglia; neu: neurons; oli: oligodendrocytes.

## References

- [1] M. Calvo-Rodriguez, S. S. Hou, A. C. Snyder et al., "Increased mitochondrial calcium levels associated with neuronal death in a mouse model of Alzheimer's disease," *Nature Communications*, vol. 11, no. 1, p. 2146, 2020.
- [2] J. Götz and L. M. Ittner, "Animal models of Alzheimer's disease and frontotemporal dementia," *Nature Reviews Neuroscience*, vol. 9, no. 7, pp. 532–544, 2008.
- [3] C. Haass and D. J. Selkoe, "Soluble protein oligomers in neurodegeneration: lessons from the Alzheimer's amyloid  $\beta$ -peptide," *Nature Reviews Molecular Cell Biology*, vol. 8, no. 2, pp. 101–112, 2007.
- [4] A. Majumdar, E. Capetillo-Zarate, D. Cruz, G. K. Gouras, and F. R. Maxfield, "Degradation of Alzheimer's amyloid fibrils by microglia requires delivery of ClC-7 to lysosomes," *Molecular Biology of the Cell*, vol. 22, no. 10, pp. 1664–1676, 2011.
- [5] R. A. Nixon, "Autophagy, amyloidogenesis and Alzheimer disease," *Journal of Cell Science*, vol. 120, no. 23, pp. 4081–4091, 2007.
- [6] J. A. Mindell, "Lysosomal acidification mechanisms," *Annual Review of Physiology*, vol. 74, no. 1, pp. 69–86, 2012.
- [7] Q. Song, B. Meng, H. Xu, and Z. Mao, "The emerging roles of vacuolar-type ATPase-dependent lysosomal acidification in neurodegenerative diseases," *Translational Neurodegeneration*, vol. 9, no. 1, p. 17, 2020.
- [8] T. Nishi and M. Forgac, "The vacuolar ( $H^+$ )-ATPases – nature's most versatile proton pumps," *Nature Reviews. Molecular Cell Biology*, vol. 3, no. 2, pp. 94–103, 2002.
- [9] M. Liu, M. Tarsio, C. M. H. Charsky, and P. M. Kane, "Structural and functional separation of the N- and C-terminal domains of the yeast V-ATPase subunit H\*," *The Journal of Biological Chemistry*, vol. 280, no. 44, pp. 36978–36985, 2005.
- [10] P. M. Kane, "The where, when, and how of organelle acidification by the yeast vacuolar  $H^+$ -ATPase," *Microbiology and Molecular Biology Reviews: MMBR*, vol. 70, no. 1, pp. 177–191, 2006.
- [11] M. B. Bagh, S. Peng, G. Chandra et al., "Misrouting of v-ATPase subunit V0a1 dysregulates lysosomal acidification in a neurodegenerative lysosomal storage disease model," *Nature Communications*, vol. 8, no. 1, p. 14612, 2017.
- [12] R. L. Proia and Y.-P. Wu, "Blood to brain to the rescue," *The Journal of Clinical Investigation*, vol. 113, no. 8, pp. 1108–1110, 2004.
- [13] W. R. Williamson and P. R. Hiesinger, "On the role of v-ATPase V0a1-dependent degradation in Alzheimer disease," *Communicative & Integrative Biology*, vol. 3, no. 6, pp. 604–607, 2010.
- [14] M. Narayanan, J. L. Huynh, K. Wang et al., "Common dysregulation network in the human prefrontal cortex underlies two neurodegenerative diseases," *Molecular Systems Biology*, vol. 10, no. 7, p. 743, 2014.
- [15] M. E. Ritchie, B. Phipson, D. Wu et al., "Limma powers differential expression analyses for RNA-sequencing and microarray studies," *Nucleic Acids Research*, vol. 43, no. 7, p. e47, 2015.
- [16] V. K. Mootha, C. M. Lindgren, K.-F. Eriksson et al., "PGC-1 $\alpha$ -responsive genes involved in oxidative phosphorylation are coordinately downregulated in human diabetes," *Nature Genetics*, vol. 34, no. 3, pp. 267–273, 2003.
- [17] A. Subramanian, P. Tamayo, V. K. Mootha et al., "Gene set enrichment analysis: a knowledge-based approach for interpreting genome-wide expression profiles," *Proceedings of the National Academy of Sciences of the United States of America*, vol. 102, no. 43, pp. 15545–15550, 2005.
- [18] C. W. Law, Y. Chen, W. Shi, and G. K. Smyth, "Voom: precision weights unlock linear model analysis tools for RNA-seq read counts," *Genome Biology*, vol. 15, no. 2, p. R29, 2014.
- [19] F. N. Soria, A. Pérez-Samartín, A. Martín et al., "Extrasynaptic glutamate release through cystine/glutamate antiporter contributes to ischemic damage," *The Journal of Clinical Investigation*, vol. 124, no. 8, pp. 3645–3655, 2014.
- [20] B. Zhang and S. Horvath, "A general framework for weighted gene co-expression network Analysis," *Statistical Applications in Genetics and Molecular Biology*, vol. 4, no. 1, 2005.
- [21] P. Langfelder and S. Horvath, "WGCNA: an R package for weighted correlation network analysis," *BMC Bioinformatics*, vol. 9, no. 1, p. 559, 2008.
- [22] Q. Yang, R. Wang, B. Wei et al., "Candidate biomarkers and molecular mechanism investigation for glioblastoma multi-forme utilizing WGCNA," *BioMed Research International*, vol. 2018, Article ID 4246703, 10 pages, 2018.
- [23] E. Fredlund, J. Staaf, J. K. Rantala, O. Kallioniemi, A. Borg, and M. Ringnér, "The gene expression landscape of breast cancer is shaped by tumor protein p53 status and epithelial-mesenchymal transition," *Breast Cancer Research: BCR*, vol. 14, no. 4, p. R113, 2012.
- [24] D. Szklarczyk, J. H. Morris, H. Cook et al., "The STRING database in 2017: quality-controlled protein-protein association networks, made broadly accessible," *Nucleic Acids Research*, vol. 45, no. D1, pp. D362–D368, 2017.
- [25] D. Otasek, J. H. Morris, J. Bouças, A. R. Pico, and B. Demchak, "Cytoscape automation: empowering workflow-based network analysis," *Genome Biology*, vol. 20, no. 1, p. 185, 2019.
- [26] D.-M. Ma, Z. Wang, L. Wang, F. Alejos-Gonzales, M.-A. Sun, and D.-Y. Xie, "A genome-wide scenario of terpene pathways in self-pollinated *Artemisia annua*," *Molecular Plant*, vol. 8, no. 11, pp. 1580–1598, 2015.
- [27] H. Sun, Y. Zhou, M. F. Skaro et al., "Metabolic reprogramming in cancer is induced to increase proton production," *Cancer Research*, vol. 80, no. 5, pp. 1143–1155, 2020.
- [28] P. Sonego, A. Kocsor, and S. Pongor, "ROC analysis: applications to the classification of biological sequences and 3D structures," *Briefings in Bioinformatics*, vol. 9, no. 3, pp. 198–209, 2008.
- [29] A. T. Mckenzie, M. Wang, M. E. Hauberg et al., "Brain cell type specific gene expression and co-expression network architectures," *Scientific Reports*, vol. 8, no. 1, p. 8868, 2018.
- [30] Y. Zhang, S. A. Sloan, L. E. Clarke et al., "Purification and characterization of progenitor and mature human astrocytes reveals transcriptional and functional differences with mouse," *Neuron*, vol. 89, no. 1, pp. 37–53, 2016.
- [31] M. Wang, A. Li, M. Sekiya et al., "Transformative network modeling of multi-omics data reveals detailed circuits, key regulators, and potential therapeutics for Alzheimer's disease," *Neuron*, vol. 109, no. 2, pp. 257–272.e14, 2021.
- [32] M. Grundman, J. Corey-Bloom, T. Jernigan, S. Archibald, and L. J. Thal, "Low body weight in Alzheimer's disease is associated with mesial temporal cortex atrophy," *Neurology*, vol. 46, no. 6, pp. 1585–1591, 1996.
- [33] M. Forgac, "Vacuolar ATPases: rotary proton pumps in physiology and pathophysiology," *Nature Reviews. Molecular Cell Biology*, vol. 8, no. 11, pp. 917–929, 2007.



- [34] Y. Wang, H. Fathali, D. Mishra et al., "Counting the number of glutamate molecules in single synaptic vesicles," *Journal of the American Chemical Society*, vol. 141, no. 44, pp. 17507–17511, 2019.
- [35] P. J. Yao, "Synaptic frailty and clathrin-mediated synaptic vesicle trafficking in Alzheimer's disease," *Trends in Neurosciences*, vol. 27, no. 1, pp. 24–29, 2004.
- [36] E. Masliah, M. Mallory, M. Alford et al., "Altered expression of synaptic proteins occurs early during progression of Alzheimer's disease," *Neurology*, vol. 56, no. 1, pp. 127–129, 2001.
- [37] R. D. Terry, E. Masliah, D. P. Salmon et al., "Physical basis of cognitive alterations in Alzheimer's disease: synapse loss is the major correlate of cognitive impairment," *Annals of Neurology*, vol. 30, no. 4, pp. 572–580, 1991.
- [38] O. El Far and M. Seagar, "A role for V-ATPase subunits in synaptic vesicle fusion?," *Journal of Neurochemistry*, vol. 117, no. 4, pp. 603–612, 2011.
- [39] S. Poëa-Guyon, M. Amar, P. Fossier, and N. Morel, "Alternative splicing controls neuronal expression of v-ATPase subunit a1 and sorting to nerve terminals\*," *The Journal of Biological Chemistry*, vol. 281, no. 25, pp. 17164–17172, 2006.
- [40] S. Vavassori and A. Mayer, "A new life for an old pump: V-ATPase and neurotransmitter release," *The Journal of Cell Biology*, vol. 205, no. 1, pp. 7–9, 2014.
- [41] A. Dubos, A. Castells-Nobau, H. Meziane et al., "Conditional depletion of intellectual disability and Parkinsonism candidate gene ATP6AP2 in fly and mouse induces cognitive impairment and neurodegeneration," *Human Molecular Genetics*, vol. 24, no. 23, pp. 6736–6755, 2015.
- [42] B. Goldstein, R. C. Speth, and M. Trivedi, "Renin-angiotensin system gene expression and neurodegenerative diseases," *Journal of the Renin-Angiotensin-Aldosterone System: JRAAS*, vol. 17, no. 3, p. 147032031666675, 2016.
- [43] G. T. Saffi and R. J. Botelho, "Lysosome fission: planning for an exit," *Trends in Cell Biology*, vol. 29, no. 8, pp. 635–646, 2019.
- [44] J. Westman, S. A. Freeman, and S. Grinstein, "Unconventional role of lysosomes in phagocytosis," *Cell Calcium*, vol. 91, p. 102269, 2020.
- [45] B. Wilkinson, J. Koenigsnecht-Talboo, C. Grommes, C. Y. D. Lee, and G. Landreth, "Fibrillar  $\beta$ -amyloid-stimulated intracellular signaling cascades require Vav for induction of respiratory burst and phagocytosis in monocytes and microglia\*," *The Journal of Biological Chemistry*, vol. 281, no. 30, pp. 20842–20850, 2006.
- [46] M. Fuhrmann, T. Bittner, C. K. E. Jung et al., "Microglial *Cx3cr1* knockout prevents neuron loss in a mouse model of Alzheimer's disease," *Nature Neuroscience*, vol. 13, no. 4, pp. 411–413, 2010.
- [47] U. Neniskyte, J. J. Neher, and G. C. Brown, "Neuronal death induced by nanomolar amyloid  $\beta$  is mediated by primary phagocytosis of neurons by microglia\*," *The Journal of Biological Chemistry*, vol. 286, no. 46, pp. 39904–39913, 2011.
- [48] M. Calvo-Rodriguez and B. J. Bacskai, "Mitochondria and calcium in Alzheimer's disease: from cell signaling to neuronal cell death," *Trends in Neurosciences*, vol. 44, no. 2, pp. 136–151, 2021.
- [49] H. du, L. Guo, S. Yan, A. A. Sosunov, G. M. McKhann, and S. ShiDu Yan, "Early deficits in synaptic mitochondria in an Alzheimer's disease mouse model," *Proceedings of the National Academy of Sciences of the United States of America*, vol. 107, no. 43, pp. 18670–18675, 2010.
- [50] D. D. Newmeyer and S. Ferguson-Miller, "Mitochondria: releasing power for life and unleashing the machineries of death," *Cell*, vol. 112, no. 4, pp. 481–490, 2003.
- [51] M. Saraste, "Oxidative phosphorylation at the fin de siècle," *Science*, vol. 283, no. 5407, pp. 1488–1493, 1999.
- [52] V. Rhein, X. Song, A. Wiesner et al., "Amyloid-beta and tau synergistically impair the oxidative phosphorylation system in triple transgenic Alzheimer's disease mice," *Proceedings of the National Academy of Sciences of the United States of America*, vol. 106, no. 47, pp. 20057–20062, 2009.
- [53] C. Caspersen, N. Wang, J. Yao et al., "Mitochondrial Abeta: a potential focal point for neuronal metabolic dysfunction in Alzheimer's disease," *FASEB Journal: official publication of the Federation of American Societies for Experimental Biology*, vol. 19, no. 14, pp. 2040–2041, 2005.
- [54] H. Hu, C.-C. Tan, L. Tan, and J.-T. Yu, "A mitocentric view of Alzheimer's disease," *Molecular Neurobiology*, vol. 54, no. 8, pp. 6046–6060, 2017.
- [55] J. M. Shoffner, P. M. Fernhoff, N. S. Krawiecki et al., "Subacute necrotizing encephalopathy: oxidative phosphorylation defects and the ATPase 6 point mutation," *Neurology*, vol. 42, no. 11, pp. 2168–2174, 1992.
- [56] G. Uziel, I. Moroni, E. Lamantea et al., "Mitochondrial disease associated with the T8993G mutation of the mitochondrial ATPase 6 gene: a clinical, biochemical, and molecular study in six families," *Journal of Neurology, Neurosurgery, and Psychiatry*, vol. 63, no. 1, pp. 16–22, 1997.
- [57] E. J. Bowman, A. Siebers, and K. Altendorf, "Bafilomycins: a class of inhibitors of membrane ATPases from microorganisms, animal cells, and plant cells," *Proceedings of the National Academy of Sciences of the United States of America*, vol. 85, no. 21, pp. 7972–7976, 1988.
- [58] A. V. Zhdanov, R. I. Dmitriev, and D. B. Papkovsky, "Bafilomycin A1 activates respiration of neuronal cells via uncoupling associated with flickering depolarization of mitochondria," *Cellular and Molecular Life Sciences: CMLS*, vol. 68, no. 5, pp. 903–917, 2011.
- [59] J. A. Covi, W. D. Treleaven, and S. C. Hand, "V-ATPase inhibition prevents recovery from anoxia in *Artemia franciscana* embryos: quiescence signaling through dissipation of proton gradients," *The Journal of Experimental Biology*, vol. 208, no. 14, pp. 2799–2808, 2005.
- [60] D. J. Colacurcio and R. A. Nixon, "Disorders of lysosomal acidification—the emerging role of v-ATPase in aging and neurodegenerative disease," *Ageing Research Reviews*, vol. 32, pp. 75–88, 2016.
- [61] M. Torres, S. Jimenez, R. Sanchez-Varo et al., "Defective lysosomal proteolysis and axonal transport are early pathogenic events that worsen with age leading to increased APP metabolism and synaptic Abeta in transgenic APP/PS1 hippocampus," *Molecular Neurodegeneration*, vol. 7, no. 1, p. 59, 2012.
- [62] B. De Strooper and E. Karran, "The cellular phase of Alzheimer's disease," *Cell*, vol. 164, no. 4, pp. 603–615, 2016.